Thermodynamic simulation of compressed air energy storage systems

Ghady Dib

N°d'ordre NNT : 2020LYSEI092

THESE de DOCTORAT DE L'UNIVERSITE DE LYON
opérée au sein de
L'Institut National des Sciences Appliquées de Lyon

Ecole Doctorale N° 162
(MÉCANIQUE, ÉNERGÉTIQUE, GÉNIE CIVIL, ACOUSTIQUE)

Spécialité / discipline de doctorat : Thermique Energétique

Soutenue publiquement le 27/10/2020, par :
Ghady Dib

Thermodynamic simulation of compressed air energy storage systems

---

Devant le jury composé de :

Lemort Vincent	Professeur	Université de Liège	Rapporteur
Grosu Lavinia	Maître de conférences, HDR	Université Paris Ouest	Rapporteure
Lanzetta François	Professeur	Université de Franche-Comte	Examinateur
Revellin, Rémi	Professeur	INSA Lyon	Directeur de thèse
Rullière, Romuald	Maître de conferences	INSA Lyon	Encadrant
Haberschill, Philippe	Maître de conférences, HDR Emérite	INSA Lyon	Co-directeur de thèse
Perroit, Quentin	Ingénieur chef de projet	AIA Life Designers	Invité

Département FEDORA – INSA Lyon - Ecoles Doctorales – Quinquennal 2016-2020

SIGLE	ECOLE DOCTORALE	NOM ET COORDONNEES DU RESPONSABLE
CHIMIE	**CHIMIE DE LYON** http://www.edchimie-lyon.fr Sec. : Renée EL MELHEM Bât. Blaise PASCAL, 3e étage secretariat@edchimie-lyon.fr INSA : R. GOURDON	**M. Stéphane DANIELE** Institut de recherches sur la catalyse et l'environnement de Lyon IRCELYON-UMR 5256 Équipe CDFA 2 Avenue Albert EINSTEIN 69 626 Villeurbanne CEDEX directeur@edchimie-lyon.fr
E.E.A.	**ÉLECTRONIQUE, ÉLECTROTECHNIQUE, AUTOMATIQUE** http://edeea.ec-lyon.fr Sec. : M.C. HAVGOUDOUKIAN ecole-doctorale.eea@ec-lyon.fr	**M. Gérard SCORLETTI** École Centrale de Lyon 36 Avenue Guy DE COLLONGUE 69 134 Écully Tél : 04.72.18.60.97 Fax 04.78.43.37.17 gerard.scorletti@ec-lyon.fr
E2M2	**ÉVOLUTION,ÉCOSYSTÈME, MICROBIOLOGIE, MODÉLISATION** http://e2m2.universite-lyon.fr Sec. : Sylvie ROBERJOT Bât. Atrium, UCB Lyon 1 Tél : 04.72.44.83.62 INSA : H. CHARLES secretariat.e2m2@univ-lyon1.fr	**M. Philippe NORMAND** UMR 5557 Lab. d'Ecologie Microbienne Université Claude Bernard Lyon 1 Bâtiment Mendel 43, boulevard du 11 Novembre 1918 69 622 Villeurbanne CEDEX philippe.normand@univ-lyon1.fr
EDISS	**INTERDISCIPLINAIRE SCIENCES-SANTÉ** http://www.ediss-lyon.fr Sec. : Sylvie ROBERJOT Bât. Atrium, UCB Lyon 1 Tél : 04.72.44.83.62 INSA : M. LAGARDE secretariat.ediss@univ-lyon1.fr	**Mme Sylvie RICARD-BLUM** Institut de Chimie et Biochimie Moléculaires et Supramoléculaires (ICBMS) - UMR 5246 CNRS – Université Lyon 1 - Bâtiment Curien 3ème étage Nord 43 Boulevard du 11 novembre 1918 69622 Villeurbanne Cedex Tel : +33(0)4 72 44 82 32 sylvie.ricard-blum@univ-lyon1.fr
INFOMATHS	**INFORMATIQUE ET MATHÉMATIQUES** http://edinfomaths.universite-lyon.fr Sec. : Renée EL MELHEM Bât. Blaise PASCAL, 3e étage Tél : 04.72.43.80.46 infomaths@univ-lyon1.fr	**M. Hamamache KHEDDOUCI** Bât. Nautibus 43, Boulevard du 11 novembre 1918 69 622 Villeurbanne Cedex France Tel : 04.72.44.83.69 hamamache.kheddouci@univ-lyon1.fr
Matériaux	**MATÉRIAUX DE LYON** http://ed34.universite-lyon.fr Sec. : Stéphanie CAUVIN Tél : 04.72.43.71.70 Bât. Direction ed.materiaux@insa-lyon.fr	**M. Jean-Yves BUFFIÈRE** INSA de Lyon MATEIS - Bât. Saint-Exupéry 7 Avenue Jean CAPELLE 69 621 Villeurbanne CEDEX Tél : 04.72.43.71.70 Fax : 04.72.43.85.28 jean-yves.buffiere@insa-lyon.fr
MEGA	**MÉCANIQUE, ÉNERGÉTIQUE, GÉNIE CIVIL, ACOUSTIQUE** http://edmega.universite-lyon.fr Sec. : Stéphanie CAUVIN Tél : 04.72.43.71.70 Bât. Direction mega@insa-lyon.fr	**M. Jocelyn BONJOUR** INSA de Lyon Laboratoire CETHIL Bâtiment Sadi-Carnot 9, rue de la Physique 69 621 Villeurbanne CEDEX jocelyn.bonjour@insa-lyon.fr
ScSo	**ScSo*** http://ed483.univ-lyon2.fr Sec. : Véronique GUICHARD INSA : J.Y. TOUSSAINT Tél : 04.78.69.72.76 veronique.cervantes@univ-lyon2.fr	**M. Christian MONTES** Université Lyon 2 86 Rue Pasteur 69 365 Lyon CEDEX 07 christian.montes@univ-lyon2.fr

*ScSo : Histoire, Géographie, Aménagement, Urbanisme, Archéologie, Science politique, Sociologie, Anthropologie

« Science says the first word on everything, and the last word on nothing. »

Victor Hugo

Acknowledgments/Remerciements

Enfin, nous y voici !

Une thèse de doctorat est un travail de longue haleine où l'implication et le soutien sans faille de nombreuses personnes sont indispensables au succès du doctorant. Ces trois années de thèse ont été pour moi une expérience immensément riche et formatrice et surtout une histoire de relations, de rencontres et d'amitié. Je tiens à exprimer ma profonde gratitude à tous ceux qui de près ou de loin ont contribué à ce projet.

Cette thèse CIFRE a été réalisée entre AIA Life Designers et le Centre d'Énergétique et de Thermique de Lyon (CETHIL UMR5008) sous la direction académique du Professeur *Rémi Revellin*, du Docteur *Romuald Rullière,* du Docteur HDR *Philippe Haberschill* et la direction technique (coté entreprise) de *Simon Davies* et *Quentin Perroit.*

Je tiens tout d'abord à remercier l'ensemble des membres de jury. *Vincent Lemort* et *Lavinia Grosu* d'avoir accepté d'étudier et de rapporter cette thèse de doctorat, avec enthousiasme. *François Lanwetta*, d'avoir accepté d'examiner mes travaux et fait l'honneur de présider ce jury de thèse.

Je remercie chaleureusement mes encadrants du CETHIL pour leurs conseils avisés et le soutien qu'ils m'ont apporté tout au long de ces années de doctorat. J'ai apprécié la confiance et l'autonomie que vous m'avez accordé au cours de ce projet, elles m'ont permis de développer ma confiance en moi. *Rémi Revellin*, pour ton expertise et tes remarques toujours pertinentes. Merci pour la confiance que tu m'as accordée. J'ai eu la chance de mener ce long travail doctoral avec une personne toujours optimiste et ex-vice-champion de monde d'aviron. *Romuald Rullière*, pour ton soutien, ta disponibilité et nos fréquents échanges. Merci pour l'aide que tu m'as apportée, en particulier, lors de notre participation à la 10ème conférence internationale « system simulation in buildings » à Liège, Belgique. *Philippe Haberschill*, pour ton imagination et tes idées qui sont toujours originales et parfois nécessitent plusieurs minutes de réflexion afin de te suivre. Merci pour le temps consacré pour m'aider à établir les équations du système de stockage et à le modéliser avec plusieurs langages de programmation. Un grand merci pour tes nombreux conseils, remarques et retours à n'importe quel moment et jour de la semaine.

Je tiens aussi à remercier l'ensemble des mes collègues au sein de l'équipe d'AIA ENVIRONNEMENT à l'agence de Lyon (Alice Donguy, Clément Prevost et Clara Galletti)

pour m'avoir accueilli en Février 2017. Merci pour votre soutien. *Simon Davies*, pour ton soutien et ta disponibilité surtout au début de la thèse. Merci pour ta motivation pour le projet et pour l'excellent modèle AIR4POWER que tu as pu développer. Nos discussions à la sortie du travail en allant prendre le métro ont été inoubliables et fructueuses pour le développement de cette thèse. *Quentin Perroit*, merci de m'avoir conseillé et guider surtout pour les deux dernières années de thèse. Merci pour ton soutien au quotidien et ta disponibilité sans faille. J'apprécie le temps consacré pour le suivi de mon avancement et la pression que tu m'as mis dans certains moments afin de respecter les échéances du projet.

Merci également à toute l'équipe du CETHIL, le groupe EHTIS et toute l'équipe de doctorants. Je garderai un souvenir indélébile de la superbe ambiance entre les doctorants du CETHIL, Merci Martin et Eloise pour la pause de 17h dans votre bureau, Rémi G. pour me donner l'idée de faire un triathlon, Mathilde pour la licence de MétéoNorm, Paul pour tous les conseils concernant le vélo, Jean pour la fermeture de la porte une seule fois en 2021, Georges pour tes conseils de ne pas travailler les week-ends, Sébastien pour m'apprendre la coinche, Nicolas C., Samuel, Damien, Sophie, Julie, David, Thomas, Khriscia, Christophe L., Janett, Naveed (My Friend). David Bou Saba, Merci pour ton aide au niveau du code numérique et des équations différentielles. Merci les amis !

Enfin, un grand merci à ma famille, je pense à mes parents (Georges et Marie), mes sœurs et frères (Patricia, Pauline, Khalil et Wissam) mes beaux-frères et belles-sœurs (Youssef, Dany, Juliana et Elsy) pour leur soutien et encouragement quotidien qui m'ont permis d'en arriver là. Une forte pensée pour mes dix neveux/nièces (Karl, Marc, Alexandre, Charbel, Joey, Elie, Marita, Jovana, Emma et Mila).

Mes derniers remerciements reviennent à Nihale, qui a été un soutien moral et émotionnel constant et toujours à mes côtés.

Abstract

In the context of developing renewable energies, storing energy improves energy efficiency and promotes the insertion of intermittent renewable energies. It consists of accumulating energy for later use in a place that may be the same or different from the place of production. Converting electrical energy to high-pressure air seems a promising solution in the energy storage field: it is characterized by a high reliability, low environmental impact and a remarkable stored energy density (kWh/m^3).

Currently, many researchers are focusing on developing small scale of the compressed air energy storage system (CAES) coupled to a building applications based on the work done for multiple large scale CAES systems installed in the world.

A global numerical model of trigeneration CAES system coupled to a building model and renewable energy modules was developed in order to analyze the CAES system behavior responding to electrical, building heating and cooling demands. Different energy scenarios (autonomous and connected to the grid modes), geographical locations and building typologies were proposed and analyzed. The CAES numerical model development is based on solving energy and heat transfer equations for each system component (compressor/expander, heat exchanger, high pressure air reservoir, thermal water storage tank).

Adiabatic compressor and expander were firstly selected to investigate the trigeneration advanced adiabatic compressed air energy system (AA-CAES) coupled to the building and to grids with the different scenarios described above. Connected mode showed more benefits sides from using the CAES system coupled to the building and to grids with an electrical load management of 75.9 % (Nice location). In addition, the trigeneration AA-CAES system offered a compromise between the electrical roundtrip efficiency (output/input), hot and cold coverage in function of building applications and the renewable energy modules size.

Similar to adiabatic components, quasi-isothermal compressor and expander developed by LightSail Energy and Enairys Powertech were also analyzed by solving the energy and heat transfer equations for each phase of the compression and expansion processes. These analytical models allowed us to have a better understanding of these technologies operations and to have several orders of magnitudes of different physical parameters. The LightSail Energy technology showed more interests for hot/cold water production while compressing/expanding air than the Enairys Powertech technology which presented a nearly quasi-isothermal air compression/expansion process.

I-CAES and AA-CAES were also compared from a financial point of view based on compressed air market analysis. Three different prototypes were studied: Two AA-CAES systems (ideal and virtual (some of which are based on commercial units found in the compressed air market)) and one I-CAES system (based on LightSail Energy CAES prototype). The compressed air market is concentrated on the small power units which make the small scale AA-CAES prototype building complicated specially for high storage pressure. Based on LCOE analysis, the LightSail Energy prototype presented the lowest cost of energy delivered (€/kWh) for a 20 years of operational period.

Résumé

Le développement des énergies renouvelables pose la question du stockage de l'énergie électrique. L'utilisation du stockage par air comprimé semble une solution prometteuse dans le domaine du stockage d'énergie : elle se caractérise par une grande fiabilité, un faible impact environnemental et une remarquable densité énergétique stockée (kWh/m^3). Jusqu'à présent, l'air comprimé a été utilisé dans de nombreux domaines comme vecteur d'énergie pour stocker différentes formes d'énergies (transport routier, poste pneumatique, plongée sous-marine). Néanmoins, actuellement de nombreux chercheurs se concentrent sur le développement de stockage d'énergie par air comprimé (CAES) à petite échelle couplé à une application de bâtiment en se basant sur les travaux développés pour les multiples systèmes de CAES à grande échelle installés dans le monde.

Un modèle numérique global du système de stockage par air comprimé à petite échelle, couplé à un modèle de bâtiment et à des modules d'énergie renouvelable a été développé dans le but de modéliser différents compresseurs/détendeurs et structures d'installation développés par plusieurs startups (LightSail Energy et Enairys Powertech) et chercheurs. Plusieurs scénarios énergétiques (autonomes et connectés aux réseaux), localisations géographiques et typologies de bâtiments ont été proposés et analysés. Le développement du modèle numérique CAES a été basé sur la résolution de l'équation de conservation de l'énergie et des équations de transferts pour chaque composant du système (compresseur/détendeur, échangeur, réservoir d'air haute pression, réservoir de stockage d'eau chaude/froide).

Les compresseurs et détendeurs adiabatiques ont d'abord été sélectionnés pour étudier le système de trigénération de stockage d'énergie par air comprimé adiabatique avancé (AA-CAES) couplé au bâtiment et aux réseaux avec les différents scénarios décrits ci-dessus. Le mode connecté aux réseaux (électrique, chaud et froid) a montré l'importance d'utiliser le système CAES couplé au bâtiment et aux réseaux avec un effacement électrique de 75,9 % (Nice). En outre, le système AA-CAES de trigénération (électrique, chaud et froid) offre un compromis entre l'efficacité du système électrique, le taux de couverture du chaud et le taux de couverture du froid en fonction de l'application du bâtiment et de la taille des modules d'énergie renouvelable.

Les compresseurs et détendeurs quasi-isothermes développés par LightSail Energy et Enairys Powertech ont été modélisés pour chaque phase de la compression et de la détente. Ces modèles analytiques ont permis une meilleure compréhension du fonctionnement principal de ces

technologies et d'avoir l'ordre de grandeur de différents paramètres physiques. La technologie LightSail Energy a montré plus d'intérêt par la production d'eau chaude/froide lors de la compression/détente de l'air que la technologie Enairys Powertech qui présente une compression/détente d'air d'avantage isotherme avec des rejets thermiques trop proches de la température ambiante pour être récupérable.

Les systèmes I-CAES et AA-CAES sont comparés d'un point de vue financier en se référant à une analyse du marché des systèmes de production/utilisation de l'air comprimé. Trois prototypes différents ont été étudiés: deux systèmes AA-CAES (idéal et virtuel (basés sur des unités commerciales trouvées sur le marché de l'air comprimé)) et un système I-CAES (basé sur le prototype LightSail Energy CAES). Le marché de la turbine est concentré sur les petites plages de pression et pour cela le montage d'un prototype AA-CAES avec une pression de stockage importante est compliqué. A partir de l'analyse économique LCOE (levelized cost of energy), il apparaît que le prototype LightSail Energy présente le coût d'énergie livré le plus bas (€/kWh) pour une période opérationnelle de 20 ans.

Table of contents

List of figures

List of tables

Nomenclature

a	length constant
c	specific heat, $J.kg^{-1}.K^{-1}$
D	diameter, m
E	energy, Wh
H	enthalpy, J
h	specific enthalpy, $J.kg^{-1}$
he	heat transfer coefficient, $W.m^{-2}.K^{-1}$
K	global heat transfer coefficient, $W.m^{-2}.K^{-1}$
L	length, m
$\dot{m}$	mass flow rate, $kg.s^{-1}$
m	mass, kg
n	polytropic index
nu	number of water droplets
nt	number of tubes
$\dot{n}$	number of water droplets per seconds
P	pressure, Pa
Q	heat transfer, J
$\dot{Q}$	heat transfer rate, W
r	specific gas constant, $J.kg^{-1}.K^{-1}$
ra	radius, m
S	Surface, m^2
t	time, s
T	temperature, K
U	internal energy, J
u	specific internal energy, $J.kg^{-1}$
$\dot{V}$	volume flow rate, $m^3.s^{-1}$
V	volume, m^3
Ve	velocity, $m.s^{-1}$
v	specific volume, $m^3.kg^{-1}$
w	specific work, $J.kg^{-1}$
W	work, J
$\dot{W}$	work rate, $J.s^{-1}$
x	Absolute humidity

Subscripts

Amb	ambient
av	average
BD	building
c	compressor
cy	cycle
CBD	cold building demand
co	cold
d	displacement
Dr	droplets
DA	dry air
EBD	electrical building demand
ELEC	electricity
from grid	energy from grid
GR	grid
HA	humid air
HE	heat exchanger
ho	hot
HBD	hot building demand
i	stage number
in	input
j	time step
k	kinetic
max	maximum
min	minimum
out	output
PV	photovoltaic
p	constant pressure
pol	polytropic
RE	renewable energy
rel	released
res	reservoir
ret	return
SAT	saturated
ST	storage
t	turbine
to grid	energy to grid
tot	total
tu	tube
va	vapor

vo	volumetric
v	constant volume

Greek letters

β	compression/expansion ratio
Δ and δ	delta
ρ	density, kg.m^{-3}
η	efficiency
γ	heat capacity ratio
ε	effectiveness
α	boolean coefficient
θ	exergy factor

Superscript

w	water
wv	water vapor

Abbreviation

AA-CAES	advanced adiabatic compressed air energy
acs	active compression stage
ats	active turbine stage
CAES	compressed air energy storage
C-CAES	classical compressed air energy storage
CCR	cold coverage ratio
CR	cold ratio
EBD	electrical building demand
ECR	electrical coverage ratio
ELM	electrical load management
ESE	electrical system efficiency
ETSE	exergy trigeneration system efficiency
HCR	hot coverage ratio
HE	heat exchanger
HR	hot recovered
I-CAES	isothermal compressed air energy storage
Nc	number of compression stages
NTU	number of Transfer Units
PV	photovoltaic
RE	renewable energy
RES	reservoir
RH	relative humidity
RTE	round trip efficiency
RPM	rotation per minute
SE	system efficiency
SP	system parameters
Sta	stage
T-CAES	trigeneration compressed air energy storage
TCR	total coverage ratio
TES	thermal energy storage
TSE	Trigeneration system efficiency
VR	volume ratio

Introduction

The spectacular growth of the world population during the 21st century, the industrial development and the rapid urbanization are reflecting a significant increase in the world energy demand. Based on the world energy outlook 2018 published by the international energy agency, the global energy demand will rise more than 25 % by 2040 [1]. With government policies and decisions, renewable energy has become the technology of choice in order to ensure sustainable clean energy and reduce carbon emissions. This fact can justify the expected growth of the renewable share by one-fifth to reach 12.4 % in responding to global energy demand in 2023.

For instance, the act of 17 august 2015 on energy transition for green growth allows France to contribute more effectively in fighting against climate change and to strengthen its energy independence by ensuring a right balance among its different energy resources. These objectives are achieved by fixing many medium and long term objectives [2]:

1. Cut greenhouse gas emissions to contribute to the target of a 40 % decrease in EU emissions by 2030 (compared with 1990 levels);
2. Cut France's consumption of fossil fuels by 30 % by 2030;
3. Reduce the share of nuclear energy to 50 % of electricity production by 2025;
4. Increase the share of renewables to 32 % of final energy consumption by 2030 and to 40 % of electricity production;
5. Halve France's final energy consumption by 2050 (compared with 2012);

6. Cut waste going into landfills by 50% by 2050.

Objective numbers 3 and 4 are focusing on increasing the share of the green energy resources based on renewables in the final energy consumption. Looking deeply into these two points, existing renewable energy technologies need to be modified in order to achieve the above goals. As a matter of fact, renewable resources intermittency presents a major obstacle and challenge in ensuring a constant answer especially to high energy demands. The energy storage technology can be a solution for the energy fluctuating issues and thus stabilizing the grid by allowing excess energy production to be saved for periods of higher customer demand. In 2017, the share of the world renewable electricity generation was 24 % where hydropower-hydraulic storage technology (STEP) presented the important part (75 %) and the rest of electricity demand was answered through the import of electricity and the use of gas, fuel and coal conventional power plants [3].

Based on the French ministry for the ecological transition, the share of tertiary and residential sectors in the final energy consumption is 42 % ahead of the transport sector (30 %), industrial sector (25 %) and agricultural sector (3 %) [4]. The tertiary and residential sectors are responsible for more than 123 million tons of CO_2 emissions making it two of the important key areas in the fight against the global warming and the energy transition. Energy storage technology is proposed in this context where it can make the building model more energy efficient [5].

The present work was carried out in a context of a PhD Cifre between CETHIL laboratory and AIA LIFE DESIGNERS company which filed a patent in 2014 (INPI) and international extension (PCT) filed in 2015 based on the AIR4POWER research project. The last mentioned project is launched by AIA LIFE DESIGNERS officially in 2013. The present thesis is therefore aimed at bringing a new contribution to knowledge on the fundamentals of micro energy storage systems designed for building application related to AIR4POWER project. Different energy storage technologies were investigated and analyzed. Numerical investigations were carried out for each component of the global energy storage system coupled with a building model. This thesis is divided into four chapters (with several appendices) as follows:

Chapter 1: This chapter introduces the energy storage technology context and gives a general overview of different energy storage technologies with focusing on mechanical and liquid piston technology developed by LightSail Energy and Enairys Powertech.

Chapter 2: This chapter is aimed at describing the numerical model conducted for the global adiabatic micro energy storage system for building application. The analytical analysis for each component of the system as well as the post processing methods are described in the chapter.

Chapter 3: Quasi-isothermal compressor and expander are investigated in this chapter focusing on the compressor/expander model developed by LightSail Energy and Enairys Powertech. The chapter offers a close look on the quasi-isothermal compression and expansion and a comparison between the mechanical and liquid piston technology.

Chapter 4: Quasi-isothermal compressor/expander models are integrated into the global model described in chapter 2. These two CAES systems (AA-CAES and I-CAES) are investigated from a financial point of view with three prototypes (Virtual, ideal and LightSail prototype).

Chapter 1 Overview of compressed air energy storage (CAES) systems

The intention of this chapter is to give an overview of the compressed air energy storage technology from concept going through research and development project to final a large scale installation or small scale prototype. Different compressed air energy storage system types are explained in this chapter based on presenting real or future CAES installation examples and many scientific researches for the purpose of overcoming the different technology barriers.

1.1 Key figures for renewable energies and main barriers

Renewable energy development is a major challenge in today's context with energy demand growth, potential depletion of fossil resources and the urgency of reducing greenhouse gas emissions. The European Union has decided to achieve a share of renewable energies in its gross final energy consumption of at least 32 % by 2030 [6]. Based on the report published by the French ministry of ecological and solidarity transition, the renewable energy share in France energy mix has increased from 6.6 % (2007) to 10.7 % (2017). It can be seen from Figure 1.1 that the renewable energy part presents the fourth largest energy source behind nuclear energy (40 %), petroleum products (28.9 %) and gas (15.7 %) [6].

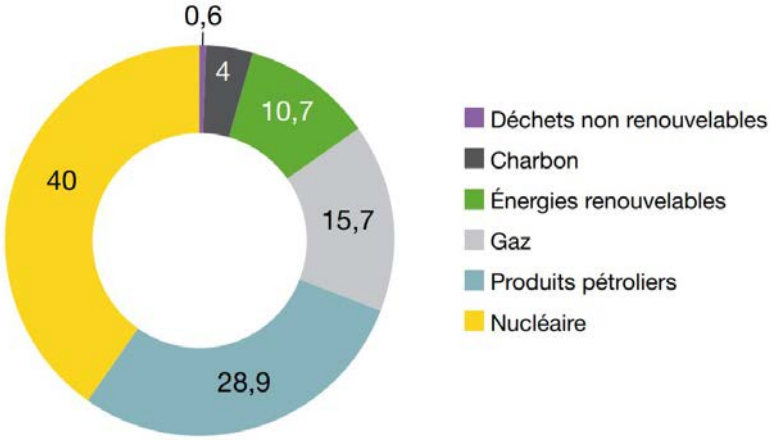

Figure 1.1: Primary energy consumption by energy source in 2017 [6]

Figure 1.2 and Figure 1.3 show different renewable energy sources answering the 10.7 % share in the primary energy consumption and electricity consumption respectively for France.

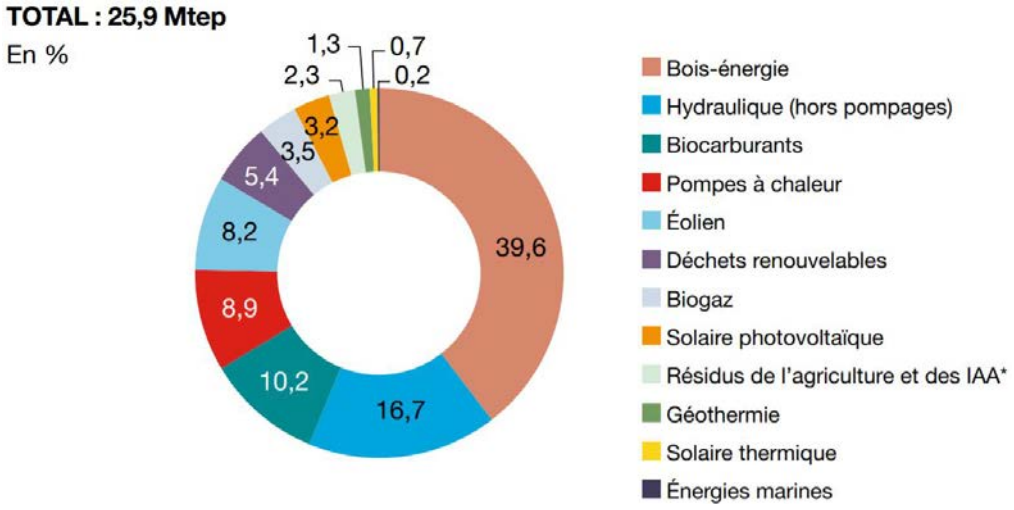

Figure 1.2: Primary production of different renewable energy sources in 2017 [6]

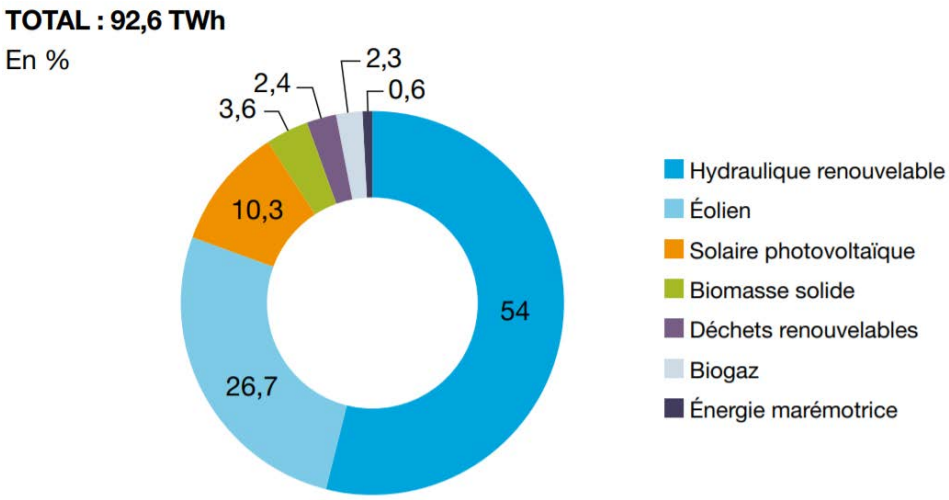

Figure 1.3: Gross renewable electricity production by technology in 2017 [6]

Wood energy, hydropower, biofuel, wind turbine come in the first places in the primary renewable production and renewable electricity production. In order to become competitive with coal, natural gas and nuclear power, renewable energy is facing major obstacles (installation cost, technical, social,…).

Two of the main barriers are the geographical and natural conditions that limit the development in different regions and lead to intermittent renewable resources. For instance, hydropower that is the most important share in the French renewable electricity presents several environmental side effects by blocking, diverting or changing the natural course of river systems and therefore an important migration route for fish. In addition, damming rivers also often reduces water and sediment flow to dangerous levels which impacts downstream wildlife populations. The incidence of solar energy on the earth surface, for example, depends on geographic location, therefore, limiting the people of many regions from the use of solar energy as it will not be reliable. The capital cost is the second obvious barrier that challenges the development of renewable energy technologies. In fact, renewable energy technologies are cost-disadvantaged compared to commonly used non-renewable technologies (coal-fired production). In addition, the development of the infrastructure required for the renewable energy plants is highly costly and therefore holds the majority of the countries for renewable energy development that prefer a cheaper option that is more economical. Social-cultural barriers vary from region to another where lack of knowledge and awareness of renewable energy technologies can be challenging for their development. This is not the case in France where according to a survey published in December 2019 by the agency of ecological transition (ADEME), the French people selected the solar energy among other renewable resources as a priority to be more developed [7]. Figure 1.3 shows the survey results where different renewable energy technologies were compared

with different aspects (clockwise): the cheapest to produce, the least polluting, the least dangerous, exist in the future, the most efficient, allowing to fight against the greenhouse effect, the most respectful of biodiversity and landscapes, which ensures the most energy independence, average per energy. Solar energy is considered as the energy with the best qualities and took the highest percentage in most of the aspects from French people point of view.

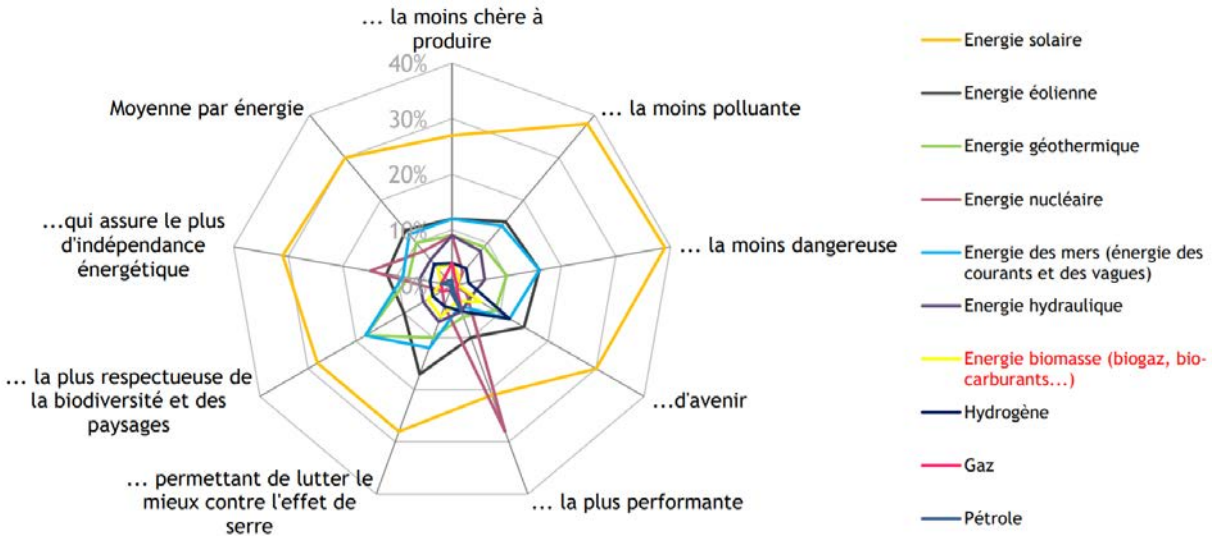

Figure 1.4: ADEME's barometer (The French and the Environment in 2019) [7]

Based on the green energy objectives fixed by the European Union, the different renewable energy barriers and in some cases an encouraging society for renewable energy development, energy storage technology is necessary at that point to boost the development of the renewable technologies at different levels.

1.2 Energy storage technology

In the current context of the development of renewable energies, energy storage improves energy efficiency and promotes the integration of intermittent renewable energies [8]. It also brings security and flexibility to energy networks. Energy storage involves both heat and electricity. It consists of accumulating energy for later use in a place that may be the same or different from the place of production. Note that the storage allowing to shift the use in time without shifting it in space is called stationary storage and in turn that aimed at mobile applications is called on-board or portable storage [8]. The deployment of low environmental impact storage systems can help to lower the cost of imported electricity necessary to answer the high electrical energy demand and significantly reduce the CO_2 emissions generated by the use of thermal power plants and the dependence on fossil resources. The "French Alternative

Energies and Atomic Energy Commission" (CEA) [8] and Luo et al. [9] detailed different energy storage technologies that provide flexibility and enhance the reliability of energy systems (Flywheel, batteries, thermal storage, supercapacitors, hydrogen storage and compressed air energy storage). Each technology depending on its application presents several technical and economic reasons that limit certain of its advantages [9],[10]. In the next section, the main focus is the electrical storage that aims to respond to four main issues: recovering excess energy production, supplying energy to compensate the lack of energy due to the intermittent nature of the energy supply especially during high energy demand and supplying energy in the case of an electrical system failure or poor local network quality. Heat storage is primarily intended for heating and cooling buildings, a single-family house in a neighborhood or in a village.

Electricity is a very convenient vector for transporting energy but difficult to store in its own form. It is therefore generally transformed to be stored in another form: mechanical energy (potential mechanical [hydraulic storage, compressed air storage], kinetic mechanics [flywheel]), thermal or chemical energy. On the contrary, thermal energy (sensible heat storage, latent heat storage) is usually stored in its original form (heat). Figure 1.5 reveals the different energy storage technologies showing each for technology its application based on output power range (x-axis) and discharge time (y-axis) where it can be noticed that pumped storage hydroelectricity (Light green square) present the highest output power (1 GW) for the longest discharge time (days). Batteries (Light orange rectangle) can operate for output power between few kilo-watt till hundreds of kilo-watt and for discharge time varying from seconds to minutes.

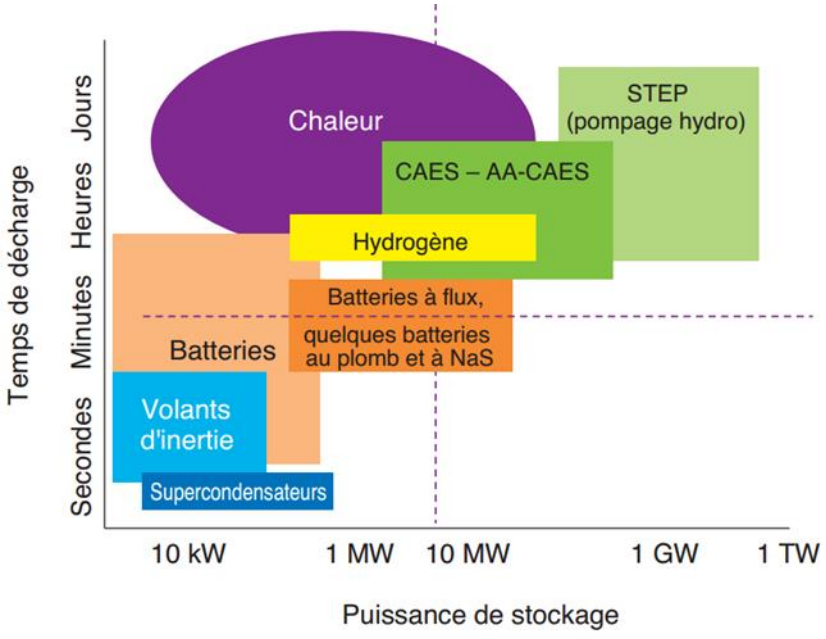

Figure 1.5: Different storage technologies function of output power and discharge time [11]

1.3 Compressed air energy storage (CAES) concept and timeline

Compressed air energy storage system can store large amounts of energy for a period of time in the range of hours making it a possible alternative solution to pumped-storage hydroelectricity. Like the latter storage technology, the large scale CAES system generally requires a particular geographic environment (underground cavities, aquifers, etc.) to store compressed air. The main concept behind the compressed air energy storage is to use the excess electrical energy to turn a compressor during the storage phase and therefore compress the air at ambient temperature and pressure up to high pressure (50 bar – 100 bar) in order to be stored in a reservoir (underground cavities for example) as shown in Figure 1.6. During the discharge phase the compressed air (potential energy) is expanded in a turbine which drives a generator and therefore responds to the lack of electrical energy. During the expansion process, the compressed air is heated before entering the turbine through the passage in a combustion chamber or through a recuperator at the inlet of the turbine (classical CAES system type discussed in the next section). The compressed air energy storage (CAES) is classified for large scale technology (Megawatt) with hours for responding time. The compressed air energy storage system (CAES) is one of the most promising technologies in the field of smart grid and poly-generation systems in the near future [10],[12],[13],[14]. CAES presents several significant advantages due to its cleanliness, reliability, economic feasibility, long service life and low environmental impact [13],[14]. Venkataramani et al. [14] concluded that the integration of CAES with renewable resources, such as solar and wind, will improve the

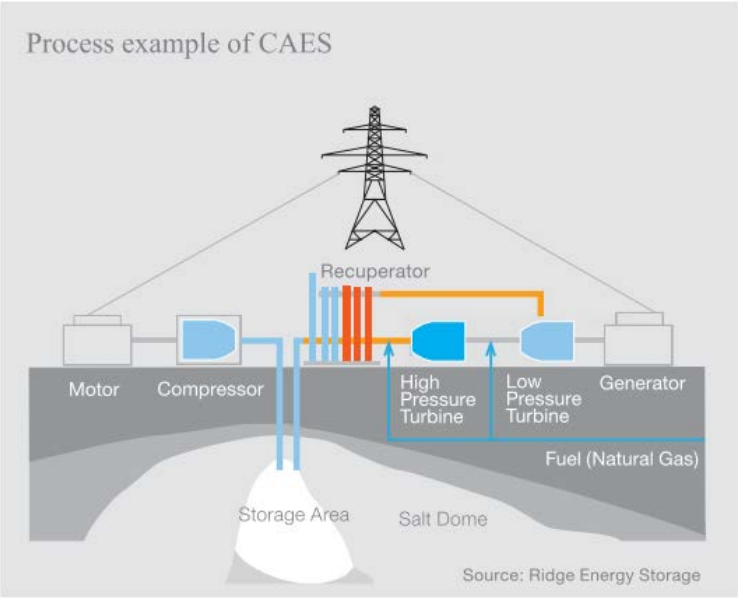

Figure 1.6: Compressed air energy storage process [15]

of these resources through demand side management toward increasing renewable power recovery. According to CEA, CAES technology presents between the lowest investment cost per power and energy unit (€/kW, €/kWh) compared to Li-ion batteries and hydropower technology [8].

Compressed air energy storage can be classified into three main categories:

- Classical diabatic CAES system (C-CAES)
- Adiabatic CAES system (A-CAES) / Advanced adiabatic CAES system (AA-CAES)
- Isothermal CAES system (I-CAES)

The idea to store electrical energy by means of compressed air is 80 years old. Figure 1.7 lists the different main large scale worldwide installations and research and development projects.

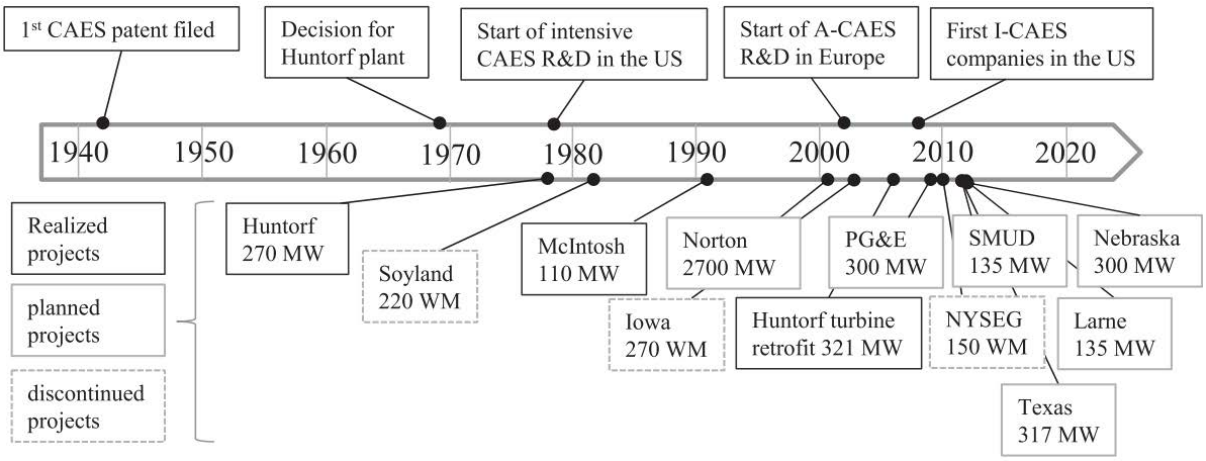

Figure 1.7: Timeline of different CAES systems large scale installations and projects [10]

In France, the usage of the compressed air as an energy vector dates back to 1866 where Napoleon III decided to set up a pneumatic network for sending letters based on the system invented by the engineer William Murdoch in 1800 and tested in London in 1853. Figure 1.8 shows the Paris pneumatic network that was put into service until 1984 where the pneumatic tube total distance was equal to 467 km [16]. In 1879, the tramway company in Nantes put the first compressed air tramway into operation. Figure 1.9 shows the tramway invented by Louis Mékarski that was based on expending compressed air at high pressure (around 80 bar) to low pressure (around 8 bar). The high pressure was produced in a central factory and then distributed via compressed air pipeline network to the called points “feeding stations” [17].

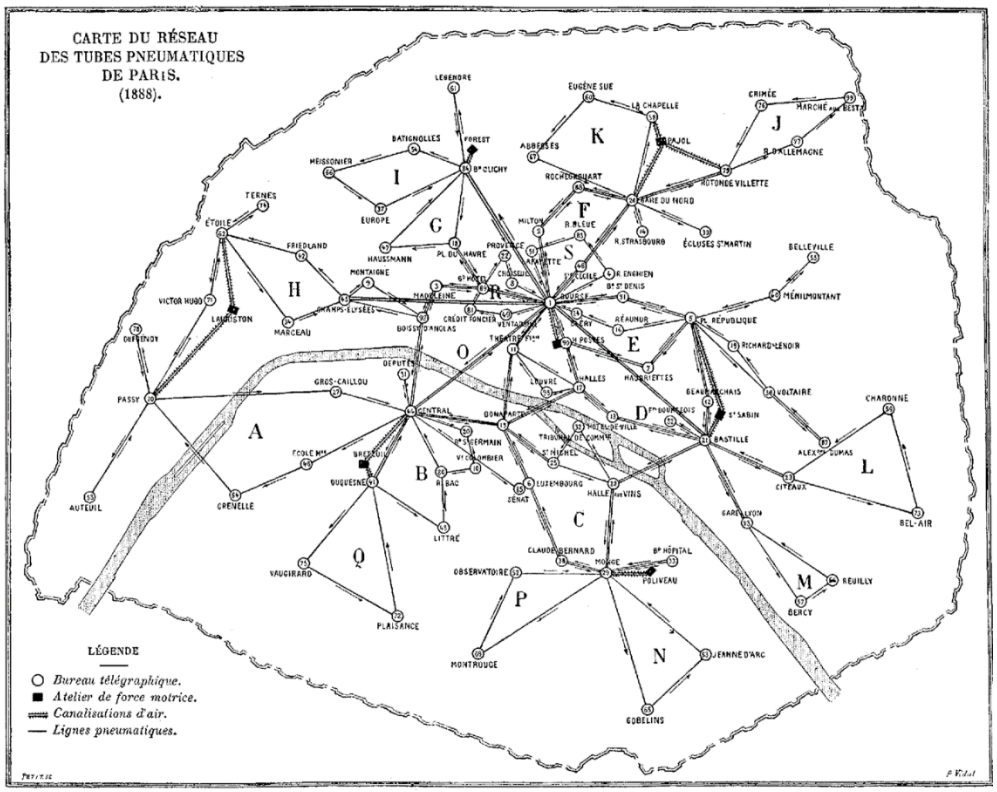

Figure 1.8: Paris pneumatic tube network map in 1888 [18]

Figure 1.9: Mékarski compressed air system motor – Tramway Nantes [17]

1.3.1 Classical diabatic CAES system (C-CAES)

The two main and well known classical CAES plants in the world running more than 20 years [19]: Huntorf in Germany (built in 1978) with a capacity of 290 MW for 2 hours – 3 hours

of operation (Figure 1.10) and the McIntosh Alabama plant in the United States (built in 1991) with a capacity of 110 MW for 26 hours of operation (Figure 1.11) [20], [11] and with an electric efficiency (electrical energy output divided by electrical energy input) of 46 % and 54 % respectively. In these classical compressed air energy storage plants (C-CAES) air is compressed adiabatically in the range of 45 bar – 70 bar and stored in former salt cavities or coal mines. Heat resulting from the compression phase is wasted to the ambient. External heat source combustion is used to raise the air temperature before entering the turbine for adiabatic expansion [11],[21].

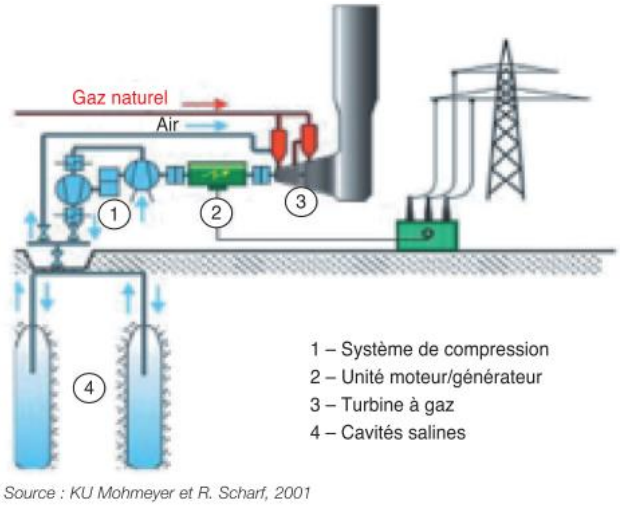

Figure 1.10: Principle components of Huntorf installation [11]

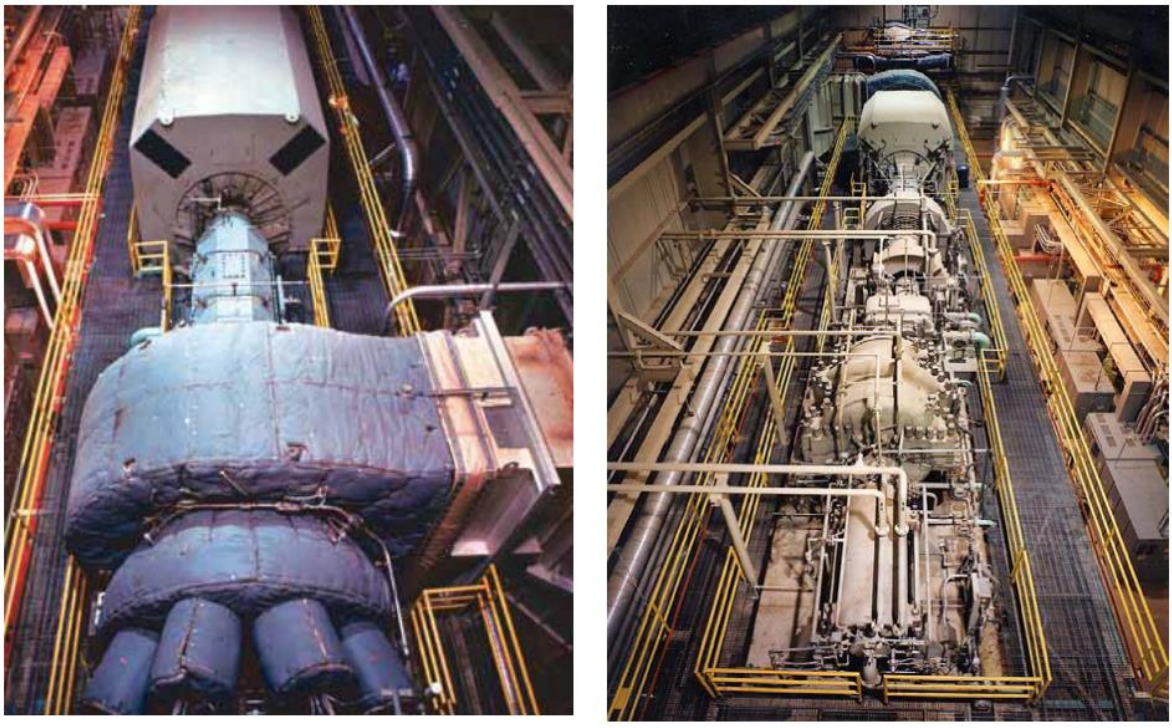

Figure 1.11: McIntosh Alabama CAES plan power train [22]

Table 1.1 compares the two classical CAES systems (Huntorf and McIntosh) based on collecting different technical parameters:

- Performance
- Geology
- Air expansion process

Table 1.1: Huntorf and McIntosh installation comparison [20], [21]

	Caracteristic	Huntorf (1978)	McIntosh (1991)
Performance	Output power (MW)	290	110
	Input power (MW)	60	53
	Charge time (h)	12	41.6
	Storage autonomy (h)	3	23
	Air mass flow kg/s	425 (discharge); 108 (charge)	157 (discharge); 94 (charge)
	System efficiency (Out/In)	46 %	54 %
Geology	Cavern number	2	1
	Storage medium	Salt	Salt
	Total volume (m3)	300 000	540 000
	Cavern temperature (°C)	37	35
	Cavern Pressure (bar)	45 – 70	45 – 75
Air expansion process	Combustible	Gas	Gas/Fioul
	Temperature/1st Turbine(°C)	550	530
	Pressure (bar)/1st Turbine (bar)	43	43
	Temperature/2nd Turbine(°C)	825	870
	Pressure (bar)/2nd Turbine (bar)	11	15

1.3.2 Adiabatic CAES system (A-CAES and Micro AA-CAES)

Advanced CAES systems allow an electrical efficiency ranging from 40 to 70 % depending on the heat/cold management resulting from air compression/expansion [23]. Thus, if the heat of compression and cold of expansion are stored separately in a thermal energy storage for reuse respectively during air expansion and compression, the storage system is said advanced adiabatic (AA-CAES) and its electrical efficiency can reach up to 70 % according to National Institute for the Industrial Environment and Risks (INERIS) [24]. The world's first large scale AA-CAES project-ADELE designed by RWE Power General Electric and other partners is seen

in Figure 1.12 Depending on the installation range scale, thermal energy storage (TES) takes different forms and physical properties. TES can be classified into three categories depending directly on the temperature (indirectly on the pressure):

- High temperature TES (> 400 °C): resistant to the combination of thermal and mechanical stress and therefore requires special materials as well as a complex system engineering [24].
- Medium temperature TES (200 °C – 400 °C).
- Low temperature TES (< 200 °C): usage of liquid TES which can be pumped through heat exchangers in series or parallel.

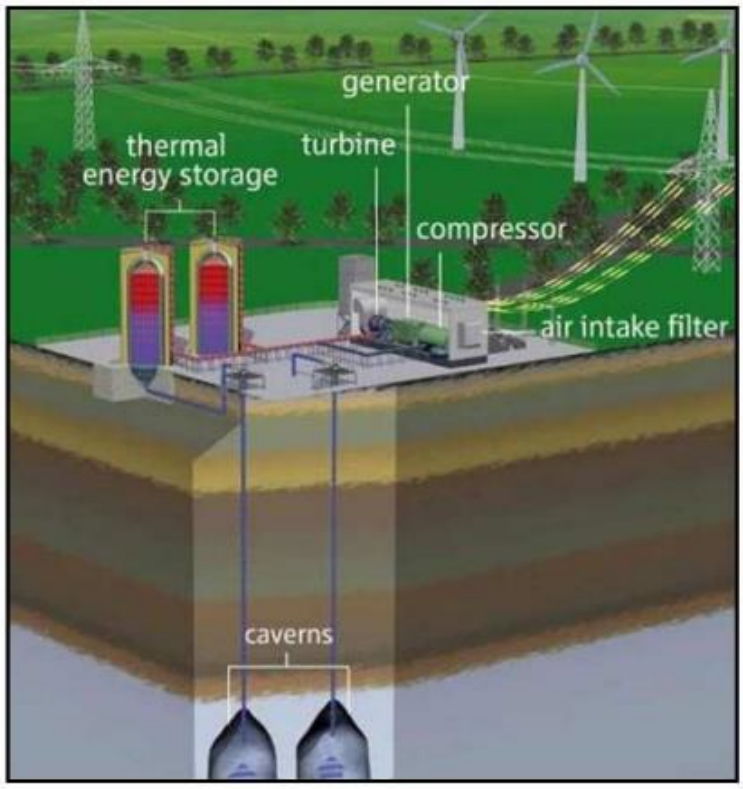

Figure 1.12: AA-CAES installation/ ADELE project [24]

While most large-scale (>50 MW) CAES systems depend on various geological factors (underground storage) that are difficult to control for air storage, micro-CAES systems (<1 MW) with specifically developed air tanks may be more adaptable and effective solutions in meeting the electricity, heat and cold needs [13]. Many researchers have focused on the micro AA-CAES system.

Sizing different system configurations

Kim et al. [25] studied the energy and exergy analysis of eight different system configurations for achieving high efficiencies. They found that a micro AA-CAES system with

heat recovery is a very effective system for distributed power networks because it can be a combination of energy storage, generation, air-cycle, heating and cooling system and it has a good efficiency (about 60 %). Xue et al. [26] developed thermodynamic and economic models for hybrid AA-CAES systems combining solid and liquid TES (thermal energy storage). The hybrid system presented a lower cost for a given efficiency. A modified model for the AA-CAES structure was conducted by Liu et al. [27]. They reported an improvement of the exergy efficiency by 3 % due to the reuse of the discharged air where its temperature is still high. Chen et al. [28] developed a mathematical model based on thermodynamic laws that shows an improvement of 3 % of the roundtrip efficiency (RTE) compared to C-CAES by pre-cooling the air entering the compressor. Hartman et al. [29] found that the efficiency of the polytropic configuration is more realistic (60 %) than the adiabatic system (70 %). These differences in system efficiency depend on many design parameters and assumptions used in specific studies based on steady thermodynamic models. Zhang et al. [30] stated that air reservoir modeling is an important AA-CAES design factor. Based on their study, a constant volume and temperature reservoir model has the highest system efficiency. The air storage temperature and pressure influence on RTE was pointed out by Guo et al. [31] where they developed a dynamic compressed air storage model. An optimal after-valve-throttle pressure was shown while taking maximum energy density as goal with constant expander inlet pressure. They added that more heat transfer between the reservoir and the atmosphere results in more stored air in charging and more released air in discharging.

Trigeneration system studies

In the literature on micro AA-CAES systems, many scientific papers focused on the design of a trigeneration (T-CAES) system coupled with renewable resources in order to respond to electrical, heating and cooling users' demand. Li et al. [32] showed a comprehensive efficiency of the storage system (~50 %) in winter where no cooling power is needed. Jannelli et al. [33] studied the purpose of polygeneration small-scale compressed air energy storage system integrated with photovoltaic power plant of a radio base station for mobile telecommunications where energy storage strategy and cooling energy production are essential. They proposed a novel T-CAES with 57% of efficiency for a small scale photovoltaic power (3.7 kW compressor constant input power) plant to satisfy the electric power demand (1.7 kW expander output power) and to cool the equipment of the radio base station. Li et al. [32] and Jannelli et al. [33] used the same compression/expansion ratio for all the stages. An analytical model based on energy balance and heat transfer equations was developed by Simpore et al. [34] where they simulated a micro AA-CAES system coupled to solar panels and building

without heat/cold recovery treatment. Using different energy situation scenarios, the building coverage ratio is higher with the increase of the solar panel area and compressor swept volume. Air tank volume has lower impact in this case. Working at low pressure (15 bar), Lv et al. [35] found the efficiency of T-CAES model to reach 76.3%. Lv et al. worked without air preheating before entering the turbine and supposed that the air charging of the reservoir is an isothermal process.

Experimental work

A pilot AA-CAES plant "TICC-500" was proposed by Wang et al. [36] with 22.6% of RTE. Round trip efficiency is defined as the electrical energy output divided by the electrical energy input. Ambient air is compressed via five intercooled compressors (1375 kWh input electric energy; 315 kW for 260 minutes of air compression) and released through a regulating valve that keeps the pressure constant at the inlet of three preheated turbines (326 kWh output electric energy). Cheayb et al. [37] carried out an experimental/numerical approach of a T-CAES composed of three ventilated compression stages driven by 4 kW motor, 300 L air reservoir and air motor coupled to a DC generator of 2 kW. Despite the RTE of 15.6%, a good match between the experimental and numerical model was noticed in their work. Heat removed during the compression phase is supposed to answer the heating demand and is not reused to preheat the air entering the turbine.

1.3.3 Isothermal CAES system (I-CAES)

Isothermal compressed air energy storage (I-CAES) is an emerging technology where isothermal compression and expansion are applied. Heat is removed continuously during the air compression cycle and added continuously during the air expansion cycle. This will result in collecting the cold at the end of the expansion phase that will be added to the next air compression cycle. In fact, it allows to reduce the compensated work during the air compression and to increase the work recovered during the air expansion. Two important innovative technologies are currently developed: mechanical piston with water injection by LightSail Energy [38] and liquid piston with integrated heat exchanger by Enairys [39]. In addition to SustainX that also developed I-CAES system by using foam as a matter to improve the heat transfer during air compression/expansion [40]. The two next sections (1.3.3.1, 1.3.3.2) focus on the two previously mentioned technologies developed by LightSail Energy and Enairys Powertech from technical and company backgrounds.

1.3.3.1 Mechanical piston with water injection

In the following section, the air storage solution proposed by LightSail Energy (LSE) will be investigated from the unit power (air compressor/expander) point of view. The Berkeley-based startup was created in 2009 with 55 employees and drew funding from various organizations including Khosla Ventures, Peter Thiel, Bill Gates and Total Energy Ventures for a total of more than 80 M$ (2017).

The company developed a new compressor/expander technology where quasi-isothermal air compression/expansion were introduced. Recently LSE focused on CAES aboveground storage by developing specialized high pressure carbon fiber tanks. LSE filed more than 50 patents and more than 1000 claims granted related to engine development, thermodynamics, electronics, pressure vessels and composite materials.

Mechanical air compressor/expander technology overview

Compressing air using traditional technology creates heat which is a wasted form of mechanical energy need for the compression process. LightSail Energy (LSE) has developed an advanced method of capturing this heat and regenerating useful energy from it. A fine, dense mist of water is injected into the compression chamber during the compression process. The cold water absorbs the heat of compression and returns it during expansion process as is illustrated in Figure 1.13. Based on LSE, this increases the round-trip efficiency of the energy storage system.

The regenerative air energy storage (RAES) proposed by LSE presents the following principle (Figure 1.13):

- Electricity drives a motor
- The motor drives the quasi-isothermal air compressor
- Water spray absorbs the heat released during air compression
- Energy is stored in the form of compressed air and warm water
- The same mechanism operates in reverse to deliver power

Crane et al. [38] introduced the technology behind the energy storage and recovery system that employs compressed air utilizing power from an operating wind turbine. They depicted the embodiment of the compressed air energy storage system as seen in Figure 1.14. The present system introduces an innovative design consisting of mixing a liquid with the air to facilitate heat exchange during air compression and expansion processes and a new electronic control of the valve timing in order to obtain the highest possible work output from a given volume of

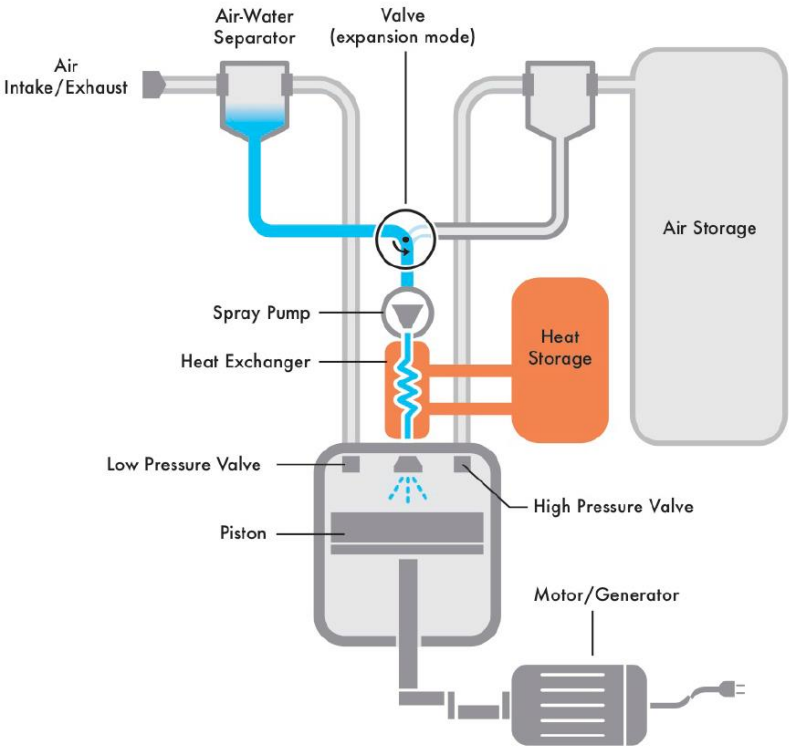

Figure 1.13: The RAES system operation presented by LSE

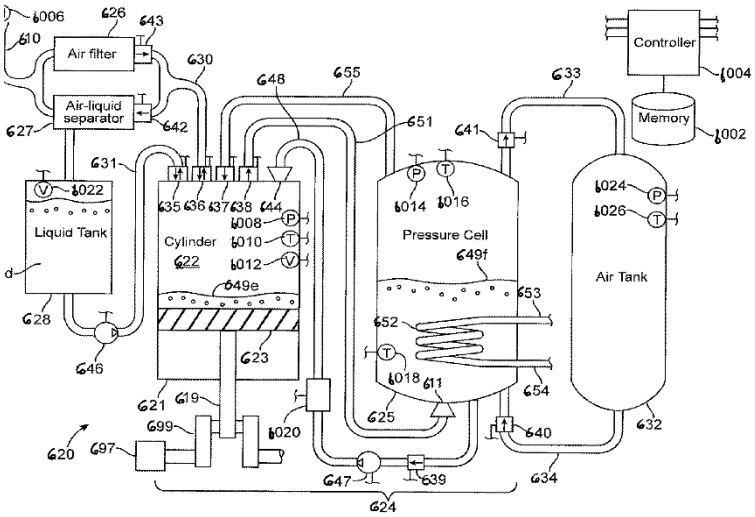

Figure 1.14: Energy storage system developed by LSE

compressed air. The system presented in Figure 1.14 is composed (from left to right):

- Air filter
- Air-liquid separator
- Liquid tank
- Cylinder device
- Pressure cell
- Air tank
- Controller and memory

The compression cycle presents 5 steps described from Figure 1.15 to Figure 1.19. Initially the mechanical piston is at bottom dead center. During step 1 of the compression cycle, as illustrated in Figure 1.15, liquid (light purple) is added to the cylinder chamber such that when the piston reaches top dead center the dead volume in the cylinder is zero. At the same time air is introduced in the cylinder device.

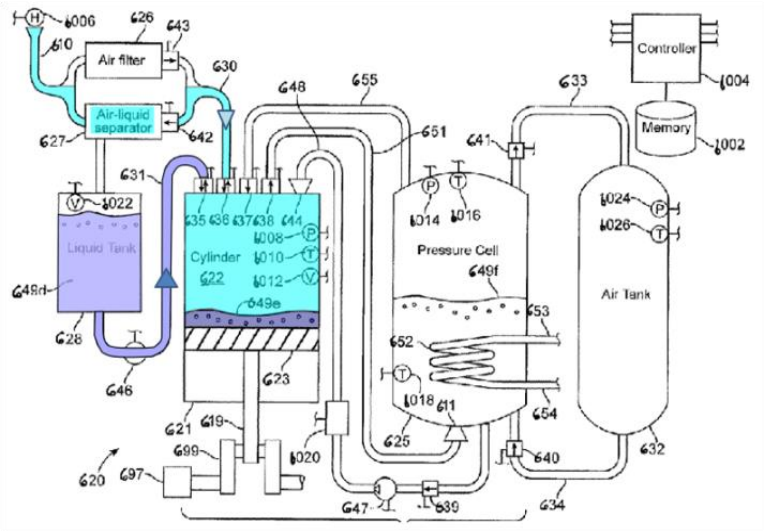

Figure 1.15: Step 1 of the compression cycle (Air intake + liquid addition to cylinder device)

As can be seen in Figure 1.16 that presents step 2 of compression cycle, the piston is at bottom dead center. During this process cold liquid mist is pumped from the pressure cell into the cylinder in order to absorb heat generated during compression step (step 3). The pressure difference between the pressure cell and the cylinder chamber is sufficiently high so that the operation of a pump is not required.

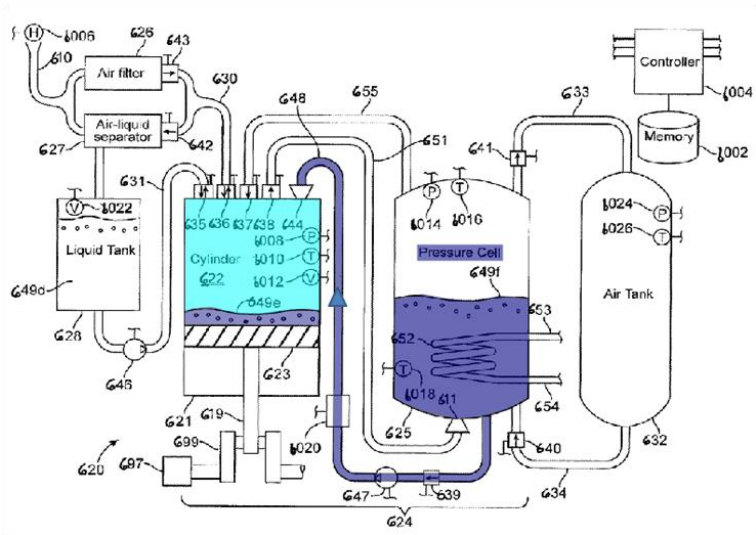

Figure 1.16: Step 2 of the compression cycle (add liquid mist to cylinder device)

Figure 1.17 shows step 3 where the piston is driven upward by a crankshaft coupled to a piston rod and therefore compressing the air and the mist contained in the cylinder chamber. All the valves are closed at that moment, ready for the air and mist compression.

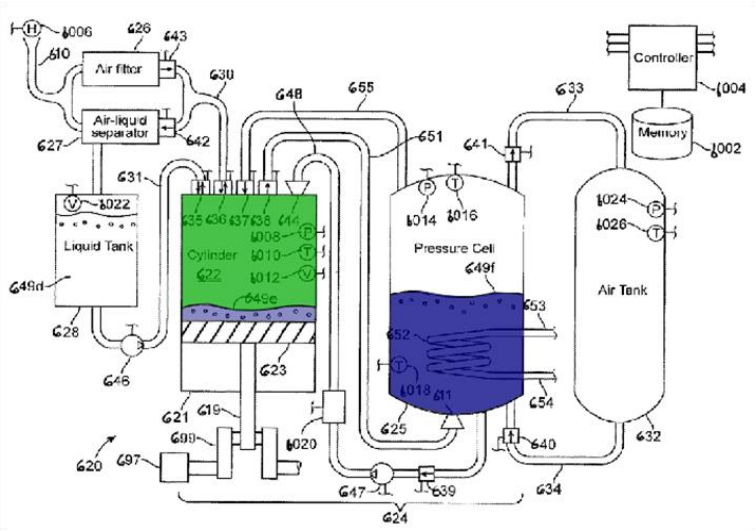

Figure 1.17: Step 3 of the compression cycle (air compression phase)

In Figure 1.18 step 4 of the compression cycle is introduced. During this step, the compressed air discharge begins once the pressure inside the cylinder chamber is substantially equal to the pressure of the pressure cell. The compressed air with the liquid mist are introduced into the pressure cell from its bottom side (green pipe) creating fine bubbles so that the heat generated during compression will exchange with the liquid (dark blue) in the pressure cell rapidly. After air mist separation, compressed cooled air (light blue) is stored in the air tank. Crane et al. [38]

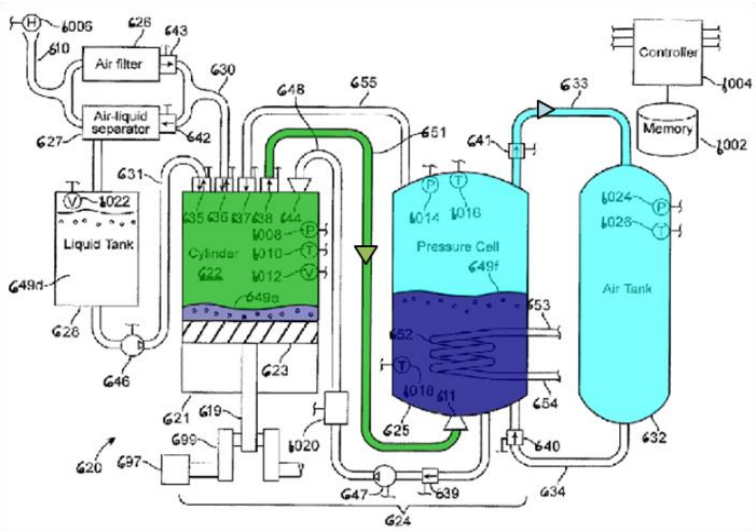

Figure 1.18: Step 4 of the compression cycle (compressed air discharge)

mentioned in their work that the liquid contained in the pressure cell is connected to a heat exchanger in order to remove the heat absorbed after air compression or to add heat to the chamber to be absorbed by the compressed air released for the expansion process. The

circulating liquid inside the heat exchanger in turn exchanges with a thermal reservoir external to the system via an external heat exchanger.

During the step 5 as presented in Figure 1.19 the piston is pulled down allowing low-pressure air to refill the cylinder chamber in order to begin with another compression cycle.

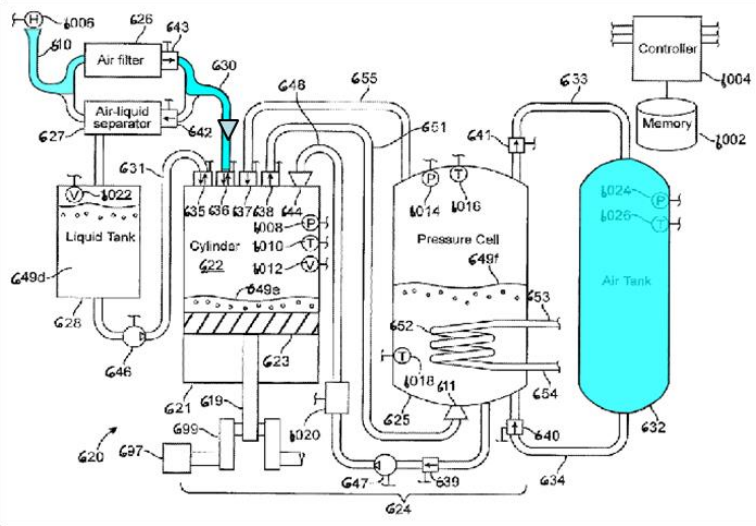

Figure 1.19: Step 5 during the compression cycle (cylinder device refill)

The expansion cycle presents 4 steps described from Figure 1.20 to Figure 1.23. The piston is considered to be at top dead center at the beginning of step 1 of the expansion cycle. This step where liquid (light purple) is added to the cylinder to eliminate the dead volume in the system, is used rarely during the process (Figure 1.20).

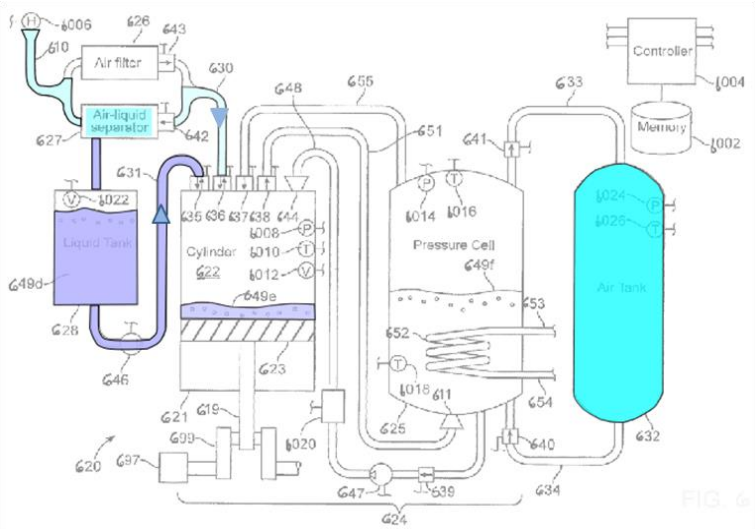

Figure 1.20: Step 1 of the expansion cycle (add liquid to cylinder chamber)

At the start of the step 2, the piston is considered to be at the top dead center. During this step of the expansion cycle, the pre-determined amount of compressed stored air (light blue) is added to the cylinder chamber after it was preheated by passing through hot liquid present inside the

pressure cell. At the same time of the compressed air introduction into the cylinder chamber, hot liquid mist (red) is being pumped from the pressure cell into the cylinder (Figure 1.21).

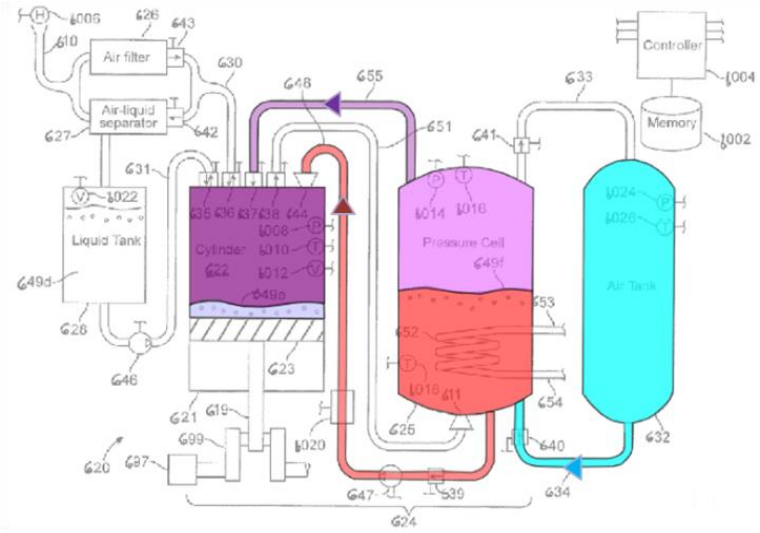

Figure 1.21: Step 2 of the expansion cycle (add compressed air and liquid mist to cylinder)

For step 3 of the expansion cycle, all the valves are closed. The piston initially at top dead center will be pushed down by the compressed air introduced during the previous step allowing air to expand in the chamber. As mentioned in Crane et al. work [38], liquid mist can also continue to be pumped into the chamber in order to add heat to the system to keep the temperature substantially constant during air expansion (Figure 1.22).

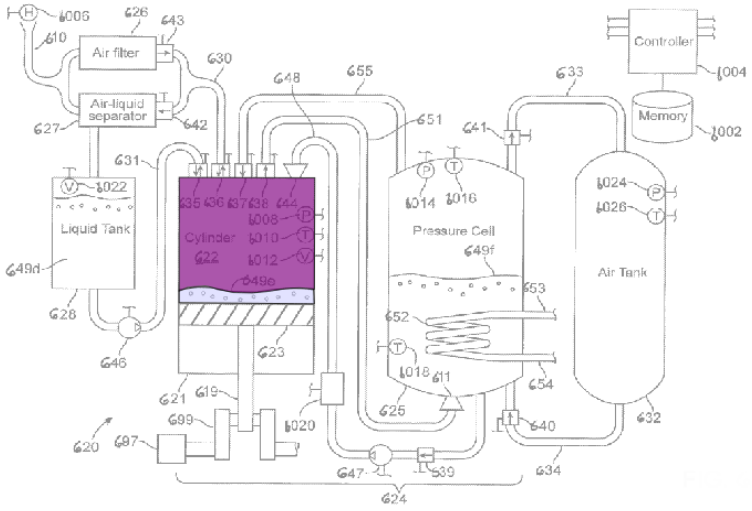

Figure 1.22: Step 3 of the expansion cycle (air expansion phase)

During step 4 of the expansion cycle, the crankshaft will move the piston upward back to the top dead center which will push out the spent air and liquid mist from the cylinder device. The power required to drive the piston comes from the momentum of the system and/or from the motion of other out-of-phase pistons. The discharged air passes through an air-liquid separator where the separated liquid is returned to the liquid tank as seen in Figure 1.23.

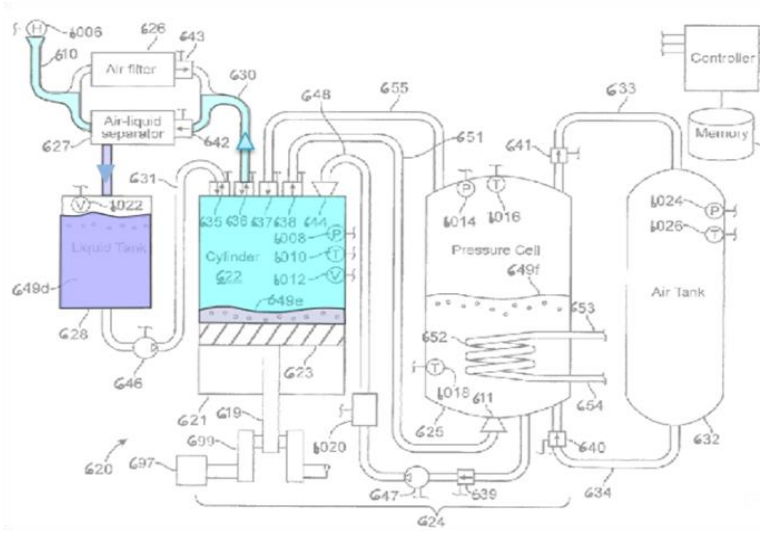

Figure 1.23: Step 4 of the expansion cycle (air discharge phase)

1.3.3.2 Liquid piston with integrated heat exchanger

Enairys Powertech is a Swiss startup incorporated in 2008 with an initial team of about six persons and develops compressed air storage solutions and energy management based on patented liquid piston compressor/expander technology. These environmentally harmless and affordable solutions mainly aim at enhancing the exploitation of intermittent renewable energy sources like photovoltaic and wind sources and therefore provide the customers with a sustainable power supply while improving the energy efficiency and power quality of electricity producers and consumers [41].

In 2011 Enairys Powertech presented its first non-commercial prototype that can absorb 10 kW of input electricity in order to store it in the form of compressed air. During the same year, they launched a pilot project with Mont-Soleil photovoltaic power plant organization and F.M.B Energie in order to develop a first commercial hydropneumatic energy storage system (HyPES) prototype of 25 kW [42]. The canton of Vaud has announced its support for the development of the HyPES system, in the form of a grant of 1.66 million francs and support intended to promote the HyPES devices entry into the market. Four patents related to storage system based on liquid piston and scroll compressor/expander technology have been filed [41]. A combination of lack of funding and technical limits is the main actual responsible for Enairys Powertech projects delay.

Technology overview

HyPES solution concept is based on the use of elasticity of air as energy vector in order to store electrical energy after converting it to mechanical energy as noticed in Figure 1.24. This is

achieved through an advanced technology that combines a new liquid piston compression/expansion concept with a specific power electronics and control units.

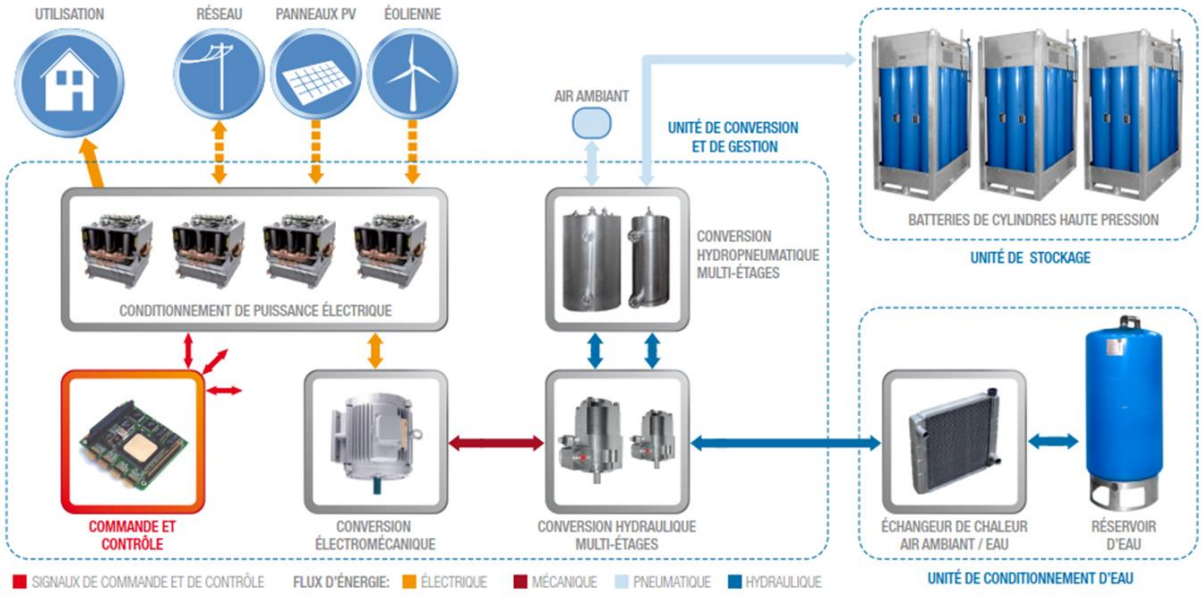

Figure 1.24: System operation of Enairys storage solution technology

Three modules can be defined in the global system (Figure 1.24):

- Conversion and management module: it manages and transforms electrical energy to compressed air. It integrates the motor/generator, the various conversion stages (reversible pumps and liquid piston chambers) as well as the control unit. The size of this module depends on the maximum power (kW) of the system.
- Storage module: High pressure cylinders in steel or carbon fiber are used to store the compressed air. The total volume defines the energy capacity of the system (kWh).
- Water storage module: The water unit has the role of cleaning and maintaining the system water at room temperature. It basically consists of a tank, a filter and a heat exchanger with the ambient air.

Enairys Powertech developed two multistage hydraulic gas compression/expansion systems [43] based on the same energy storage technology. The differences between the two systems are mainly the hydraulic circuit, hydraulic power conversion unit and the heat exchanger locations in the storage system. In addition, the compression/expansion chamber is modified at the level of the liquid ports. In the following section, the first system proposed by Enairys Powertech is considered for the analysis.

Technology overview of liquid piston air compressor

The compression/expansion chamber seen in Figure 1.25 presents the concept of the air compression and air expansion using pumped water between stainless steel tubes used to separate water and air and therefore creating an important heat exchange surface between the two working fluids [44]. Four phases are identified for the air compression cycle (Figure 1.26 - Figure 1.30):

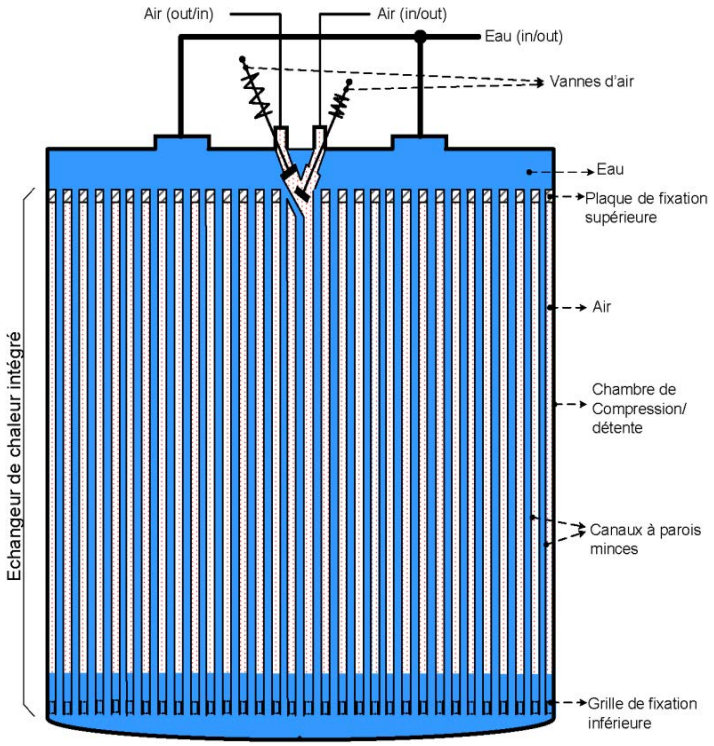

Figure 1.25: Liquid piston chamber in the conversion unit developed by Enairys Powertech

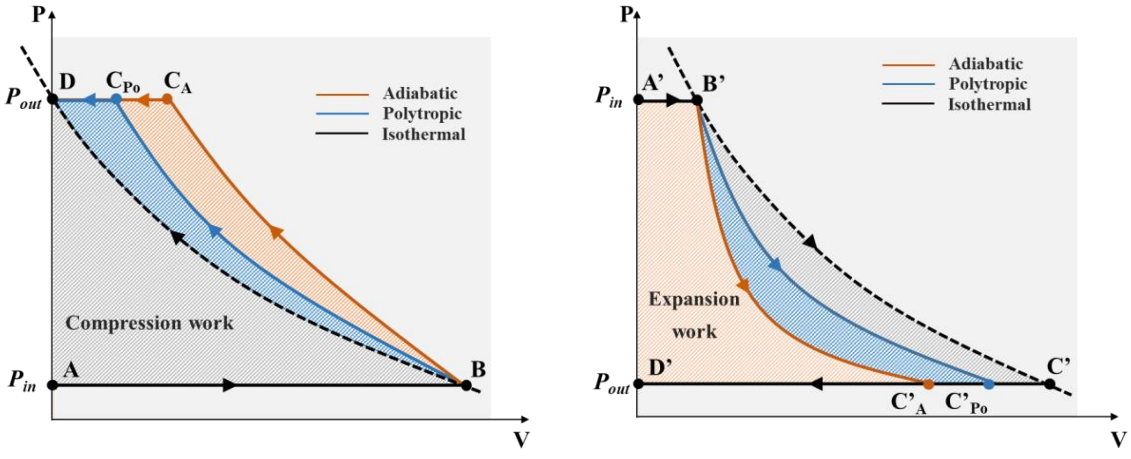

Figure 1.26: PV diagram for air compression and expansion processes

- **<u>Phase 1 (A →B)</u>:** *Air intake and water discharge*

Humid air is introduced into the compression chamber. At the same time, water in the tubes is evacuated using a reversible pump. Air water interface moves down the chamber during this process (Figure 1.27).

- **Phase 2 (B → C):** *Air compression and cold water injection*

Cold water is injected into the tubes. Air water interface moves upward of the chamber. The air in the chamber between the tubes is compressed (Figure 1.28).

- **Phase 3 (C → D):** *Air discharge and water injection*

When the pressure in the chamber reaches the discharge pressure, the air is evacuated through the air outlet valve. Water is injected to ensure the delivery of compressed air, especially when the pressure difference (chamber-reservoir) is low (Figure 1.29).

- **Phase 4 (D → A):** *Isochoric air expansion*

At the end of compressed air discharge, air input and water output valves are opened.

This fact creates pressure drop in the chamber (Figure 1.30).

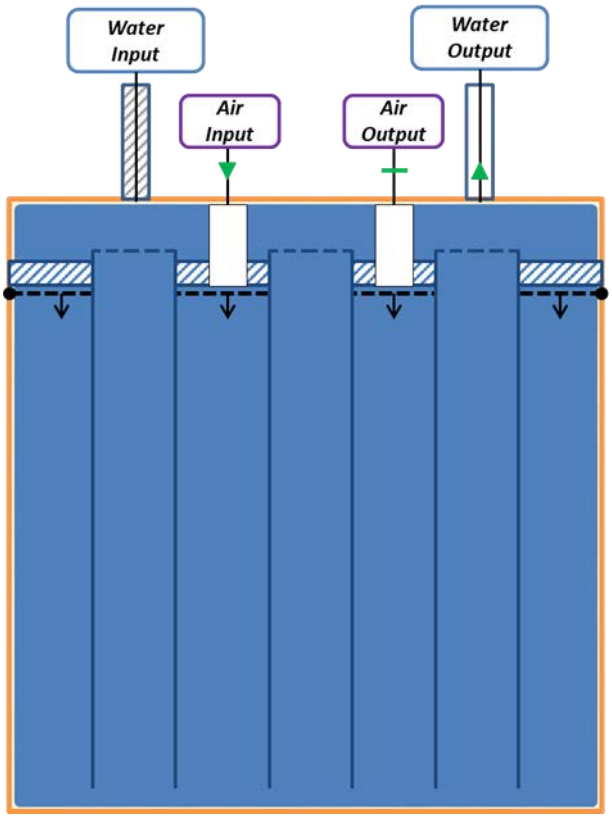

Figure 1.27: Phase 1 of the compression cycle

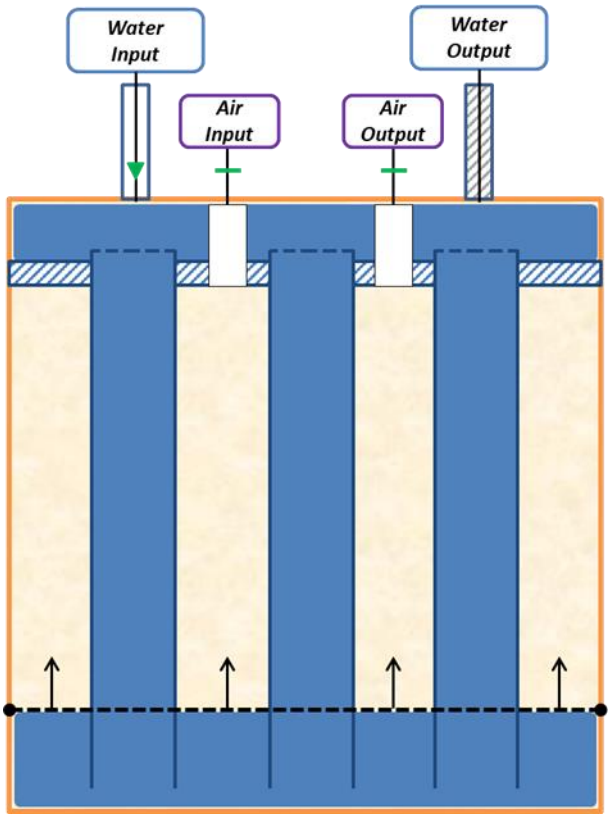

Figure 1.28: Phase 2 of the compression cycle

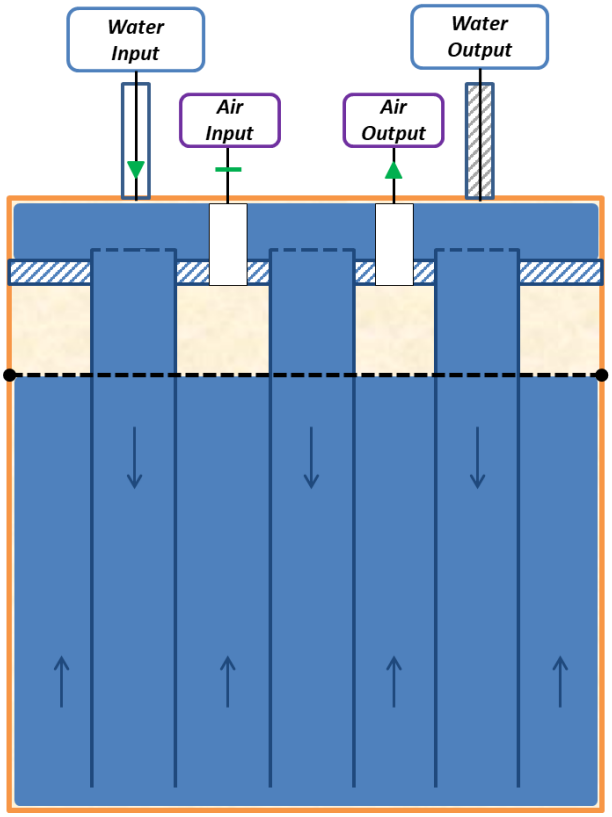

Figure 1.29: Phase 3 of the compression cycle

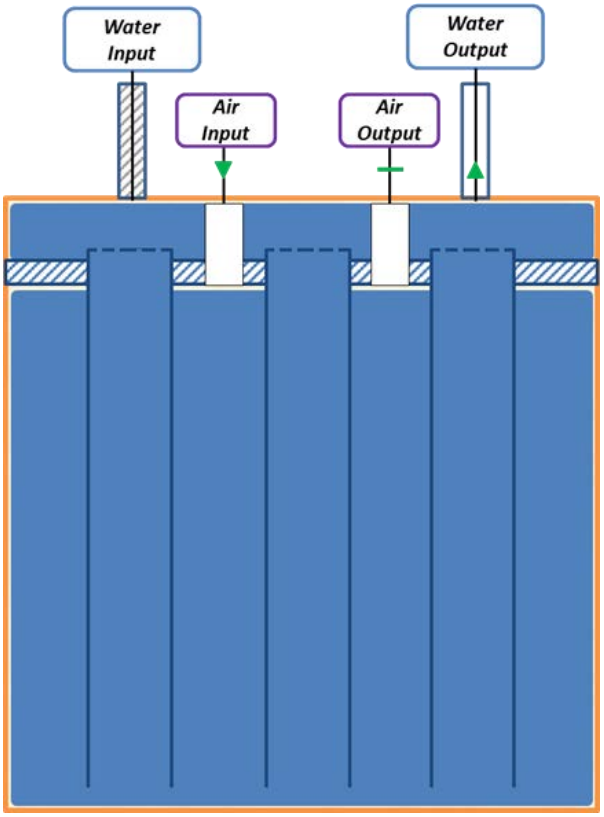

Figure 1.30: Phase 4 of the compression cycle

Technology overview of liquid piston air expander

The technology behind the liquid piston air expander is almost similar to the one of the compressor detailed in the previous section. The four phases mainly the same but with different order (Figure 1.26):

- **Phase 1 (A' →B'):** *Compressed Air intake and water discharge*

This phase can be seen in Figure 1.29 but with considering the compressed air that is entering to the chamber and therefore push the air/water interface downward.

- **Phase 2 (B' → C'):** *Compressed Air expansion and water discharge*

Figure 1.28 can also be used to show the end of compressed air expansion where water is pumped into the tubes in order to evacuate expanded air.

- **Phase 3 (C' → D'):** *Expanded air discharge and water injection*
- **Phase 4 (D' → A'):** *Isochoric air and water compression*

1.4 Conclusion

Compressed air energy was used as an important energy vector from the middle of the nineteenth century up to date. In fact, many old and new concepts were developed into real large scale installations and advanced small scale prototypes. A-CAES can be considered as a mature technology on a large scale approach. Many ideas were proposed by researchers to increase the electrical roundtrip efficiency of the A-CAES. LightSail Energy and Enairys Powertech are presenting two promising isothermal compressed air energy storage technologies that are taking the compressed air energy storage to a high level in global energy efficiency. This latter goal is achieved through the focus on the different important factors: reduction of energy storage volume by increasing the stored energy density (kWh/m^3) and developing the trigeneration energy concept (global efficiency).

Chapter 2 Numerical model of micro trigeneration advanced adiabatic compressed air energy storage system for building application

This chapter carries out a novel numerical global model of micro trigeneration advanced adiabatic compressed air energy storage (AA-CAES) coupled to building model and to electrical, hot and cold grids. Developed in VBA Excel, the numerical model which is based on thermodynamics and energy analysis offers a wide range of design factor analysis of each component of the global system. The ideal prototype proposed in this chapter is based on a new approach taking commercial units available in the actual market in order to develop the micro coupled global storage system and to propose new component concept in the case of non-availability in the market. The ideal prototype is studied and analyzed in different energy and geographical scenarios

2.1 Global system operation

The global system is composed of four main modules as seen in Figure 2.1:

1) Renewable energy module: solar and wind energy combined to deliver electricity to building model, storage system and electrical grid.
2) Building model module: different building typologies with electrical, hot and cold energy demand profiles are proposed in this chapter.
3) Energy storage system module: system that stores electrical energy and delivers electrical, hot and cold energy to building and/or electrical grid.
4) Electrical, hot and cold grids module: energy storage system is connected to the electrical grid in the "connected mode operation" for economic advantages. In addition, hot and cold grids are always connected to the building model as an energy backup at all operation modes.

The global system is modeled based on multiple energy scenarios as follows:

A. The first priority is to supply the electrical energy building demand using the renewable energy production.
B. If the renewable energy production is higher than the electrical energy building demand then the rest of the green energy is sent to the storage system.
C. Once the storage is saturated, all the excess of the renewable energy production is sent to the electrical grid.
D. If the renewable energy production is lower than the electrical energy building demand then the storage system is introduced to fill the electrical energy gap. In the same context, the storage system answers building heating and cooling demands.
E. When the global system is in "connected mode operation", AA-CAES system has the possibility to sell electrical energy to the grid after satisfying building electrical load.
F. In any lack of energy response case, electrical, hot and cold grids are considered to answer the rest of energy building demand.
G. In "connected mode operation" the electrical grid is connected to the AA-CAES system. When the cost of electricity is cheap (for example: during the night), the electrical grid can provide electrical energy to the storage system in order to store it for high peak energy consummation.

In summary, the studied global model focuses on two functional modes:

- Autonomous mode operation: A + B + C + D + F.

- Connected mode operation: A + B + C + D + **E** + F + **G**.

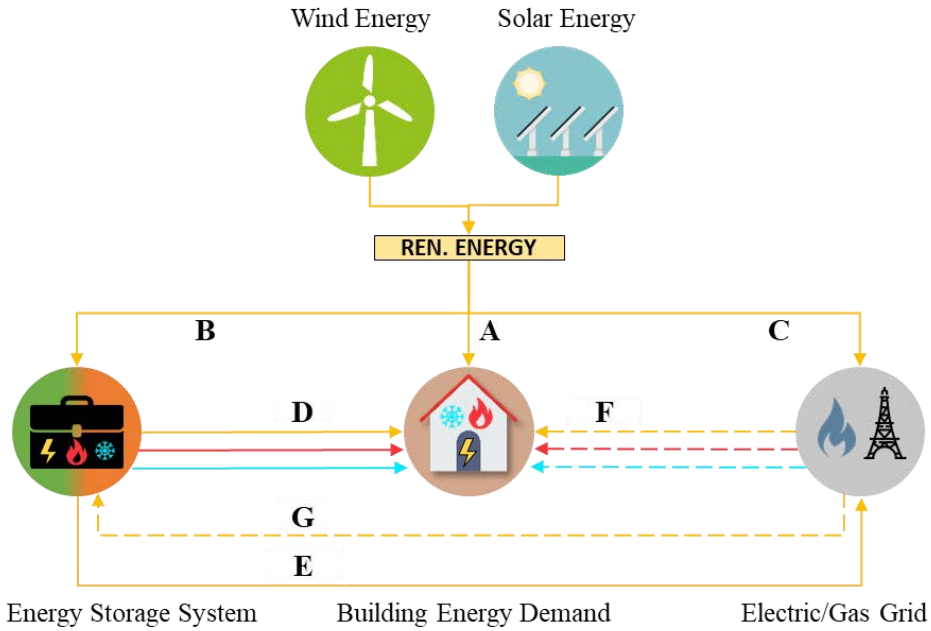

Figure 2.1: Global system operation (autonomous and connected mode)

2.1.1 Micro advanced adiabatic compressed air energy storage system description

The micro AA-CAES system configuration is based on four main elements: Compressor, compressed air reservoir, turbine and hot/cold water reservoir as seen in Figure 2.2. This system is designed in order to satisfy the energy demand of a building model by storing the excess of renewable energy production. The surplus renewable energy production (solar and wind energy) is used to power the electrical motor that will convert electrical energy to mechanical energy that in turn will run the intercooled compressor. During the critical high peak energy building demands, the energy storage system responses by introducing the compressed air into preheated turbine that turns a generator in order to deliver electrical energy to the user.

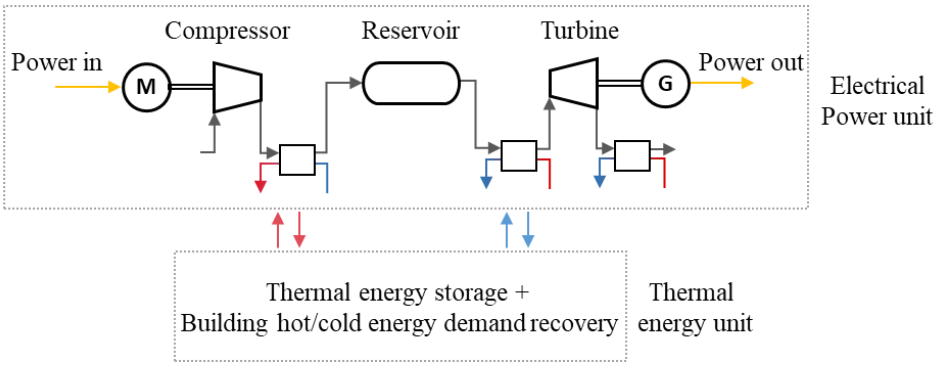

Figure 2.2: Advanced adiabatic compressed air energy storage system configuration

Figure 2.3 shows a system configuration example by selecting three compressors and two turbines. Four main phases can be distinguished:

- Charge phase: three intercooled compressors powered by electric motor are used to compress the ambient air to a fixed reservoir pressure (left upper side).
- Storage phase: high pressure reservoir model is considered as constant-volume (middle upper side).
- Discharge phase: compressed air is introduced to a set of heat exchangers and turbines that turn an electrical generator (right upper side).
- Thermal energy unit: multiple heat exchangers are used to cool air at the outlet of the compressor stages and at the same time to preheat the compressed air before entering the turbine stages (left and right middle side). Heat and cold storage are sized based on maximum power daily storage system function: 8 hours for compression phase time and 4 hours for expansion phase time.

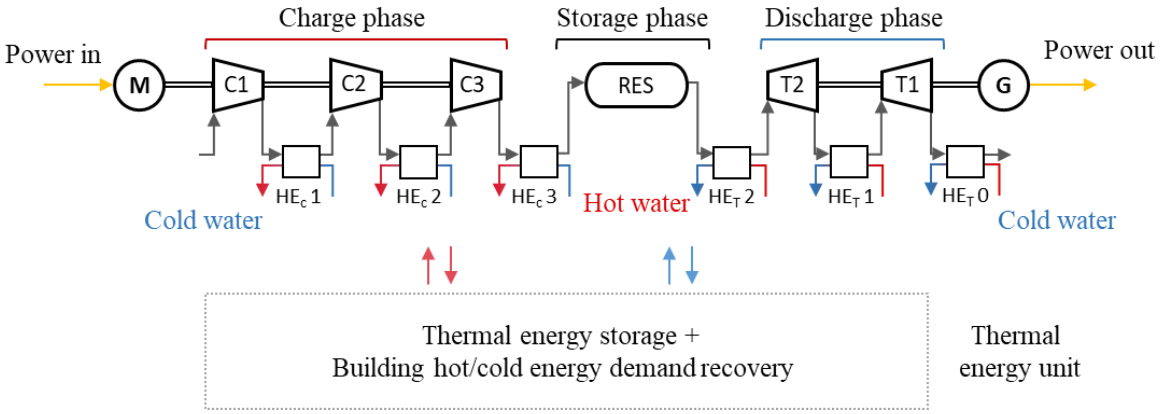

Figure 2.3: Adiabatic compressed air energy system configuration (for example: 1 reservoir (RES), 3 compressors (C1, C2 and C3), 2 turbines (T1 and T2) and 6 heat exchangers (HE_C1, HE_C2, HE_C3, HE_T2, HE_T1, and HE_T0)).

Thermal energy storage is connected to the building model through two heat exchangers in order to answer building heating and cooling demands. Figure 2.4 shows that the heat recovered from air cooling during compression phase is used to respond building heating demand. In the same manner, cold recovered from compressed air preheating during expansion phase is collected to answer the building cooling demand. After responding to building heating and cooling demands, hot and cold return water will end up into hot and cold reservoir.

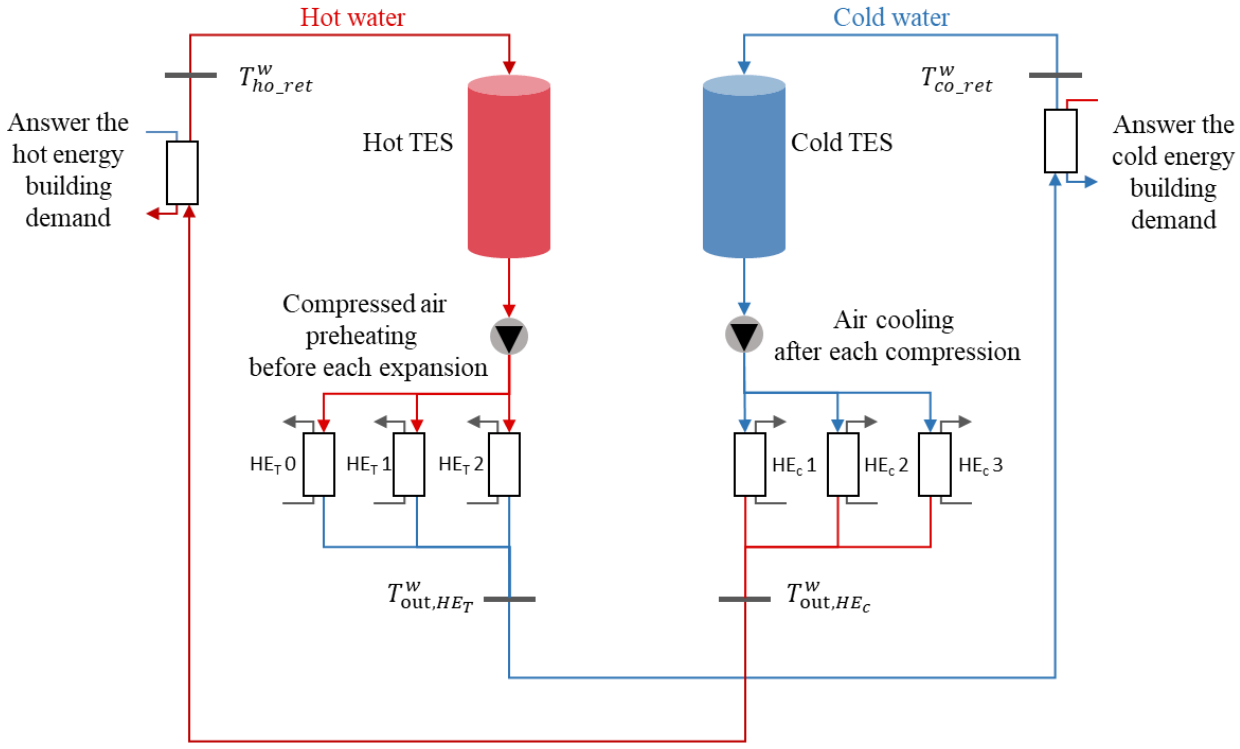

Figure 2.4: Thermal energy unit configuration for 3 compressors and 2 turbines case

2.1.2 Renewable energy module description

The system includes a wind turbine and photovoltaic panels whose size and surface as well as other parameters related to their production are the global model inputs. The renewable energy module supply the building model as a priority and the rest of the renewable production is stored and/or send to the grid. The electrical energy produced by the renewable energy module is in the form of direct current and therefore an inverter is needed to convert it to alternating current in order to be injected into the grid [45]. In this study, the renewable energy module is not the main concern, therefore multiple numerical and experimental studies on solar and wind energy are used in order to choose the right renewable energy model inputs [45], [46].

2.1.3 Building model description

The building model used in this chapter is modeled and calibrated in another research project "AIR4POWER" that is part of the sustainable production and renewable energy program of ADEME's research, development and innovation (RDI) strategy. In this latter project, a dynamic thermal simulation was conducted in order to predict the building energy needs model. The building model is composed of different typologies:

- Office: 2908 m^2
- Housing: 1337 m^2
- Hotel: 1971 m^2
- Commercial space: 597 m^2
- Total surface: 6813 m^2

2.2 Thermodynamic analysis

2.2.1 Model assumptions

2.2.1.1 Energy storage system module

- Air is considered as ideal gas.
- Maximum and minimum reservoir pressure are fixed (P_{max}, P_{min}).
- High pressure reservoir is considered as constant volume.
- The product of reservoir wall thermal conductivity and its surface ($(KS)_{res}$) is assumed to be known to 125 W.m/K.
- Cylinder piston volumetric compressor/turbine are considered in this system.
- Displacement volume for the first stage of compressor and turbine are fixed.
- Compressors and turbines are mounted on the same crankshaft separately.
- The efficiencies of heat exchangers (for charge and discharge phases) are fixed to 90 %.
- After each air compression, hot water exits the heat exchanger at 70 °C ($T^{w}_{\mathrm{out},HE_c}$).
- After each air expansion, cold water exits the heat exchanger at 5 °C ($T^{w}_{\mathrm{out},HE_t}$).
- Hot water return temperature ($T^{w}_{ho\_ret}$) is fixed at minimum 40 °C.
- Cold water return temperature ($T^{w}_{co\_ret}$) is fixed at maximum 15 °C.
- Hot and cold water reservoirs are considered to be adiabatic.
- Volumetric efficiency is considered equal to be equal to 100 %.
- Potential and kinetic energy are negligible.

2.2.1.2 Renewable energy module

- Solar panels chosen for the study is described below:
    - Material: monocrystalline.
    - Maximum power output: 180 W/m^2.
    - Total surface: 1000 m^2.
- Micro wind turbine chosen for the analysis is described as follow:
    - Blade radius: 1.5 m.
    - Maximum power output: 25 kW.
    - The output power is calculated from multiplying the specific kinetic energy ($E_k = \frac{1}{2} Ve^2$) and the air mass flow rate passing through the wind turbine ($\dot{m} = Ve\ S\ \rho$). And therefore the output power final equation is as follows:

      $Power = \frac{1}{2}\ Ve^3\ S\ \rho$.

2.2.1.3 Building model module

In order to calculate the energy building needs, a dynamic thermal simulation is achieved during the AIR4POWER project over one meteorological year. Multiple hypotheses were assumed related to wall characteristics, glazing, and lighting. For instance, real occupancy profiles were used where heat generated from one person is estimated to 115W/occupant: 70 W sensible heat and 45 W latent heat. The assumed occupancy according to different typologies are as follows:

- Commercial space : 5 m²/person ;
- Office : 2 occupants per office ;
- Open-spaces : 7 m²/person ;
- Meeting rooms : 4 m²/person ;
- Hall and circulations : 1 person for 25 m² ;
- Housing, depends on the type
    - Type 1 hotel room = 1 person ;
    - Type 2 = 2 people ;
    - Type 3 = 3 people ;
    - Type 4 = 4 people.

2.2.2 Analytical model of the energy storage system module

The modelling of the global system is based on thermodynamic equations of each component of the global system: storage system, renewable energy module and building model. The details of the equations are presented in the appendix A. Air is considered for all the parameters calculated in this chapter (temperature, pressure, mass, mass flow rate) while the superscript "w" is written to indicate water as working fluid. In the chapter, the main concern is to develop an analytical model for the AA-CAES system.

- Charge phase (energy consumption phase)

Real work of compressor "i" is calculated by integrating the reversible work ($v\mathrm{d}p$) throughout the compression cycle (Figure 2.5) and by dividing by the polytropic efficiency. In appendix A.1. the details of the compression work calculation are presented.

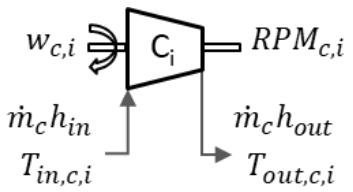

Figure 2.5: Compressor block representation (input, output)

The i[th] polytropic compression work can be calculated by the following:

$$w_{c,i} = \left(\frac{n_c}{n_c - 1} r T_{in,c,i} (\beta_c(t)^{\frac{n_c - 1}{n_c}} - 1)\right) \frac{1}{\eta_{pol}} \tag{2.1}$$

Where n_c is the polytropic index during the compression phase, r is the gas constant, $\beta_c = \frac{P_{out,c}}{P_{in,c}}$ is the compression ratio, $\eta_{pol}$is the polytropic efficiency and $T_{in,c,i}$ is the air inlet temperature of the compressor "i".

As a result, the outlet air compressor temperature of each stage can be written as:

$$T_{out,c,i} = T_{in,c,i}\, \beta_c(t)^{\frac{n_c - 1}{n_c}} \tag{2.2}$$

The different global system operations depend on the difference between the electrical energy incomes and outcomes of the energy storage system which can be expressed as follows:

$$\Delta E = R.E. - E.B.D. + Grid - to - Storage - Storage - to - Grid \tag{2.3}$$

$(R.E.)$ represents the hourly renewable energy production and $(E.B.D.)$ the hourly electrical energy building demand. In addition to two terms related to the "connected mode operation"

where the storage has the possibility to sell/store electricity to/from the electrical grid. The detailed form of the Eq. (2.3) leads to the following relation:

$$\Delta E = (E_{PV}(t) + E_W(t)) - E_{EBD}(t) + \left(\alpha E(t)\right)_{GR-ST} - \left(\alpha E(t)\right)_{ST-GR} \quad (2.4)$$

Where α is the Boolean coefficient that is related to the grid connection scenarios.

This calculated electrical energy difference (ΔE) imposes the input air mass flow rate to the compressor stages ($\dot{m}_c$) which is function of the total compressor work ($\sum_{i=1}^{Nc} w_{c,i}$) and in other words function of the working reservoir pressure (β_c) as seen in the two following equations:

$$\dot{m}_c = \frac{\Delta E}{\sum_{i=1}^{Nc} w_{c,i}\, \Delta t} \quad (2.5)$$

$$\dot{m}_c = \frac{(E_{PV}(t) + E_w(t)) - E_{EBD}(t) + \left(\alpha E(t)\right)_{GR-ST} - \left(\alpha E(t)\right)_{ST-GR}}{\sum_{i=1}^{Nc} w_{c,i}\, \Delta t} \quad (2.6)$$

In this study, the compressors are assumed to be mounted on the same crankshaft. Consequently, the revolution per minute is the same for all the compressors and is calculated by fixing the displacement volume of the first compressor stage:

$$RPM_c = \frac{\dot{V}_{c,1}}{V_{d,c,1}} 60 \quad (2.7)$$

Where $\dot{V}_{c,1}$, $V_{d,c,1}$ are the air volume flow rate and displacement volume of the 1st compressor stage respectively. The displacement volume of the ith stage (i > 1) of compressor is calculated with the following equation:

$$V_{d,c,i} = \frac{\dot{V}_{c,i}}{RPM_c} 60 = \frac{\left(\dot{m}_c / \rho_{c,i}\right)}{RPM_c} 60 \quad (2.8)$$

Where $\rho_{c,i}$ is the air density of the compressor ‘’i’’ which is related to the inlet compressor air pressure.

- Storage phase (air entering/released to/from high pressure reservoir):

As mentioned above the high pressure reservoir model is considered to be constant-volume ($W = 0$). The reservoir model used in this study is based on the investigations carried out by Simpore [46] who developed an analytical reservoir model that takes into consideration the heat loss/gain to/from the surroundings. The energy balance equation for the air entering the reservoir with air mass flow rate (Figure 2.6) calculated in the previous section is as follows:

$$\mathrm{d}(m\,u) = +\dot{m}_c h_{in}\mathrm{d}t + \delta Q = h_{in}\mathrm{d}m\ + \delta Q \tag{2.9}$$

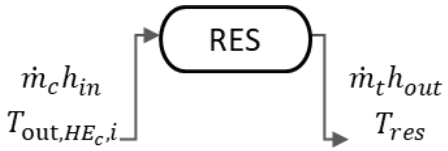

Figure 2.6: Reservoir block representation (input, output)

Substituting the enthalpy and internal energy formulas into Eq. (2.9), results in the following ordinary differential equation:

$$\frac{\mathrm{d}T}{\mathrm{d}t} = \frac{(\gamma T_{in,res} - T_{res})}{m}\frac{\mathrm{d}m}{\mathrm{d}t} + \frac{(KS)_{res}}{mC_v}(T_{amb} - T_{res}) \tag{2.10}$$

From this latter equation, the reservoir temperature is calculated as a function of the mass flow rate ($\dot{m}_c$) entering the air reservoir and its temperature ($T_{in,res} = T_{out,HE_c,i}$). By integrating Eq. (2.10) between j and j+1 time step, the numerical air reservoir temperature at j+1 time step can be expressed by the following (see Appendix A.2.):

$$(T_{res})_{j+1} = \left[\frac{(\gamma T_{in,res} - T_{res})_j}{m_j + \dot{m}_c\Delta t}\dot{m}_c + \frac{(KS)_{res}}{(m_j + \dot{m}_c\Delta t)C_v}(T_{amb} - T_{res})_j\right]\Delta t + (T_{res})_j \tag{2.11}$$

The ideal gas equation is used to calculate the increase of reservoir pressure at each time step or the pressure decrease for the air releasing phase.

$$(P_{res})_{j+1} = \frac{m_{j+1}(T_{res})_{j+1}r}{V_{res}} \tag{2.12}$$

With the reservoir air mass at j+1 time step equals to the following:

$$m_{j+1} = \dot{m}_c\,\Delta t + m_j \tag{2.13}$$

Where $\dot{m}_c$ is the air mass flow rate introduced the air reservoir a time step j and m_j is the reservoir air mass equal to $\frac{(P_{res})_j V_{res}}{r(T_{res})_j}$. In the same way, as for the air entering reservoir phase, the energy conservation equation for the air leaving the high pressure reservoir is described by:

$$\mathrm{d}(m\,u) = -\dot{m}_t h_{out}\mathrm{d}t + \delta Q = +h_{out}\mathrm{d}m\ + \delta Q \tag{2.14}$$

Which yields the following differential equation:

$$\frac{\mathrm{d}T}{\mathrm{d}t} = \frac{(\gamma T_{out,res} - T_{res})}{m}\frac{\mathrm{d}m}{\mathrm{d}t} + \frac{(KS)_{res}}{mC_v}(T_{amb} - T_{res}) \tag{2.15}$$

In this case $T_{out,res} = T_{res}$. Equation (2.15) which is an ordinary differential equation can be solved numerically by calculating the air reservoir temperature at j+1 time step after releasing air mass m_{j+1} as follows:

$$(T_{res})_{j+1} = \left[\frac{(\gamma T_{res} - T_{res})_j}{m_j + \dot{m}_t \Delta t}\dot{m}_t + \frac{KS_{res}}{(m_j + \dot{m}_t \Delta t)C_v}(T_{amb} - T_{res})_j\right]\Delta t + (T_{res})_j \quad (2.16)$$

- Discharge phase (energy production phase)

The turbine is based on a hypothetical model in this study due to the non-availability of the inlet high pressure turbine in the compressor/turbine market. The proposed cylinder piston volumetric turbine with inlet and outlet parameters is shown in Figure 2.7.

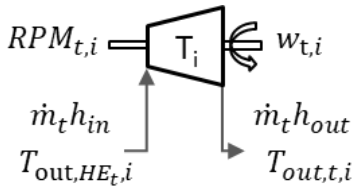

Figure 2.7: Turbine block representation (input, output)

Once the compressed air is released to pass through the heat exchanger and therefore the turbine, the real work obtained from that turbine "i" is obtained by the following (see Appendix A.3.):

$$w_{t,i} = \left(\frac{n_t}{n_t - 1} r T_{in,t,i}(\beta_{t,i}(t)^{\frac{n_t - 1}{n_t}} - 1)\right)\eta_{pol} \quad (2.17)$$

The outlet turbine air temperature is calculated by using the polytropic expansion equation as follows:

$$T_{out,t,i} = T_{in,t,i}\,\beta_{t,i}(t)^{\frac{1-n_t}{n_t}} \quad (2.18)$$

Where n_t is the polytropic index for the expansion phase, r is the gas constant, $\beta_t = \frac{P_{out,t}}{P_{in,t}}$ is the expansion ratio and η_{pol} is the polytropic efficiency. $T_{in,t,i}$, $T_{out,t,i}$ are the air inlet/outlet temperature of the turbine "i".

Similar to compressors, the turbines are supposed to be mounted on the same crankshaft that is rotating at the same revolution per minute calculated by fixing the displacement volume of the

first turbine stage. The upper equations Eqs. (2.7) (2.8) are also used for the discharge phase with the same assumptions:

$$RPM_t = \frac{\dot{V}_{t,1}}{V_{d,t,1}} 60 \tag{2.19}$$

$$V_{d,t,i} = \frac{\dot{V}_{t,i}}{RPM_t} 60 = \frac{\left(\dot{m}_t / \rho_{t,i}\right)}{RPM_t} 60 \tag{2.20}$$

Where RPM_t, $\dot{V}_{t,1}$, $V_{d,t,1}$ are the turbines rotation per minute, air volume flow rate and displacement volume of the 1st turbine stage respectively. $\dot{m}_t$, $\rho_{t,i}$ are the air mass flow rate entering the turbine and the air density of the turbine ‘’i’’.

- Thermal energy unit

Thermal energy unit is composed of hot and cold water storage reservoirs and multiple heat exchangers inserted between compressor and turbine stages. During the air compression process, cold water storage is called two times: for cooling air after each compression and for answering building heating demand at the same time step (j). Hot water storage is also called to preheat the compressed air before expanding it and to answer building cooling demand at the same time step (j). A countercurrent heat exchanger was selected as seen in the Figure 2.8. The heat transfer during charge and discharge phases are calculated by the following equations respectively:

$$\dot{Q}_{c,\mathrm{i}} = \dot{m}_c c_p \left(T_{in,HE_c,i} - T_{out,HE_c,i}\right) = \dot{m}^w_{co} c^w_p \left(T^w_{out,HE_c,i} - T^w_{in,HE_c,i}\right) \tag{2.21}$$

$$\dot{Q}_{t,i} = \dot{m}_t c_p \left(T_{in,HE_t,i} - T_{out,HE_t,i}\right) = \dot{m}^w_{ho} c^w_p \left(T^w_{out,HE_t,i} - T^w_{in,HE_t,i}\right) \tag{2.22}$$

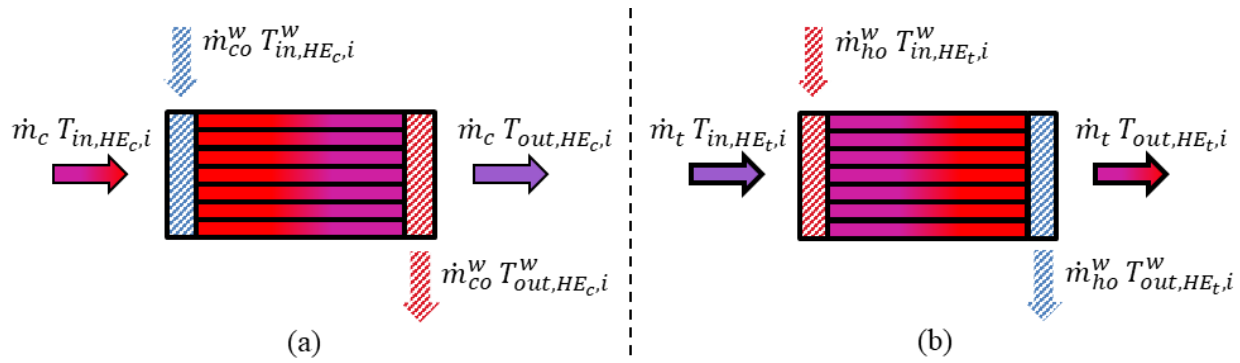

Figure 2.8: Heat exchanger model inserted between the compressor/turbine stages during the charge phase (a) and the discharge phase (b)

With:

$$T_{out,c,i} = T_{in,HE_c,i} \tag{2.23}$$

$$T_{out,HE_c,i} = T_{in,c,i+1} \tag{2.24}$$

$$T_{out,res} = T_{in,HE_t,i} \tag{2.25}$$

$$T_{out,HE_t,i} = T_{in,t,i} \tag{2.26}$$

Using the effectiveness–NTU method, the air outlet from the heat exchanger during the charge and discharge phases are described in the Eq. (2.27) and Eq. (2.28) respectively:

$$T_{out,HE_c,i} = T_{out,c,i} - \varepsilon_{HE,c}(T_{out,c,i} - T^w_{in,HE_c,i}) \tag{2.27}$$

$$T_{out,HE_t,i} = T_{in,HE_t,i} + \varepsilon_{HE,t}(T^w_{in,HE_t,i} - T_{in,HE_t,i}) \tag{2.28}$$

Where ε is the heat exchanger efficiency.

Focusing on charge phase:

Based on Eq. (2.21), cold water mass flow rate needed to cool compressed air is calculated as follow:

$$\dot{m}^w_{out,co,i} = \frac{\dot{m}_c c_p \left(T_{in,HE_c,i} - T_{out,HE_c,i}\right)}{c^w_p \left(T^w_{out,HE_c,i} - T^w_{in,HE_c,i}\right)} \tag{2.29}$$

Where $T^w_{out,HE_c,i}$ = 70 °C and $T^w_{in,HE_c,i} = T^w_{co\_ST}(j)$. It should be noted that this water mass flow rate will end up by entering the hot water storage. After cold water storage response, the temperature of that storage $T^w_{Cold\_ST}(j)$ is assumed to remain constant. Therefore, the cold water storage mass is calculated with Eq. (2.30):

$$\mathrm{d}m_{co\_ST} = -\dot{m}^w_{co,i}\mathrm{d}t \tag{2.30}$$

In turn, hot water recovered during the air cooling process answers the h building heating demand. This hot energy answer is limited by a minimum hot return temperature ($T^w_{ho\_ret}$) that is equal to 40 °C. The mass and temperature of hot water storage are then calculated as following:

$$\mathrm{d}m_{ho\_ST} = +\dot{m}^{w}_{co}\mathrm{d}t = +\dot{m}^{w}_{ho}\mathrm{d}t \tag{2.31}$$

$$\frac{\mathrm{d}T^{w}_{ho\_ST}}{\left(T^{w}_{out,HE_c,i} - T^{w}_{ho\_ST}\right)} = \frac{\mathrm{d}m}{m} \tag{2.32}$$

The previous equation Eq. (2.32) can be solved numerically as follows:

$$T^{w}_{ho\_ST}(j+1) = \left(T^{w}_{ho\_ST}(j)\frac{m_{ho\_ST}(j)}{m_{ho\_ST}(j+1)}\right) + \left(T^{w}_{ho\_ret}\left(1 - \frac{m_{ho\_ST}(j)}{m_{ho\ ST}(j+1)}\right)\right) \tag{2.33}$$

Focusing on discharge phase:

Based on Eq. (2.22), hot water mass flow rate needed to preheat the compressed air before expanding it is described in the following:

$$\dot{m}^{w}_{out,ho,i} = \frac{\dot{m}_t c_p\left(T_{out,HE_t,i} - T_{in,HE_t,i}\right)}{c^{w}_{p}\left(T^{w}_{out,HE_t,i} - T^{w}_{in,HE_t,i}\right)} \tag{2.34}$$

Where $T^{w}_{out,HE_t,i}$ = 5 °C and $T^{w}_{in,HE_t,i} = T^{w}_{ho\_ST}(j)$. It should mentioned that the hot water mass flow rate will end up by entering the cold water storage. After hot water storage response, the temperature of that storage $T^{w}_{ho\_ST}(j)$ is assumed to remain constant. Therefore, the hot water storage mass is calculated with Eq. (2.35):

$$\mathrm{d}m_{ho\_ST} = -\dot{m}^{w}_{ho,i}\mathrm{d}t \tag{2.35}$$

In turn, cold water recovered during the air preheating process answers the building cooling demand. This cold energy answer is limited by a maximum cold return temperature ($T^{w}_{co\_ret}$) that is equal to 15 °C. The mass and temperature of cold water storage are then calculated as following:

$$\mathrm{d}m_{co\_ST} = +\dot{m}^{w}_{ho}\mathrm{d}t = +\dot{m}^{w}_{co}\mathrm{d}t \tag{2.36}$$

$$\frac{\mathrm{d}T^{w}_{co\_ST}}{\left(T^{w}_{out,HE_t,i} - T^{w}_{co\_ST}\right)} = \frac{\mathrm{d}m}{m} \tag{2.37}$$

The previous equation Eq. (2.37) can be solved numerically as follows:

$$T^{w}_{co\_ST}(j+1) = \left(T^{w}_{co\_ST}(j)\frac{m_{co\_ST}(j)}{m_{co\_ST}(j+1)}\right) + \left(T^{w}_{co\_ret}\left(1-\frac{m_{co\_ST}(j)}{m_{co\_ST}(j+1)}\right)\right)$$

2.3 Numerical analysis of the energy storage system module

2.3.1 Iterative approach

The iterative approach used in this numerical global model to solve these equations detailed above are represented in the flowchart of Figure 2.9. Four inputs modules (wind turbine, solar production, energy building demand and system parameters) are called at each hourly time step (j) for each single day (a) of the year. The data collected is analyzed and then based on energy condition (ΔE), the energy scenario discussed in section 3.1 being chosen. Therefore, within the same time step (j), the electrical loop that deals with electrical energy coming/going from/to different energy resource/user is analyzed at first place. And then comes the investigation of the thermal unit module. Figure 2.10 to Figure 2.13 present the micro AA-CAES system (in charge and discharge phase), the electrical loop and the thermal energy unit loop in details.

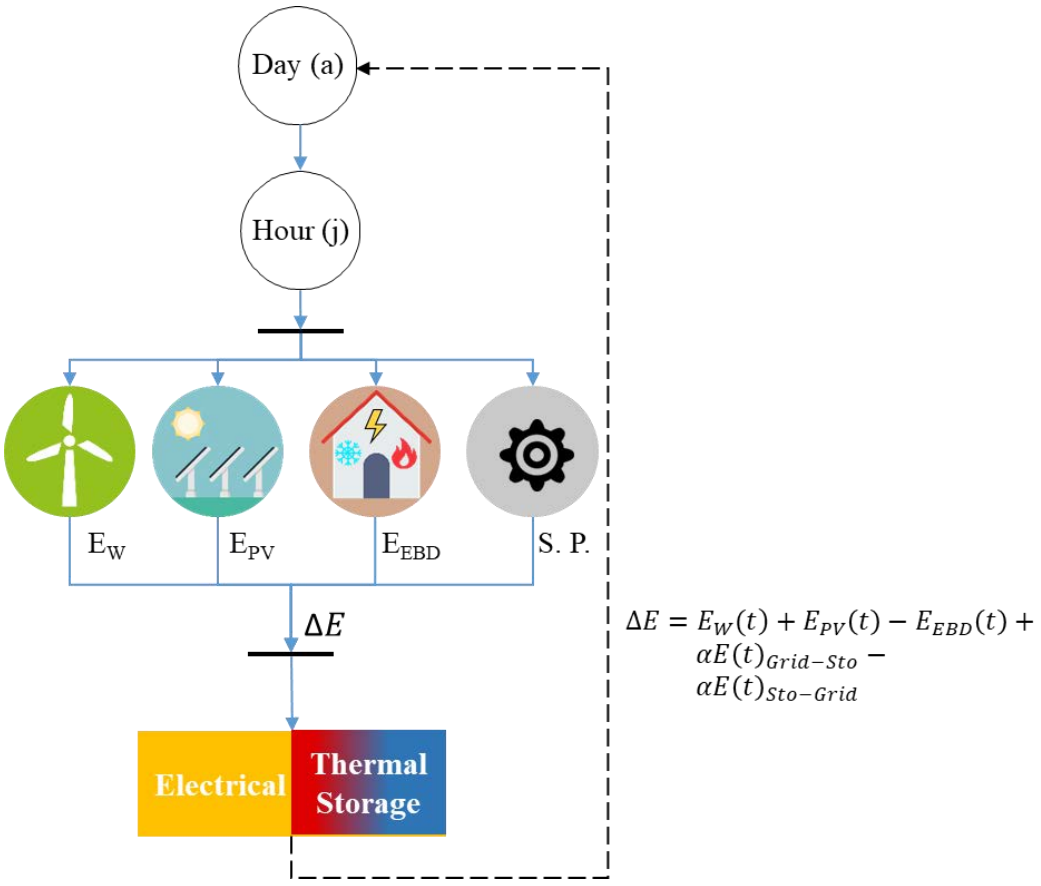

Figure 2.9: Global numerical code of the micro AA-CAES flow chart

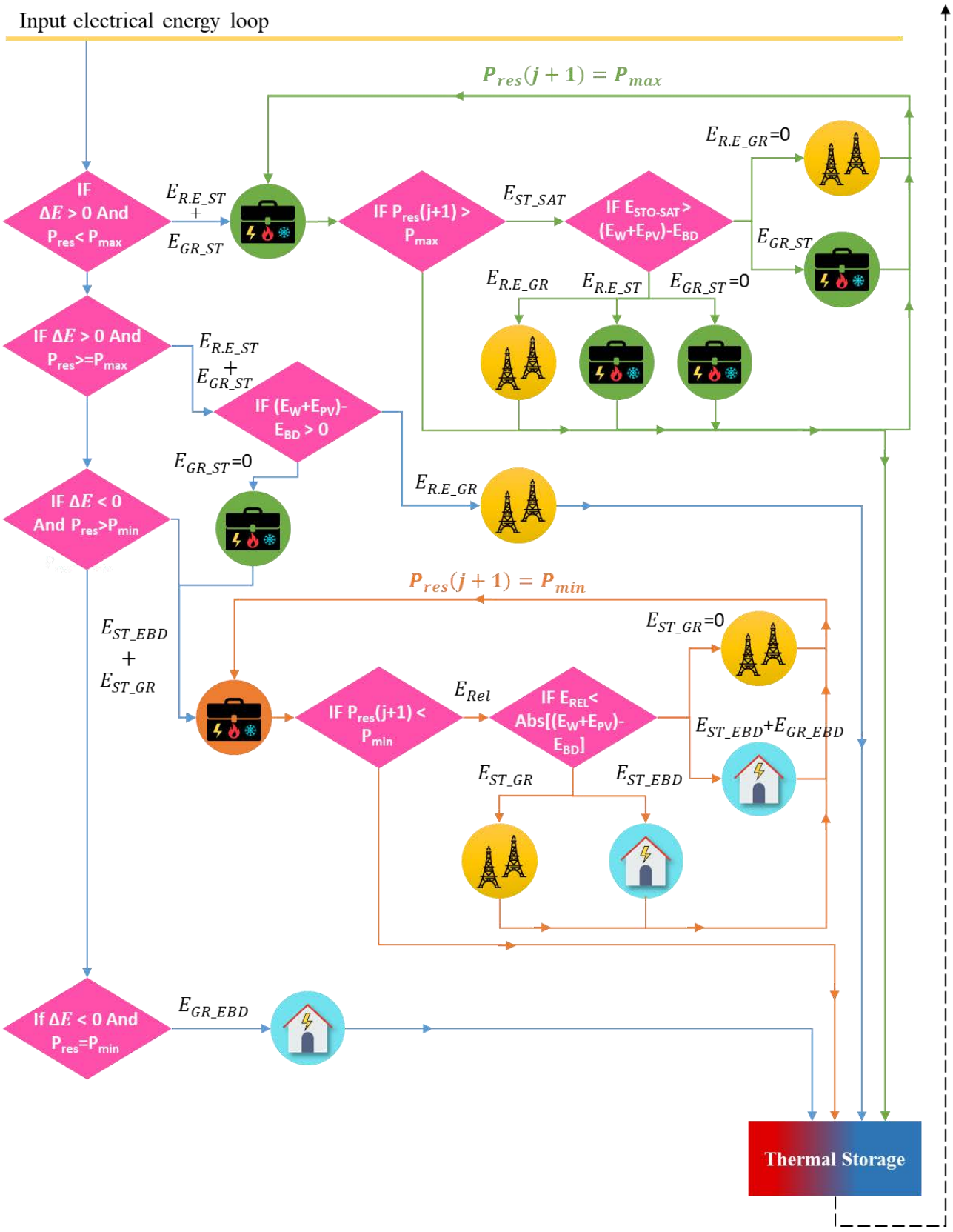

Figure 2.10: Numerical electrical loop of the micro AA-CAES flow chart

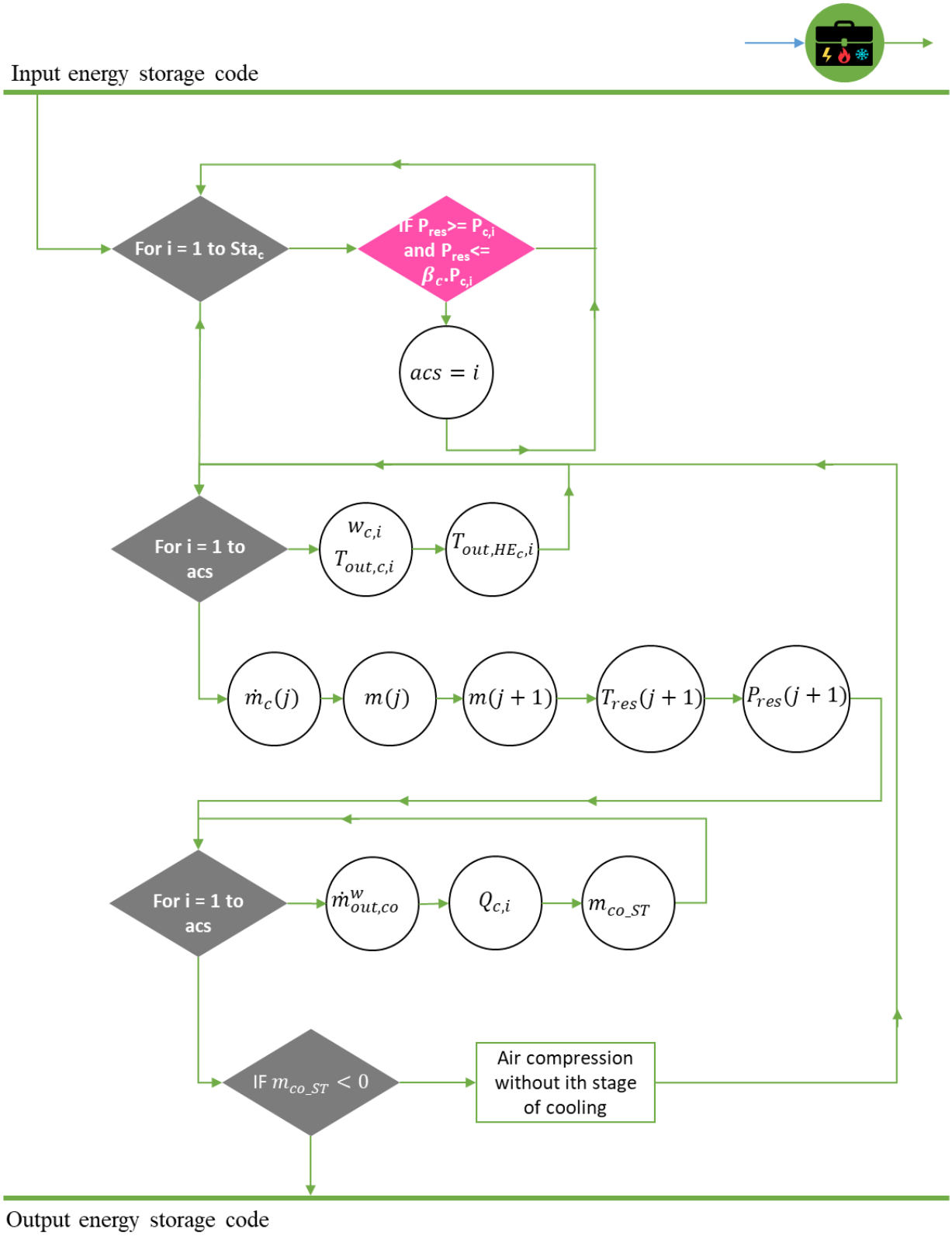

Figure 2.11: Flow chart representing the numerical code of the energy storage phase

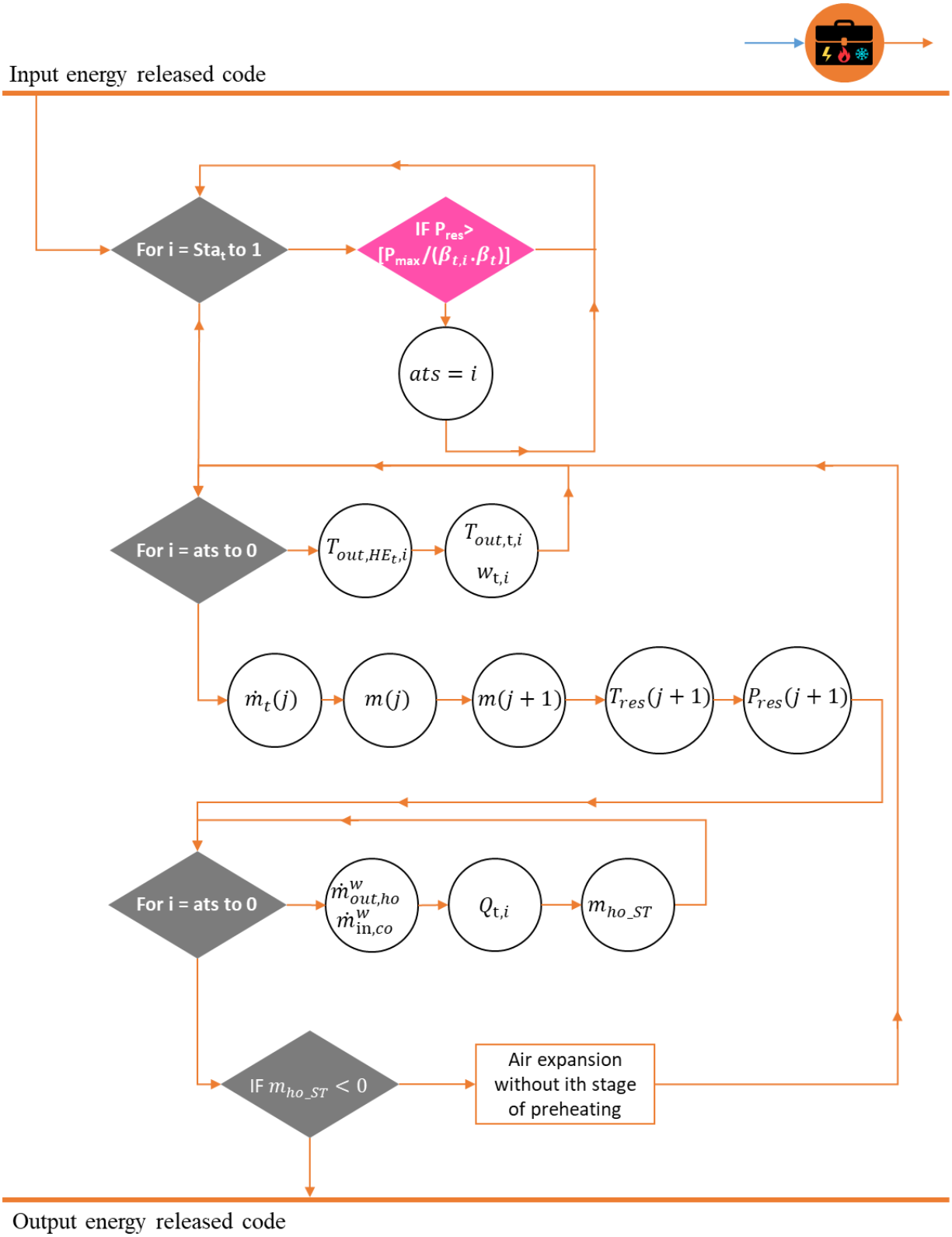

Figure 2.12: Flow chart representing the numerical code of the energy released phase

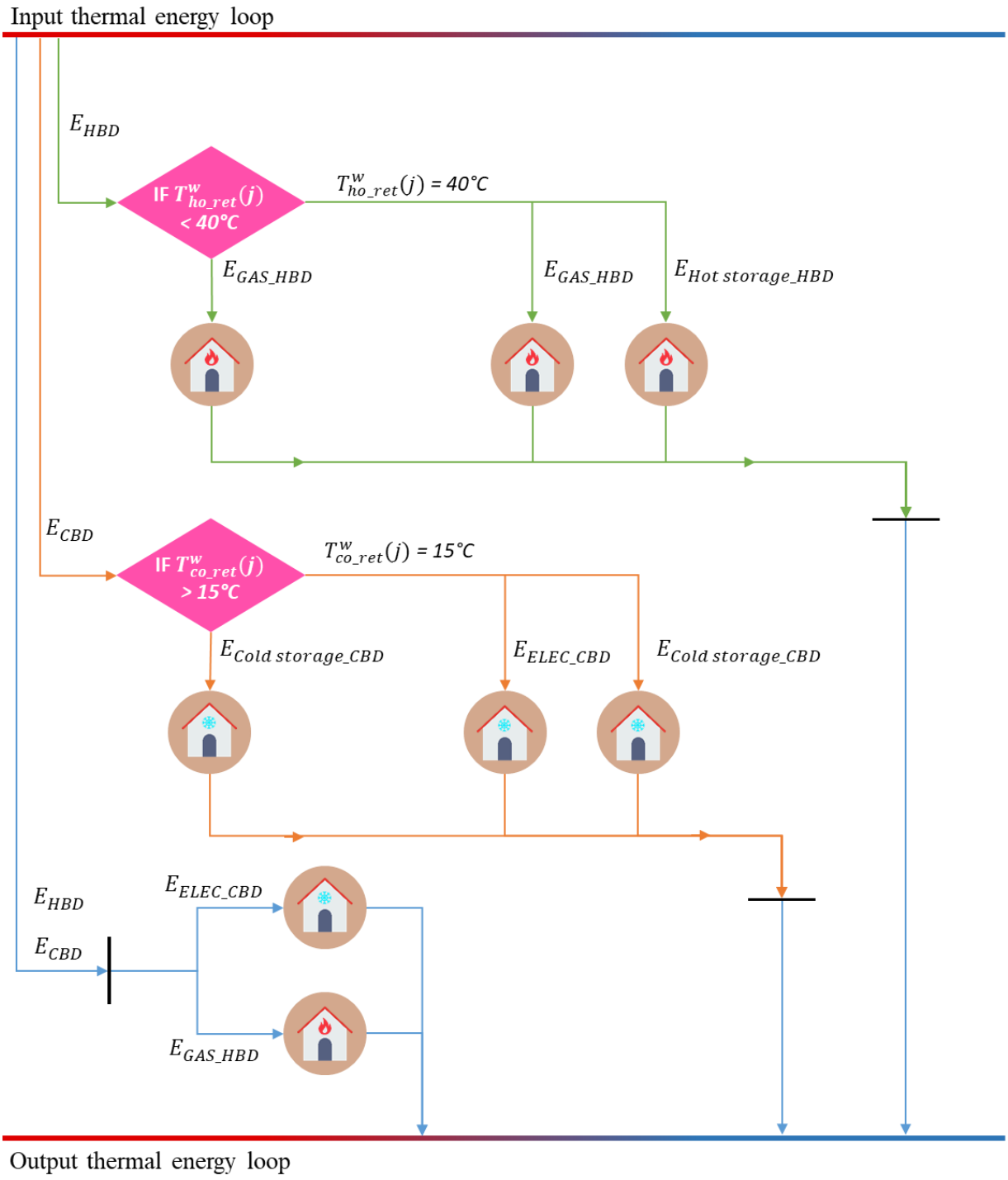

Figure 2.13: Numerical thermal loop of the micro AA-CAES flow chart

2.3.2 Excel VBA

The global model is coded using EXCEL VBA program. Different main and sub modules of the numerical tool used to dynamically calculate and analyze the performance of the global system are shown in Figure 2.14.

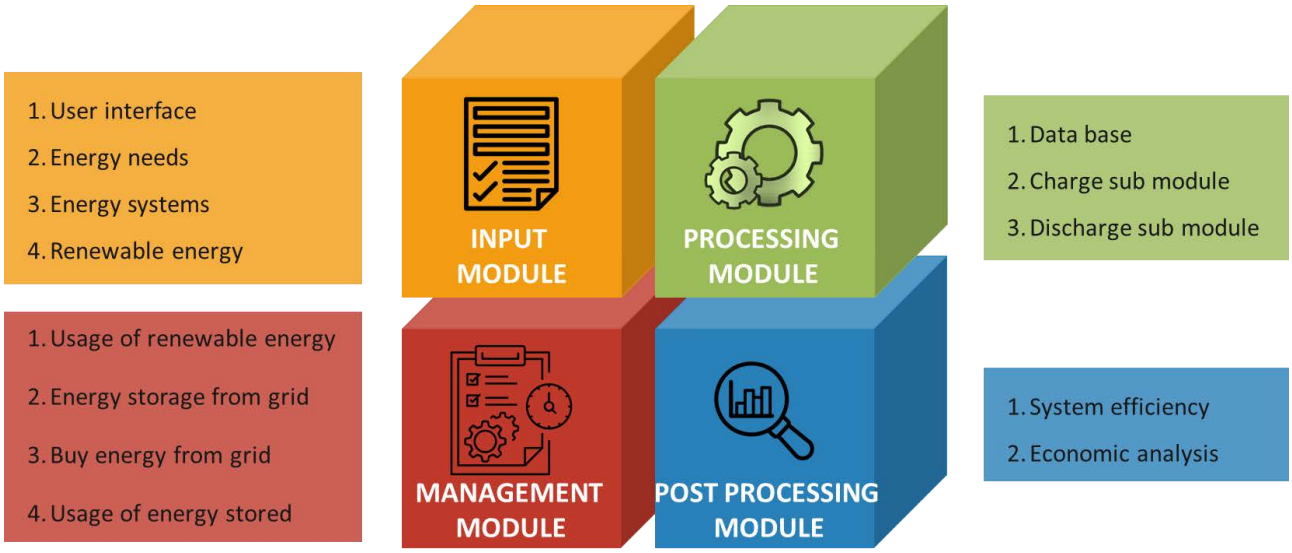

Figure 2.14: 3D matrices representing the main and sub modules of EXCEL VBA code

Input module consists of grouping most of the input parameters related to different system components in order to be modified by the user in a simple way. The main function of the storage system depends on different energy management strategies related to economic situations. These strategies are defined in the management module. Processing module offers a close look on all the system variables at each time step during the system function. The different results are plotted and shown in the post processing module.

2.4 Results and discussion

- Three compressors and two turbines are chosen to be modeled in this section. ”Nice” a French city is chosen as a geographical scenario. Other inputs and constraints required for the sizing procedure are listed in three tables:
  - Table 2.1: related to compressed air energy storage system and to renewable energy module (solar panels and wind turbine).
  - Table 2.2: related to thermal energy module (thermal storage and heat exchanger)

Table 2.1: Input data and constraints related to CAES and R.E. unit

CAES unit		**R.E. unit**	
Air reservoir volume	35 m^3	*Solar panel*	
Initial reservoir temperature	20 °C	Surface	1000 m^2
Max. air reservoir pressure	200 bar	Efficiency	20%
Min. air reservoir pressure	10 bar	Maximum	180 W/m^2
Max. power input/output	100 kW	power output	
Number of compression stages	3	Material	Monocrystalline
Compression ratios ($\beta_{c,1}$, $\beta_{c,2}$, $\beta_{c,3}$)	10, 5, 4	*Wind turbine*	
1st compressor displacement volume	0.0006 m^3	Blade diameter	1.5 m
Number of expansion stages	2	Maximum	25 kW
Expansion ratios ($\beta_{t,1}$, $\beta_{t,2}$)	5, 10	power output	
1st turbine displacement volume	0.0006 m^3		
Polytropic index	1.4		
Polytropic efficiency	80%		

Table 2.2: Input data and constraints related to thermal energy unit

Thermal energy unit			
Thermal Storage		*Heat exchangers*	
Initial cold water temp	20 °C	Efficiency	90 %
Cold storage volume	8 m^3	Outlet temperature	70 °C
Initial hot water temp	20 °C	*(compressor)*	
Hot storage volume	8 m^3	Outlet temperature	5 °C
Minimum input temperature	40 °C	*(turbine)*	
(hot storage)			
Maximum input temperature	15 °C		
(cold storage)			

Monthly renewable energy production (R.E.) and electrical building demand (E.B.D.) are shown in Figure 2.15.

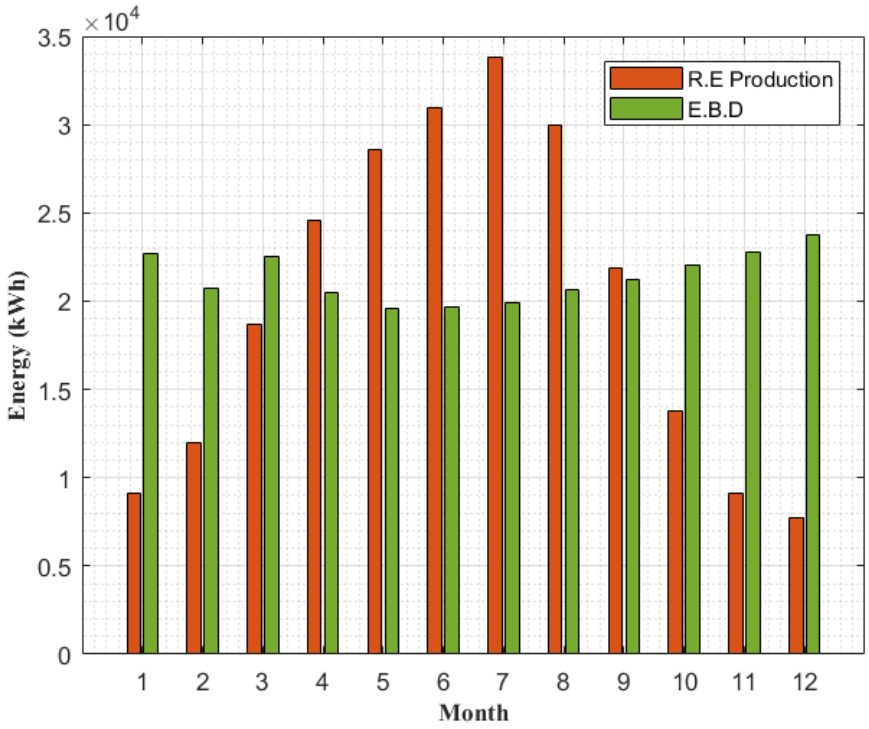

Figure 2.15: Monthly renewable energy production (R.E.) and electrical building demand (E.B.D.) for Nice location

2.4.1 Autonomous mode operation

2.4.1.1 Monthly energy analysis

The autonomous mode operation is applied in order to satisfy in the first place the energy building demand based on renewable energy production (solar and wind). The energy grids are on standby in case renewable energy production is not sufficient. As discussed before in section 3.1, autonomous mode is applied in the first place to ensure the electrical, hot and cold building demands. By applying the proposed numerical methodology, four different energy sources can be represented in Figure 2.16. It can be noticed that the energies derived directly from the renewable energy production (R.E. self-production) and from the AA-CAES system (Energy from storage) have the same behavior all over the year. This fact can be seen clearly during summer days (May, June, July and August) where energy derived from the storage scores the highest values (in July around 4 833 kWh). It is worth mentioning that in some cases (for example: July) the electrical energy building demand is totally answered and the rest of renewable energy production is sent to the electrical grid (4 000 kWh in July).

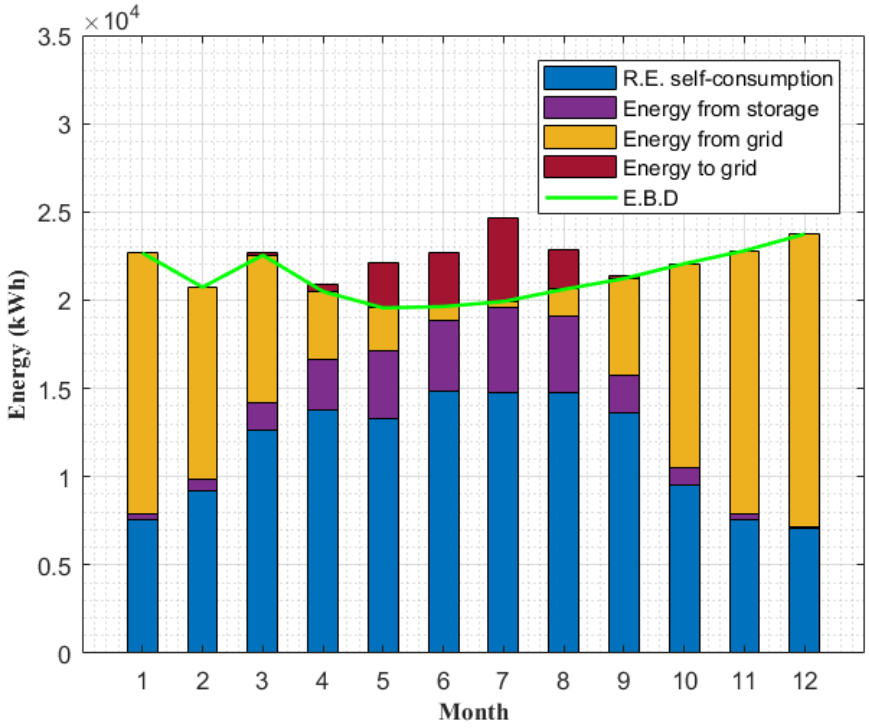

Figure 2.16: Different sources of electrical energy responding to electrical energy building demand

It must be noted that Figure 2.15 and Figure 2.16 present the cumulative/sum of different energy sources (renewable energy, energy from storage, energy from grid and energy to grid) and the energy building demand over each month of the year. The global system operation for different energy scenarios (discussed in section 3.1) is analyzed at each hour time step where in many situations renewable energy production does not answer the energy building demand. As a result, different energy sources (R.E. production, storage and energy from the grid) must be used to answer the hourly energy demand. For example, during the month of May, even though the sum of renewable energy production is higher than the building energy demand (Figure 2.15), multiple energy sources are used (Figure 2.16).

Figure 2.17 and Figure 2.18 show the hot/cold building demand answered by hot/cold water storage and an alternative energy. As discussed in section 3.1.1, the hot water recovered after cooling the air during compression phase responds to building heating demand. The renewable energy production increases from May to July and then begins to decrease till November (Figure 2.15). This R.E. production behavior affects directly the air compression operation and consequently the hot water respond (Figure 2.17). It should me mentioned that the hot and cold water storage are sized (8 m^3) based on daily AA-CAES operation: 8 hours of air compression at maximum power (100 kW) and 4 hours of air expansion at the same power. Building heating demand answered by the thermal unit is around 8 % per the year.

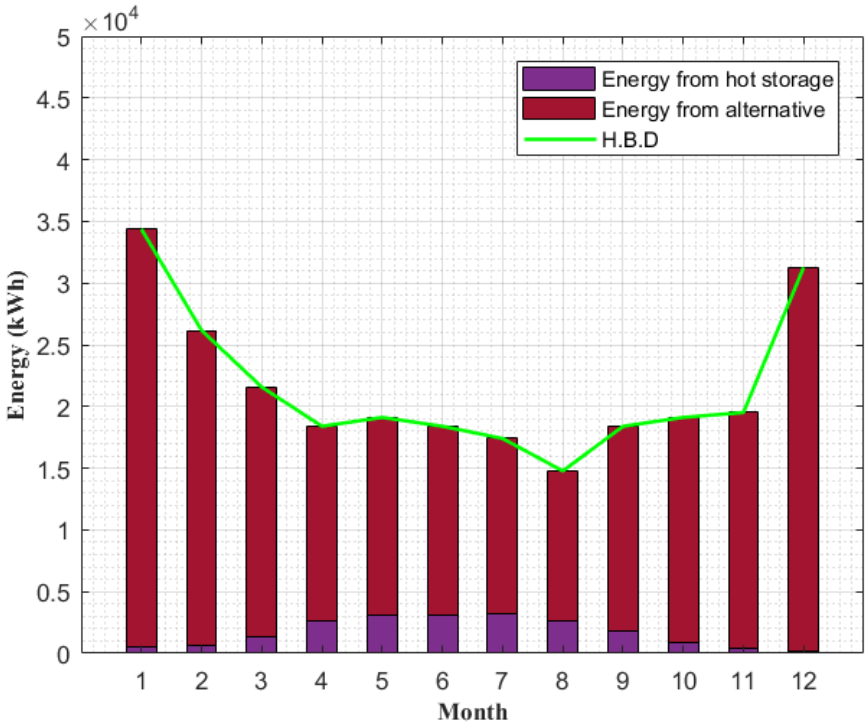

Figure 2.17: Monthly building heating demand answered by hot water storage and non R.E. source

As it can be seen in Figure 2.18, building cooling demand answered by the thermal energy unit is considered low (4 %). This is justified in some cases where the air reservoir temperature is higher than the hot water storage temperature. This fact has two important contradictory consequences:

- An important air reservoir temperature ensures a better air expansion and therefore a better AA-CAES electrical output power.
- No preheating for air before expansion and therefore no hot energy building respond.

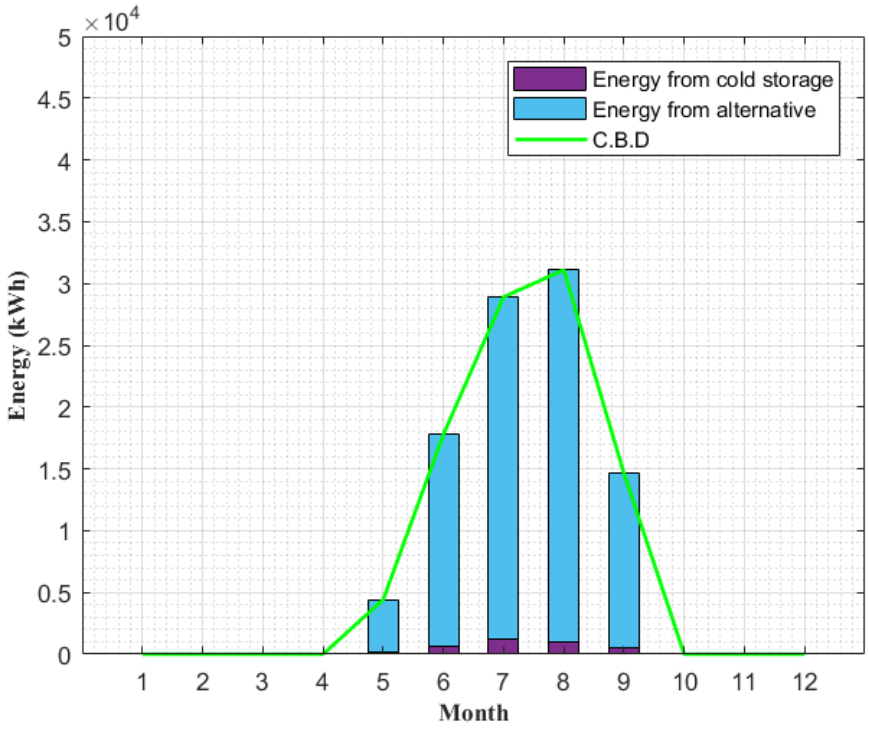

Figure 2.18: Monthly building cooling demand answered by cold water storage and non R.E. source

2.4.1.2 Daily energy analysis

As it can be seen in Figure 2.19, the micro AA-CAES answers the building electrical energy demand (green) over the year by managing the energy scenarios discussed in the global system operation (section 3.1). The total energy consumed by the compressors (blue) is proportional to the solar production (yellow) whereas the energy recovered from storage (orange) is inversely proportional to the solar production. Figure 2.20 and Figure 2.21 show the evolution of the daily hot water storage volume and temperature throughout the year. Also Figure 2.22 and Figure 2.23 present the daily cold water storage volume and temperature. As a first observation, the two water storages are communicating vessels and affected by the electrical energy difference (ΔE) that in turn will play the major role in order to choose the energy scenario. The main parameters that influence the hot and cold water storage temperatures are the hot and cold building energy responds and the energy scenarios (energy storing, energy discharging,…). While cooling the air during the air compression phase, hot water recovered at 70 °C answers the hot energy building to be stored afterwards at minimum 40 °C. From the 100th day to 250th day of the year, the energy storage scenario is frequently called and therefore recovering more hot water at 70 °C and in parallel answering more building heating demand. While the air is expanded, the cold water is recovered and stored at 5°C. The cold water storage temperature is shown to increase while answering the building cooling demand.

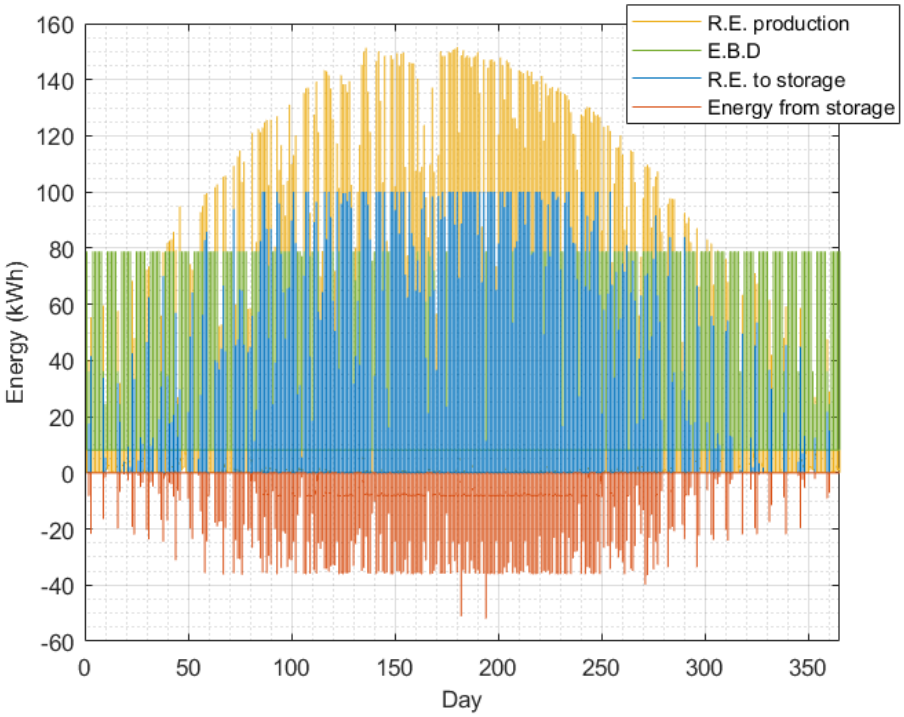

Figure 2.19: Daily renewable energy production, electrical building demand, renewable energy stored and stored energy delivered to building

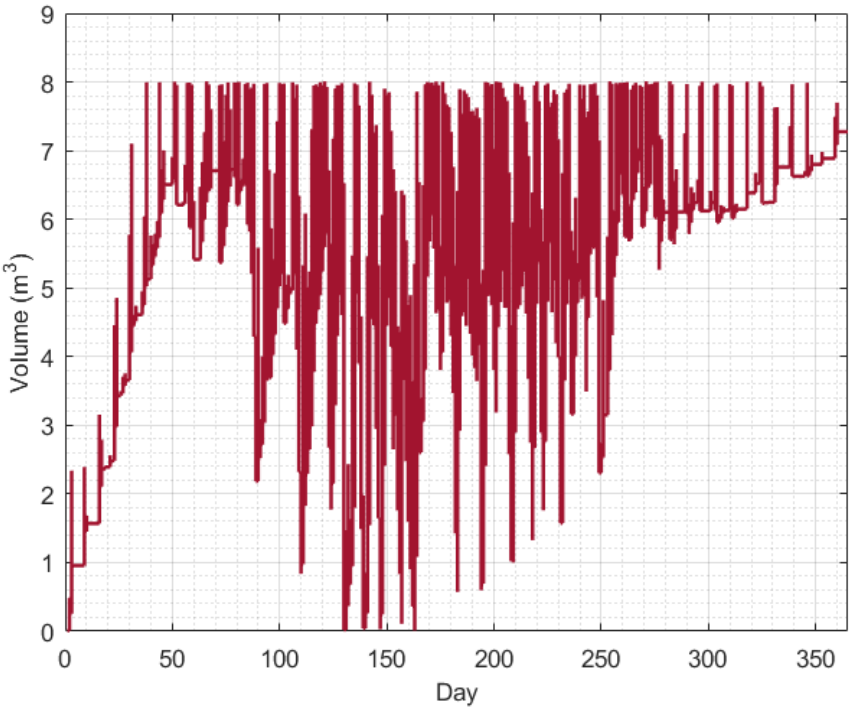

Figure 2.20: Daily hot water storage volume

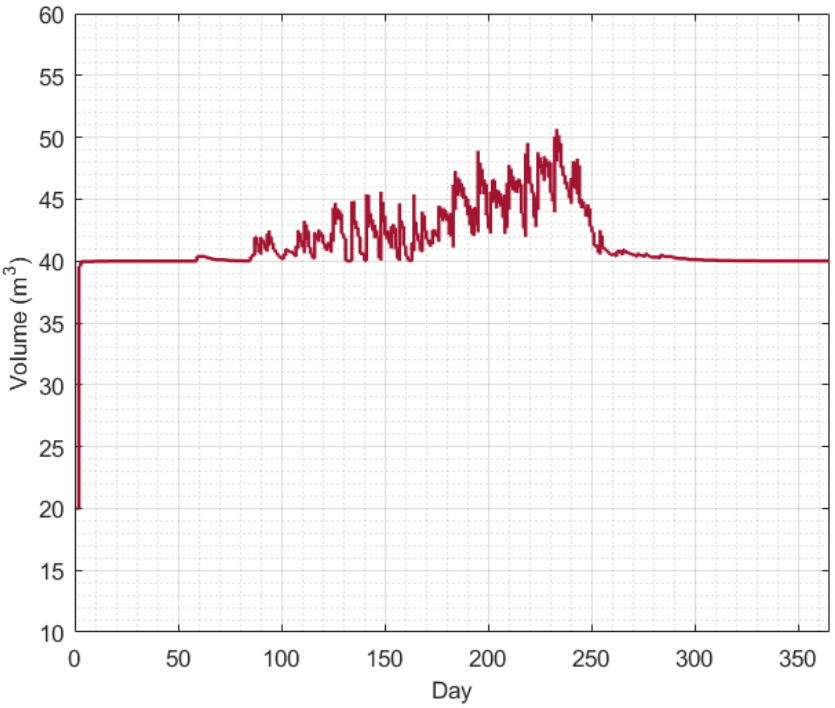

Figure 2.21: Daily hot water storage temperature

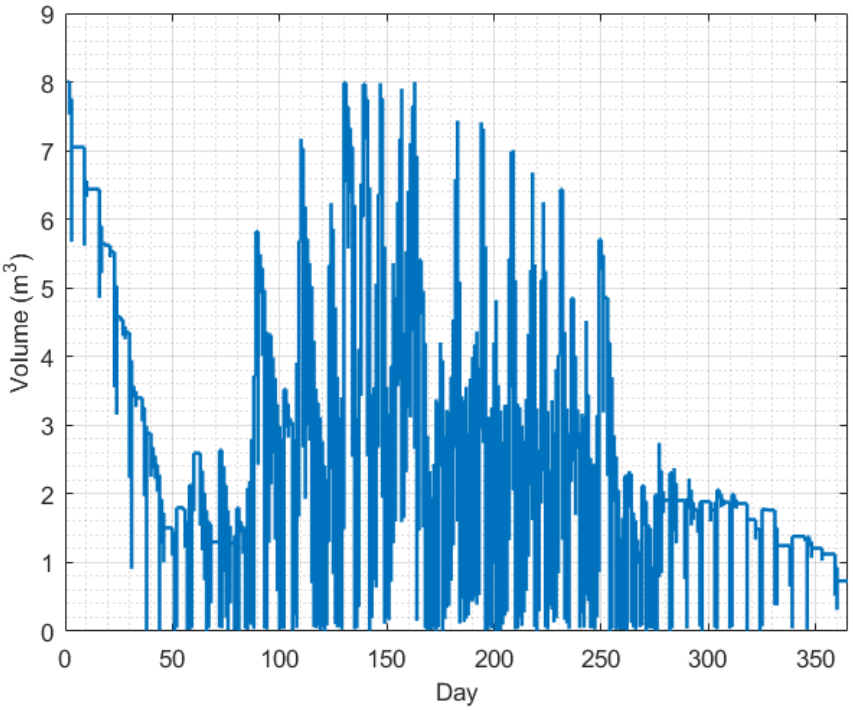

Figure 2.22: Daily cold water storage volume

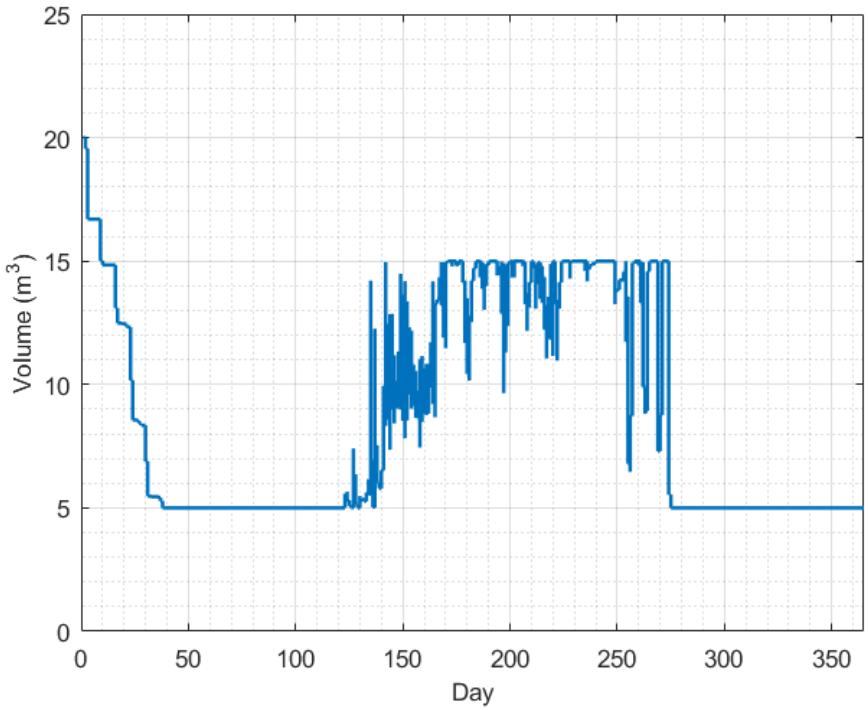

Figure 2.23: Daily cold water storage temperature

2.4.2 Connected mode operation

The connected mode operation takes the economic advantage where the system can store/sell electricity coming from/to the electrical grid in addition to the storing of renewable energy, in order to answer the energy building demand. Figure 2.24 to Figure 2.27 show the different hourly and monthly energy scenarios used for the connected mode operation. The blue rectangles mean that the operation is on whereas the meaning of the grey rectangles is that the operation is off. The scenario of the electric energy consumption based on renewable energy production is shown in Figure 2.24. The renewable energy self-consumption is considered to be operational all the time during the year. Storing energy using the electrical grid is seen in Figure 2.25 with the focus on morning hours (0:00 to 9:00) where the electric energy purchase cost is relatively low. Similar to electric energy purchase, Figure 2.26 shows the energy scenario for selling stored electricity to the grid. It can be seen that selling electricity is concentrated during the night (18:00 to 23:00) for economic benefits. Stored electrical energy is programmed to answer the electrical building demand all the time (Figure 2.27).

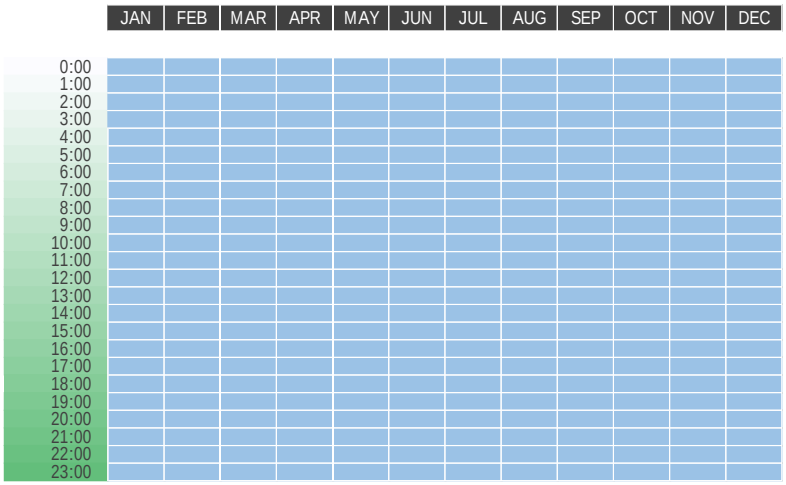

Figure 2.24: Renewable energy self-consumption schedule

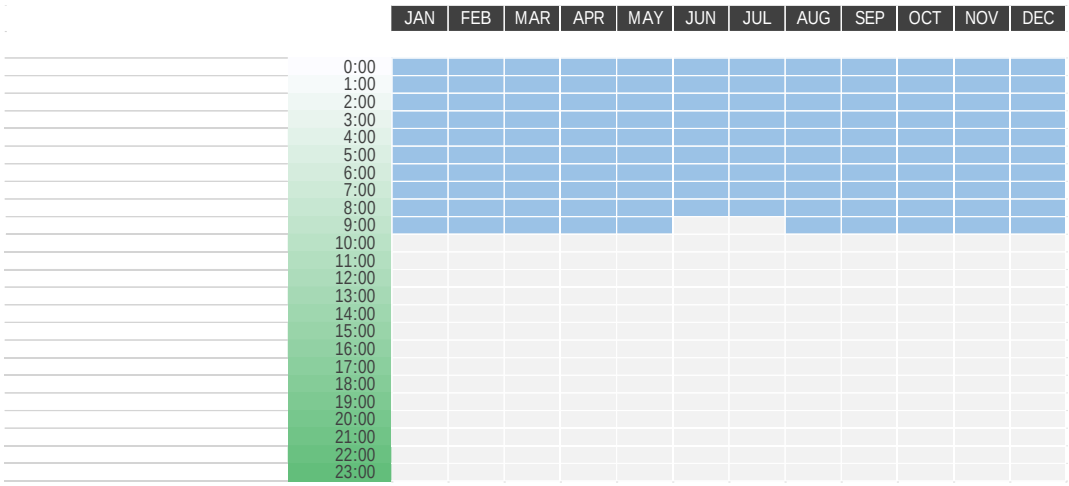

Figure 2.25: Schedule of energy storage from electrical grid

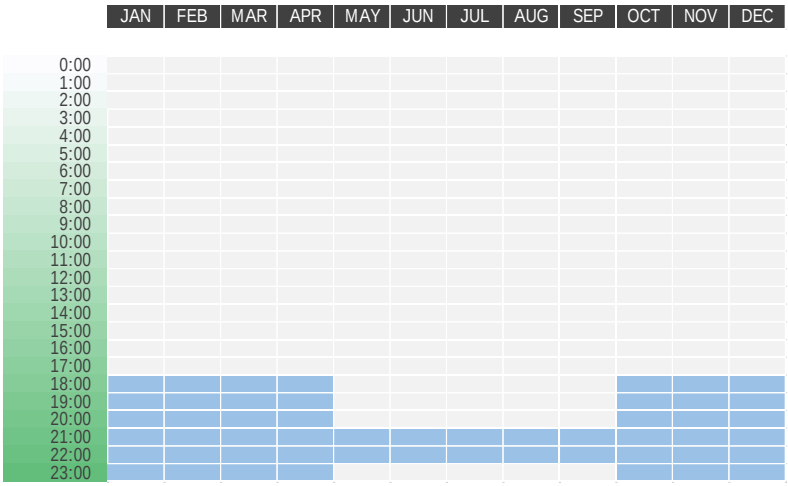

Figure 2.26: Stored energy sold to the electrical grid schedule

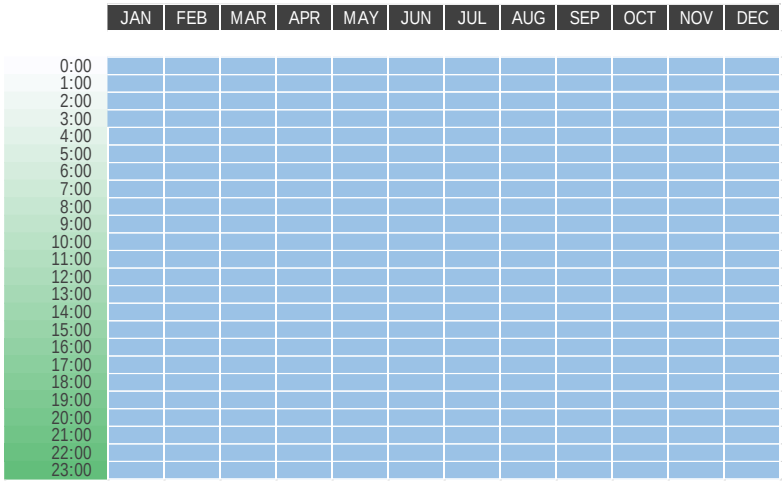

Figure 2.27: Stored energy answering building schedule

2.4.2.1 Monthly energy analysis

Unlike the autonomous mode operation, Figure 2.28 shows that the share of energy answered by the storage system is more important. An important part of renewable energy (R.E.) is sent to the electrical grid due to the storage saturation based on storing energy from the grid during morning hours. In the connected mode operation, the high pressure reservoir achieves rapidly the maximum pressure (200 bar) and thus the storage system has a tendency to more deliver energy to the building and to the electrical grid.

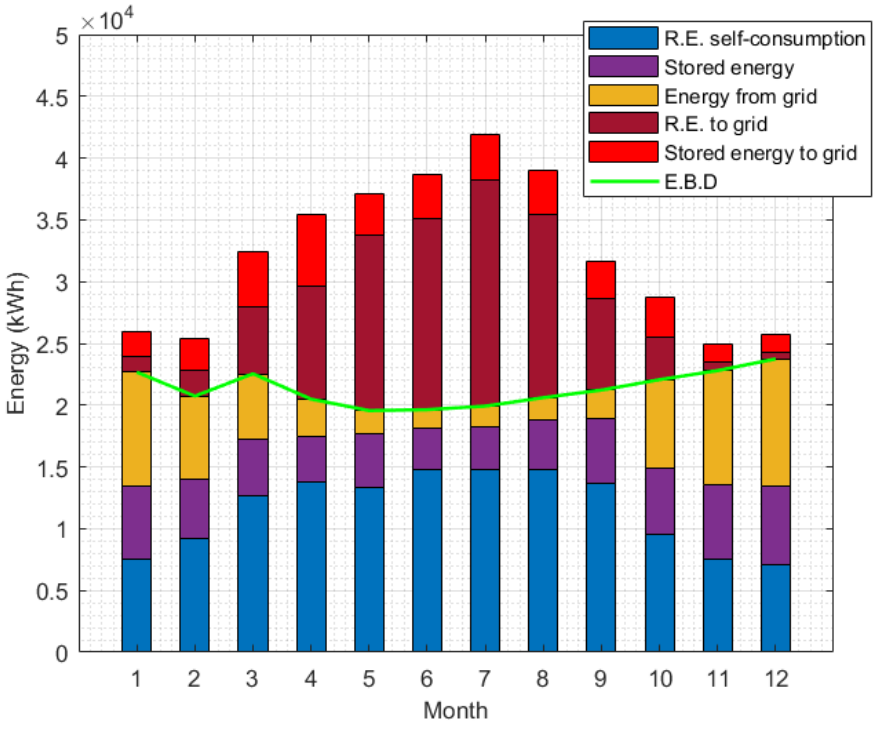

Figure 2.28: Different sources of electrical energy responding to electrical energy building demand

It should be noted that in Figure 2.29 and Figure 2.30 the building heating and cooling demands answered by the thermal energy unit is more favorite in the connected mode operation. 20 % of the hot energy building covered by the hot water storage whereas 5 % for cold energy. Cold part remains relatively low because of the high temperature (around 100 °C) stored in high pressure reservoir. This fact promotes higher electrical output power but on the other hand reduces the cold water recovered from preheated turbines and therefore less cold energy building response.

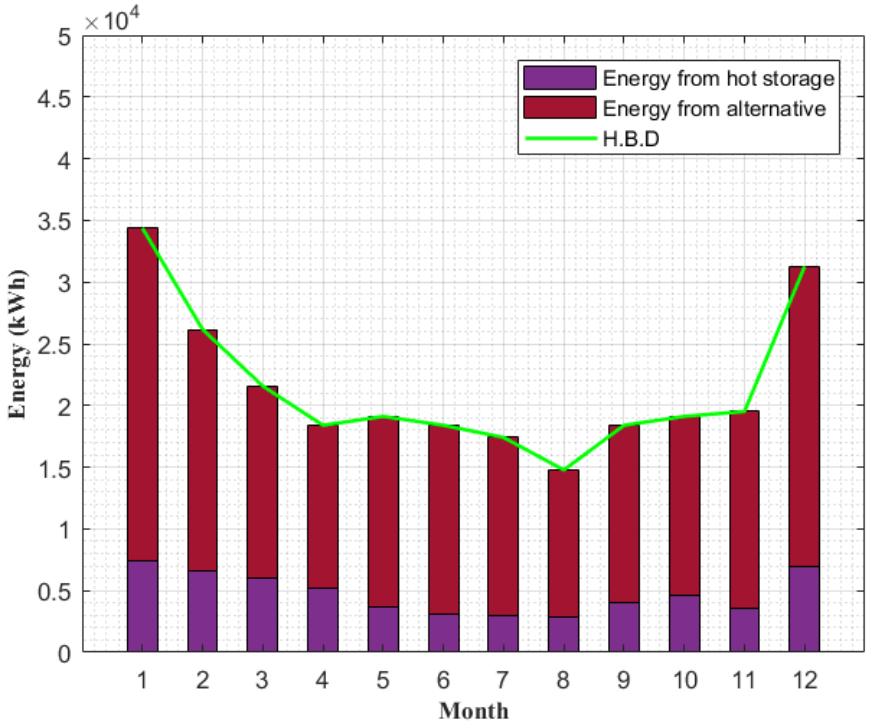

Figure 2.29: Monthly building heating demand answered by hot water storage and non R.E. source

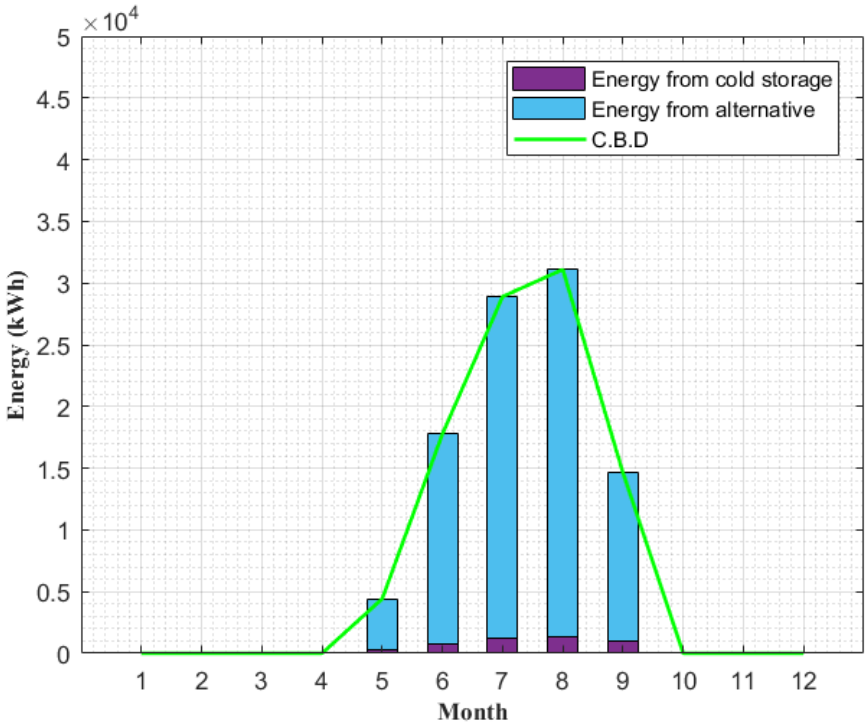

Figure 2.30: Monthly building cooling demand answered by cold water storage and non R.E. source

2.4.2.2 Daily energy analysis

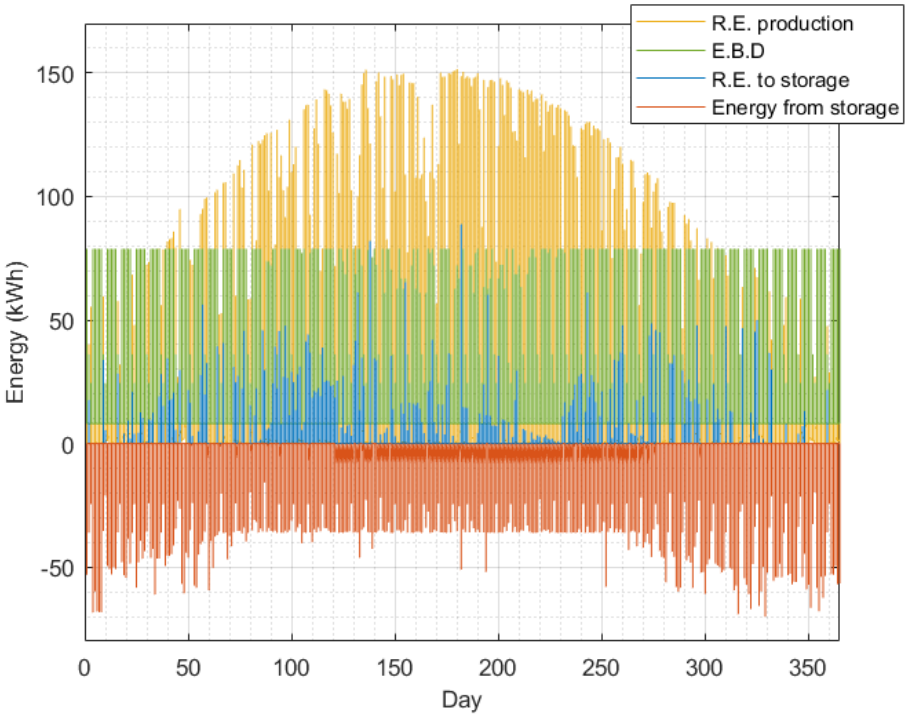

Figure 2.31: Daily renewable energy production, electrical building demand, renewable energy stored and stored energy delivered to building

Figure 2.31 shows that with the connected mode operation the micro AA-CAES has more tendency to rapidly store energy in order to deliver it more frequently. Like the autonomous mode operation, both water storages are always acting as a communicating vessels. The main difference from previous mode operation is the hot water storage temperature behavior. As mentioned above, the connected mode has more tendency to store energy and therefore recovers more hot water at 70 °C after cooling the air during compression phase. Thus increasing the hot energy building response. The cold water storage response is similar to previous mode operation.

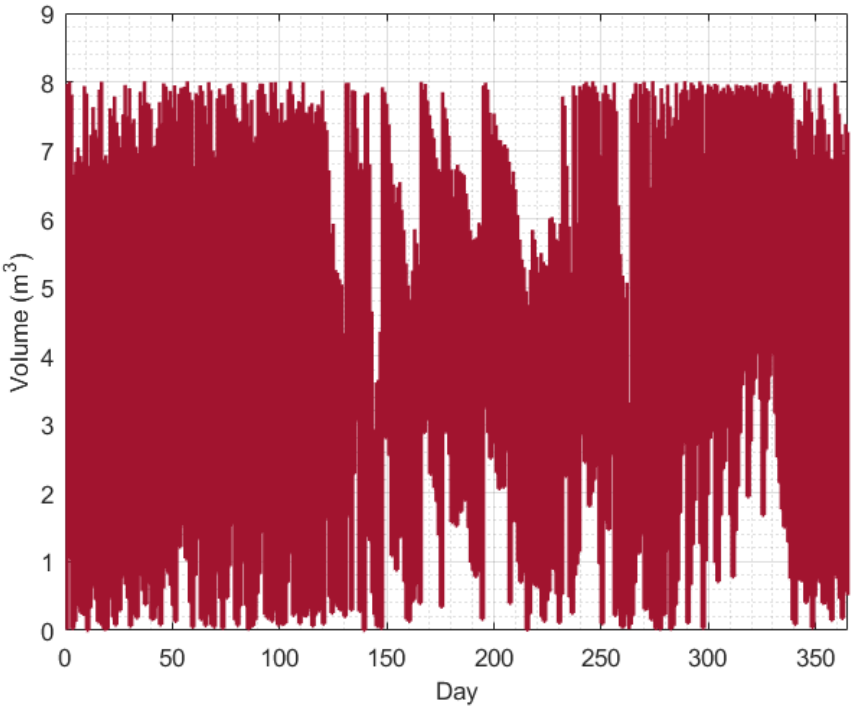

Figure 2.32: Daily hot water storage volume

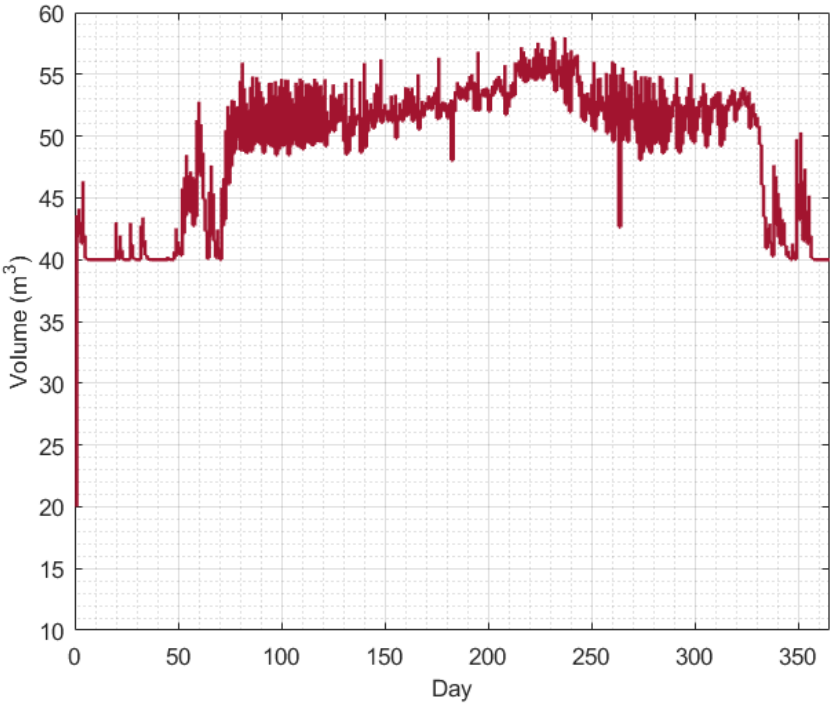

Figure 2.33: Daily hot water storage temperature

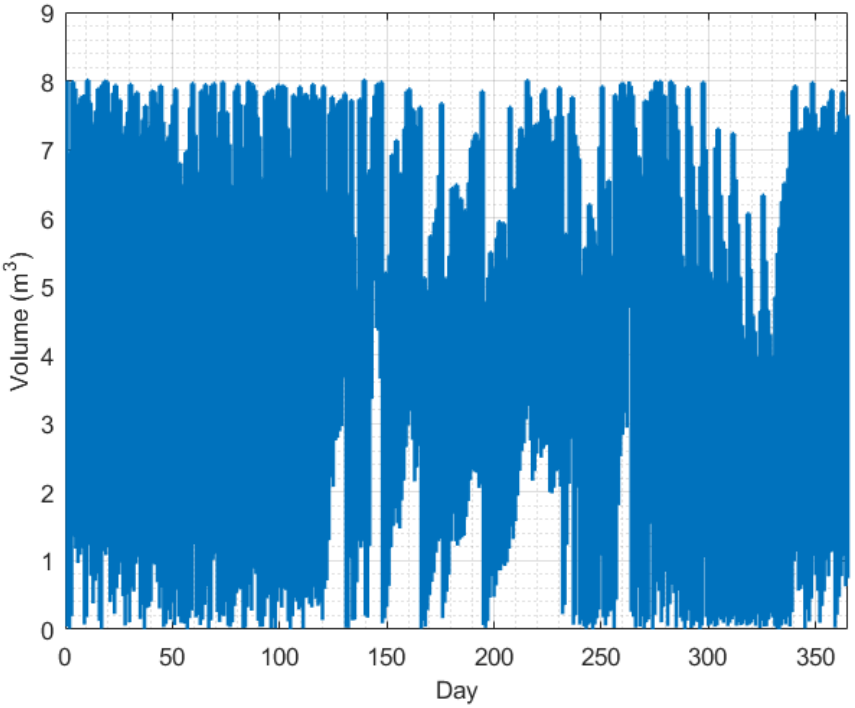

Figure 2.34: Daily cold water storage volume

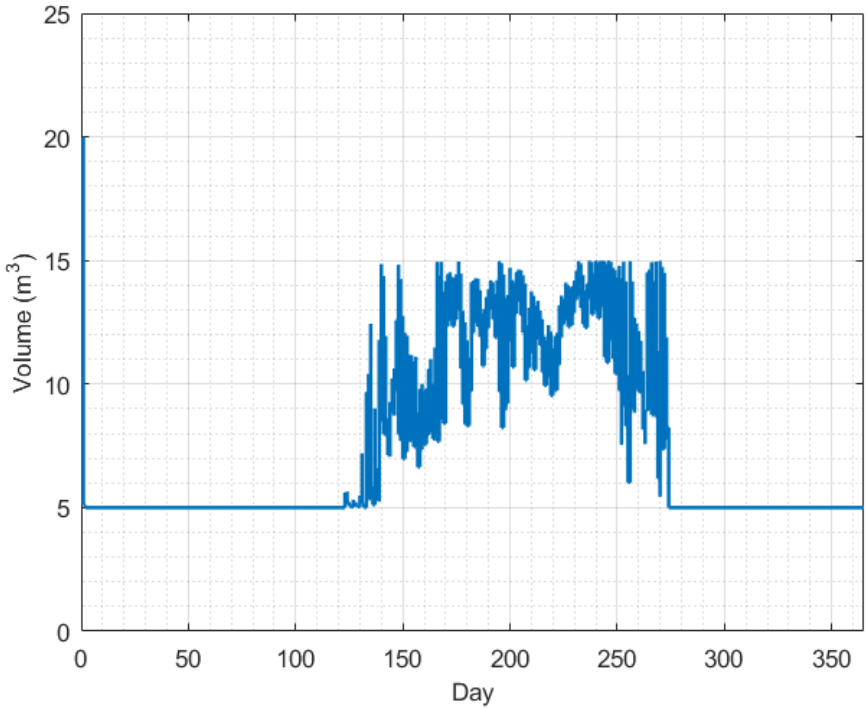

Figure 2.35: Daily cold water storage temperature

2.4.3 Parametric analysis

In order to analyze the upper results of the micro AA-CAES, nine indicators are defined in this chapter as follows:

- Electrical load management (E.L.M.):

$$E.L.M. = \frac{Min\,(R.E.,\ E.B.D.)\ +\ W_t}{Electrical\ total\ consumption} = 1 - \frac{(E_{GR-ST}\ +\ E_{ST-GR})}{Electrical\ total\ consumption} \tag{2.38}$$

- Electrical coverage ratio (E.C.R.):

$$E.C.R. = \frac{W_t}{Electrical\ total\ consumption} \tag{2.39}$$

- Hot coverage ratio (H.C.R.):

$$H.C.R. = \frac{Energy\ from\ hot\ water\ storage}{Hot\ energy\ building\ demand} \tag{2.40}$$

- Hot recovered (H.R.):

$$H.R. = \frac{Energy\ from\ hot\ water\ storage}{W_c} \tag{2.41}$$

- Cold coverage ratio (C.C.R.):

$$C.C.R. = \frac{Energy\ from\ cold\ water\ storage}{Cold\ energy\ building\ demand} \tag{2.42}$$

- Cold recovered (C.R.):

$$C.R. = \frac{Energy\ from\ cold\ water\ storage}{W_t} \tag{2.43}$$

- Total coverage ratio (T.C.R):

$$T.C.R. = \frac{W_t + Energy\ from\ (hot + cold)\ water\ storage}{(Electrical + Hot + Cold)\ total\ consumption} \tag{2.44}$$

- Electrical CAES efficiency (E.S.E.):

$$E.S.E. = \frac{W_t}{W_c} \tag{2.45}$$

- Trigeneration CAES system efficiency (T.S.E.):

$$T.S.E. = \frac{E_{ST-B} + Energy\ from\ (hot + cold)\ water\ storage}{W_c} \tag{2.46}$$

- Exergy trigeneration CAES system efficiency (E.T.S.E.):

$$E.T.S.E. = \frac{|E_{ST-BD} + \theta_{ho}Q_{ho} + \theta_{co}Q_{co}|}{W_c} \tag{2.47}$$

Where:

$$\theta_{ho} = (1 - \frac{T_{amb}}{T^{w}_{out,HE_c,i}}) \tag{2.48}$$

and

$$\theta_{co} = (1 - \frac{T_{amb}}{T^{w}_{out,HE_t,i}}) \tag{2.49}$$

and

$$Q_{ho} = Energy\ from\ hot\ water\ storage \tag{2.50}$$

$$Q_{co} = Energy\ from\ cold\ water\ storage \tag{2.51}$$

Table 2.3 shows the results of these indicators described above for the micro AA-CAES in the autonomous and the connected mode operation (Nice location).

Table 2.3: Parametric analysis results

	Autonomous mode	Connected mode
E.L.M.	63.9 %	75.9 %
E.C.R.	9.74 %	21.8 %
H.C.R	7.56 %	19.92 %
H.R.	22 %	19.41 %
C.C.R.	4 %	5 %
C.R.	14.59 %	5.55 %
T.C.R.	7.87 %	18.39 %
E.S.E.	28.22 %	34.61 %
T.S.E.	54.37 %	42.37 %
E.T.S.E.	31.66 %	37.54 %

In best energetic case configuration, micro AA-CAES system in the connected mode operation presents more advantages than the autonomous mode operation. This result is justify by the fact that the storage system is connected to the electrical grid meaning more air compression/expansion cycles. However, the electrical coverage ratio (E.C.R.) remains low in both modes (10.24 % and 22.3 %). This latter coverage ratio shows a fair agreement with the one resulted numerically by Simpore [46]. More air compression cycles led to an increase in the heat coverage ratio with the connected operation mode while the important air reservoir temperature limit the cold coverage ratio in both modes operation. Heat recovered (H.R.) and cold recovered (C.R.) show to be important in autonomous mode operation. The latter fact is due to the important increase of the total compression work (W_c) and total expansion work (W_t) compared to the increase of the hot/cold energy from hot/cold storage while switching from autonomous to connected mode operation.

2.4.4 Geographical scenario

Three different geographical locations of France (Figure 2.36) are chosen to be studied in this section in order to have a global view related to the micro AA-CAES behavior. Table 2.4 and Table 2.5 list the different parameters studied in section 3.4.3 (Parametric analysis).

Figure 2.36: Geographical locations considered for the study

Table 2.4: Parametric analysis results for Strasbourg location

	Autonomous mode	Connected mode
E.L.M.	50 %	69.5 %
E.C.R.	6.04 %	25.52 %
H.C.R	3.24 %	12.23 %
H.R.	22.64 %	22.93 %
C.C.R.	4 %	5 %
C.R.	10.06 %	2 %
T.C.R.	4.28 %	16.42 %
E.S.E.	25.71 %	42.08 %
T.S.E.	50.92 %	52.41 %
E.T.S.E.	29.15 %	45.44 %

Table 2.5: Parametric analysis results for Nantes location

	Autonomous mode	Connected mode
E.L.M.	54 %	71.2 %
E.C.R.	7.52 %	24.75 %
H.C.R	5.03 %	17.43 %
H.R.	23.72 %	21.69 %
C.C.R.	6 %	8 %
C.R.	8.02 %	2.55 %
T.C.R.	6.32 %	20.05 %
E.S.E.	27.21 %	34.29 %
T.S.E.	53.08 %	46.16 %
E.T.S.E.	30.79 %	37.49 %

Western France regions (example: Nantes) are characterized by oceanic climate defined by mild temperature and experience low rainfall. While in North East France regions (example: Strasbourg) the semi-continental climate is dominant where annual rainfall is relatively high. The rains are more important in summer, often stormy. This fact explains the higher numbers in Nantes case where more solar production over a year than Strasbourg.

2.5 Conclusion

In this chapter, a novel numerical micro AA-CAES model is proposed in order to satisfy electrical, building heating and cooling demands. Different design parameters are grouped and therefore an ideal prototype is proposed based on a global numerical sizing tool which in turn based on solving energy balance and heat transfer equations for each system components. Connected mode operation scores more advantages points than the autonomous mode operation in most of the energy and geographical scenarios. The thermal storage response is related to the compression/expansion cycles frequency and to the electrical system efficiency. The

trigeneration system efficiency is a compromise between electrical system efficiency, hot coverage ratio and cold coverage ratio.

Chapter 3 Quasi-isothermal air compressor and expander

The quasi-isothermal air compressor and expander technologies were investigated by many researchers in different specific fields in order to have higher system efficiency by reducing the compression work and increasing the expansion work. This chapter presents the numerical code of two new quasi-isothermal compressors and expanders developed by LightSail Energy and Enairys Powertech detailed in chapter 2. The regenerative air energy storage (RAES) system introduced by Light Sail Energy is based on advanced mechanical piston compressor/expander technology with water injection inside the cylinder chamber. Whereas Enairys Powertech technology presents multistage hydraulic gas quasi-isothermal compressor/expander systems.

Quasi-isothermal compressor/expander are desired for many applications that request high efficiency performance. Many concepts were proposed in order to improve multiple factors that have a big impact on the overall compressor/expander operation. High heat transfer was a must in order to achieve nearly isothermal air compression/expansion and to circumvent the reduction in efficiency. Water spray and liquid piston concepts were proposed, developed and completed by many researchers seeking to have the effective solution that can provide a high total surface area for heat transfer [47],[48],[49],[50],[51]. Herein, these published scientific works that are mostly similar to LightSail Energy and Enairys Powertech technologies development were used in this study to have a better understanding of different sizing parameters. In the following chapter, analytical simplified model simulations of mechanical piston compressor/expander with water injection (LightSail Energy technology) and liquid piston with integrated heat exchanger (Enairys Powertech technology) are completed to determine the main conditions required for high efficiency and the potential improvement in overall performance.

3.1 Numerical analysis of the mechanical piston compressor and expander with water injection

The main motivation for this work is to propose a simplified and an innovative numerical model based on physics equations in order to have a better understanding of the main sizing parameters for the concerned technology. As seen in Figure 3.1, the modelling of the quasi-isothermal compressor/expander is based on solving the principles of energy and mass conversation applied to the flows passing through the compressor/expander in a steady state: humid air at input temperature (T_{in}) and water in the form of droplets at input temperature (T_{in}^{w}). Humid Air is considered for all the parameters calculated in this chapter (temperature, pressure, mass, mass flow rate…) while the superscript "w" is written to indicate water as the working fluid.

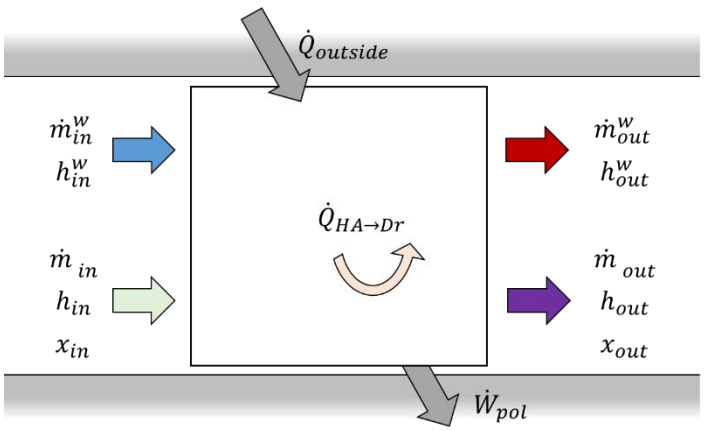

Figure 3.1: Conservation of energy for a steady-flow, open system

3.1.1 Numerical model assumptions

The following assumptions have been taken into account:

- Perfect gas is considered.
- Heat transfers between the compression/expansion chamber and the outside are taken into account using a single uniform wall temperature T_{wall}.
- Air compression phase is cooled by heating cold water droplets.
- Air expansion phase is heated by cooling hot water droplets.
- The compressor outlet air wet temperature is equal to that of the water. (see appendix B.1.1.)
- Mass exchange between air and injected water droplets during compression/expansion will be guided by the difference in water vapor pressure contained in the air and in the vicinity of the water droplets. (see appendix B.1.1.)B.1.1.
- Water is introduced into the compressor along with air in the form of incompressible droplets which heat up and vaporize.
- The kinetic energy of the air is neglected.

Figure 3.2 shows the PV diagram for the air compression and expansion cycles.

- Air suction (1→2) and compressed air introduction (1'→2') phases are considered to be an isobaric and an isothermal processes.
- Compressed air discharge (3→4) and expanded air discharge (4'→5') phases are considered to be also an isobaric and isothermal processes.
- An isochoric expansion (3'→4') is considered after the compressed air expansion phase (2'→3').

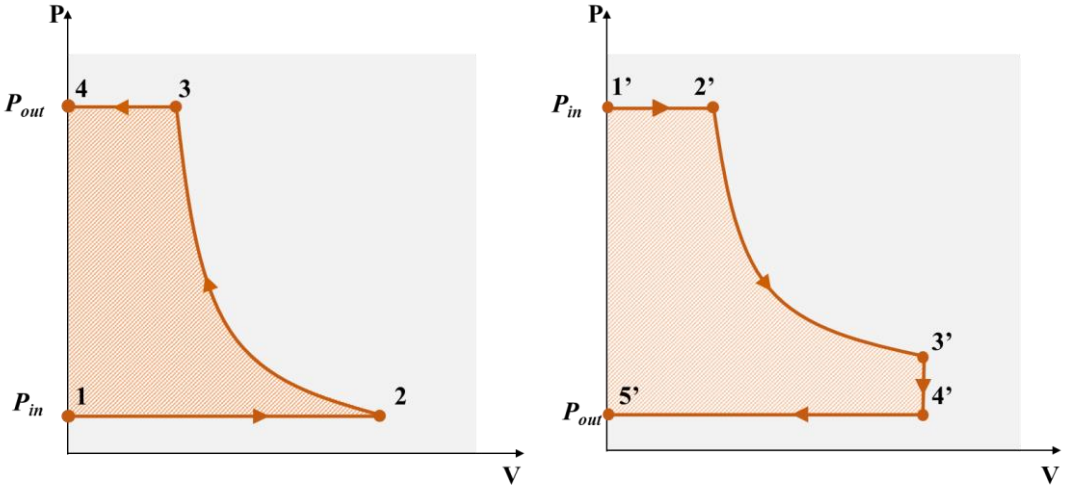

Figure 3.2: PV diagram of the air compression (left) and expansion (right) cycles

3.1.2 Analytical analysis of mechanical piston compressor with water injection

3.1.2.1 Air energy conservation

a) Energy conservation for humid air running through the compressor:

$$\dot{m}_{DA}(h_{out} - h_{in}) = \dot{m}_{DA}\frac{1}{\eta_{pol}}\frac{n_c}{n_c - 1}(P_{out}v_{out} - P_{in}v_{in}) - \dot{Q}_{HA\to Dr} + he_{wa}\,S_{wa}(T_{wa} - T_{av}) + \dot{m}_{DA}\,(x_{out} - x_{in})\,h_{va} \quad (3.1)$$

From above equation, $\dot{Q}_{HA\leftrightarrow Dr}$ is the thermal energy shared between the humid air and water droplets inside the mechanical cylinder chamber during the air compression phase. $\dot{m}_{DA}$ is the dry air mass flow rate entering and leaving the chamber at the respective enthalpies h_{in} and h_{out} and at respective absolute humidity x_{in} and x_{out}. Internal wall conductance is represented by $he_{wa}\,S_{wa}$ with internal wall temperature T_{wa} (This term is negligible if wall is considered as adiabatic). The average humid air temperature T_{av} is given by the following equation:

$$T_{av} = \frac{T_{out} + T_{in}}{2} \quad (3.2)$$

Specific enthalpy of humid air is described as follow:

$$h_{HA} = c_p T + h_{va}x \quad (3.3)$$

Where the specific enthalpy for the steam (or vapor) is shown in the equation below:

$$h_{va} = \Delta h_{lv} + c_{p,va}T \quad (3.4)$$

Δh_{lv} is the specific enthalpy of water vaporization at 0°C. The two enthalpy equations described above are used for air input and output of the compressor. Absolute humidity x of the humid air is a function of the temperature and of the air relative humidity at the compressor inlet. Considering the wet air temperature equal to that of water, the compressor outlet absolute humidity is obtained from the following:

$$x_{out} = d\frac{P_{SAT}^{wv}}{P_{out} - P_{SAT}^{wv}} \quad (3.5)$$

With *d* (equal to 0.62198) is the water vapor density (relative to the air). It should be mentioned that the "*SAT*" nomenclature does not refer to all the air particles founded in the cylinder chamber; In fact it refers to the air particles founded around the water droplet at the outlet of the compressor/expander. Therefore, the saturated water vapor pressure P_{SAT}^{wv} at temperature T is given by the following equation:

$$\ln(P_{SAT}^{wv}) = \frac{a_0}{T_{out}^{w}} + a_1 + a_2\, T_{out}^{w} + a_3 (T_{out}^{w})^2 + a_4 ln(T_{out}^{w}) \quad (3.6)$$

The a_i values are given in Table 3.1.

Table 3.1*:* Coefficients of correlation for the calculation of the saturation vapor pressure of water [52]

a_0 (K)	a_1	a_2(K^{-1})	a_3(K^{-2})	a_4
-6096.9385	21.2409642	-2.711 193x10^{-2}	1.673952x10^{-2}	2.433502

3.1.2.2 Air mass conservation

The dry air flow sucked by the compressor is deduced from the volumetric efficiency by:

$$\dot{m}_{DA} = \frac{\dot{V}_c}{v_{in}}\, \eta_{vo} \quad (3.7)$$

With $\dot{V}_c$ volumetric flow generated (product of displacement by the rotation speed for a piston compressor) and η_{vo} the volumetric efficiency.

3.1.2.3 Water energy conservation

$$\dot{m}_{out}^{w}\, h_{out}^{w} - \dot{m}_{in}^{w}\, h_{in}^{w} = \dot{Q}_{HA\leftrightarrow Dr} - \dot{m}_{DA}\, (x_{out} - x_{in})\, (h_{va}) \quad (3.8)$$

where $\dot{m}_{out}^{w}$ and $\dot{m}_{in}^{w}$ the outlet and inlet flow rates of the water droplets with respective specific enthalpies h_{out}^{w} and h_{in}^{w}.

3.1.2.4 Water mass conservation

$$\dot{m}_{in}^{w} = \rho^{w}\, \dot{nu}_{Dr}\, \frac{4}{3}\pi\, (ra_{Dr})_{in}^{3} = \dot{m}_{DA}\, (x_{out} - x_{in}) + \dot{m}_{out}^{w} \quad (3.9)$$

where $\dot{nu}_{Dr}$ is the number of water droplets per second, ρ^{w} is the water density and ra_{Dr} is the droplet radius.

$$\dot{m}_{out}^{w} = \rho^{w}\, \dot{nu}_{Dr}\, \frac{4}{3}\pi\, (ra_{Dr})_{out}^{3} \quad (3.10)$$

3.1.2.5 Complementary equations

The heat transfer exchanged between water and humid air is given by the following equation:

$$\dot{Q}_{HA\rightarrow Dr} = he\; 4\,\pi (ra_{Dr})_{av}^{2}\, nu_{Dr} (T_{av} - T_{av}^{w}) \quad (3.11)$$

where T_{av}, T_{av}^{w} are the humid air and water average temperature and $(ra_{Dr})_{av}$ is the droplet average radius. The heat transfer coefficient was studied numerically and measured experimentally by many researchers. Most of the water spray injection numerical models used

the Ranz-Marshall correlation which indicated convective heat transfer for spheres as Qin and Loth [48] and Odukomaiya [50] did in their works. The range of heat transfer coefficient applied in this study is however based on an experimental work conducted by Guanwei [49] where a transient temperature measurement method was developed to investigate the heat transfer behavior while cooling the air by injecting water spray. Based on the measurements carried out by Guanwei [49], the value of the heat transfer coefficient is in the range of 10 $W.m^{-2}.K^{-1}$ - 120 $W.m^{-2}.K^{-1}$. Furthermore the water droplet number is expressed as follows:

$$nu_{Dr} = \dot{n}u_{Dr}\, t_{ST} \tag{3.12}$$

t_{st} is the water droplets residence time in the compressor chamber during air compression phase which will depend on the rotation speed (among other parameters). It is also necessary to write the energy conservation for the compressor wall as the following (wall conduction neglected due to the assumption of low wall thermal resistance with respect to the thermal resistance between the ambient air and the outer wall of the compressor):

$$\begin{aligned} \dot{Q}_{conduction} = -he_{wa} S_{wa}\,(T_{wa} - T_{av}) + \\ he_{outside}\, S_{outside}\,(T_{\infty} - T_{wa}) = 0 \end{aligned} \tag{3.13}$$

Where $he_{outside}\, s_{outside}$ is the external conductance of the compressor and T_{∞} is the external temperature. With this latter equation, the outside heat transfer rate can be expressed as follows:

$$\dot{Q}_{outside} = he_{wa} S_{wa}\,(T_{wa} - T_{av}) = KS\,(T_{\infty} - T_{av}) \tag{3.14}$$

With *KS* the global conductance ($KS = [1/(he_{wa}S_{wa}) + 1/(he_{outside}\, S_{outside})]^{-1}$).

Equation (3.1) becomes:

$$\begin{aligned} \dot{m}_{DA}(h_{out} - h_{in}) \\ = \dot{W}_{real} - \dot{Q}_{HA\to Dr} + \dot{m}_{DA}\,(x_{out} - x_{in})\, h_{va} + \dot{Q}_{outside} \end{aligned} \tag{3.15}$$

With the total polytropic work rate:

$$\dot{W}_{real} = \dot{m}_{DA} \frac{1}{\eta_{pol}} \frac{n_c}{n_c - 1} (P_{out} v_{out} - P_{in} v_{in}) \tag{3.16}$$

Using the definition of polytropic process:

$$P_{in} v_{in}^{n_c} = P_{out} v_{out}^{n_c} \tag{3.17}$$

Finally, the use of the equation of state for humid air at the compressor inlet and outlet is a must:

$$P_{in/out} v_{in/out} = \left(r + x_{in/out} r^{w}\right) T_{in/out} \tag{3.18}$$

$r\ et\ r^{w}$ are the air and water vapor gas constant respectively (r = 287.05 J.kg^{-1}.K^{-1} and r^{w} = 461.52 J.kg^{-1}.K^{-1})

3.1.3 Analytical analysis of mechanical piston expander with water injection

The analytical model of the mechanical piston expander with water injection is similar to the compressor model detailed above. Based on the assumption regarding the isochoric expansion, multiple different equations are added in the section below in order to build the expander model.

In the expander case, Eq. (3.1) that presents the energy conservation for humid air running through the compressor, is as follows (see appendix B.1.2.):

$$\dot{m}_{DA}(h_{out} - h_{in}) = \left[\frac{1}{n_t - 1}\left(\eta_{pol}\right)(P_{in} V_{2'})[(VR)^{n_t - 1} - 1] + P_{out} V_{4'} - P_{in} V_{2'}\right] {}^{1}\!/_{\Delta t_{cy}} - \dot{Q}_{HA \to Dr} + he_{wa}\, S_{wa}(T_{wa} - T_{av}) + \dot{m}_{DA}(x_{out} - x_{in})\, h_{va} \tag{3.19}$$

From above equation, VR is the volume ratio ($\frac{V_{2'}}{V_{3'}}$), Δt_{cy} is the time needed to expand the compressed air and the rest of the variables are the same used as in Eq. (3.1). The air temperature at state 3' is calculated from the following equation:

$$T_{3'} = T_{in} VR^{(n_t - 1)} \tag{3.20}$$

At state 3', the air pressure is given by the ideal gas formula:

$$P_{3'} = P_{in} VR^{(n_t)} \tag{3.21}$$

Since the expanded air discharge phase (4'→5') is isothermal, therefore the outlet air temperature is equal to the following:

$$T_{out} = T_{4'} = T_{3'}\left(\frac{P_{out}}{P_{3'}}\right) \tag{3.22}$$

The compressed air mass flow rate introduced into the expander, is a function of the volume ratio (VR) as described in the following equation:

$$\dot{m}_{DA} = VR \frac{\dot{V}_c}{v_{in}} \eta_{vol} \tag{3.23}$$

3.1.4 Numerical resolution of the mechanical piston compressor and expander

Both numerical models coded in MATLAB are based on multiple iterative loops and multiple convergence conditions. Three iterative loops are used for each model where polytropic index, outlet absolute humidity and outlet water temperature are chosen to be the convergence parameters. For compressor and expander the conditions are described below:

First condition (A) is related to the polytropic index, where it is initialized in the beginning and then corrected (n_c^*) using Eq. (3.16). At the end of the initial loop, condition (A) is verified:

$$\left|\frac{n_c^* - n_c}{n_c}\right| > 0.001 \tag{3.24}$$

If condition (A) is true, therefore $n_c = \max(n_c^*, n_c^{**})$ where:

$$n_c^{**} = \left(1 - \frac{ln\frac{T_{out}^w}{T_{in}}}{ln\frac{P_{out}}{P_{in}}}\right)^{-1} \tag{3.25}$$

If condition (A) is false, the loop is ended.

Second condition (B) focuses on average water temperature and outlet absolute humidity. Both variables are initialized in the beginning and then corrected ($(T_{av}^w)^*; x_{out}^*$) using Eq.(3.9) and Eq.(3.5) respectively. The two sub conditions are the following:

$$(T_{av}^w)^* - T_{av}^w > 0.001 \tag{3.26}$$

If above condition is true, therefore: $T_{av}^w = (T_{av}^w)^*$. In case it is not true, the numerical code will exit the loop to go through the next sub condition (Eq. (3.27)).If the latter equation is correct, then: $x_{out} = x_{out}^*$.

$$\left|\frac{x_{out}^* - x_{out}}{x_{out}}\right| > 0.001 \tag{3.27}$$

In the case of Eq. (3.27) is not satisfied, the numerical compressor code is ended Figure 3.3 and Figure 3.4 show the flow charts of the compressor and expander numerical codes. The meaning of the geometric form of the flow chart is as follows: the circle symbol means a variable, double circles symbol defines an initialized variable, the square symbol refers to a constant and the diamond symbol stands for the convergence condition.

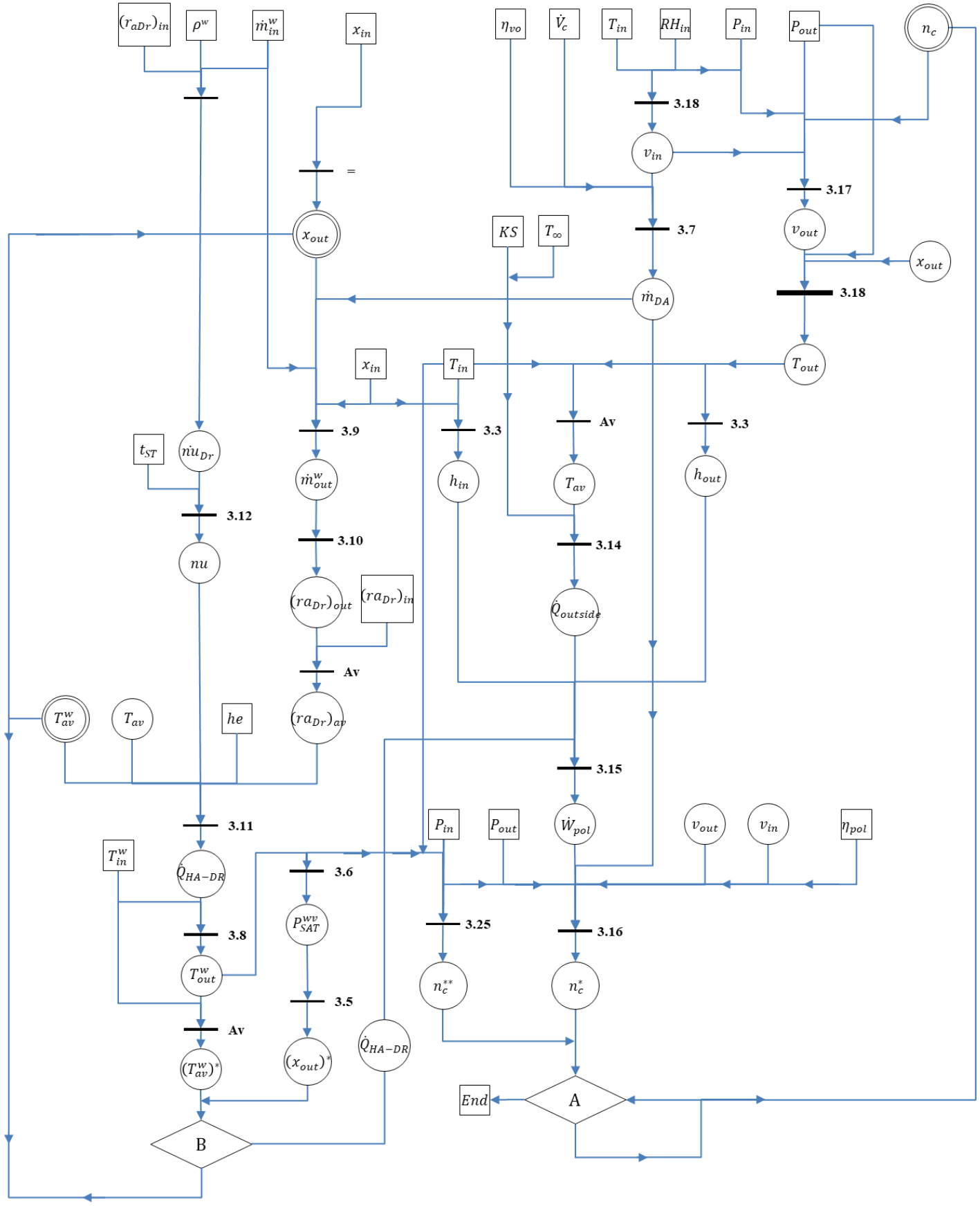

Figure 3.3: Classical piston compressor numerical code flow chart

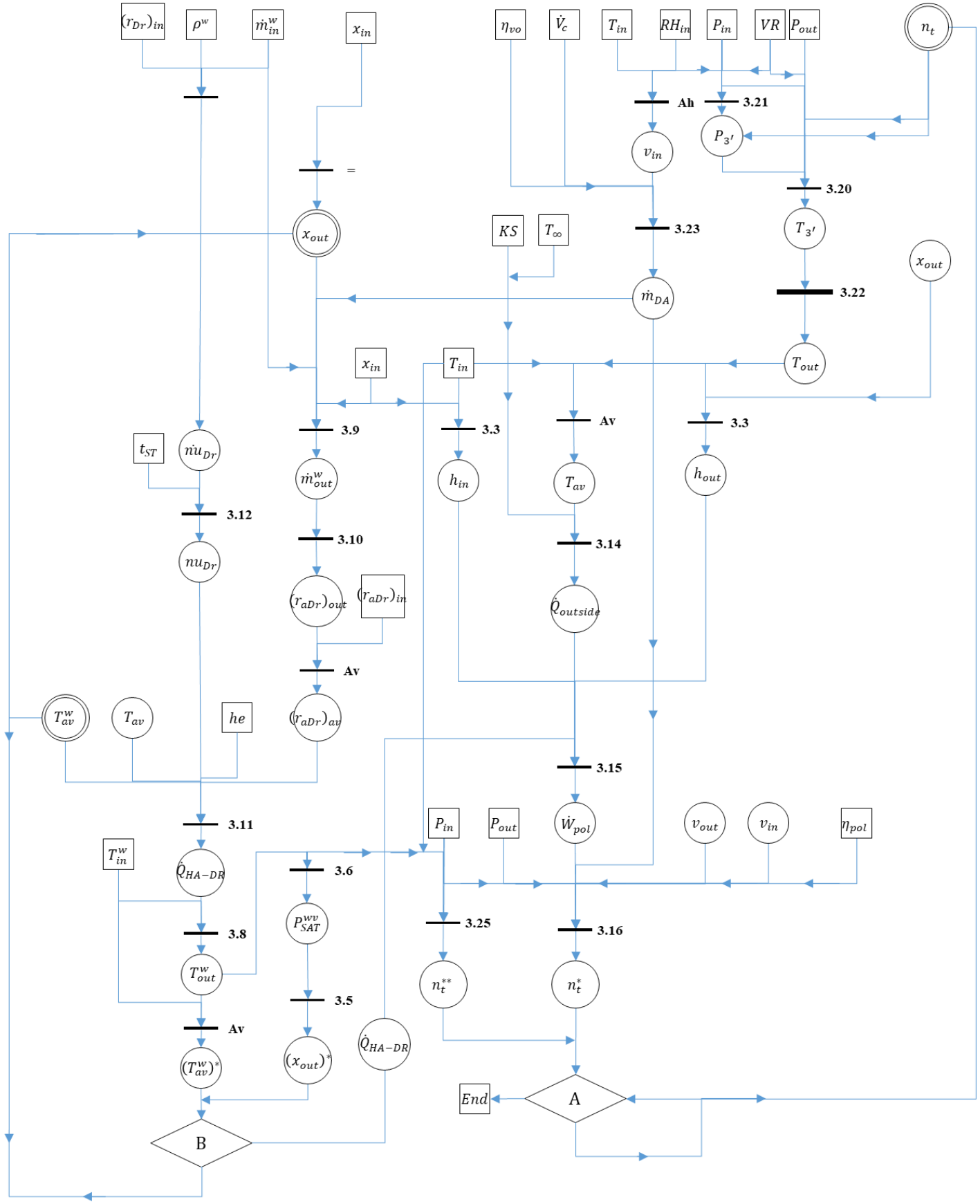

Figure 3.4: Classical piston expander numerical code flow chart

3.1.5 Results and discussion

The compressor and expander numerical model explained in the section above are considered for a specific architecture composed of three stage air compressors/expanders in order to underline the influence of design parameters such as heat transfer coefficient, mass loading (the mass of water spray over the mass of sucked air), droplet diameter and cooling method (during air compression) and heating method (during air expansion).

3.1.5.1 Mechanical piston air compressor

The mechanical piston compressor numerical model consists of modeling three air stage compressors described with the fixed and initialized inputs in the table below:

Table 3.2: Numerical compressor model inputs

	Low pressure	Middle pressure	High pressure
Pressure range (bar)	1 → 6	6 → 36	36 → 216
Inlet air temperature (°C)	20	Outlet 1st comp.	Outlet 2nd comp.
Inlet water temperature (°C) (series cooling case)	10	Outlet 1st comp.	Outlet 2nd comp.
Inlet water temperature (°C) (parallel cooling case)	10	10	10
Inlet absolute air humidity ($g_{water}/kg_{dry\ air}$)	8.9	Output first stage absolute air humidity	Output second stage absolute air humidity
Inlet air mass flow rate (kg/s)	0.01744	0.01744	0.01744
Inlet water mass flow rate(kg/s)	0.0872	0.0872	0.0872
Polytropic efficiency	0.8	0.8	0.8
Inlet water droplet radius (μm)	16	16	16
Infinite air temperature (°C)	20	20	20
Residence time of the droplets in the cylinder (s)	0.02	0.02	0.02
Global conductance	5	5	5
Initialized variables			
Polytropic index	1.10	1.10	1.10
Average water temperature (°C)	25	25	25

Outlet absolute humidity ($g_{water}/kg_{dry\ air}$)	8.9	8.9	8.9

First, the parallel cooling mode is considered for the three stage air compressors. As a matter of fact, the cold water is injected separately in each of the three cylinders with the same inlet water temperature (10 °C). The evolution of the air/water temperature, total work rate, total heat transfer described in Eq. (3.11), outlet absolute humidity, polytropic index and isothermal efficiency are plotted versus the heat transfer coefficient as seen in Figure 3.5, Figure 3.6 and Figure 3.7. It can be noticed from Figure 3.5 that for a fixed droplet diameter (16 µm) and mass loading (ML = 5), the outlet air temperatures for the three compressors decrease with the increase of the heat transfer coefficient. In fact this air temperature drop justifies the increase of the outlet water temperature of each compressor (Figure 3.6). For instance, for 100 W/m^2.K, the water injected in the third compressor at 10 °C, left it with the highest outlet water temperature of 23.52 °C (a difference of 13.52 °C). It should also be pointed out that after 400 W/m^2.K - 450 W/m^2.K, the outlet air/water compressor temperature remains relatively constant.

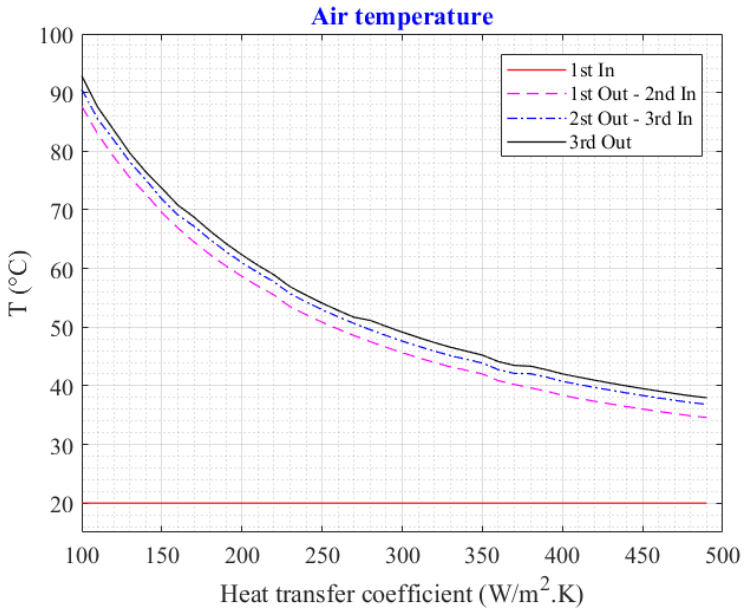

Figure 3.5: Air temperature going through the three air stage compressors in function of heat transfer coefficient

Figure 3.7 confirms the relationship between the total work rate and the total heat transfer rate expressed in Eq. (3.11) and in Eq. (3.16). After 150 W/m^2.K the heat transfer coefficient impact on work rate and heat transfer variable is negligible. It is also noticed from Figure 3.7 that the compression of the humid air inside each cylinder leads to a less humid compressed air at the outlet compressor.

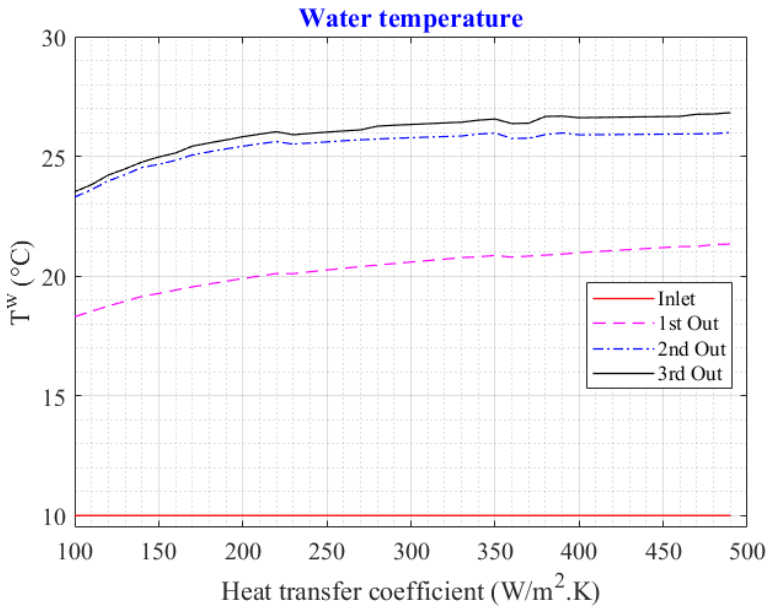

Figure 3.6: Water temperature going through the three air stage compressors in function of heat transfer coefficient

This fact is seen clearly during the first compression process with the huge decrease of the air humidity where at 100 W/m^2.K the absolute humidity drops from 8.9 g $_{water}$/kg $_{dry\ air}$ to 2.18 g $_{water}$/kg $_{dry\ air}$. This humidity drop explains the important rise in air temperature for the first air compression stage (see Eq. (3.18)). In fact, from Eq. (3.5) and Eq. (3.6), it can be seen that the outlet water compressor temperature (T_{out}^w) and the saturated water vapor pressure (P_0^w) are inversely proportional to the absolute humidity (x_{out}). This explains the low increase of the absolute humidity with the increase of the heat transfer coefficient which induces enhance in compressor outlet water temperature. By the increase of the heat transfer coefficient, the outlet air compressor temperature as well the polytropic index decrease as seen in Figure 3.7. This latter observation can be deduced from Eq. (3.17) and Eq. (3.18). The isothermal efficiency is defined as the real compression work divided by the isothermal work. The increase of heat transfer coefficient leads to an increase of compensated total work rate which reduces the isothermal efficiency as noticed in Figure 3.7.

Second, the series cooling method effect is next investigated while varying the heat transfer coefficient and fixing the droplet diameter (16 µm) with the mass loading (ML= 5).

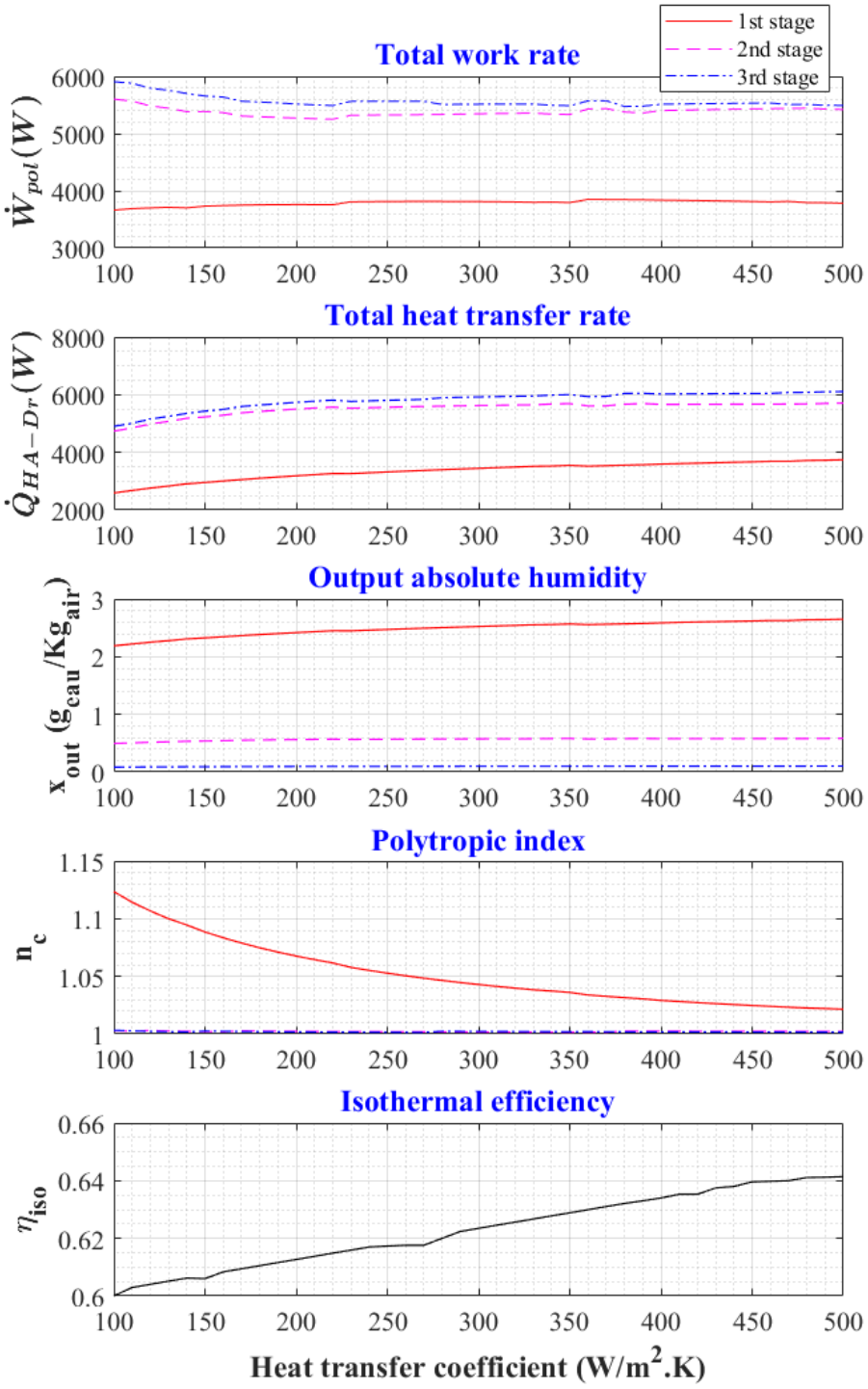

Figure 3.7: Several outlet parameters as function of the heat transfer coefficient. The legend of the first figure at the top has to be considered for the other figures below

In this cooling method the cold water is injected in the first cylinder to absorb the heat released during the first stage air compression. At the outlet of that cylinder, warm water resulted is collected in order to be injected in the second and later on in the third cylinder. As can be

observed from Figure 3.9, the outlet water compressor temperatures score higher values than the temperatures resulted with the parallel cooling method. At 100 W/m^2.K, water enters the first compressor at 10 °C and leaves the third one with a temperature of 40.66 °C. This warmer water has a negative on the air cooling effect while increasing the heat transfer coefficient (see Figure 3.8). The responses of air/temperature, total work/heat transfer rate, polytropic index and isothermal efficiency while varying the heat transfer coefficient are similar to the one of the parallel cooling method studied above.

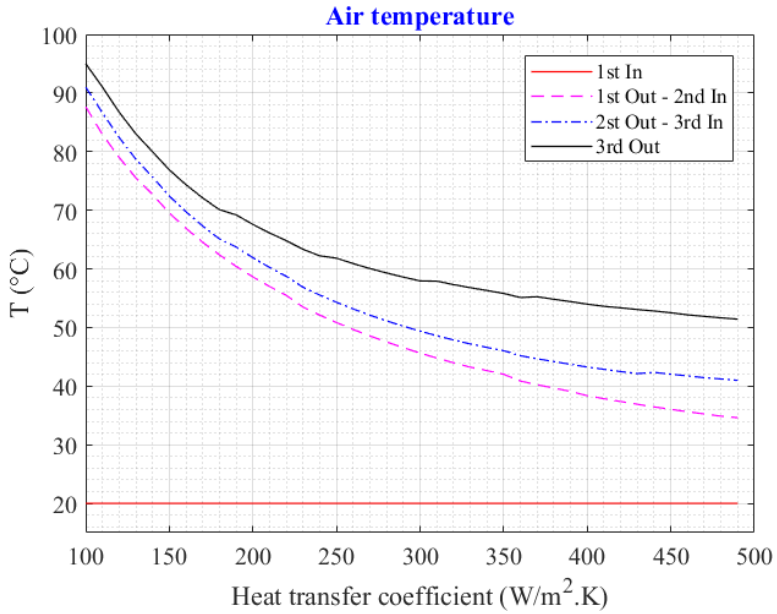

Figure 3.8: Air temperature as a function of the heat transfer coefficient (compressor series cooling)

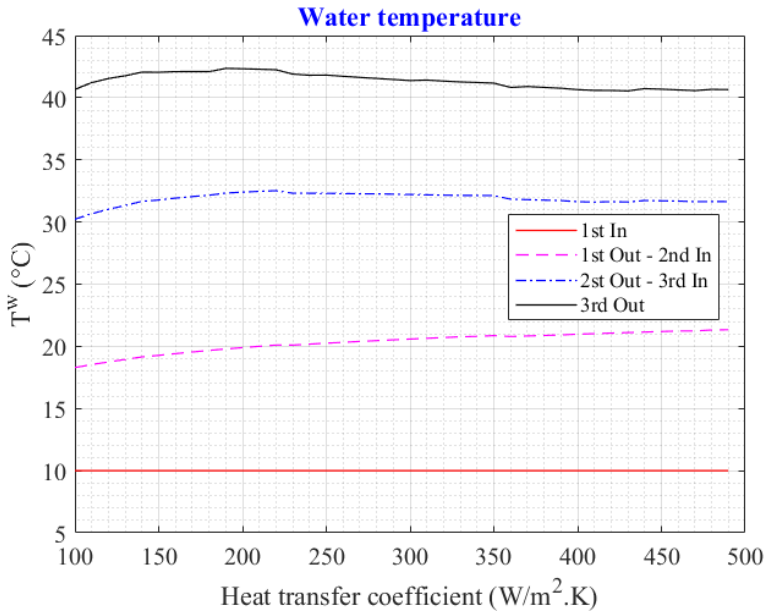

Figure 3.9: Water temperature as a function of heat transfer coefficient (compressors series cooling)

The water droplet size influence is next investigated with a fixed heat transfer coefficient (400 W/m^2.K), fixed mass loading (ML = 5) and the assumption of parallel cooling method. The droplet diameter range (16 µm – 36 µm) used in this analysis is similar to the one used in Qin and Loth work [48] which is reasonably achievable by most spray nozzles. Figure 3.10 and Figure 3.11 show the air/water temperatures for varying the droplet diameters from 16 µm to 36 µm. The result is a lower injected surface area as droplet diameter increases. Conversely, the performance of small droplets, such as 16 µm, is more encouraging and toward isothermal process. These results show a perfect match with the experimental work done by Qin and Loth [48] where they investigated the efficiency of the air compression with the water injection.

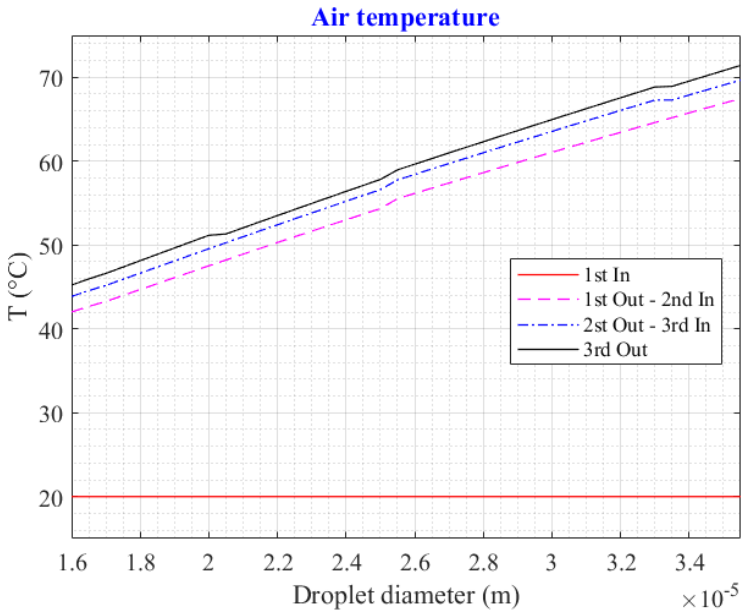

Figure 3.10: Air temperature in function of water droplet diameter

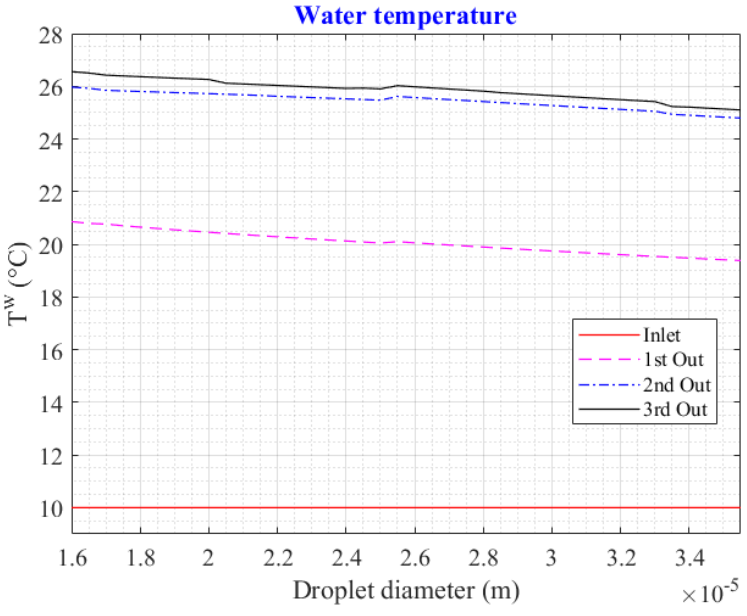

Figure 3.11: Water temperature in function of water droplet diameter

The mass loading variation impact for a fixed heat transfer coefficient (400 W/m^2.K) and droplet diameter (16 µm) is seen in Figure 3.12 and Figure 3.13. The higher the water mass flow rate the lower the compressor outlet air/water temperature and the closer to an isothermal air compression process. This fact was also observed by Qin and Loth in their investigation of the droplet spray solution for achieving high heat transfer during air compression using a sinusoidally driven piston in a 5 kW first-stage cylinder with various compression ratios [48].

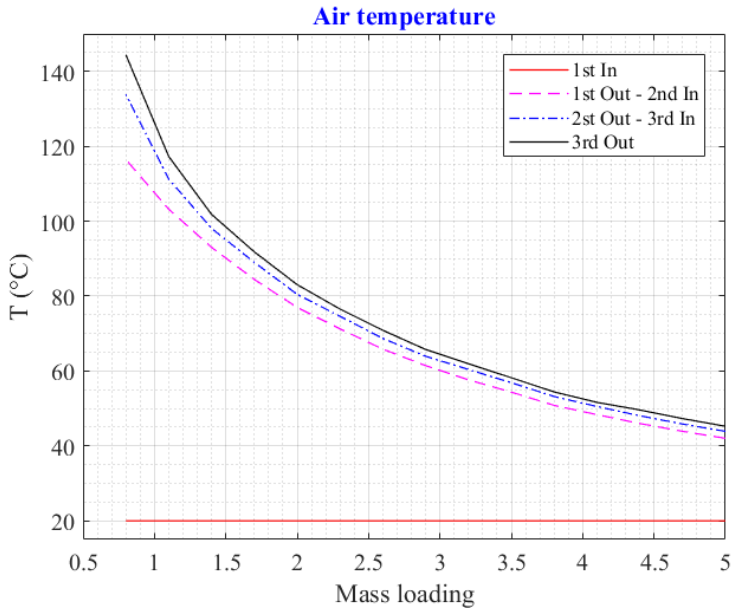

Figure 3.12: Air temperature in function of mass loading

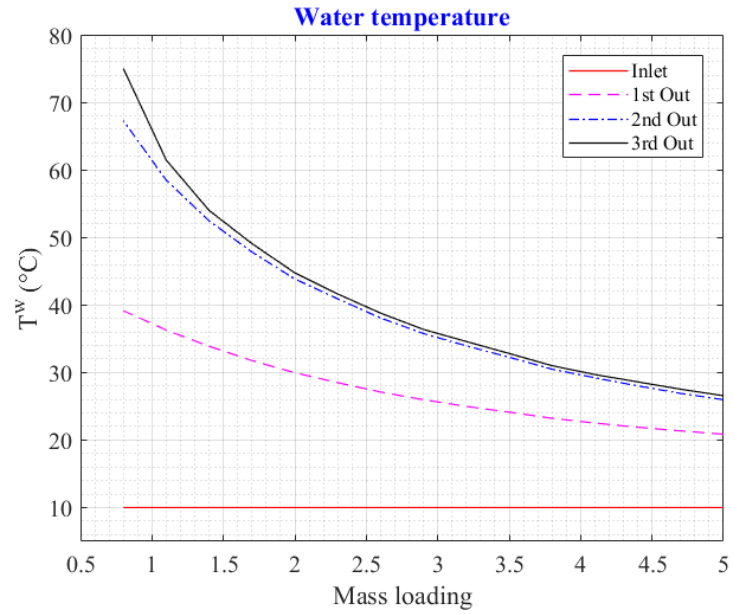

Figure 3.13: Water temperature in function of mass loading

3.1.5.2 Mechanical piston air expander

The fixed input parameters showed in Table 3.2 are similar for the expander numerical model. In this case, compressed air stored at 216 bar with a temperature of 20°C is expanded through three air expanders (216 bar →1 bar). Table 3.3 lists the expander fixed inputs dissimilar to those of the compressor model:

Table 3.3: Numerical expander model inputs

	High pressure	Middle pressure	Low pressure
Inlet air temperature (°C)	20	Outlet 1st comp	Outlet 2nd comp
Inlet water temperature (°C) (series cooling case)	60	Outlet 1st comp	Outlet 2nd comp
Inlet water temperature (°C) (parallel cooling case)	60	60	60
Initialized variables			
Polytropic index	1.10	1.10	1.10
Average water temperature (°C)	40	40	40
Outlet absolute humidity ($g_{water}/kg_{dry\ air}$)	8.9	8.9	8.9

Similar to the compressor model analysis, the parallel heating mode is first investigated for the three stage air expanders. In this case, hot water is injected separately in each of the three expanders with the same inlet water temperature (60 °C) in order to preheat the compressed air before expanding process. Fixing droplet diameter (16 μm) and mass loading (ML= 5), Figure 3.14 shows that the outlet air temperatures for the three expanders increase with the increase of the heat transfer coefficient. This fact indicates that the more air/water heat transfer, the higher air temperature and the lower water temperature leaving the expander (Figure 3.15). Figure 3.16 shows a coherent results of the total work rate, heat transfer rate, absolute humidity and polytropic index. In fact, the most total work rate recovered is during the first air stage expander where the air temperature difference is small. It should also be pointed that the outlet absolute humidity is increasing while passing through expander stages. This fact is explained by the relation between the absolute humidity and the outlet air pressure described in Eq. (3.5). In fact, it was noticed that the outlet air pressure has more impact on the absolute humidity than the water saturation vapor pressure and the outlet water temperature.

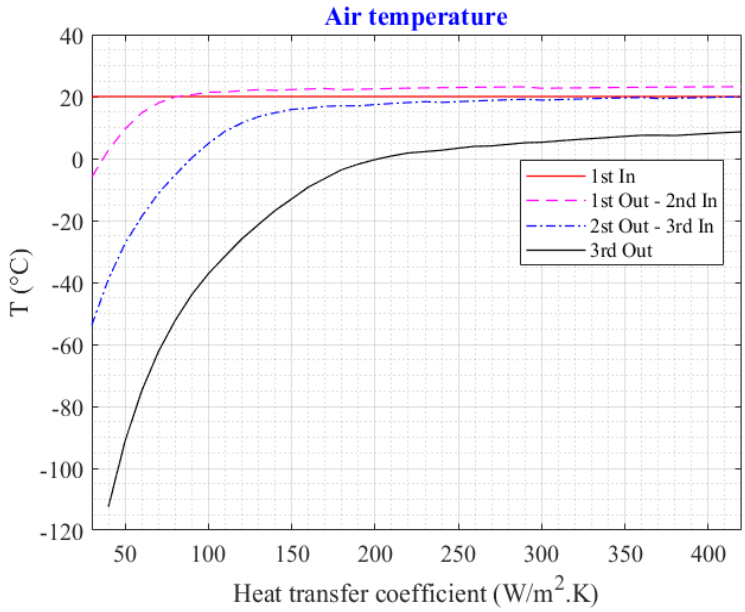

Figure 3.14: Air temperature going through the three air stage expanders in function of heat transfer coefficient

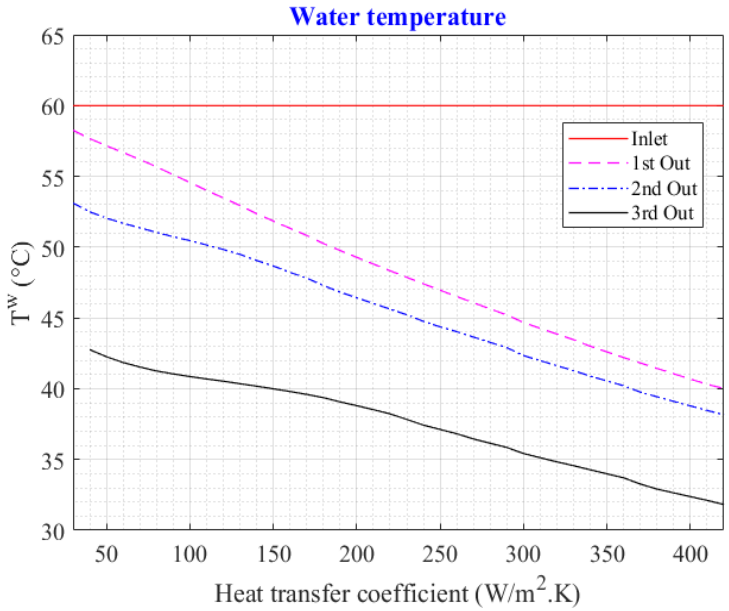

Figure 3.15: Water temperature going through the three air stage expander in function of heat transfer coefficient

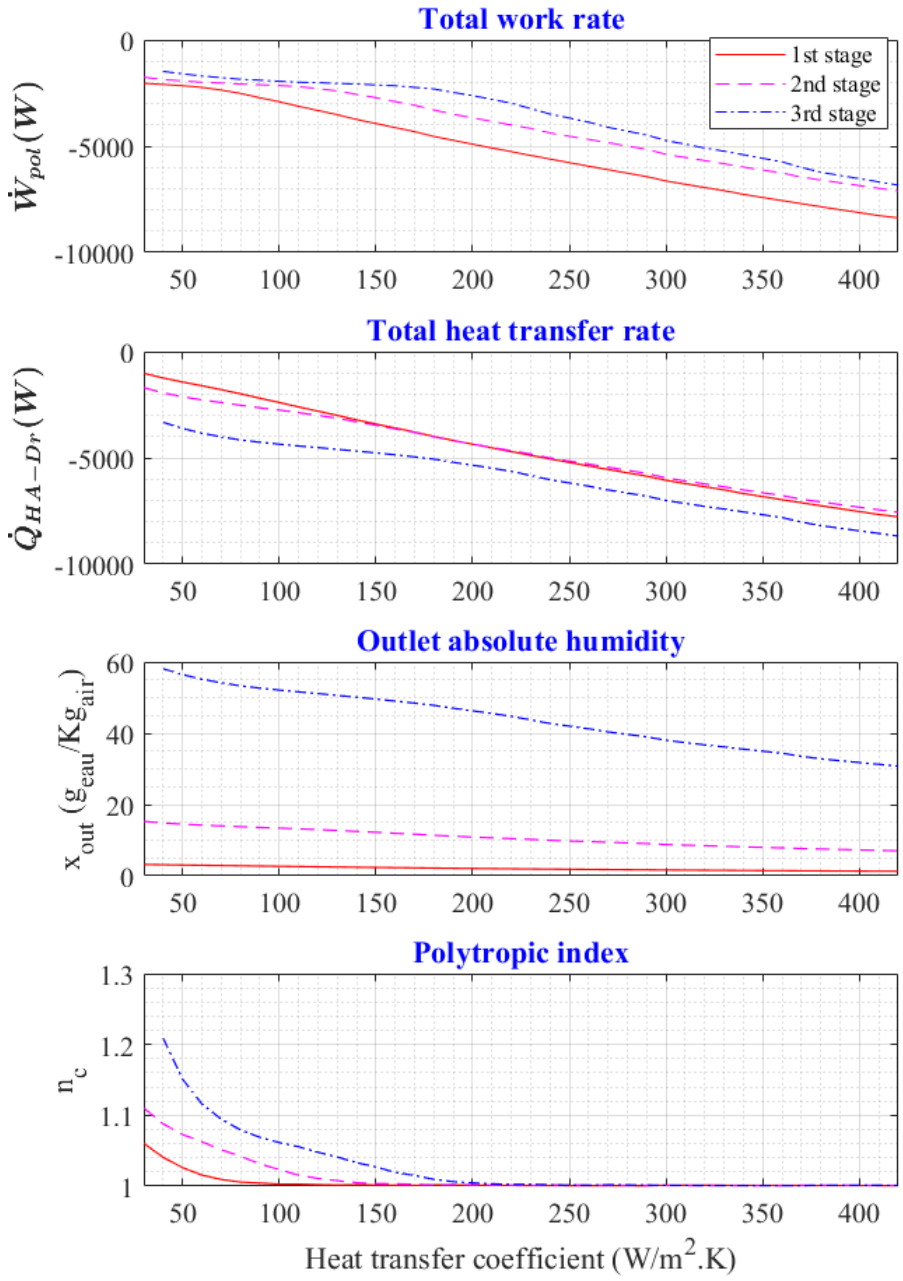

Figure 3.16: Several outlet parameters in function of the heat transfer coefficient. The legend of the first figure at the top has to be considered for the other figures below

Second investigation concerns the expander series heating method as seen in Figure 3.17 and Figure 3.18. Similar to the compressor series cooling model, the water collected after each expander stage is injected for the next one. The result shows that applying this heating method helps the air at the outlet of the expander to be warmer than the parallel heating method especially for the third air stage expander. It can be noticed from Figure 3.18 that water reaches lower temperatures than the previous case and therefore pushing the air to be warmer.

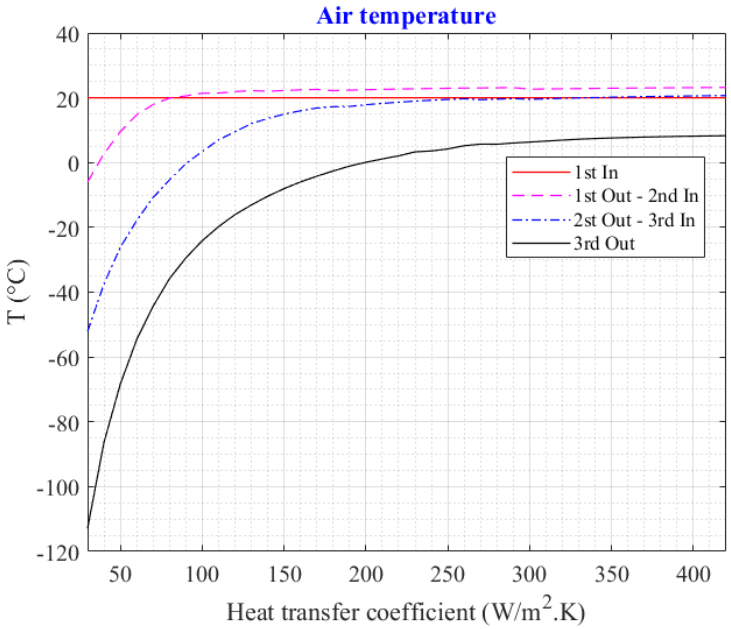

Figure 3.17: Air temperature in function of the heat transfer coefficient (expanders series heating)

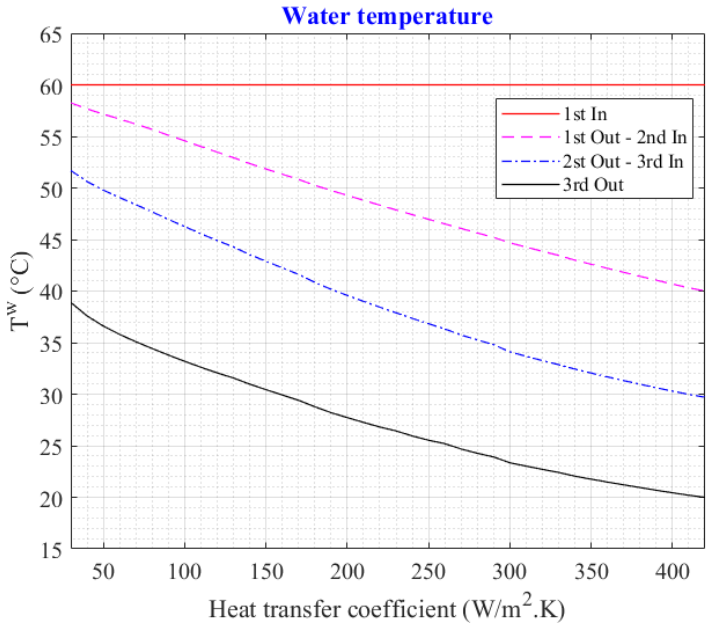

Figure 3.18: Water temperature in function of heat transfer coefficient (expanders series heating)

Third case study is focusing on the influence of the droplet diameter on the air and water temperature going through the three air stage expanders as seen in Figure 3.19 and Figure 3.20. For a fixed heat transfer coefficient (250 W/m^2.K) and mass loading (ML= 5), the increase of the droplet diameter shows a significant decrease of the air temperature especially for the second and third air stage expander while an increase of the water temperature is noticed. As a matter of fact, the increase of the droplet diameter implies a decrease of the droplet numbers injected in the expander which will decrease the air/water heat transfer (see Eq. (3.9)).

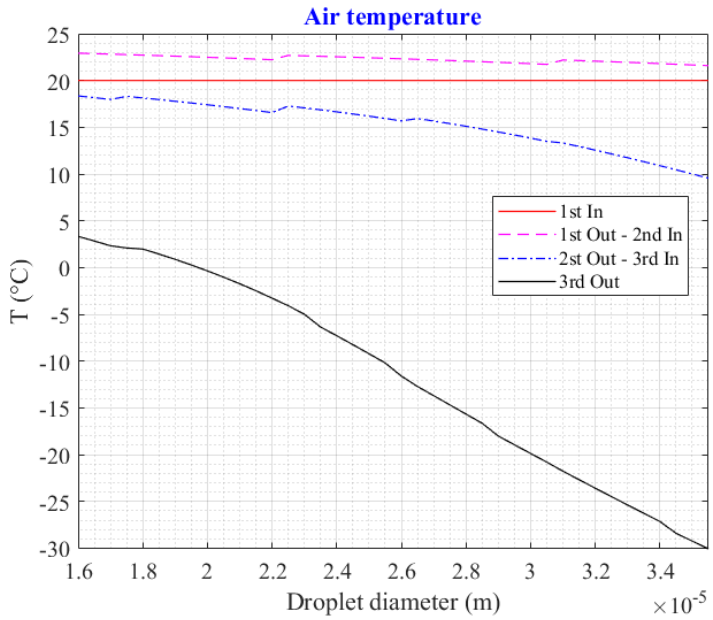

Figure 3.19: Air temperature in function of water droplet diameter

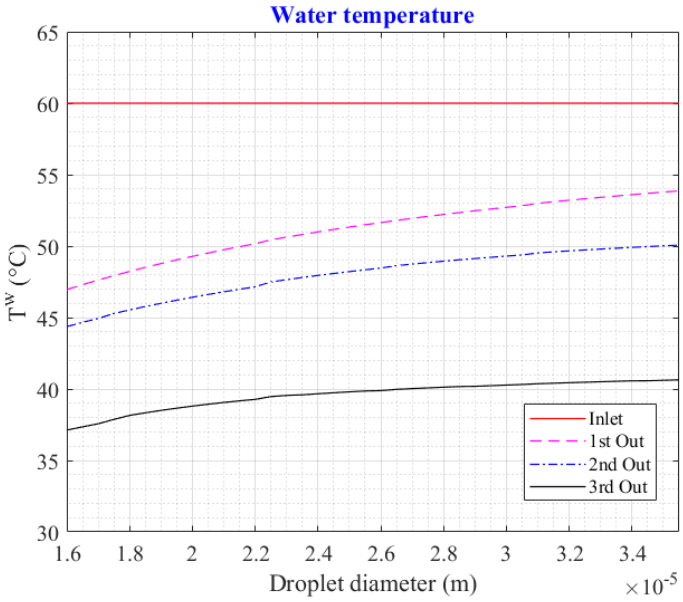

Figure 3.20: Water temperature in function of water droplet diameter

The mass loading variation impact for a fixed heat transfer coefficient (250 W/m^2.K) and droplet diameter (16 µm) is presented in Figure 3.21 and Figure 3.22. The higher the water mass flow rate the higher the expander outlet air/water temperature. Equations Eq. (3.5) (3.9) (3.18) justify the relations between the outlet water temperature, absolute humidity and the outlet air temperature.

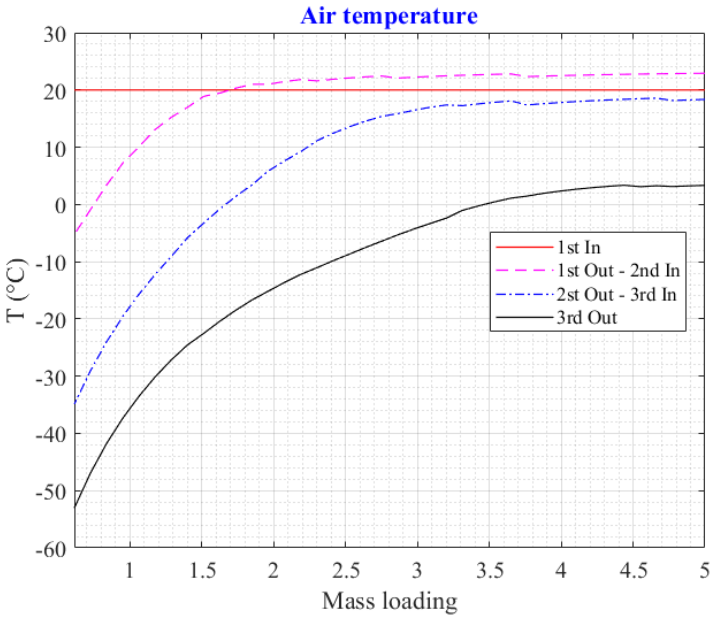

Figure 3.21: Air temperature in function of mass loading

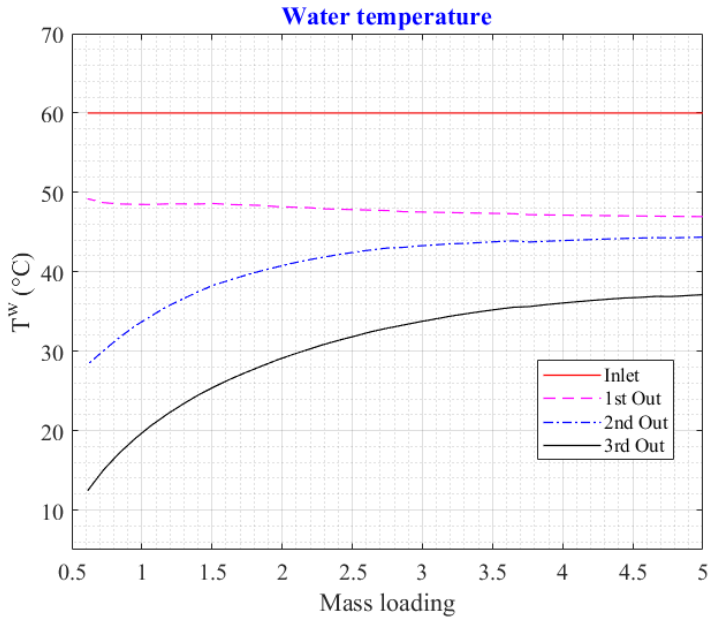

Figure 3.22: Water temperature in function of mass loading

3.2 Numerical analysis of the liquid piston compressor and expander with integrated heat exchanger

In order to simulate liquid piston air compression and air expansion developed by Enairys Powertech, a numerical code was developed in MATLAB that presents iterative calculations based on the principles of energy and mass conservation and heat transfer equation (described in the section below). The core of the numerical code is based on two main iterative loops using the compressor/expander outlet water temperature ($T_{F^-}^{w}$, $T_{G'_{Po}}^{w}$) and the air temperature at the end of the compression/expansion phase ($T_{C_{Po}}, T_{C'_{Po}}$) as convergence parameters (Figure 3.23). Dichotomy method is used specially for the air temperature at the end of the compression/expansion phase calculation where it is limited between the air temperature at the beginning of the compression phase (T_B)/expansion phase ($T_{B'}$) and the adiabatic air temperature at the end of the compression phase (T_{C_A})/expansion phase ($T_{C'_A}$). Air is considered for all the parameters calculated in this chapter (temperature, pressure, mass, mass flow rate,…) while the superscript "w" is written to indicate water as working fluid.

3.2.1 Numerical model assumptions

The following assumptions have been taken into account:

- Perfect gas is considered.
- Air compression phase is cooled by heating the water tubes inside the chamber.
- Inlet water mass flow rate introduced into the liquid piston chamber is equal to outlet mass flow rate leaving the chamber ($\dot{m}_{in}^{w} = \dot{m}_{out}^{w} = \dot{m}^{w}$).
- Air volume introduced to compressor/expander is equal to water volume pumped into the compression/expansion chamber.
- Water is considered incompressible and non-expandable.
- The heat transfer at the air-water interface is negligible taking into account the length to diameter ratio of the air space (space between the tubes) which is important.
- The heat transfer coefficient is assumed to be the same during the three phases of the compression cycle (suction + compression + discharge).
- The dead volume is considered to be equal to zero at the end of compressed air discharge phase (State D).
- Water temperature at state E (T_E^w: beginning of the water discharge) is equal the one at state F ($T_{F^-}^{w}$: end of water discharge).

- State F is divided into two sub states: F^- (end of water discharge) and F^+(beginning of the water injection).

3.2.2 Analytical model of liquid piston compressor

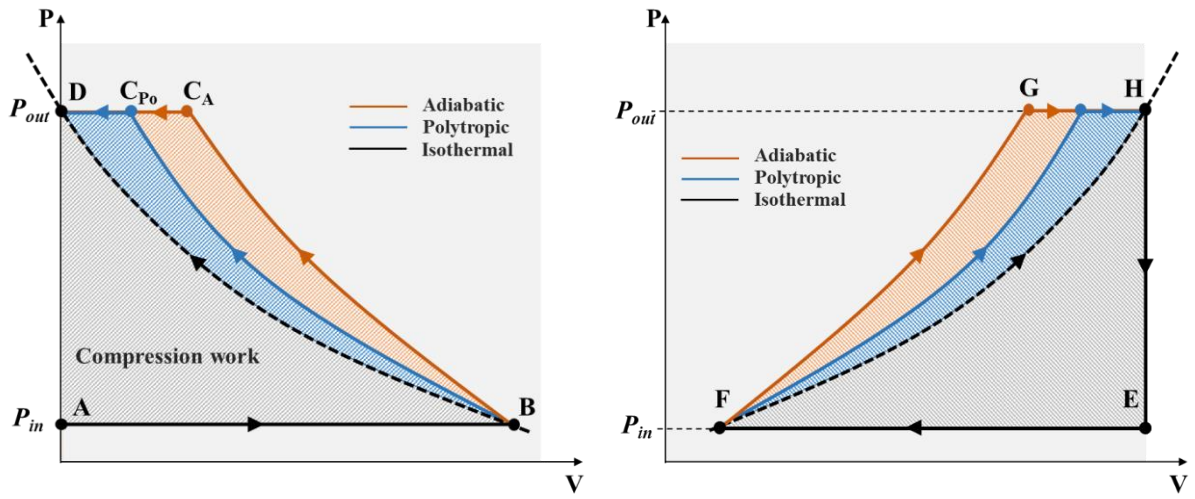

Figure 3.23: PV diagram of the air (left) and water (right) compression cycle

3.2.2.1 Air energy conservation

- Phase 1 (A → B): Air intake

$$U_B - U_A = -P_{in}(V_B - V_A) + \int_A^B \dot{m}\, h_{in}\, dt + Q_{AB} \tag{3.28}$$

- Phase 2 (B → C_{Po}): Air compression

$$U_{C_{Po}} - U_B = \frac{1}{\eta_{pol}} \frac{P_{in} V_B}{n_c - 1} \left[\left(\frac{V_B}{V_{C_{Po}}} \right)^{n_c - 1} - 1 \right] + Q_{BC_{Po}} \tag{3.29}$$

- Phase 3 (C_{Po} → D): Air discharge

$$U_D - U_{C_{Po}} = -P_{out}\left(V_D - V_{C_{Po}}\right) - \int_{C_{Po}}^{D} \dot{m}\, h_{out}\, dt + Q_{C_{Po}D} \tag{3.30}$$

Based on Eq. (3.28), an analytical expression of the air temperature at state B (end of air suction) is proposed in the next section:

$$\frac{dU}{dt} = \dot{m}_{AB} h_{AB} + \dot{Q}_{AB} - P \frac{dV}{dt} \tag{3.31}$$

By replacing the internal energy, enthalpy and air-water heat transfer rate by their expressions, Eq.(3.31) can be written as (see appendix B.2.1.):

$$\dot{m}_{AB} c_p \, t \, \frac{dT}{dt} + \left(\dot{m}_{AB} c_p + he_{AB} \, S_{tu}(t)\right) T(t) = \dot{m}_{AB} c_p T_A + he_{AB} \, S_{tu}(t) T_E^w \quad (3.32)$$

With the air water exchange surface $S_{tu}(t)$ calculated as follow:

$$S_{tu}(t) = \frac{4}{D_{tu}} V_B = \frac{4}{D_{tu}} \frac{\pi D_{tu}^2}{4} L(t) \, nt = \pi \, D_{tu} \, nt \, a \, t \quad (3.33)$$

Where D_{tu} is the tube diameter, $L(t) = a \, t$ is the air active column length where a is a constant and t is the operational time; nt is the number of the tubes inside the compression/expansion chamber used to form the integrated heat exchanger. Eq.(3.32) becomes:

$$\begin{aligned} \dot{m}_{AB} c_p \, t \, \frac{dT}{dt} + \left(\dot{m}_{AB} c_p + he_{AB} \, \pi \, D_{tu} \, a \, nt \, t \right) T(t) \\ = \dot{m}_{AB} c_p T_{in} + he_{AB} \, \pi \, D_{tu} \, nt \, a \, t \, T^w \end{aligned} \quad (3.34)$$

With analytical approach, equation (3.34) can be simplified to:

$$\frac{\tau \, t}{\tau + t} \frac{dT}{dt} + T = \frac{\tau \, T_{in}}{\tau + t} + \frac{t \, T^w}{\tau + t} \quad (3.35)$$

With $\tau = \frac{\dot{m}_{AB} \, c_p}{a \, nt \, he_{AB} \, D_{tu} \pi}$;

The air temperature (during air suction phase) expression is written as follows:

$$T(t) = T_{F^-}^w + \frac{\tau}{t} \left(T_A - T_E^w\right) \left(1 - e^{-t/\tau}\right) \quad (3.36)$$

In this study, the air suction phase time is equal to half the air compression cycle time as considered by Lemofouet [44]. The air temperature at state B is found to be:

$$T_B = T_{F^-}^w + \frac{\tau}{\frac{t_{cy}}{2}} \left(T_A - T_E^w\right) \left(1 - e^{-\frac{t_{cy}}{2}/\tau}\right) \quad (3.37)$$

The energy equation (Eq. (3.30)) written in another form for the air discharge phase ($C_{Po} \rightarrow D$) is:

$$\frac{dH}{dt} = \dot{m}_{C_{Po}D} h_{C_{Po}D} + he_{C_{Po}D} \, S_{tu}(t) \left(T_G^w - T\right) \quad (3.38)$$

$$M \frac{dh}{dt} + h_{C_{Po}D} \frac{dM}{dt} = h_{C_{Po}D} \frac{dM}{dt} + he_{C_{Po}D} \, S_{tu}(t) \left(T_G^w - T\right) \quad (3.39)$$

$$M \frac{dh}{dt} = he_{C_{Po}D} \, S_{tu}(t) \left(T_G^w - T\right) \quad (3.40)$$

$$Mc_p \frac{dT}{dt} = he_{C_{Po}D}\, S_{tu}(t)\, (T_G^w - T) \tag{3.41}$$

From Eq. (3.41), the air temperature at state D (end of air discharge phase) is found to be:

$$T_D = T_G^w + (T_{C_{Po}} - T_G^w)\, e^{-NTU\left(\frac{1}{2}-\frac{t_C}{tcy}\right)} \tag{3.42}$$

With $\boldsymbol{NTU} = \frac{\boldsymbol{nt\, he_{AB}\, D_{tu}\, \pi\, L_0}}{\boldsymbol{\dot{m}_{AB}\, c_p}}$.

3.2.2.2 Air mass conservation

The air mass flow rate sucked during a compression cycle is given by the next equation:

$$\dot{m}_{AB} = \frac{V_B(\frac{t_{cy}}{2})\, \rho\, \eta_{vo}}{t_{cy}/_2} \tag{3.43}$$

The displacement volume in all the compression chamber is given by:

$$V_B = nt\, \frac{\pi\, D_{tu}^2}{4} L(\frac{t_{cy}}{2}) \tag{3.44}$$

And therefore the tube numbers is calculated as the following:

$$nt = \frac{4\, V_B}{L(\frac{t_c}{2})\, \pi\, D_{tu}^2} \tag{3.45}$$

The volume at the end of the compression phase (V_C) depends on the aspirated air volume (V_B) and the polytropic index (n_c). It will be shown later in Eq. (3.63) that the polytropic index depends on the air temperature at the end of the compression phase. At the state C, the compressed air volume is calculated as follows:

$$V_C = \left(\frac{P_{in}}{P_{out}}\right)^{\frac{1}{n_c}} V_B \tag{3.46}$$

3.2.2.3 Water energy conservation

- Phase 1 (E → F): Water discharge

$$U_F - U_E = -P_{in}(V_F - V_E) - \int_E^F \dot{m}_w h\, dt + Q_{EF} \tag{3.47}$$

- Phase 2 (F → G): Water injection and water compression

$$U_F - U_G = \frac{-1}{n_c - 1}[P_{out}V_F - P_{in}V_G] + \int_F^G \dot{m}_w h\, dt + Q_{FG} \tag{3.48}$$

- Phase 3 (G → H): Water injection

$$U_H - U_G = -P_{out}(V_H - V_G) + \int_G^H \dot{m}_w h \, dt + Q_{GH} \tag{3.49}$$

- Phase 4 (H → E): Isochoric water expansion

$$U_E - U_H = Q_{HE} \tag{3.50}$$

These four equations Eqs. (3.47), (3.48), (3.49), (3.50) can be grouped in one water energy balance equation as shown below (assuming phase 4 as adiabatic):

$$\dot{m}^w(h_{EF}^w - h_{FG}^w - h_{GH}^w)t_{cy} = \left(\dot{W}_{tot}\right)_c + \dot{Q}_{EF} + \dot{Q}_{FG} + \dot{Q}_{GH} \tag{3.51}$$

To calculate the outlet water temperature it is necessary to express its enthalpy as a function of its pressure and its temperature, by separating the internal energy from the mechanical content of the enthalpy (neglecting the kinetic and gravitational energies):

$$h^w = C_w T + \frac{P}{\rho^w} \tag{3.52}$$

To simplify the problem, the transfer of mechanical energy is supposed to be isothermal; In this case the outlet water temperature is given by the following expression:

$$T_{F^-}^w = T_{in}^w - \frac{\dot{Q}_{(tot)_c}}{c_w \dot{m}^w} = T_{F^+}^w - \frac{\dot{Q}_{EF} + \dot{Q}_{FG} + \dot{Q}_{GH}}{c_w \dot{m}^w} \tag{3.53}$$

3.2.2.4 Water mass conservation

Since pumped water volume is equal to air volume (V_B) introduced into the compression chamber, the input/output water mass flow rate is equal to:

$$\dot{m}_{in}^w = \dot{m}_{out}^w = \frac{V_B \, \rho_{F^+}^w}{t_{cy}} \tag{3.54}$$

3.2.2.5 Complementary equations

The total air compression work rate is defined by the following equation:

$$\dot{W}_{(tot)_c} = (W_{AB} + W_{BC_{Po}} + W_{C_{Po}D}) \frac{1}{\eta_{po} \, t_{cy}} \tag{3.55}$$

With the air suction, compression and discharge work expressed as follows:

$$W_{AB} = -P_{in} V_B \tag{3.56}$$

$$W_{BC} = \frac{1}{n_c - 1}(P_{out} V_{C_{Po}} - P_{in} V_B) \tag{3.57}$$

$$W_{CD} = P_{out} V_{C_{Po}} \tag{3.58}$$

The total heat transfer exchanged between water and air is given by the following:

$$\dot{Q}_{(tot)_c} = \dot{Q}_{AB} + \dot{Q}_{BC_{Po}} + \dot{Q}_{C_{Po}D} \tag{3.59}$$

With:

$$\dot{Q}_{AB} = \dot{m}_{AB}\, c_p\, (T_B - T_A) \tag{3.60}$$

$$\dot{Q}_{BC_{Po}} = he_{BC_{Po}} \left(\frac{V_B + V_{C_{Po}}}{0{,}5\, D_{tu}}\right)\left(T^{w}_{F^+} - \left(\frac{T_{C_{Po}} + T_B}{2}\right)\right) \tag{3.61}$$

$$\dot{Q}_{C_{Po}D} = \dot{m}_{C_{Po}D}\, c_p\, (T_D - T_{C_{Po}}) \tag{3.62}$$

Many scientific researchers studied and analyzed the heat transfer coefficient for the liquid piston during the air compression phase. Van de Ven and Li [47] used a fully developed pipe flow analysis to model the liquid piston system in order to roughly estimate the heat transfer between the air and the liquid. The studied heat transfer coefficient was between 50-350 $W.m^{-2}.K^{-1}$. Odukomaiya [50] developed GLIDES (Ground-Level Integrated Diverse Energy Storage) technology which is based on liquid piston compression/expansion. In his work, Odukomaiya conducted numerical model calibrated by his collected experimental data. The gas-liquid heat transfer coefficient was found to be in the range of 200-500 $W.m^{-2}.K^{-1}$. These later heat transfer coefficient ranges are used in this study. The polytropic index of the compression phase is calculated from the following:

$$n_c = log\frac{P_{in}}{P_{out}} \Big/ log\frac{T_{C_{Po}}}{T_B} + log\frac{P_{in}}{P_{out}} \tag{3.63}$$

3.2.3 Analytical model of liquid piston expander

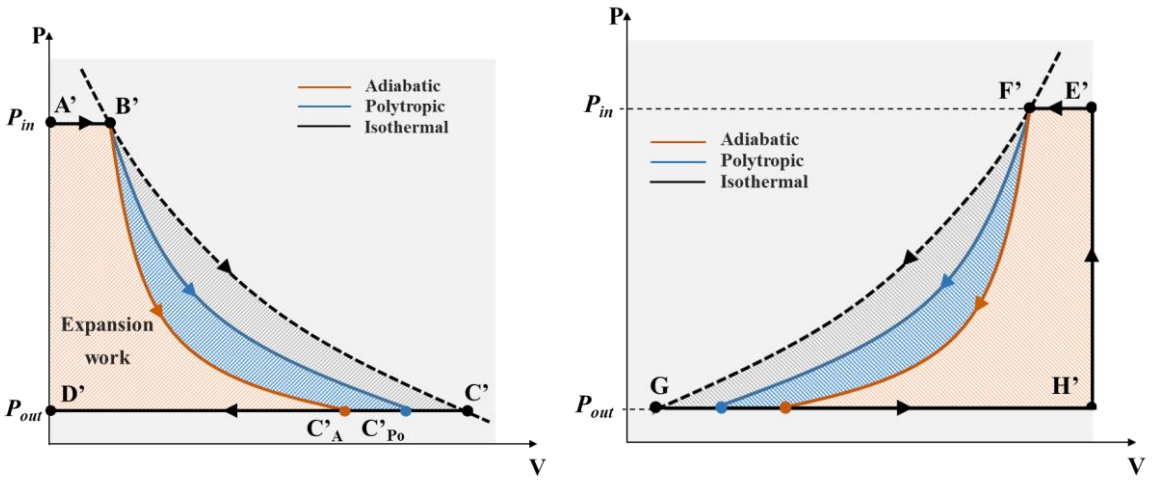

Figure 3.24: PV diagram of the air (left) and water (right) expansion cycle

The liquid air expansion mode is similar to the liquid air compression mode developed and discussed in the previous section. The mass conservation and the complementary equations are the same as those used for the compression mode.

3.2.3.1 Air energy conservation

Equation (3.31) is also applicable for the compressed air suction phase (A'→B'). Equation (3.34) is solved in this case and the air temperature at state B' (end of air suction phase) is:

$$\begin{aligned} T_{B\prime} = \; & T_{out}^{w} + \frac{\tau}{t}\left(T_{A\prime} - T_{out}^{w}\right)\left(1 - e^{-t/\tau}\right) \\ & = T_{E\prime}^{w} + \frac{\tau}{t}\left(T_{A\prime} - T_{E\prime}^{w}\right)\left(1 - e^{-t/\tau}\right) \end{aligned} \tag{3.64}$$

The air discharge phase is also similar to that developed for the compression mode. Equation (3.41) is solved to calculate the air temperature at state D' (end of air discharge phase):

$$T_{\mathrm{D}\prime} = T_{in}^{w} + \left(T_{C_{Po}^{\prime}} - T_{in}^{w}\right) e^{\frac{-NTU}{2}} = T_{\left(G_{Po}^{\prime}\right)^{+}}^{w} + \left(T_{C_{Po}^{\prime}} - T_{\left(G_{Po}^{\prime}\right)^{+}}^{w}\right) e^{\frac{-VR_t\, NTU}{2}} \tag{3.65}$$

With ($VR_t \frac{t_{cy}}{2}$) is the compressed air introduction time into the expander. VR_t is the volume ratio that defines as follows:

$$VR_t = \frac{V_{B\prime}}{V_{C_{Po}^{\prime}}} \tag{3.66}$$

3.2.3.2 Air mass conservation

The compressed air mass flow rate introduced into the expander is expressed as follows:

$$\dot{m}_{A\prime B\prime} = \frac{V_{B\prime}\, \rho\, \eta_{vo}}{t_{cy}} \tag{3.67}$$

With expended air volume calculated from the following equation:

$$V_{C_{Po}^{\prime}} = \left(\frac{P_{in}}{P_{out}}\right)^{\frac{1}{n_t}} V_{B\prime} \tag{3.68}$$

3.2.3.3 Water energy conservation

Total heat transfer calculated in Eq. (3.75) which is based on the air temperature evolution through the air expansion cycle, is considered to be equal of the total heat transfer calculated with water temperature evolution during the air expansion cycle. Therefore the outlet water temperature of the expansion chamber is calculated as follows:

$$T_{\left(G_{Po}^{\prime}\right)^{-}}^{w} = T_{in}^{w} - \frac{\dot{Q}_{(tot)_t}}{c_w \dot{m}^{w}} = T_{\left(G_{Po}^{\prime}\right)^{+}}^{w} - \frac{\dot{Q}_{E\prime F\prime} + \dot{Q}_{F\prime G\prime} + \dot{Q}_{G\prime H\prime}}{c_w \dot{m}^{w}} \tag{3.69}$$

3.2.3.4 Water mass conservation

Inlet water mass flow rate is assumed to be equal the outlet water mass flow rate and calculated from the following equation:

$$\dot{m}_{out}^{w} = \dot{m}_{in}^{w} = \frac{V_{C'_{Po}} \rho_w}{t_{cy}} \tag{3.70}$$

3.2.3.5 Complementary equations

The total air expansion work rate is defined as follows:

$$\dot{W}_{(tot)_t} = \eta_{po}(W_{A'B'} + W_{B'C'_{Po}} + W_{C'_{Po}D'}) \frac{1}{t_{cy}} \tag{3.71}$$

With the air suction, expansion and discharge work expressed as follows:

$$W_{A'B'} = -P_{in} V_{B'} \tag{3.72}$$

$$W_{B'C'_{Po}} = \frac{1}{n_t - 1}(P_{out} V_{C_{Po}} - P_{in} V_{B'}) \tag{3.73}$$

$$W_{C'_{Po}D'} = P_{out} V_{C'_{Po}} \tag{3.74}$$

The total heat transfer exchanged between water and air during air expansion cycle is given by the following equation:

$$\dot{Q}_{(tot)_t} = \dot{Q}_{A'B'} + \dot{Q}_{B'C'_{Po}} + \dot{Q}_{C'_{Po}D'} \tag{3.75}$$

The heat transfer for each phase during the expansion cycle is described below with the following equations:

$$\dot{Q}_{A'B'} = \dot{m}_{A'B'}\, c_p \left(T_{B'} - T_{A'}\right) \tag{3.76}$$

$$\dot{Q}_{B'C'_{Po}} = he_{B'C'_{Po}} \left(\frac{V_{B'} + V_{C'_{Po}}}{0{,}5\, D_{tu}}\right) \left(T_{E'}^{w} - \left(\frac{T_{C'_{Po}} + T_{B'}}{2}\right)\right) \tag{3.77}$$

$$\dot{Q}_{C'_{Po}D'} = \dot{m}_{C'_{Po}D'}\, c_p \left(T_{D'} - T_{C'_{Po}}\right) \tag{3.78}$$

The polytropic index for the air expansion phase is given by the following equation:

$$n_t = log\frac{P_{in}}{P_{out}} \Big/ log\frac{T_{C'_{Po}}}{T_{B'}} + log\frac{P_{in}}{P_{out}} \tag{3.79}$$

3.2.4 Numerical resolution of liquid piston compressor and expander

The dichotomy method is applied for both numerical codes where the air temperature at the end of the compression/expansion phase is chosen to be the convergence parameter. This parameter can have a maximum or minimum temperature values during compression and expansion phases that are the following respectively:

- Compressor model:

$$T_B \leq T_{C_{Po}} \leq T_{C_A} \tag{3.80}$$

$$T_B \leq T_{C_{Po}} \leq \left(\frac{P_{in}}{P_{out}}\right)^{\frac{1-\gamma}{\gamma}} T_B \tag{3.81}$$

$$T_{C_{Po}} = \frac{T_B + T_{C_A}}{2} \tag{3.82}$$

The dichotomy function used for the compressor numerical codes is described below:

$$f(T_D) = \left[\dot{W}_{(tot)_c} + \dot{Q}_{(tot)_c} - \dot{m}_{AB}\, C_p(T_C - T_A)\right] / \dot{W}_{(tot)_c} \tag{3.83}$$

- Expander model:

$$T_{C'_A} \leq T_{C'_{Po}} \leq T_{B'} \tag{3.84}$$

$$\left(\frac{P_{in}}{P_{out}}\right)^{\frac{1-\gamma}{\gamma}} T_{B'} \leq T_{C'_{Po}} \leq T_{B'} \tag{3.85}$$

$$T_{C'_{Po}} = \frac{T_{B'} + T_{C'_A}}{2} \tag{3.86}$$

The dichotomy function used for the expander numerical codes is the following:

$$f\left(T_{D'}\right) = \left[\dot{W}_{(tot)_t} + \dot{Q}_{(tot)_t} - \dot{m}_{A'B'}\, C_p\left(T_{D'} - T_{A'}\right)\right] / \dot{W}_{(tot)_t} \tag{3.87}$$

The second convergence parameter is the discharge water temperature which is initialized in the beginning ($T_{F^-}^{w}$). These two parameters are used to set two main conditions for the iterative loop as seen in Figure 3.25 and Figure 3.26. For the compression phase, the first condition (A) is described below:

$$|(T_{F^-}^{w})^{*} - (T_{F^-}^{w})| \leq 0.001 \tag{3.88}$$

Where $(T_{F^-}^{w})^{*}$ is calculated from Eq. (3.53). If condition (A) is true, the solution is converged (END). If condition (A) is false, the following equation is applied before the next iterative loop begins:

$$(T_{F^-}^{w}) = (T_{F^-}^{w})^{*} \tag{3.89}$$

The second condition (B) depends on the dichotomy function:

$$f(T_D) \leq 0 \tag{3.90}$$

If condition (B) is true, then the next equation is applied

$$T_{C_A} = T_{C_{Po}} \tag{3.91}$$

If condition (B) is false, then the next equation is applied

$$T_B = T_{C_{Po}} \tag{3.92}$$

In the expansion phase case, the first applied condition (A):

$$\left|\left(T_{(G'_{Po})^-}^{w}\right)^{*} - T_{(G'_{Po})^-}^{w}\right| \leq 0.001 \tag{3.93}$$

Equation (3.69) is used to calculate $\left(T_{(G'_{Po})^-}^{w}\right)^{*}$ If condition (A) is true, the solution is converged (END). If condition (A) is false, the following equation is applied before the next iterative loop begins:

$$\left(T_{(G'_{Po})^-}^{w}\right) = \left(T_{(G'_{Po})^-}^{w}\right)^{*} \tag{3.94}$$

The second condition (B) depends on the dichotomy function:

$$f(T_{D'}) \leq 0 \tag{3.95}$$

If condition (B) is true, then the next equation is applied

$$T_{C'_A} = T_{C'_{Po}} \tag{3.96}$$

If condition (B) is false, then the next equation is applied

$$T_{B'} = T_{C'_{Po}} \tag{3.97}$$

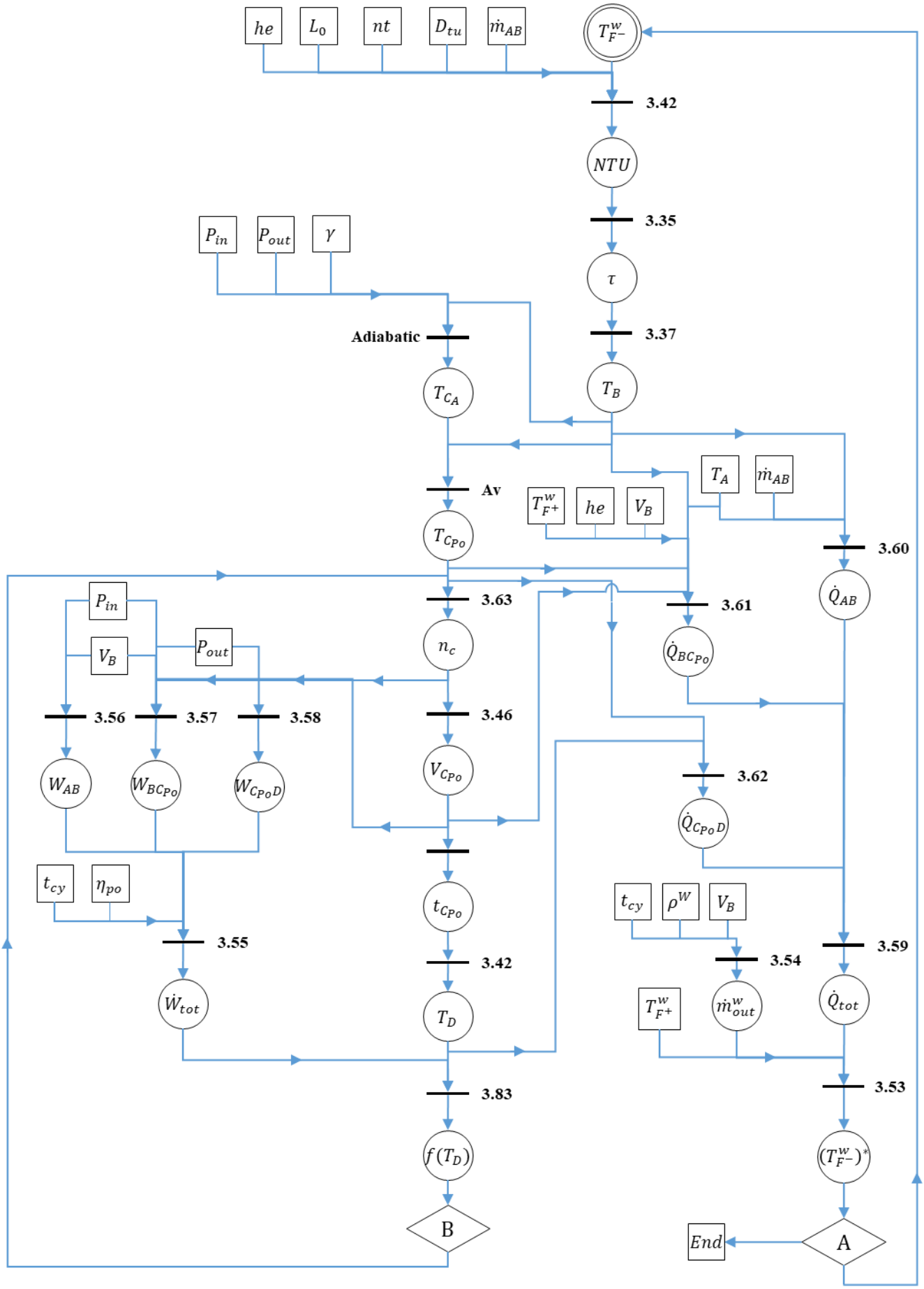

Figure 3.25: Liquid piston compressor numerical code flow chart

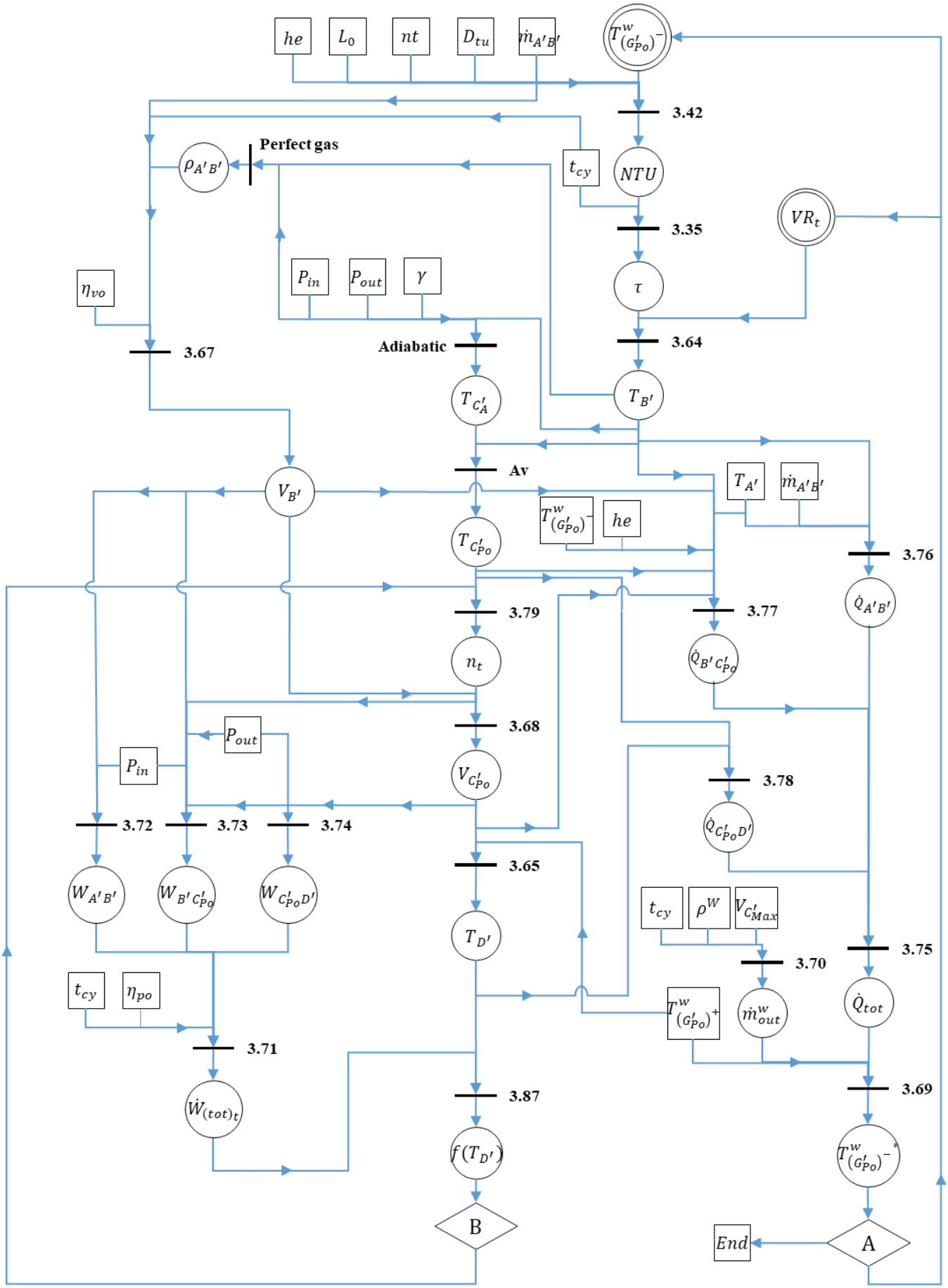

Figure 3.26: Liquid piston expander numerical code flow chart

3.2.5 Results and discussion

Based on the report published by Enairys Powertech [44], a two-stage liquid piston air compressor was tested experimentally. The experimental model inputs fixed by Enairys Powertech are listed in the table below:

Table 3.4: Experimental liquid piston compressor model inputs

	Low pressure	High pressure
Pressure range (bar)	10 → 40	40 → 160
Compression ratio	4	4
Inlet air temperature (°C)	24	Outlet 1st comp
Inlet water temperature (°C)	23	23
Cylinder volume (L)	62.8	15.7
Cylinder height (m)	0.5	0.5
Cylinder diameter (m)	0.4	0.2
Tube diameter (mm)	2	1
Cycle time (s)	20	20

3.2.5.1 Liquid piston compressor results and discussion

The model input parameters listed in Table 3.4 are considered for the numerical model described in section 4.2. Based on Enairys published work, the displacement air volume is equal to the pumped water volume which is the half the total chamber volume. Therefore the air mass flow rate sucked is equal to 0.01469 kg/s (taking into account the volumetric efficiency equal to 0.8). Three parameters were studied during the air compression phase: heat transfer coefficient, tube diameter and air mass flow rate.

The heat transfer coefficient influence on different air/water temperature states and other model outputs during the air compression phase are shown in Figure 3.28 and Figure 3.29. It should be mentioned that during the air intake phase, water that underwent a previous compression cycle is pumped out of the compressor. It is noticed that the water leaves the compressor with a small increase in temperature. At 5 $W.m^{-2}.K^{-1}$ the first and second stage water temperature difference is 0.6 and 9.8 °C respectively. This fact can explain the temperature drop while the air is introduced in the chamber. At 5 $W.m^{-2}.K^{-1}$ the highest air temperature at the end of the

compression phase is reached (47.19 °C and 61.57°C for the 1st and 2nd stage respectively). This temperature ($T_{C_{Po}}$) is rapidly decreased with the increase of the heat transfer coefficient to stabilize for 80 W.m^{-2}.K^{-1} around 24.49 °C and 25.72°C for each stage compressor. During the final phase, compressed air is pushed out of the cylinder where the water (at 23°C) is pumped into it. This air/water indirect contact justifies the air temperature drop while leaving the cylinder (at 80 W.m^{-2}.K^{-1} compressed air leaving the first compressor dropped from 24.49°C to 24.29°C and from 25.72°C to 25.54°C for the second). The input/output air temperature difference for the 1st and 2nd stage air compressor is equal to 0.49 and 1.24 °C respectively. For the water the difference is also small around 0.4 and 1.6 °C for 1st and 2nd compressor respectively. These results show a fair agreement with those presented in Enairys Powertech work [44], where the average outlet air temperature of the first stage air compressor scored an increase of 1°C and 0.2°C for water leaving the same compressor. Figure 3.29 shows consistent values for the total work rate, the total heat transfer rate and the polytropic index while varying the heat transfer coefficient. In fact as the heat transfer coefficient increases the air/water heat transfer increases which leads to a decrease in the total compensated work and therefore the polytropic index converged to unity and the isothermal compression efficiency increases. The PV diagram for the two stage air liquid piston compressor is shown in Figure 3.27

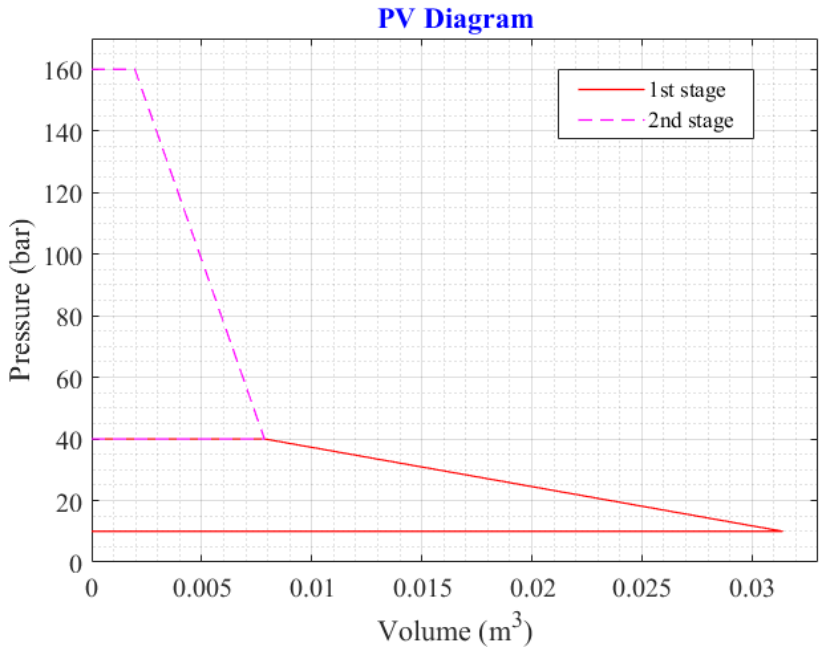

Figure 3.27: PV diagram representing two air stage liquid piston compressors

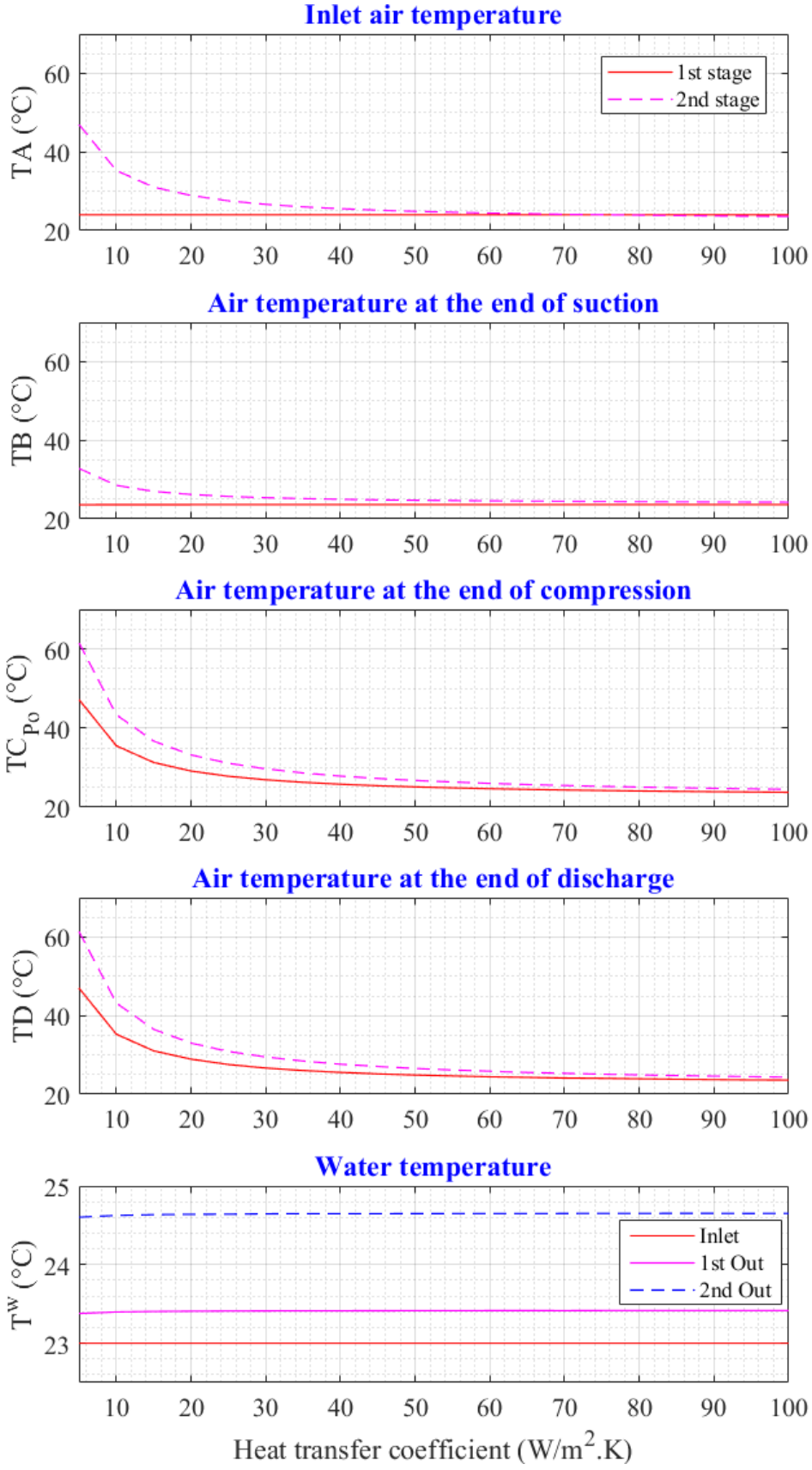

Figure 3.28: Air/Water temperature at different air compression states function of the heat transfer coefficient. The legend of the first figure at the top has to be considered for the other figures below.

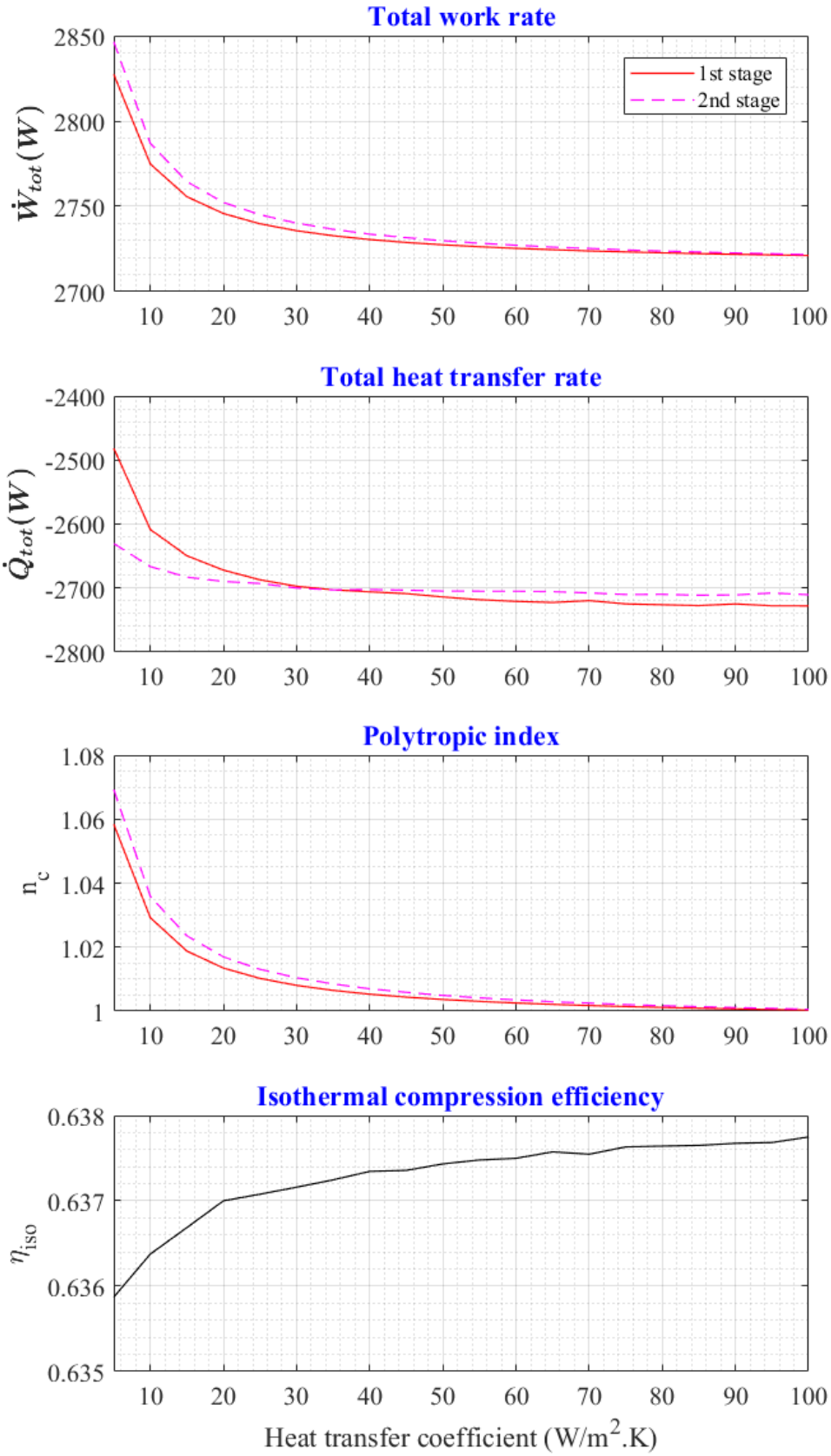

Figure 3.29: Several liquid piston compressor model outputs function of the heat transfer coefficient

The influence of the 2nd stage air compressor tube diameter on the air and water temperature at the end of compression and discharge phase respectively, is seen in Figure 3.30. While fixing

the heat transfer coefficient at 80 $W.m^{-2}.K^{-1}$ and air mass flow rate at 0.01469 kg/s, the tube diameter is varied from 1 mm to 10 mm. Based on the Eq. (3.33) the tube diameter and the number of tubes are inversely proportional, therefore increasing the diameter reduces the tube numbers and as a result reduces air/water heat transfer. This operation explains the increase of the air temperature at the end of the compression shown in Figure 3.30.

Figure 3.31 presents the influence of the air mass flow rate (varying from 0.01469 kg/s to 0.29 kg/s) on the water and air temperatures while fixing the tube diameter for second compressor at 1 mm and heat transfer coefficient at 80 $W.m^{-2}.K^{-1}$. The higher the air mass flow rate for the same water mass flow rate, the higher the air temperature at the end of the air compression phase. From above results, tube diameter and air mass flow rate have a negligible impact on water temperature.

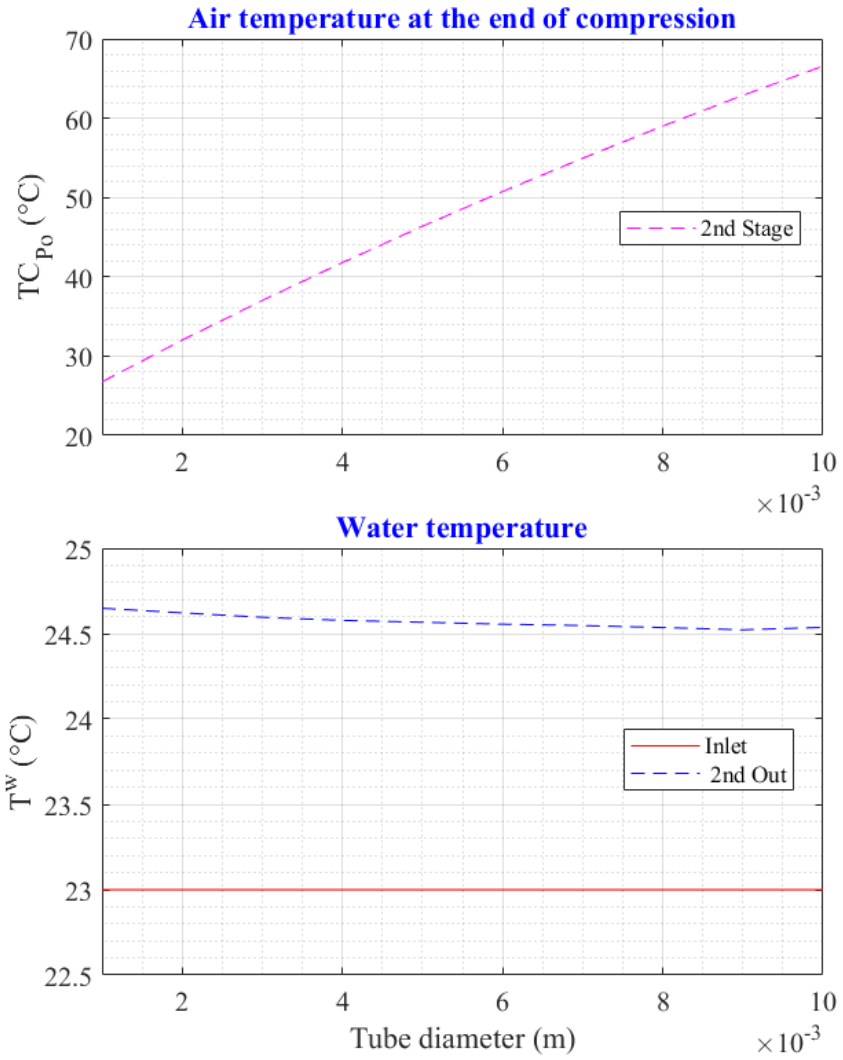

Figure 3.30: Air and water temperature at the end of compression function of 2nd stage compressor tube diameter

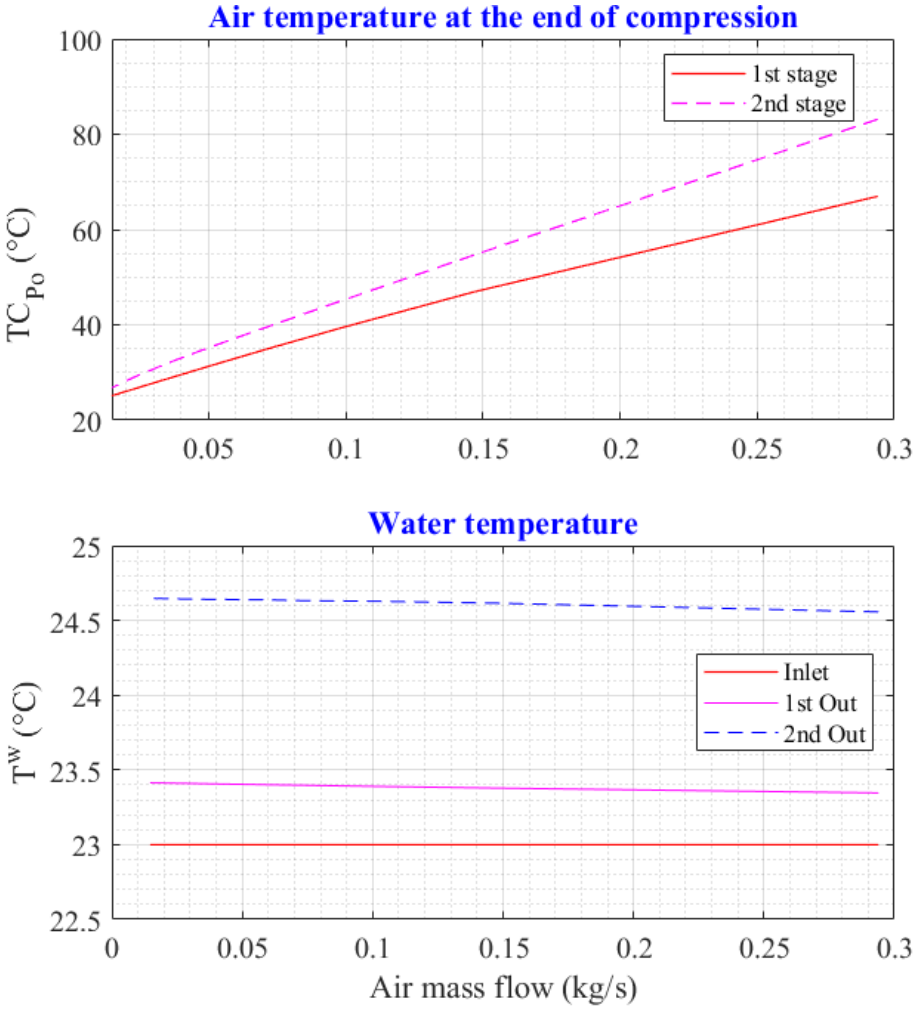

Figure 3.31: Air and water temperature at the end of compression function of air mass flow rate

3.2.5.2 Liquid piston expander results and discussion

The liquid piston expander numerical model is inspired from the liquid piston compressor experimental model designed and published by Enairys Powertech [44]. The expander numerical model inputs are similar to the ones listed in Table 3.4. In this case the first stage air expansion is the high pressure stage followed by the low pressure stage. Inlet air temperature is fixed at 20°C with 23°C for expander inlet water.

Based on Figure 3.32 the heat transfer coefficient has a fair influence on air temperature at different states during the air expansion process and minor influence on water temperature. In this case the air mass flow rate is fixed at 0.01469 kg/s for 1 mm for 1st stage and 2 mm for 2nd stage air expander. This influence is clearly seen for the air temperature at the end of the expansion especially from 5 W.m^{-2}.K^{-1} to 40 W.m^{-2}.K^{-1}. It can be seen that during compressed air suction phase, its temperature rises due to indirect contact with warm water leaving the

expander. Same approach is noticed for the air discharge phase where the warm injected water is in indirect contact with the air.

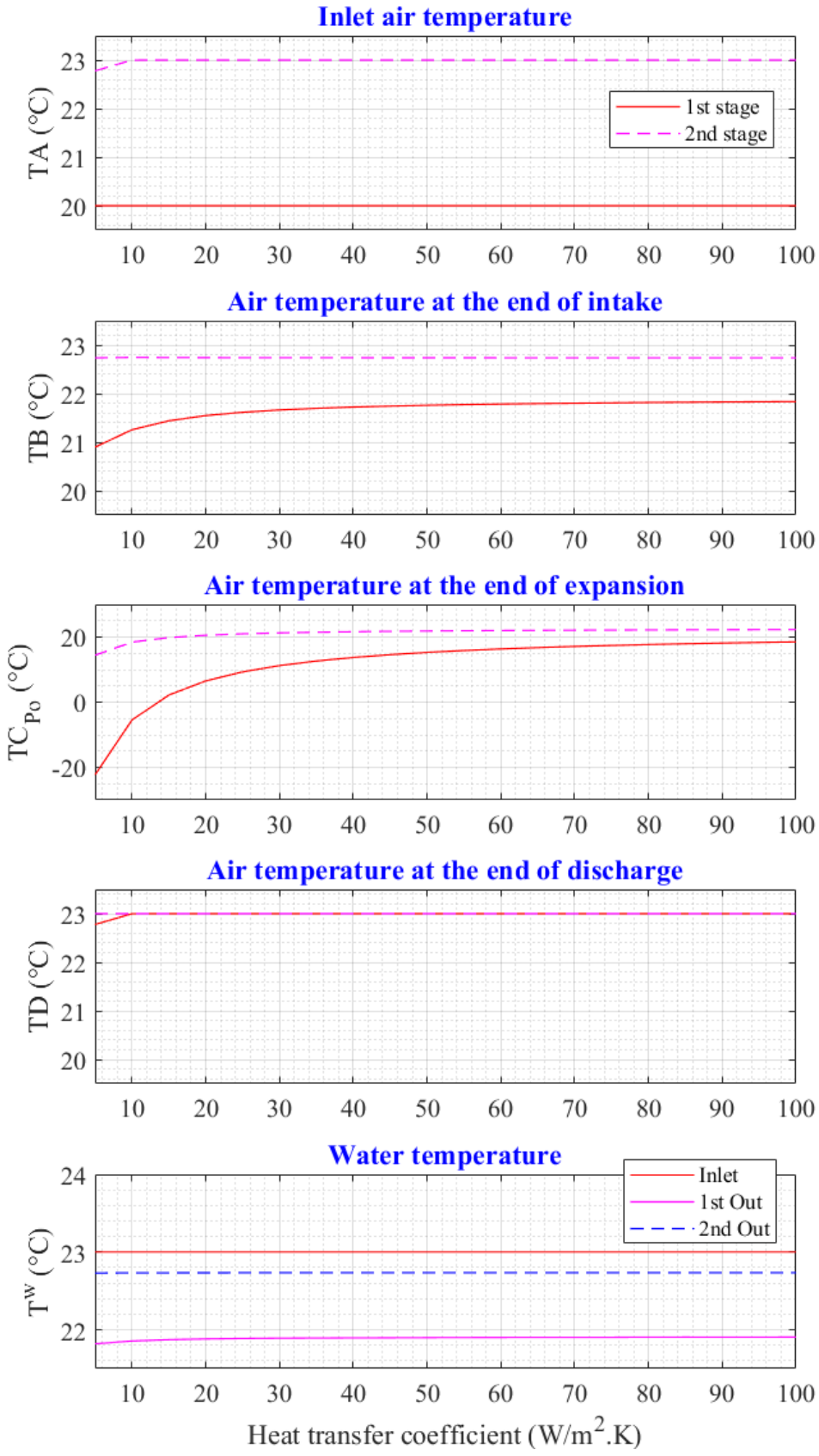

Figure 3.32: Air/Water temperature at different air expansion states function of the heat transfer coefficient

From Figure 3.33 the total work rate recovered during the first stage air expansion phase is strongly impacted while increasing the heat transfer coefficient. At 80 $W.m^{-2}.K^{-1}$ the total work rate recovered is around 1740 W for the first stage and 1750 W for the second stage. Similar to the observations noticed for the compressor model, Figure 3.34 shows that the increase of the 2nd stage air expander tube diameter is deteriorating the air temperature at the end of the expansion while fixing the heat transfer coefficient at 80 $W.m^{-2}.K^{-1}$ and 0.01469 kg/s as mass flow rate. This fact is due the drop in the heat transfer between air and water. The third parameter influence to analyze is the air mass flow rate variation with fixed tube diameters (2 mm) and heat transfer coefficient (80 $W.m^{-2}.K^{-1}$). Figure 3.35 highlights the impact of introducing more compressed air in the expander for the same water flow. This impact affects heavily the air temperature at the end of the expansion phase while in contrary water seems not heavily impacted.

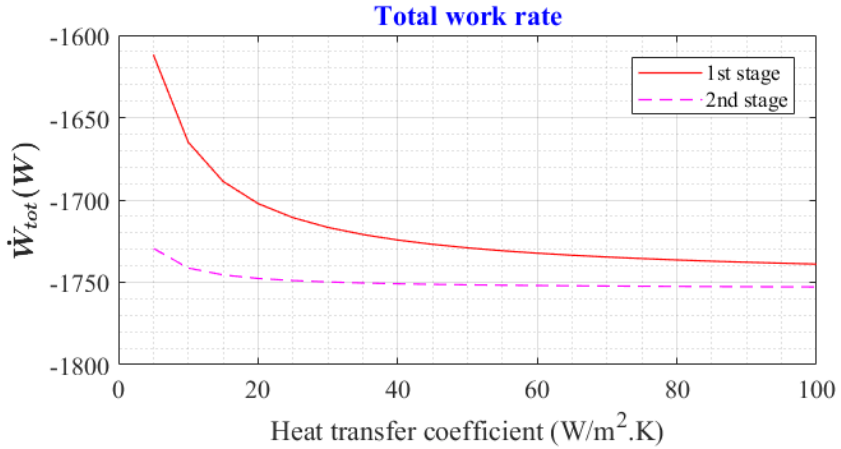

Figure 3.33: Total work rate recovered during air expansion phase function of the heat transfer

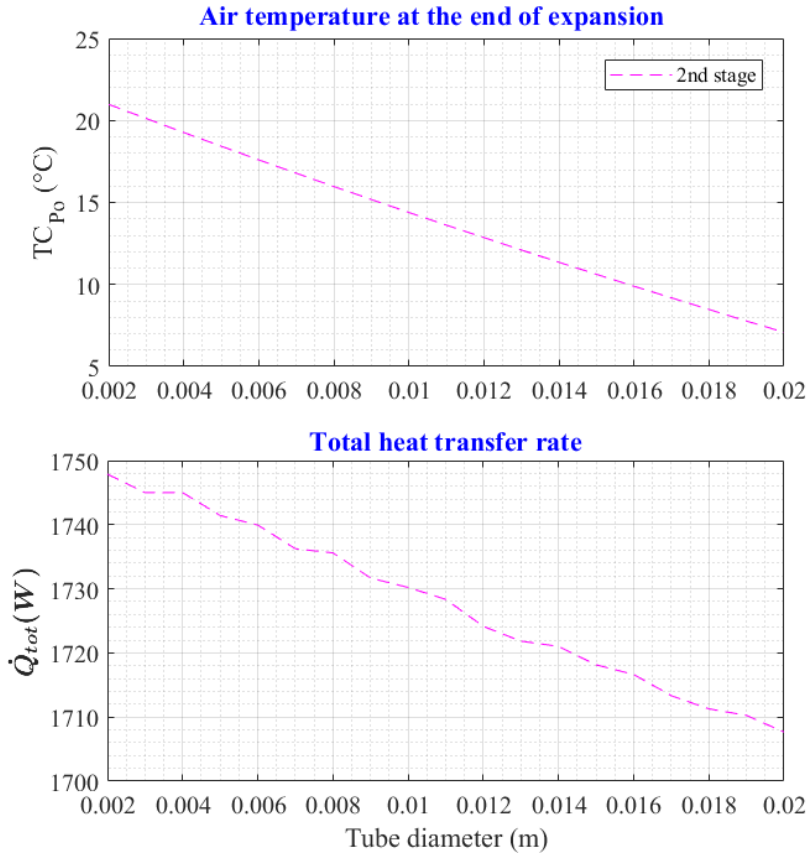

Figure 3.34: Air and water temperature at the end of expansion function of 2nd stage expander tube diameter

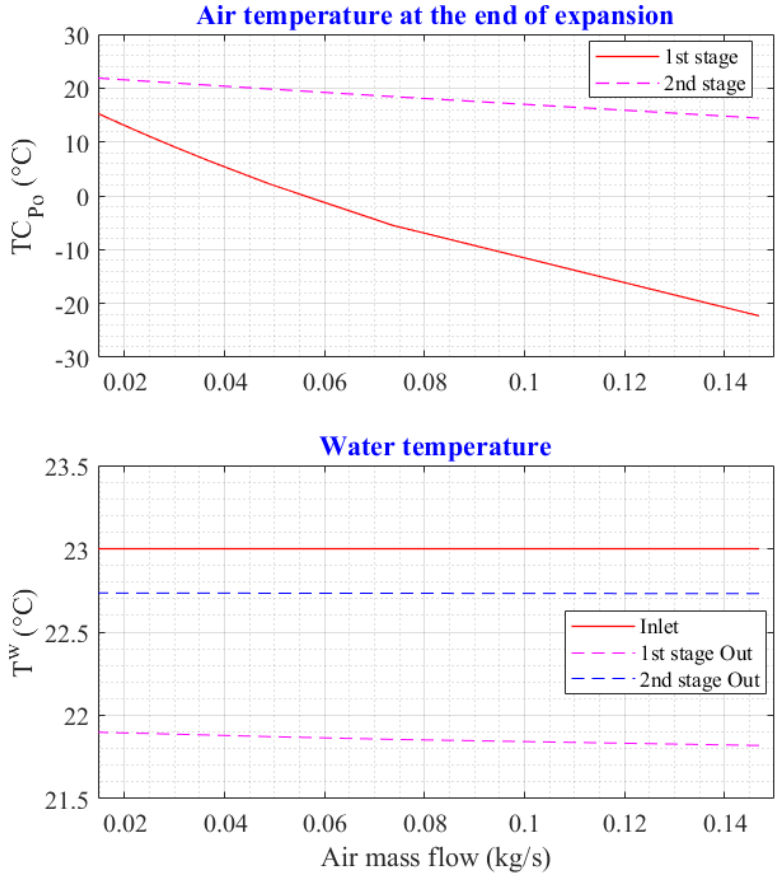

Figure 3.35: Air and water temperature at the end of expansion function of air mass flow rate

3.3 Chapter conclusion

In this chapter the quasi-isothermal compressor and expander developed by LightSail Energy (mechanical piston compressor/expander with water injection) and Enairys Powertech (liquid piston compressor/expander with integrated heat exchanger) were investigated. Multiple scientific works that describe similar technologies were used in this study. Analytical models were presented for each technology. It was notably highlighted the influence of the heat transfer coefficient, heat transfer exchange surface and mass loading on the compressor/expander operation with tracing the behavior of the system outputs (air/water temperature, humidity, work rate, heat transfer rate,…). It was evidenced that the mechanical piston compressor is more favorable for the production of hot water (or cold in case of expansion) than the liquid piston technology that presented a strong isothermal compression and expansion process.

Chapter 4 Numerical model comparison and market/financial study of micro isothermal and adiabatic compressed air energy storage system

The idea in this chapter is to integrate the quasi-isothermal compressor/expander discussed in chapter 3, into the global numerical code developed and detailed in chapter 2. A comparison is then carried on in this chapter between the micro quasi-isothermal and advanced adiabatic compressed air energy storage systems. In addition, an overview of the compressed air market is also described in order to carry on a financial analysis for three different micro prototypes: Adiabatic (virtual and ideal) and isothermal (LightSail Energy).

4.1 Quasi-isothermal compressor/expander integration in the numerical tool coupled to the building

In this section, quasi-isothermal compressors and expanders developed and detailed in chapter 3 are taken as external components in order to be integrated to the global numerical tool detailed in chapter 2 and which simulates a micro trigeneration compressed air energy storage system coupled to a building model and a renewable energy resources. Global numerical code developed in chapter 2 has a well described energy scenarios as seen in Figure 4.1.

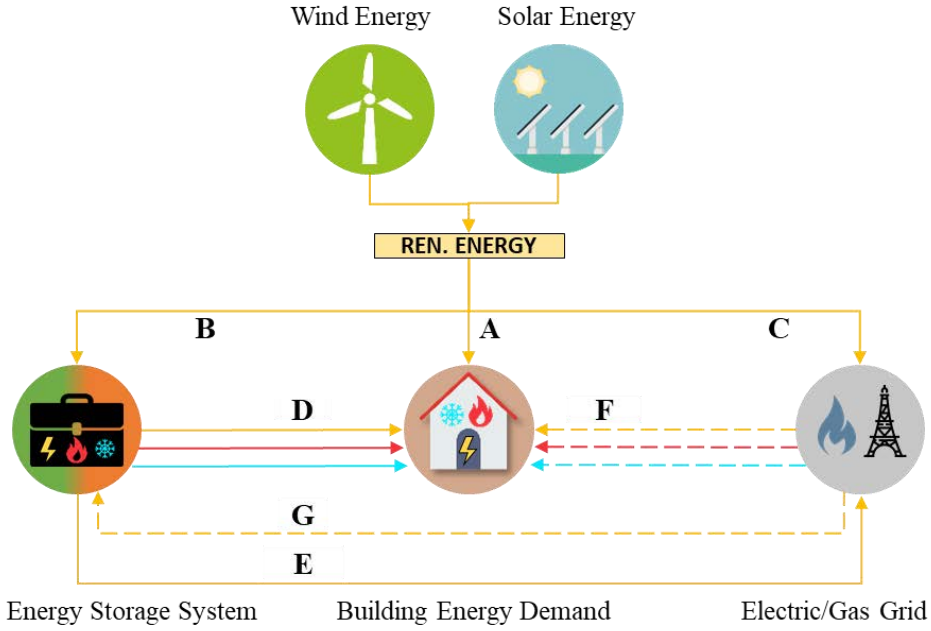

Figure 4.1: Global system operations (autonomous and connected mode)

Note to remember, the studied global model focuses on two functional modes:

- Autonomous mode operation: A + B + C + D + F.
- Connected mode operation: A + B + C + D + **E** + F + **G**.

In this chapter, the quasi-isothermal CAES system is following these same energy scenarios described above. The main difference between the adiabatic and quasi-isothermal compressed air energy storage is the system configuration. This can be seen in Figure 4.2 where no heat exchangers are added between compressors/expanders and the air reservoir like the adiabatic case. In both technologies (mechanical piston and liquid piston), heat is absorbed continuously inside the compressor and cold is absorbed continuously inside the expander.

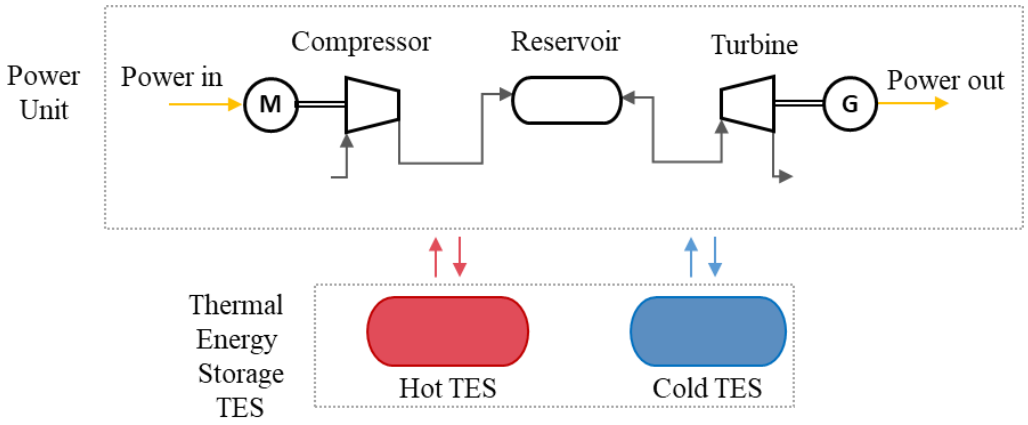

Figure 4.2: Quasi-isothermal compressed air energy storage system configuration

The second difference between quasi-isothermal and adiabatic CAES system is the working temperature range. Selecting the quasi-isothermal compressor, the maximum inlet/outlet water temperature difference is noticed to be around 15 °C for mechanical piston (Figure 3.6) and 2 °C for liquid piston (Figure 3.28). In return, the maximum inlet/outlet water temperature difference in the case of the expander is found to be around 20 °C for mechanical piston (Figure 3.15) and 1.1 °C for liquid piston (Figure 3.32). These ranges are justified for quasi-isothermal CAES system concept that is focused mainly to increase the final round trip electrical efficiency. Therefore in the quasi-isothermal CAES system case the trigeneration concept is difficult to be applicable and for the section below the focus will be on the electrical quasi-isothermal CAES system efficiency.

4.1.1 Integration of the mechanical piston compressor and expander with water injection

Table 4.1 lists the input data required to simulate the quasi-isothermal CAES global system. The energy building demand profile used in chapter 2, is also considered for this case study. It should be mentioned that cold water coming from cold water reservoir is injected in the quasi-isothermal compressor to absorb heat released during air compression and then to proceed to hot water reservoir. In the same manner, hot water is injected to quasi-isothermal expander to preheat the compressed air and then to proceed to the cold water storage. The compressed air preheating process is limited by the air reservoir temperature, meaning that if in some cases the air reservoir temperature is higher than stored hot water temperature, the compressed air is not preheated.

Table 4.1 **:** Input data and constraints related to CAES and R.E. unit

CAES unit			
Air reservoir volume	35 m^3	Mass loading (ML)	5
Initial reservoir temperature	20 °C	Droplet diameter	16 µm
Max. air reservoir pressure	200 bar	**R.E. unit**	
Min. air reservoir pressure	10 bar	*Solar panel*	
Max. power input/output	100 kW	Surface	1000 m^2
Number of compression stages	3	Efficiency	20 %
Compression ratios ($\beta_{c,1}$, $\beta_{c,2}$, $\beta_{c,3}$)	10, 5, 4	Maximum power output	180 W/m^2
1st compressor displacement volume	0.0006 m^3	Material	Monocrystalline
Number of expansion stages	2	*Wind turbine*	
Expansion ratios ($\beta_{t,1}$, $\beta_{t,2}$)	5, 10	Blade diameter	1.5 m
1st turbine displacement volume	0.0006 m^3	Maximum power output	25 kW
Polytropic index	1.4		
Polytropic efficiency	80 %		

Table 4.2 shows the parametric analysis results for the quasi-isothermal CAES and advanced adiabatic CAES global system taking Strasbourg as a geographical scenario in autonomous mode of system operation. It can be noticed the advantages brought by the I-CAES system regarding three defined parameters: electrical load management (E.L.M.), electrical coverage ratio (E.C.R.) and electrical system efficiency (E.S.E.). Figure 4.3 presents the cumulative/sum of different energy sources (renewable energy, energy from storage, energy from grid and energy to grid) and the energy building demand over each month of the year, for the I-CAES system (Strasbourg).

Table 4.2: Parametric analysis results for Strasbourg location (Autonomous mode)

	AA-CAES	I-CAES (Mechanical Piston)
E.L.M.	50 %	57.1 %
E.C.R.	6.04 %	13.19 %
E.S.E.	25.71 %	66.66 %

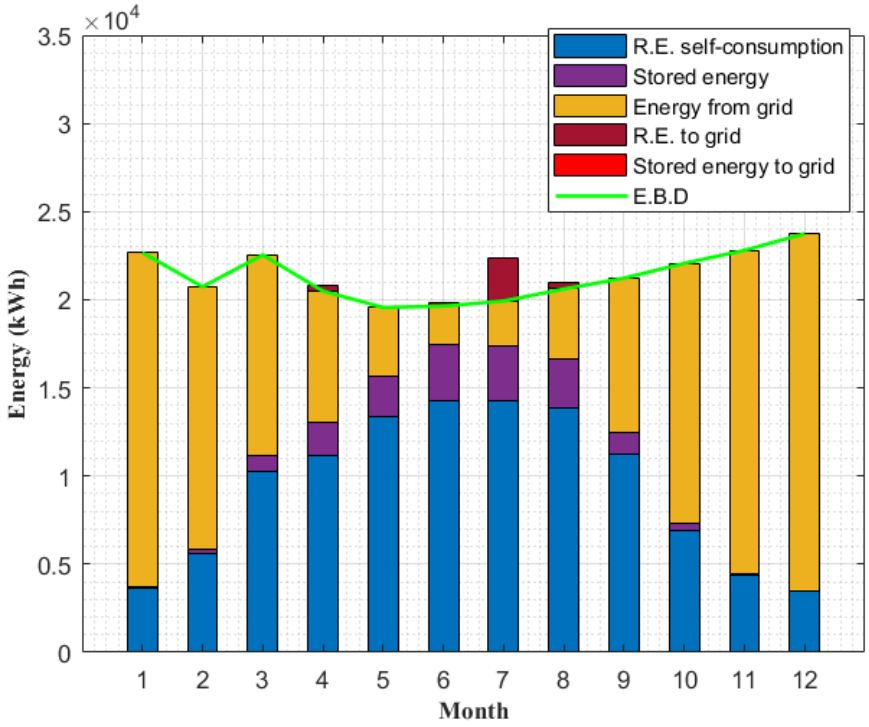

Figure 4.3: Different sources of electrical energy responding to electrical energy building demand for I-CAES (Strasbourg) – Mechanical piston

4.1.2 Liquid piston compressor and expander with integrated heat exchanger integration

Similar to mechanical piston technology, the liquid piston compressor and expander developed by Enairys Powertech detailed in chapter 3 are integrated into the global numerical tool in order to have a projection over a year of the operation of the CAES system based on the liquid piston technology. The sizing of liquid piston compressor and expander detailed in chapter 3, is based on the compressor/expander geometry data delivered by Enairys Powertech.

The CAES system architecture (compression/expansion stage number) used in the mechanical piston case (Table 4.1) is applicable for the liquid piston compressor and expander. A small numerical modification is added in order to use the same dimensional sizing of the liquid piston compressor and expander. This modification consists of initializing the compressor or expander numerical loop with air mass flow calculated based on the compressor/expander geometry fixed by Enairys Powertech. A comparison between the compression/expansion work with the solar energy/released energy respectively is completed afterwards, and therefore recalculate air mass flow if necessary.

Figure 4.4 shows the isothermal CAES system reply to the electrical energy demand based on the liquid piston compressor and expander technologies. It can be noticed that the compressed air storage answer is increased compared to mechanical piston case. This fact was also shown with the increase of the renewable energy share sold to the electrical grid. These facts can be justified by an electrical system efficiency of 73.4 % which represents an increase of almost 10 % compared to mechanical piston case.

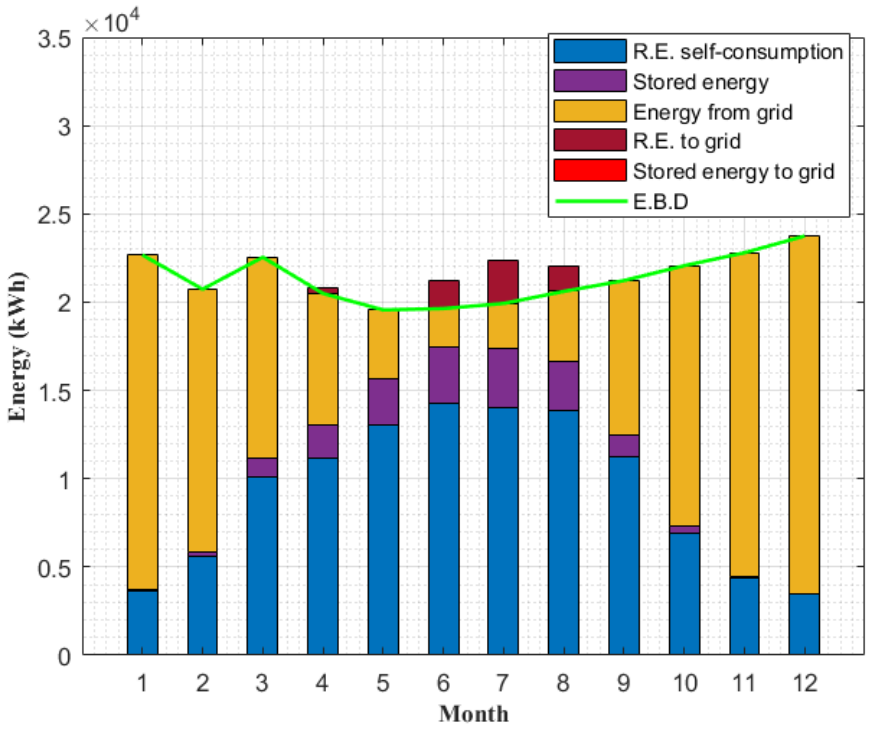

Figure 4.4: Different sources of electrical energy responding to electrical energy building demand for I-CAES (Strasbourg) – Liquid piston

4.2 Micro compressed air energy storage system current market

Even though classical compressed air energy storage (C-CAES) exists for more than 40 years, the micro CAES technology is still in development phase. In the last decade, small scale compressed air energy storage has been an interesting topic for many scientific researchers trying to find solutions to the technical restrictions and limitations presented by the storage systems. Numerical sizing tool are developed to study different system configurations in order to find the best system efficiency or to make the energy storage system more profitable within different energy context. In addition, experimental works are concentrated for the storage phase of a small power energy storage system. Beside these theoretical and experimental investigations, the compressed air market presents a missing piece to accomplish this micro energy storage system. In fact, the high inlet pressure turbine machine (> 20 bar) is difficult to find in the actual market which makes this system not applicable in the short term.

4.2.1 Air compressor and expander market

Air compressors

Air compressors are classified as follows: Positive displacement (volumetric) and dynamic (turbo-compressor) compressor as seen in Figure 4.5. In the first category, the pressure rise is obtained by reducing a certain volume of gas using mechanical action or by accumulating air mass. These positive displacement compressors fall into two families: reciprocating type (piston compressors, etc.) and rotary type (vane, lobe, screw compressors, etc.). For the second category (dynamic compressors or turbochargers), the work is done on a fluid so as to rise its pressure. Compression is achieved by applying inertial forces to the gas by the bladed impellers. Dynamic compressors are subdivided into centrifugal and axial compressors. Figure 4.6 shows the area of usage for some single-stage compressors. It is nevertheless possible to combine several compressors in parallel to increase the total mass flow or in series to increase the discharge pressure.

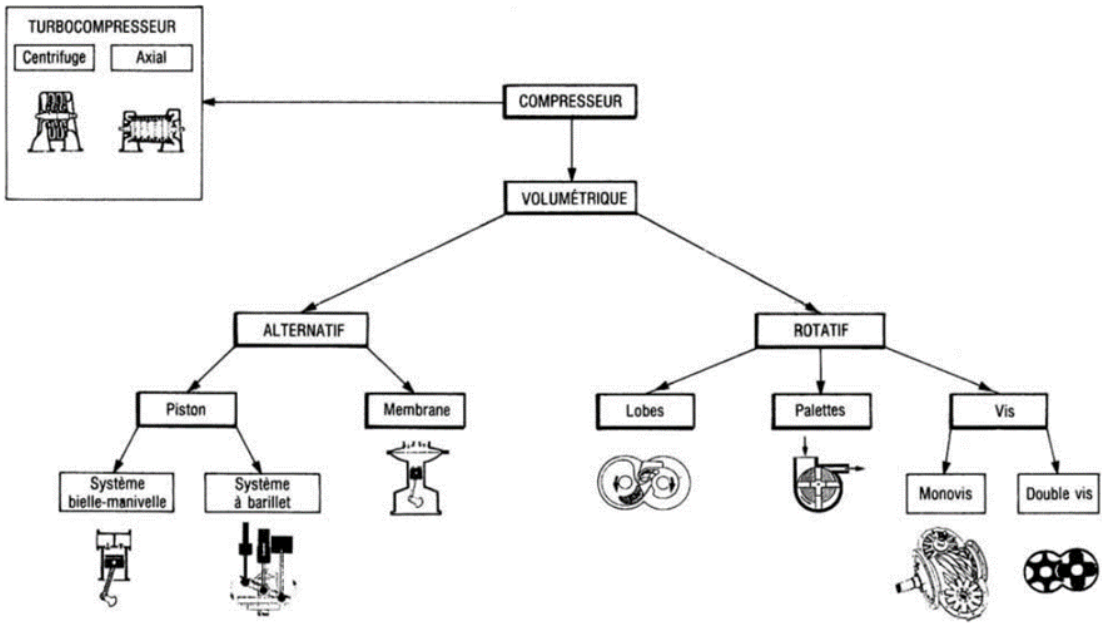

Figure 4.5: Classification of compressor operational industrial uses [53]

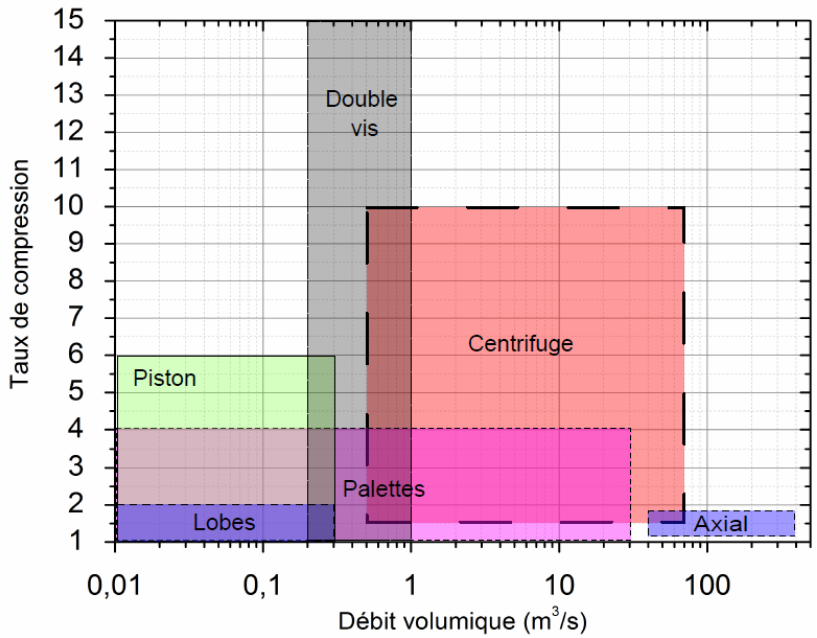

Figure 4.6: Single stage compressor application range [53]

The main actors in the air compressor market in Europe are Atlas copco (Sweden), Kaeser compressors (Germany), Boge (Germany), Bauer compressor (Germany). This commercial market is primarily focused on the screw compressor ranging from a few kilowatts to a hundred kilowatts (depending on the air mass flow sucked by the compressor which in turn depends on the application) for a maximum discharge pressure ranging from 10 to 15 bar. For a high

pressure range (from 50 to 300 bar) piston compressors are introduced to meet high pressure industrial applications from tens to hundreds of kilowatts. These compressors are used in the automotive, brewing, agri-food sector, paper manufacturing, blowing (glass), wastewater treatment, marine, medical and healthcare industries. Turbo-compressor products (centrifugal/axial) target megawatt power range for a very large intake air flow (10^3 to 10^6 m^3/h) with an outlet pressure ranging from 6 to 200 bar. This type of compressor is used for hydrocarbon and petrochemical (refining) and industrial gas (air separation) applications and to generate electricity. Table 4.3 lists some examples of compressors available on the market according to technical parameters (Pressure, outlet power, mass flow rate, and weight) and supplier.

Table 4.3: Examples of available compressors in the actual market

Compressor	Working pressure (bar)	Power (kW)	Mass flow rate delivered (m^3/h)	Weight (kg)	Provider
Screw (GR)	14 – 20	110 – 200	760 – 1 405	3140 – 3500	Atlas Copco
Screw (GA)	7 – 14	5 – 500	30 – 5 076	317 – 8400	Atlas Copco
Screw (SO)	8 – 10	45 – 355	315 – 3 060	2150 – 6600	BOGE
Lobe (SL)	8 – 10	1.5 – 7.5	9.6 – 1860	-	Renner Kompressoren
Piston (I)	360	30 – 160	78 – 432	1150 – 4000	Bauer Compressor
Piston (LB)	6 – 40	11 – 15	86 – 144		Atlas Copco
Piston (LB)	40 – 300	5.5 – 18	7.2 – 144	-	Atlas Copco
Centrifugal (ZH)	2.5 – 13	355 – 3150	4579 – 35244	6000 – 27000	Atlas Copco
Centrifugal	3.5 – 10	185 – 2240	1500 – 19 800	4500 – 13000	Almig

Air expanders

As for the turbo-expander market, the key players are Atlas Copco (Sweden), BHGE (United States), Cryostar (Switzerland), Ingersoll Rand, Man Diesel & Turbo, Siemens AG, Air Products and Chemicals (United Kingdom) and L.A. Turbine (United States). Several industrial applications use the turbo-expander technology: LNG (Liquefied Natural Gas) solutions, industrial gas applications, energy production (Natural Gas-Fired Power Plant) and renewable energy (Geothermal energy: recovery of waste heat). The turbo-expanders are available in the market with multiple different models that can withstand pressures up to 200 bar. These proposed solutions target megawatt power range. Currently, several scientific studies are focused on reducing the size of the Organic Ranking Cycle (ORC) technology where a small-scale turbo-expander (kW) is being tested. At the market level, this solution is not always

attractive because of its installation cost (€/kW) which is too high and which does not guarantee a reasonable return on investment [54]. In addition, many scientific researchers are trying to convert positive displacement compressors (scroll or screw) used in cooling and compressed air technology and which they are cheaply available in the market, into expanders integrated into small ORC in particular below 100 kW [55]. Based on Weiß [55] the small power turbines are not available in today market. In this subject, Lemort and Legros [56] detailed the selection criteria and consequences of the expander in an Organic Rankine Cycle (ORC) system and they presented particularly the main operations and limitations for the positive displacement expander (Reciprocating, orbital, and rotary). Based on Lemort and Legros the positive displacement compressor market and technical maturity in HVAC&R (Heating, Ventilation, Air-Conditioning and Refrigeration) and the compressed air industry is more advanced than the positive displacement expander market and its technical maturity in ORC systems. Daccord et al. [57] proposed a new expander prototype based on a piston expander that can be integrated in an exhaust heat recovery in a truck using an ORC technology (working fluid of the Rankine cycle used for their study is an ethanol-based mixture). Daccord et al. designed a single cylinder axial expander with nominal supply pressure of 30 bar for a maximal electric power of 3 kW (displacement volume equal to 443 cm^3). Qiu et al. [58] tested the viability for converting a market available scroll compressor into an expander. For 8.6 bar as expander inlet pressure their converted compressor produced 965 W with 3995 rpm. Ziviani et al. [59] developed a newly design open-drive oil-free scroll expander integrated in a small scale Organic Rankine Cycle applications. They successfully tested a scroll expander with an internal volume ratio of 3.5 and for the maximum output power of 3.75 kW at 2500 rpm (10 bar was the maximum expander inlet pressure). ENOGIA is one the few companies that developed an innovative small scale turbine (10 kW) while proposing wasted heat recovering and converting it into electricity based on Rankine cycle. Their prototype is capable to produce to 160 kWth from 70 °C hot source [60].

4.2.2 Micro compressed air energy storage system barriers

There are many points that catch researcher's attention in order to be solved and therefore enhance the compressed air energy storage technology. Currently, micro compressed air energy storage system built from commercial air compressors and expanders propose low power output range with low working pressure. Beside the social restrictions, high pressure storage is essential to reduce the volume storage, to have higher compression temperature and therefore

have more hot energy recovered during air compression. High pressure reservoir material (metal, carbon fiber) plays a big role in the total system cost. Increasing the storage pressure has a main technical limitation regarding the air expander and its inlet pressure limit. As explained in section 4.2.1, the compressed air market is more addressed with low power output air compressors for multiple daily applications. In this subject, many numerical and experimental studies are increasing in recent years in order to develop low power output air expander using Organic Rankine Cycle development projects for example. The main technical limitations related to low power expanders are the working pressure and temperature [56].

4.3 Levilized cost of energy analysis (LCOE)

In addition to the technical investigation, the micro AA-CAES system is analyzed from the financial point of view. In this section, LCOE analysis is considered which compares three energy storage systems with different characteristics on a comparable basis. Ideal and virtual AIR4POWER prototypes with LightSail Energy prototype will be compared and analyzed in the following part. Note that AIR4POWER project is part of the energy transition context by proposing to answer the major question of energy storage and management. The AIR4POWER project aims to demonstrate the relevance of an innovative energy storage solution in the form of compressed air at a building and/or district scale which would offer a low environmental impact, high reliability and remarkable energy density. More details about the AIR4POWER project progress and key dates are described in appendix C.

4.3.1 LCOE input data

LightSail Energy developed a reversible air motor that compresses and expands air quasi-isothermally up and from 200 bar as explained in chapter 2. In order to compare the LightSail technology, two prototypes (ideal and virtual) of micro AA-CAES are proposed. The ideal prototype is based on best energetic parameters selection (described in chapter 3) while the virtual is composed from components available in the actual compressed air market. The main input data selected for the LCOE analysis is listed in Table 4.4.

Table 4.4: Main LCOE calculator inputs

		Virtual prototype	Ideal prototype	LightSail Energy
General input	R.E. cost (€/MWh)	60	60	60
	Inflation (%)	2	2	2
	WACC (discount rate %)	7	7	7
	OPEX (%)	2 % from CAPEX	2 % from CAPEX	2 % from CAPEX
	Electrical efficiency (%) (η_{elec})	35	35	55
Technical parameters	Provider	Ingersoll Rand	-	LightSail Energy
	Input power (kW)	23.5	100	200
	Storage pressure (bar)	40	200	200
	Storage time (h)	8	8	8
	Cycles/year	365	365	365
	Margin on supplier (%)	20	20	18
	Transport (%)	-	-	10
Turbine	Cost compared to air compressor (%)	120	120	-

Ingersoll Rand is chosen to compose virtual micro AA-CAES components. Table 4.5 lists the detailed cost of the storage system composed by a group of compressor, air reservoir and other equipments needed for the compressed air storage system. Screw compressor is selected to rise the ambient pressure to 10 bar where the piston compressor will in turn increase it to 40 bar. The total input power of the compressor group is equal to 23.5 kW. The storage time for the AIR4POWER prototype is fixed to be equal to the one proposed by LightSail Energy (8 hours). Storage time is estimated to be equal to discharge time.

Table 4.5: Ingersoll Rand air equipment cost

	Cost (€)
Screw Compressor	11 170
Piston Compressor	7 669
Air reservoir (1 m^3 at 40 bar)	10 000
Heat exchanger	2 500
Air dryer	3 130
Other equipment	870
Total	35 339

The cost of these equipment are used for both prototypes taking the estimation of the cost of 1 m^3 compressed air reservoir at 200 bar (ideal prototype) equals four times the one at 40 bar (40 000 euros). In both prototypes the turbine is considered as a prototype and not commercially found in the market.

4.3.2 LCOE analysis

4.3.2.1 First level of LCOE analysis

LCOE calculator measures the cost for these three technologies discussed above over a period of 20 years. This analysis can be divided into three modules:

- Specific characteristics of the application module (
- Table 4.6)
- Storage module (Table 4.7)
- Capital and operational expenditure module (
-
- Table 4.8)

Table 4.6: Specific characteristics of the application module

	Virtual prototype	Ideal prototype	LightSail Energy
Power (kW) (***Fixed***)	23.5	100	200
Storage time (h) (***Fixed***)	8	8	8

Energy (***Power x Storage time***) (kWh)	188	800	1 600
Cycle number/year (***Fixed***)	365	365	365
Discharge time/year (h) (***Discharge time x Cycle number/year***)	2 920	2920	2 920
Analysis period (years) (***Fixed***)	20	20	20
Total cycle number (***Cycle number/year x Analysis period***)	7 300	7 300	7 300
Electrical consummation/year (kWh) (***Energy x Cycle number/year x*** $\boldsymbol{\eta_{elec}^{-1}}$)	196 057	834 286	1 061 818
Electrical production/year (kWh) (***Energy x Cycle number/year***)	68 620	292 000	584 000

Using the global numerical code detailed in chapter 3, several numerical simulations were conducted with the input parameters fixed in section 7.2.1 (maximum input power, charge time, storage pressure, polytropic coefficient) in order to set the compressed air reservoir volume.

Table 4.7: Storage module

	Virtual prototype	Ideal prototype	LightSail Energy
Storage pressure (bar)	40	200	200
Polytropic index	1.4	1.4	1.185
Total reservoir volume (Energy/Stored energy) (m^3)	55	35	75
Stored energy (kWh/m^3)	3.42	22	21.33

Based on the single unit cost described in Table 4.5 and the reservoir volume detailed in Table 4.7, the total cost of each component of the system as well as the capital expenditure (CAPEX) and the operating expenses (OPEX) are listed in the Table 4.8.

Table 4.8: Capital and operational expenditure module

	Virtual prototype	Ideal prototype	LightSail Energy
Total reservoir cost (€)	550 000	1 400 000	-
Total compressor cost (€)	25 339	25 339	-
Turbine cost (€)	30 407	30 407	-
CAPEX: Initial total technology cost (***sum of three costs above***)	726 895	1 746 895	623 040
Actual costs per kWh of usable capacity (***CAPEX / Energy***) (€/kWh)	3 866	2 184	389
OPEX: Operating costs (***2% x CAPEX***) (€/year)	14 538	34 938	12 461

The initial LightSail Energy technology cost was calculated based on their fixed objective of energy capital cost (200 $/kWh) and power capital cost (800 $/kW).

4.3.2.2 Second level of LCOE analysis

In this section, Table 4.8 is expanded for a 20-year period. Table 4.9, Table 4.10 and Table 4.11 represent 20 years analysis for the three studied prototype (virtual, ideal and LightSail Energy) successively. In the following tables (Table 4.9, Table 4.10 and Table 4.11) year 0 represents initial cost (CAPEX) detailed in Table 4.8 which also lists the operating cost (OPEX) for year 1. 2 % inflation is taken into consideration for the OPEX calculation over the years. Renewable energy (R.E.) cost (€/kWh) is estimated to be fixed during the analysis period and is used to calculate the energy cost used to charge the compressors for each prototype. Total operation cost is the sum of the maintenance and the renewable energy charge cost at declared efficiency.

Table 4.9: AIR4POWER virtual prototype

Year	Capex (€)	Maintenance (€)	R.E. cost (€/kWh)	R.E. charge cost @100% efficiency (€)	R.E charge cost @declared efficiency (€)	Total operation cost (€)	Electrical production (kWh)
0	726 895						
1	-	14 538	0.06	4 117	11 763	26 301	68 620
2	-	14 829	0.06	4 117	11 763	26 592	68 620

3	-	15 125	0.06	4 117	11 763	26 889	68 620
4	-	15 428	0.06	4 117	11 763	27 191	68 620
5	-	15 736	0.06	4 117	11 763	27 500	68 620
6	-	16 051	0.06	4 117	11 763	27 814	68 620
7	-	16 372	0.06	4 117	11 763	28 135	68 620
8	-	16 699	0.06	4 117	11 763	28 463	68 620
9	-	17 033	0.06	4 117	11 763	28 797	68 620
10	-	17 374	0.06	4 117	11 763	29 138	68 620
11	-	17 722	0.06	4 117	11 763	29 485	68 620
12	-	18 076	0.06	4 117	11 763	29 839	68 620
13	-	18 438	0.06	4 117	11 763	30 201	68 620
14	-	18 806	0.06	4 117	11 763	30 570	68 620
15	-	19 182	0.06	4 117	11 763	30 946	68 620
16	-	19 566	0.06	4 117	11 763	31 330	68 620
17	-	19 957	0.06	4 117	11 763	31 721	68 620
18	-	20 357	0.06	4 117	11 763	32 120	68 620
19	-	20 764	0.06	4 117	11 763	32 527	68 620
20	-	21 179	0.06	4 117	11 763	32 942	68 620

Table 4.10: AIR4POWER ideal prototype

Year	Capex (€)	Maintenance (€)	R.E. cost (€/kWh)	R.E. charge cost @100% efficiency (€)	R.E charge cost @declared efficiency (€)	Total operation cost (€)	Electrical production (kWh)
0	1 746 895						
1	-	34 938	0.06	17 520	50 057	84 995	292 000
2	-	35 637	0.06	17 520	50 057	85 694	292 000
3	-	36 349	0.06	17 520	50 057	86 407	292 000
4	-	37 076	0.06	17 520	50 057	87 134	292 000
5	-	37 818	0.06	17 520	50 057	87 875	292 000
6	-	38 574	0.06	17 520	50 057	88 631	292 000
7	-	39 346	0.06	17 520	50 057	89 403	292 000
8	-	40 133	0.06	17 520	50 057	90 190	292 000
9	-	40 935	0.06	17 520	50 057	90 992	292 000
10	-	41 754	0.06	17 520	50 057	91 811	292 000

11	-	42 589	0.06	17 520	50 057	92 646	292 000
12	-	43 441	0.06	17 520	50 057	93 498	292 000
13	-	44 310	0.06	17 520	50 057	94 367	292 000
14	-	45 196	0.06	17 520	50 057	95 253	292 000
15	-	46 100	0.06	17 520	50 057	96 157	292 000
16	-	47 022	0.06	17 520	50 057	97 079	292 000
17	-	47 962	0.06	17 520	50 057	98 019	292 000
18	-	48 921	0.06	17 520	50 057	98 979	292 000
19	-	49 900	0.06	17 520	50 057	99 957	292 000
20	-	50 898	0.06	17 520	50 057	100 955	292 000

Table 4.11: LightSail Energy prototype

Year	Capex (€)	Maintenance (€)	R.E. cost (€/kWh)	R.E. charge cost @100% efficiency (€)	R.E charge cost @declared efficiency (€)	Total operation cost (€)	Electrical production (kWh)
0	623 040						
1	-	12 461	0.06	35 040	63 709	76 170	584 000
2	-	12710	0.06	35 040	63 709	76 419	584 000
3	-	12 964	0.06	35 040	63 709	76 673	584 000
4	-	13 224	0.06	35 040	63 709	76 933	584 000
5	-	13 488	0.06	35 040	63 709	77 197	584 000
6	-	13 758	0.06	35 040	63 709	77 467	584 000
7	-	14 033	0.06	35 040	63 709	77 742	584 000
8	-	14 314	0.06	35 040	63 709	78 023	584 000
9	-	14 600	0.06	35 040	63 709	78 309	584 000
10	-	14 892	0.06	35 040	63 709	78 601	584 000
11	-	15 190	0.06	35 040	63 709	78 899	584 000
12	-	15 493	0.06	35 040	63 709	79 203	584 000
13	-	15 803	0.06	35 040	63 709	79 512	584 000
14	-	16 119	0.06	35 040	63 709	79 828	584 000
15	-	16 442	0.06	35 040	63 709	80 151	584 000

16	-	16 771	0.06	35 040	63 709	80 480	584 000
17	-	17 106	0.06	35 040	63 709	80 815	584 000
18	-	17 448	0.06	35 040	63 709	81 157	584 000
19	-	17 797	0.06	35 040	63 709	81 506	584 000
20	-	18 153	0.06	35 040	63 709	81 862	584 000

Table 4.12 summarizes Table 4.9, Table 4.10 and Table 4.11 by taking into assumption the 20 years studied period and a discount rate (WACC) of 7%. Note that the discount rate is the interest rate used to calculate the present value of future cash flows from a project or investment.

Table 4.12: Intermediate calculations for LCOE

	Virtual prototype	Ideal prototype	LightSail Energy
RE cost (Electrical input @ 100% efficiency)	43 618 €	185 607 €	371 214 €
RE cost (Electrical input @ declared efficiency)	124 622 €	530 306 €	674 935 €
Maintenance cost	179 108 €	430 437 €	153 518 €
Operation cost	303 730 €	960 743 €	828 453 €
Electrical production	726 961 kWh	3 093 452 kWh	6 186 904 kWh

From Table 4.12, the levelized cost of energy for the three studied technologies are presented in the table below.

Table 4.13: LCOE Final calculations

	Virtual prototype	Ideal prototype	LightSail Energy
Charge cost (€/kWh) (***RE cost @ 100% eff. / Elec. prod.***)	0.06	0.06	0.06
Efficiency penalty (€/kWh) (***RE cost @ declared eff. / Elec. Prod. – Charge cost***)	0.11	0.11	0.05
Maintenance (€/kWh)	0.25	0.14	0.02

(***Main. cost / Elec. Prod.***)			
Capital Cost (€/kWh) (***CAPEX/ Elec prod***)	1.00	0.56	0.10
Total LCOE (€/kWh)	**1.42**	**0.88**	**0.23**

Table 4.13 and Figure 4.7 show the LCOE (€/kWh) of the three studied technology in this section (virtual, ideal and LightSail Energy). It is seen clearly that the CAPEX is the most influential parameter on the total and final technology cost. Focusing on the CAPEX calculations, the reservoir cost is the most critical and causes high initial technology cost. Based on cost estimations assumed in this financial study the ideal prototype is still away of LightSail Energy technology, where the virtual prototype cannot be considered as a competitive with the two other technologies.

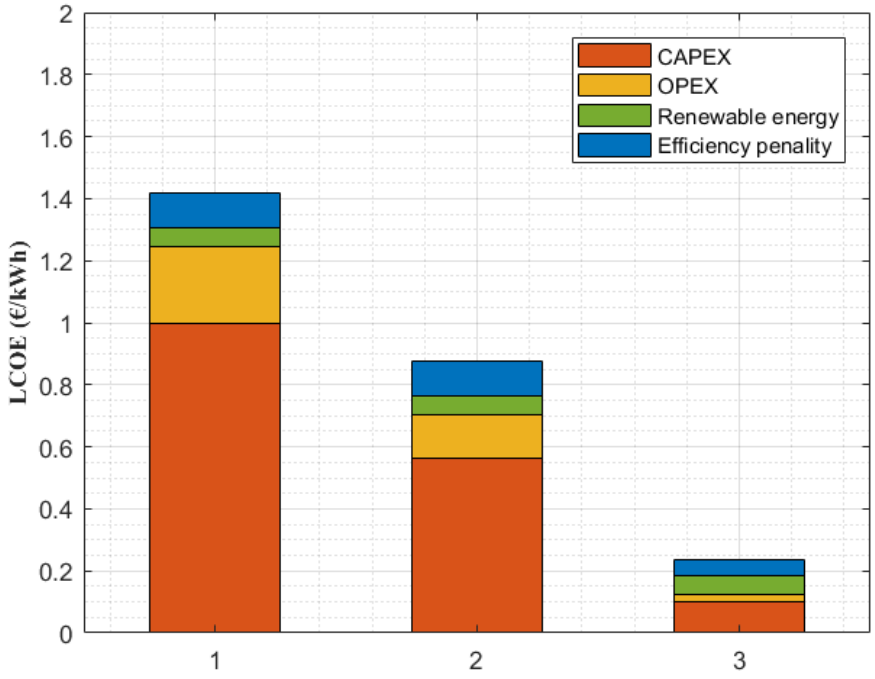

Figure 4.7: LCOE analysis for three compressed air storage technology (1: Virtual prototype, 2: ideal prototype and 3: LightSail Energy)

4.4 Building the ideal prototype

3D model of the ideal prototype discussed financially in previous section and technically in chapter 3 is presented in this section in order to have a better idea of the dimensions of the different components that compose the micro AA-CAES system. This work was applied

without focusing on applicable standards and regulations used in the compressed air industry. Based on Figure 4.8 the room dimensions needed to accommodate all the components of the storage system are as follow:

- Height: 3.88 m
- Length: 24 m
- Width: 11 m

The compressed air system installation usually consists of the following components:

- Compressor + heat transfer air/water (or air/oil or air/air)
- Compressed air reservoir
- Filter
- Air dryer
- Oil water separator
- Distribution system

The AA-CAES room can be divided into three zones (Figure 4.9):

- Power train zone
- Reservoir zone
- Control zone

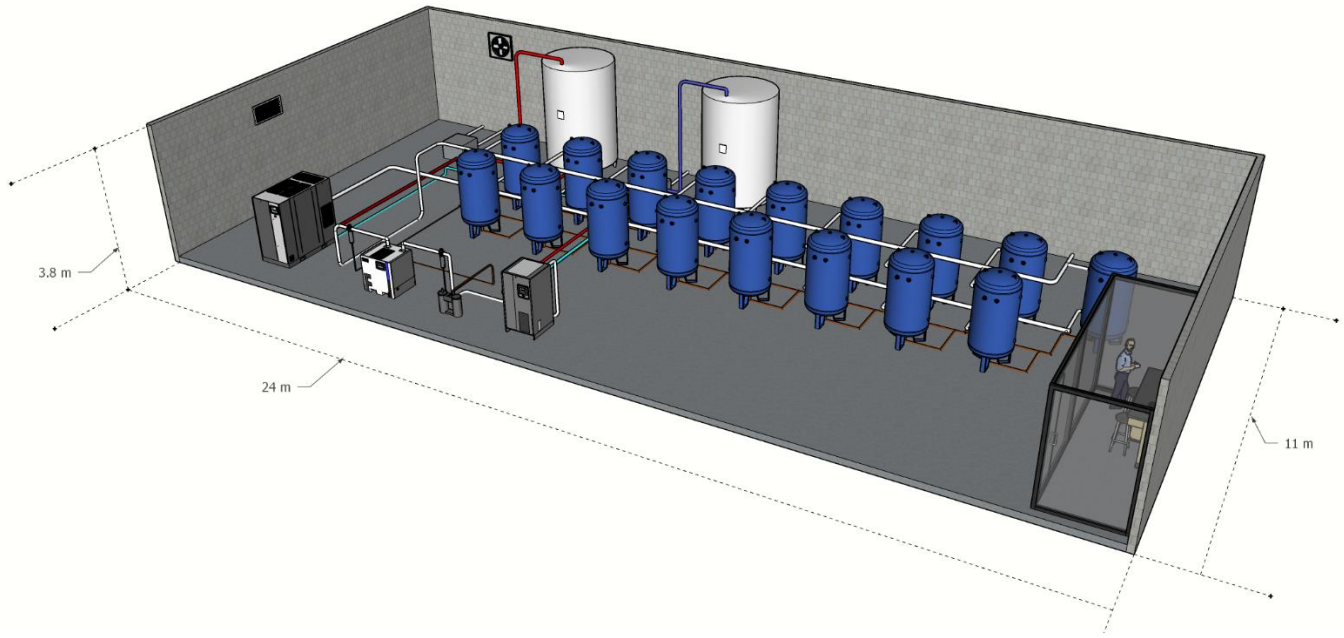

Figure 4.8: 3D model of the ideal prototype with test room dimensions

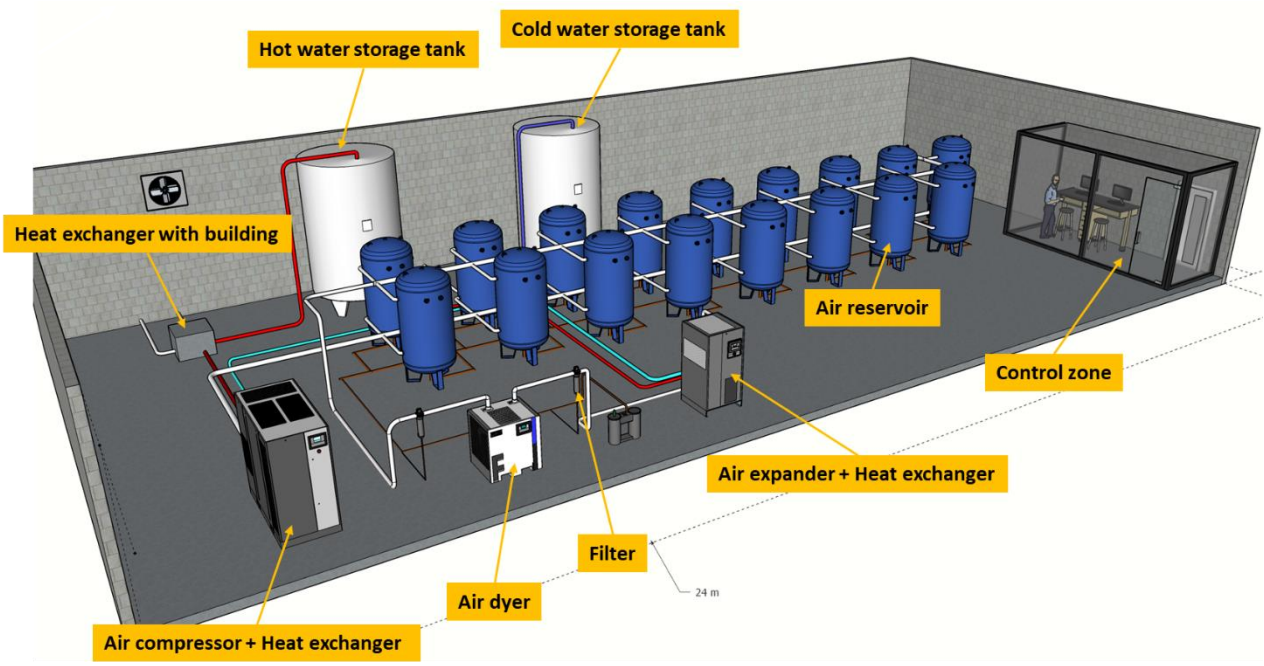

Figure 4.9: 3D model of the ideal prototype in a different angle (Ideal prototype)

4.4.1 Power train zone

Figure 4.10 shows in front of the figure the power train that is composed of (from left to right): compressor, air dryer, oil water separator and air expander. It is noticed that air filters are used at the air dryer input and output. The compressor is estimated to compress the air up to 200 bar and cooling it with an embedded heat exchanger air/water. Once the compressed air is released and before expanding it, the air goes through air filters (to purify the air and remove dust) and then air dryer that in turn removes any free water left in the system. Oil water separator is used in order to capture the oil left in compressor, compressed air reservoir and filters.

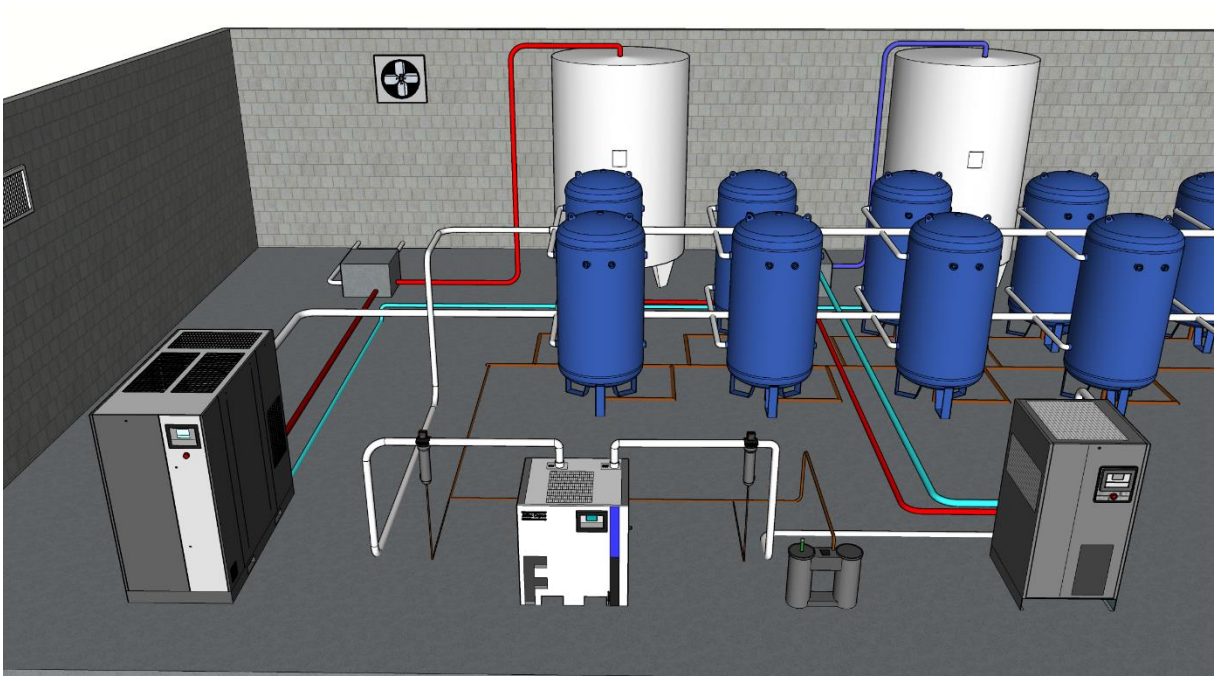

Figure 4.10: 3D model of ideal prototype with focusing on power train module (compressor, dryer, air/oil separator and expander)

4.4.2 Reservoir module

Figure 4.11 shows the two types of reservoirs used in the ideal prototype for the micro AA-CAES system. The blue reservoirs represent the compressed air reservoirs with 2 m^3 of capacity each. 34 compressed air reservoirs needed to represent the best energetic case (in other words the ideal prototype) are selected as seen in Figure 4.8. The two thermal reservoirs needed to store hot (at the top left) and cold (at the top right) water are shown in Figure 4.11. 8 m^3 is the capacity chosen for each thermal reservoir in the ideal prototype case. As explained in chapter 3 (section 3.1.1 and Figure 2.4) the thermal storage is connected to compressor, expander and to building through two heat exchangers which are represented by two grey cubes in the Figure 4.11.

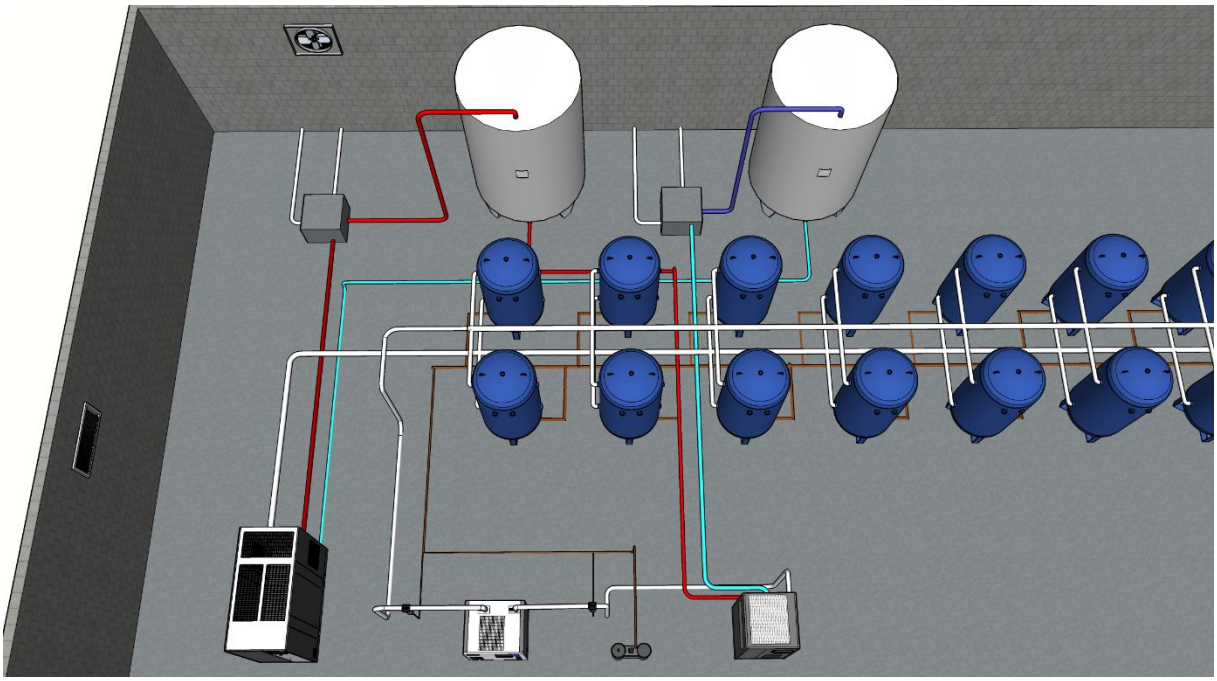

Figure 4.11: 3D model of ideal prototype with focusing on the connections between thermal energy module and power train module

Light blue pipe represents the connection used in order to cool the air during compression phase using stored cold water and recovered cold water after air expansion phase sent to the cold water storage. Before storing the recovered cold water, it passes through the heat exchanger that is connected to the building in order to answer cold building demand. In the same manner red pipes illustrate the hot water needed to preheat the compressed air before expanding it and hot water recovered after air compression phase. Before storing it, hot water passes through heat exchanger connected to the building in order to respond the building heating demand. Figure 4.12 focuses on the thermal water storage connections to the building through heat exchangers.

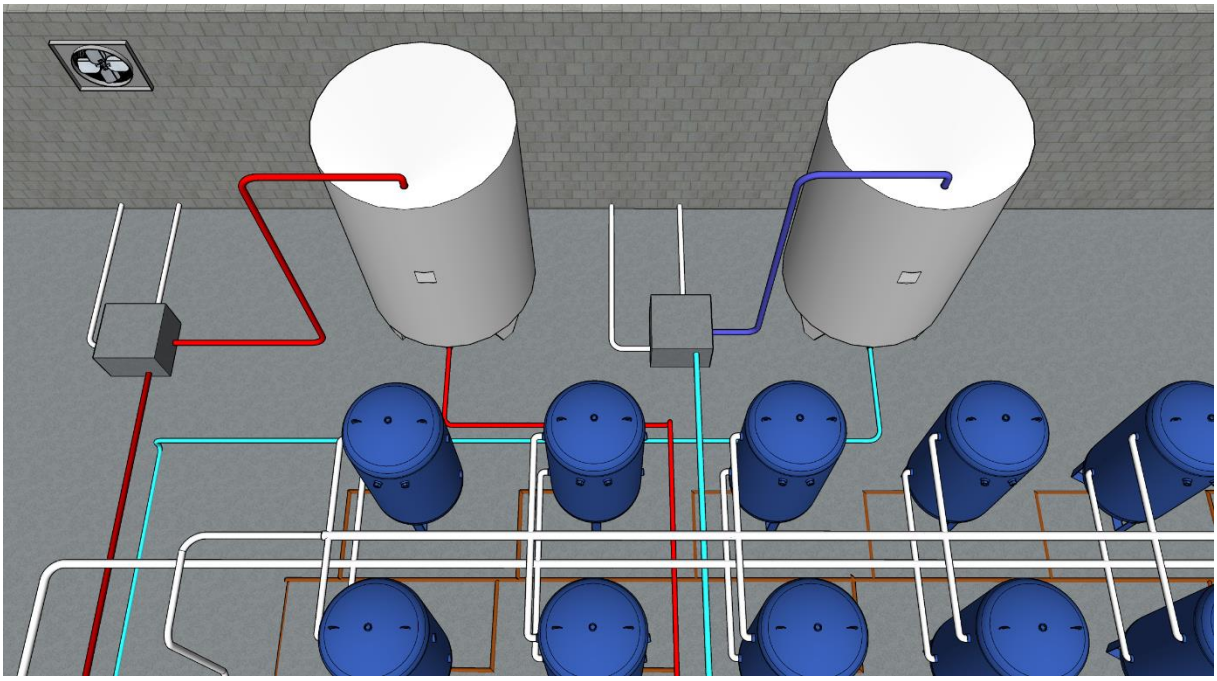

Figure 4.12: 3D model of ideal prototype with focusing the thermal energy module

4.4.3 Control module

Separate control unit is imagined as shown in Figure 4.13.

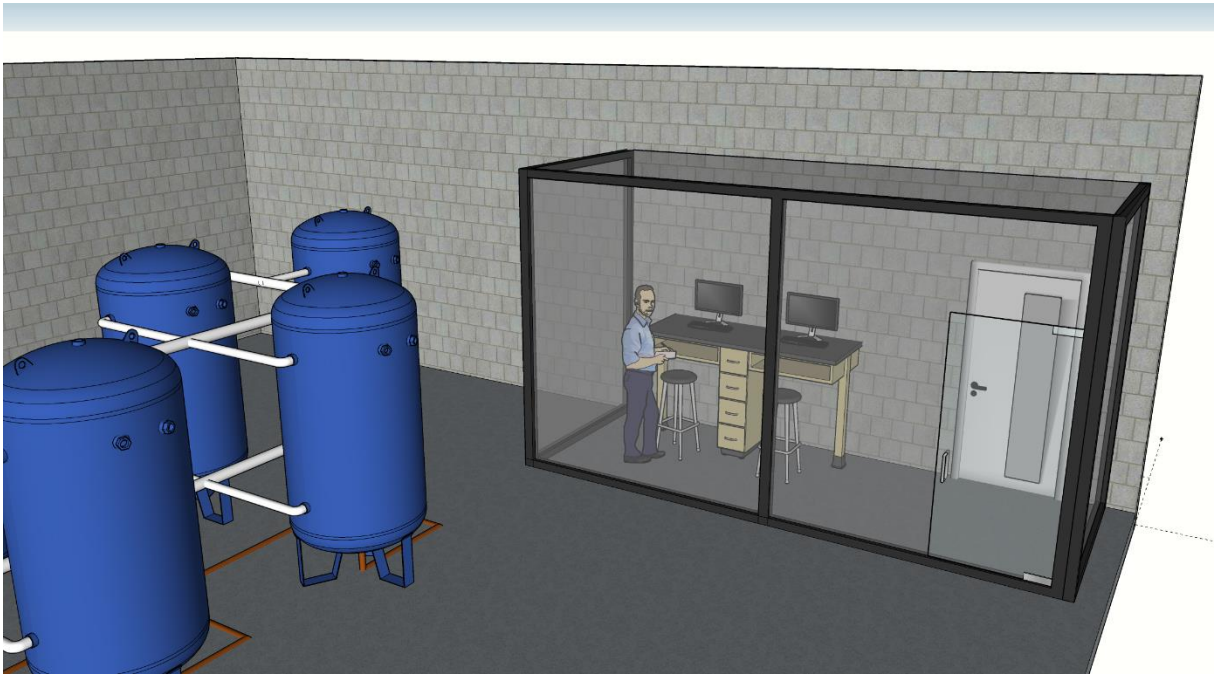

Figure 4.13: 3D model of the ideal prototype focusing the control module

4.5 Conclusion

This chapter carries out the investigation of two isothermal technologies developed in chapter 3 integrated in the global numerical tool developed in chapter 2. As a consequence, both isothermal technologies showed a remarkable advantages regarding the input/output roundtrip electrical efficiency. Moreover, the liquid piston technology compared to mechanical piston showed a nearly isothermal process with negligible air temperature variation during the compression and expansion phases. Focusing on the financial analysis, the capital cost of the different components of the CAES system is the major factor in making total LCOE (€/kWh) attractive and competitive with other storage technologies. High pressure reservoir and high inlet high pressure turbine are the first two components to be more developed and therefore reducing their cost.

Conclusion and perspectives

Conclusion

A numerical investigation has been performed on different compressed air energy storage technologies coupled to renewable energy modules and a building model. The research is focused on providing an understanding of the new environmental regulations context and the necessity of new innovative technology that specially brings the renewable energy sector to be more reliable and live up to high expectations. To date, compressed air energy has been used in many fields as an important vector to store different types of energies. Many researchers are currently focusing on developing small scale compressed air energy storage (CAES) coupled to building applications taking the advantage of the work developed for the multiple large scale systems installed worldwide. These researches are mainly concentrated on developing the hybrid architecture of the small scale CAES system going through each component (compressor, heat exchanger, turbine and high pressure reservoir) in order to increase the inlet/outlet roundtrip electrical or global efficiency.

Firstly, a small scale advanced adiabatic compressed air energy storage system (AA-CAES) is numerically investigated. Coupled to renewable energy modules (solar panels and wind turbines) and to a building model with specific detailed typologies, the AA-CAES is modeled taking the consideration of two modes of operation (Autonomous and connected mode) and three different geographical scenarios (Strasbourg, Nantes and Nice). Connected to the electrical, hot and cold grids, the AA-CAES showed more interests in responding to the building energy demands. The trigeneration (electrical, hot and cold) AA-CAES system offers a range of compromise between electrical system efficiency, hot coverage ratio and cold coverage ratio depending on the building application and the size of renewable energy modules.

Secondly, the study concentrated on the quasi-isothermal compressed air energy storage (I-CAES) system especially to two innovative technologies developed by LightSail Energy (mechanical piston with water injection) and Enairys Powertech (Liquid piston with integrated heat exchanger). For the first time, a detailed thermodynamic analysis is described for each isothermal compressor and turbine developed by the mentioned Startups, based on the limited data exchanged with AIA LIFE DESIGNERS. These mathematical models enabled the

comprehension of the main operation of these technologies and therefore having many orders of magnitudes of different physical parameters such as air/water temperature, air pressure, compensated/recovered work, heat absorbed/released, droplet diameter and heat transfer coefficient. Mechanical piston with water injection technology showed to be favorable to the production of hot water during air compression and cold water during air expansion, where liquid piston with integrated heat exchanger represented a strong isothermal compression and expansion with a minimal air temperature gradient. These facts justified the higher inlet/outlet roundtrip electrical efficiency obtained by Enairys Powertech.

Finally, a detailed financial analysis for the AA-CAES and I-CAES systems is presented in this work. With describing the compressed air market and listing the cost of each CAES component available in this market, three prototypes (virtual, ideal and LightSail Energy) were proposed to be financially investigated based on a levelized cost of energy analysis (LCOE). The main obstacles in building a small scale AA-CAES prototype is the non-availability of inlet high pressure turbine and the cost of high pressure reservoir in the actual compressed air market. LightSail Energy technology seems to have the lowest levelized cost of energy among the ideal and virtual prototypes where their own developed high pressure reservoir plays a big role in reducing their main capital cost.

Perspectives

The numerical results conducted for the small scale AA-CAES found in this work were validated by the comparison done with similar numerical work [46]. This fact does not neglect the need of an experimental test bench representing the small scale AA-CAES hybrid architecture described in chapter 2 or virtual prototype represented in chapter 4. This can be achieved for a few kilowatts system output which means low working air pressure. As for important power range CAES system, the development of small scale gas turbines is needed to be taken into serious consideration in order to work with high air pressure range.

Concerning the global small scale AA-CAES numerical model detailed in this work, many different perspectives are listed below:

- Taking into account the different physical parameters variations during the numerical time step fixed to one hour. In this work, the main objective was to have a global point of view over a year regarding the AA-CAES coupled to renewable energy module and building model using Excel VBA which is limited in terms of numerical power. Therefore, during the fixed numerical time step, the processes were considered to be permanent.

- Taking into consideration the ambient temperature variation throughout the year depending on the location where the AA-CAES system is installed which impacts the air temperature of the high pressure reservoir calculation. Therefore, this consideration will take into account the heat losses or gain from/to thermal energy storage/ambient air.
- In addition to answering energy building demand, most of the energy storage projects regarding buildings or cities or parking (for example) propose electrical vehicle concepts linked to the energy storage system. It can be interesting to insert an electrical vehicle sub-model to the developed global model in order to have a close look for the time needed to charge a specific number of electrical vehicles based on the installed compressed air energy storage system.
- It is interesting to create a sub component in the global AA-CAES numerical tool, to model a heat pump. Inserting a heat pump to the global system (AA-CAES + Building + renewable energy) is interesting regarding the management of the water temperature resulting from the AA-CAES system, in case the variation of these temperatures remains quite minimal and therefore a lukewarm loop and open water access (like sea water) are needed as proposed in Figure 0.1.

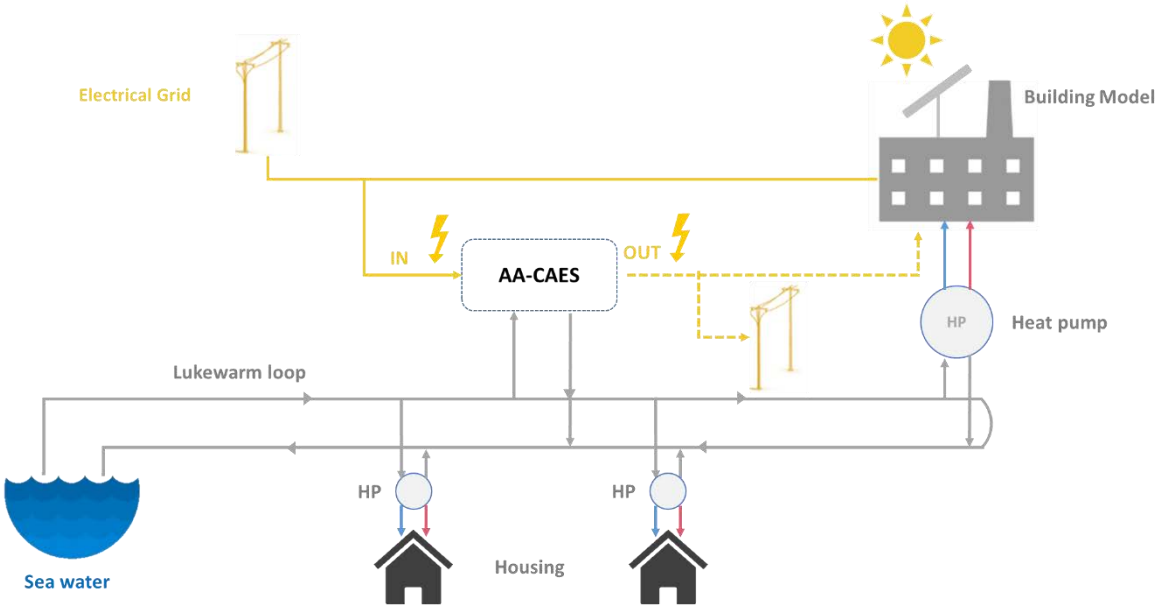

Figure 0.1: AA-CAES installation diagram and possible connected operating mode with heat pump insertion and sea water access

Appendix A *Adiabatic air compression/expansion process*

This appendix focuses on the polytropic air compression and compressed air expansion phases. In addition to the air storing and the air releasing to/from high pressure reservoir processes are theoretically described below. The equations described in this appendix complete the analysis done in chapter 2.

A.1. Charge phase

$$w_{charge} = \int_{P_{in}}^{P_{out}} vdp = \int_{P_{in}}^{P_{out}} \frac{P_{in}^{1/n}}{P^{1/n}} v_{in}\, dP = P_{in}^{1/n} v_{in} \int_{P_{in}}^{P_{out}} \frac{dP}{P^{1/n}} \tag{A.1}$$

$$\begin{aligned} w_{charge} = \int_{P_{in}}^{P_{out}} vdp &= P_{in}^{1/n}\, v_{in} \left[\frac{P^{n-1/n}}{n-1/n}\right]_{P_{in}}^{P_{out}} \\ &= \frac{n}{n-1} P_{in}^{1/n}\, v_{in} \left[P_{out}^{n-1/n} - P_{in}^{n-1/n}\right] \end{aligned} \tag{A.2}$$

$$w_{charge} = \int_{P_{in}}^{P_{out}} vdp = \frac{n}{n-1} P_{in}^{1/n}\, v_{in}\, P_{in}^{n-1/n} \left[\frac{P_{out}^{n-1/n}}{P_{in}^{n-1/n}} - 1\right] \tag{A.3}$$

$$w_{charge} = \int_{P_{in}}^{P_{out}} vdp = \frac{n}{n-1} P_{in} v_{in} \left[\frac{P_{out}^{n-1/n}}{P_{in}^{n-1/n}} - 1 \right] \quad (A.4)$$

$$w_{c,i} = \int_{P_{in}}^{P_{out}} vdp = \left(\frac{n}{n-1} r T_{in,c,i} \left[\beta_c(t)^{\frac{n-1}{n}} - 1 \right] \right) \frac{1}{\eta_{pol}} \quad (A.5)$$

And using Poisson's law:

$$P_{in} v_{in}^n = P_{out} v_{out}^n \quad (A.6)$$

$$P_{in} \left(\frac{r T_{in}}{P_{in}} \right)_{in}^n = P_{out} \left(\frac{r T_{out}}{P_{out}} \right)_{out}^n \quad (A.7)$$

$$P_{in}^{1-n} T_{in}^n = P_{out}^{1-n} T_{out}^n \quad (A.8)$$

$$T_{out,c,i} = T_{in,c,i} \, \beta_c(t)^{\frac{n-1}{n}} \quad (A.9)$$

A.2. Storage phase

A.2.1. Introducing air into the reservoir from compressors

$$d(m\,u) = +\dot{m}_c h_{in} dt \; + \delta Q = h_{in} dm \; + \delta Q \quad (A.10)$$

$$\frac{d(m\,u)}{dt} = +\dot{m}_c h_{in} + \frac{\delta Q}{dt} \quad (A.11)$$

$$\frac{u\,dm}{dt} + \frac{m\,du}{dt} = +\dot{m}_c h_{in} + \frac{\delta Q}{dt} \tag{A.12}$$

$$c_v\,T_{res}\,\dot{m}_c + mc_v\frac{dT}{dt} = \left(r\,T_{in,res} + c_v\,T_{in,res}\right)\dot{m}_c + (KS)_{res}(T_{amb} - T_{res}) \tag{A.13}$$

A.2.2. Releasing air from the reservoir into turbines

Air leaving the high pressure reservoir process is described with the equations (22-28):

$$d(m\,u) = -\dot{m}_t h_{out} dt\ + \delta Q = +h_{out} dm\ + \delta Q \tag{A.14}$$

$$\frac{d(m\,u)}{dt} = -\dot{m}_t h_{out} + \frac{\delta Q}{dt} \tag{A.15}$$

$$\frac{u\,dm}{dt} + \frac{m\,du}{dt} = -\dot{m}_t h_{out} + \frac{\delta Q}{dt} \tag{A.16}$$

$$c_v\,T_{res}\,\dot{m}_t + mc_v\frac{dT}{dt} = -\left(r\,T_{out,res} + c_v\,T_{out,res}\right)\dot{m}_t + (KS)_{res}(T_{amb} - T_{res}) \tag{A.17}$$

A.3. Discharge phase

Polytropic expansion: $Pv^n = Cte = P_{in}{v_{in}}^n = P_{out}{v_{out}}^n$

$$w_{Discharge} = \int_{P_{in}}^{P_{out}} v dp = \int_{P_{in}}^{P_{out}} \frac{P_{in}^{1/n}}{P^{1/n}} v_{in}\,dP = P_{in}^{1/n} v_{in} \int_{P_{in}}^{P_{out}} \frac{dP}{P^{1/n}} \tag{A.18}$$

$$w_{Discharge} = \int_{P_{in}}^{P_{out}} vdp = P_{in}^{1/n}\, v_{in} \left[\frac{P^{n-1/n}}{n-1/n}\right]_{P_{in}}^{P_{out}} = \frac{n}{n-1} P_{in}^{1/n}\, v_{in} \left[P_{out}^{n-1/n} - P_{in}^{n-1/n}\right] \quad (A.19)$$

$$w_{Discharge} = \int_{P_{in}}^{P_{out}} vdp = \frac{n}{n-1} P_{in}^{1/n}\, v_{in}\, P_{in}^{n-1/n} \left[\frac{P_{out}^{n-1/n}}{P_{in}^{n-1/n}} - 1\right] \quad (A.20)$$

$$w_{Discharge} = \int_{P_{in}}^{P_{out}} vdp = \frac{n}{n-1} P_{in} v_{in} \left[\frac{P_{out}^{n-1/n}}{P_{in}^{n-1/n}} - 1\right] \quad (A.21)$$

$$w_{t,i} = \int_{P_{in}}^{P_{out}} vdp = \left(\frac{n}{n-1} r T_{in,t,i} \left[\beta_t(t)^{\frac{n-1}{n}} - 1\right]\right) \eta_{pol} \quad (A.22)$$

And using Poisson's law:

$$P_{in} v_{in}^n = P_{out} v_{out}^n \quad (A.23)$$

$$P_{in} \left(\frac{rT_{in}}{P_{in}}\right)_{in}^n = P_{out} \left(\frac{rT_{out}}{P_{out}}\right)_{out}^n \quad (A.24)$$

$$P_{in}^{1-n}\, T_{in}^n = P_{out}^{1-n}\, T_{out}^n \quad (A.25)$$

$$T_{out,t,i} = T_{in,t,i}\, \beta_t(t)^{\frac{n-1}{n}} \quad (A.26)$$

Appendix B *Mechanical/Liquid piston compressor/expander*

The section below presents the details behind the study of the mechanical and liquid piston compressor/expander technology.

B.1. Mechanical piston technology

B.1.1. Mass transfer between air and water droplets

Mass transfer between the air and the injected water during compression/expansion will be guided by the difference of water vapor pressure contained in the air and in the vicinity of the water droplets where the partial water vapor pressure ($P_{partial}^{wv}$) is equal to the saturated water vapor pressure (P_{SAT}^{wv}). This partial water vapor pressure in the vicinity of the water droplet will play a big role to push away or to attract the water vapor contained in the air.

During the compression phase, the air temperature is higher than that of the cold injected water. The water vapor contained in the air will migrate towards to or escape from the water droplet as long as the partial water vapor pressure contained in the air is higher or lower than the partial water vapor pressure in the vicinity of droplet. At the compressor outlet, it is assumed that there is no more mass transfer and in this case, the partial water vapor pressure in the air is equal to the saturated water vapor pressure at the water outlet temperature. In other words the wet temperature is equal to that of water (Figure A1).

During the expansion phase (Figure A2), the compressed air is cooler than the hot injected water. This will help to fill the air with water vapor (humidification/increase of the partial water vapor pressure in the air), until the air is saturated. In fact, the water vapor in the vicinity of

droplet at water temperature have a higher pressure than the water vapor pressure in air. The mass transfer will take place from water droplet to air, until saturation.

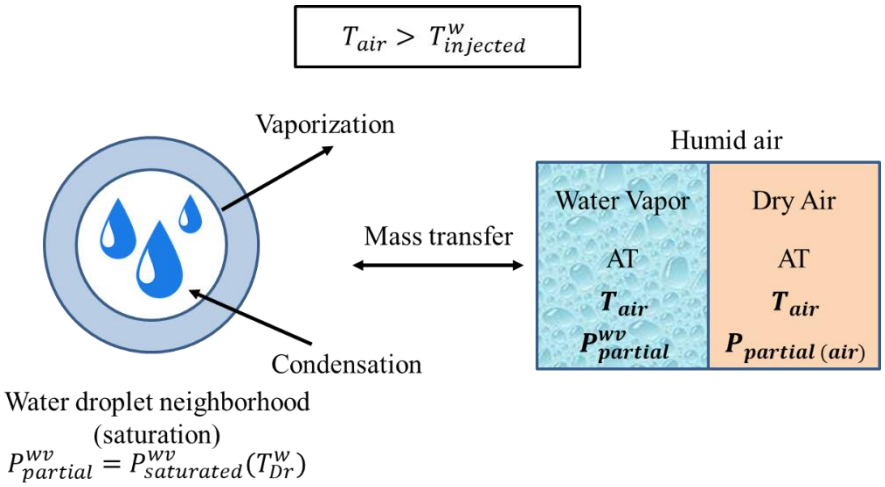

Figure 0.2: Mass transfer between water droplets injected inside the cylinder during compression

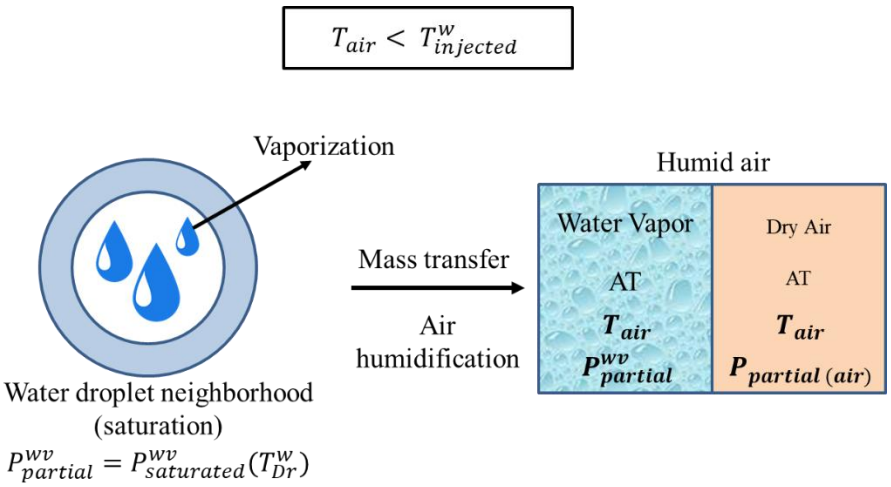

Figure 0.3: Mass transfer between water droplets injected inside the cylinder during expansion

B.1.2. Compressed air expansion process

Figure 3.2 shows the PV diagram of the compressor and expander cycle for mechanical piston technology. Equation (3.19) is detailed with the analytical equations below which in turn describe the four air expansion cycle phases (1'→5').

Compressed air introduction phase (1'→2'):

$$U_{2'} - U_{1'} = -P_{in}(V_{2'} - V_{1'}) + \int_{1'}^{2'} \dot{m}_{DA}\, h_{in}\, dt + Q_{1'2'} \qquad \text{(B.1)}$$

Compressed air expansion phase (2'→3'):

$$U_{3'} - U_{2'} = \frac{1}{n_t - 1}\left(\eta_{pol}\right)(P_{in}V_{2'})[(VR_t)^{n_t-1} - 1] + Q_{2'3'} \quad \text{(B.2)}$$

Isochoric air expansion phase (3'→4'):

$$U_{4'} - U_{3'} = -\int_{3'}^{4'} \dot{m}_{DA}\, h\, dt \quad \text{(B.3)}$$

Expanded air discharge phase (4'→5'):

$$U_{5'} - U_{4'} = -P_{out}(V_{5'} - V_{4'}) - \int_{4'}^{5'} \dot{m}_{DA}\, h_{out}\, dt + Q_{4'5'} \quad \text{(B.4)}$$

The sum of the four previous equations is as follows:

$$\begin{aligned} 0 = {} & -P_{in}(V_{2'} - V_{1'}) - P_{out}(V_{5'} - V_{4'}) \\ & + \frac{1}{n_t - 1}\left(\eta_{pol}\right)(P_{in}V_{2'})[(VR_t)^{n_t-1} - 1] + \int_{1'}^{2'} \dot{m}_{DA}\, h_{in}\, dt \\ & - \int_{4'}^{5'} \dot{m}_{DA}\, h_{out}\, dt + Q_{1'2'} + Q_{2'3'} + Q_{4'5'} \end{aligned} \quad \text{(B.5)}$$

B.2. Liquid piston technology

B.2.1. Air introduction phase

The section below present the series of analytical equations that described the air suction (phase: A ➞ B) before compression process begins and the compressed air introduction (phase: A' ➞ B') before expansion process begins. These equations based on energy conservation led to the temperature equation at state B and B'.

$$\frac{dU}{dt} = \dot{m}\, h_{in} + \dot{Q} - P\frac{dV}{dt} \quad \text{(B.6)}$$

$$\frac{dU}{dt} + P\frac{dV}{dt} = \frac{dH}{dt} \quad \text{(B.7)}$$

$$\frac{dH}{dt} = \dot{m}h_{in} + \dot{Q} \quad \text{(B.8)}$$

$$\frac{dH}{dt} = \dot{m}h_{in} + he\, S(t)(T^w - T) \quad \text{(B.9)}$$

$$M\frac{dh}{dt} + h\frac{dM}{dt} = \dot{m}h_{in} + he\ S(t)(T^w - T) \tag{B.10}$$

$$\dot{m}c_p t\ \frac{dT}{dt} + h\dot{m} - \dot{m}h_{in} = he\ S(t)(T^w - T) \tag{B.11}$$

$$\dot{m}c_p\ t\ \frac{dT}{dt} + \left(\dot{m}c_p + he\ S(t)\right)T(t) = \dot{m}c_pT_{in} + he\ S(t)T^w \tag{B.12}$$

$$S(t) = \frac{4}{D}V_2 = \frac{4}{D}\ \frac{\pi D^2}{4}L(t)\ nt = \pi\ D\ nt\ a\ t \tag{B.13}$$

$$\dot{m}c_p\ t\ \frac{dT}{dt} + \left(\dot{m}c_p + he\ \pi\ D\ a\ t\ nt\right)T(t) = \dot{m}c_pT_{in} + h\ \pi\ D\ nt\ a\ t\ T^w \tag{B.14}$$

$$\frac{\tau\ t}{\tau + t}\ \frac{dT}{dt} + T = \frac{\tau\ T_{in}}{\tau + t} + \frac{t\ T^w}{\tau + t} \tag{B.15}$$

$$\tau = \frac{\dot{m}\ c_p}{a\ nt\ h\ D\ \pi} \tag{B.16}$$

$$\tau = \frac{t_{cy}}{NTU} \tag{B.17}$$

$$NTU = \frac{he\ nt\ \pi\ DL_{initial}}{\dot{m}_{av}c_p} \tag{B.18}$$

$$T = T^w + \frac{\tau}{t}\ (T_{in} - T^w)\ \left(1 - e^{-t/\tau}\right) \tag{B.19}$$

B.2.2. Air discharge phase (Liquid piston compressor)

Equation (3.41) is a differential equation with second member that describes the phase air discharge phase after compressing the air (phase: C → D).This equation is solved based on two analysis approaching the air mass $M(t)$ and tube surface $S_{tu}(t)$.

- Mass calculation $\boldsymbol{M(t)}$

$$\frac{dM}{dt} = \dot{m} \tag{B.20}$$

$$M = \dot{m}t + b \tag{B.21}$$

The mass boundary conditions are as follow:

$$t = 0 \rightarrow M = b = M_{C_{Po}} \tag{B.22}$$

$$t = \frac{t_{cy}}{2} - t_{C_{Po}} \rightarrow M = 0$$

Using the two above boundary conditions, the mass equation is described below:

$$M = M_{C_{Po}}\left(1 - \frac{2t}{t_{cy} - 2t_{C_{Po}}}\right) \tag{B.23}$$

Substituting in Eq. (3.41):

$$M_{C_{Po}}\left(1 - \frac{2t}{t_{cy} - 2t_{C_{Po}}}\right) c_p \frac{dT}{dt} = he\, S_{tu}(t)(T_{we} - T) \tag{B.24}$$

- Tube surface calculation $\boldsymbol{S_{tu}(t)}$

$$S(t) = \alpha t + \beta \tag{B.25}$$

The surface boundary conditions are the following:

$$t = 0 \rightarrow S_{tu}(0) = S_{tu_{C_{Po}}} = \beta \tag{B.26}$$

$$t = \frac{t_{cy}}{2} \rightarrow S_{tu}\left(\frac{t_{cy}}{2} - t_{C_{Po}}\right) = 0$$

Using the two above boundary conditions, the tube surface equation is described below:

$$S_{tu}(t) = S_{tu_{C_{Po}}}(1 - \frac{2t}{t_{cy} - 2t_{C_{Po}}}) \tag{B.27}$$

Substituting Eq. (3.41):

$$M_{C_{Po}} c_p \frac{dT}{dt} = he\, S_{tu_{C_{Po}}}\,(T_{in}^{w} - T) \tag{B.28}$$

$$\frac{dT}{dt} + \frac{he\, S_{tu_{C_{Po}}}}{M_{C_{Po}} c_p} T = \frac{he\, S_{tu_{C_{Po}}}}{M_{C_{Po}} c_p}\, T_{in}^{w} \tag{B.29}$$

The solution is therefore :

$$y(t) = \frac{c}{b} + cte\ e^{\frac{-b}{a}t} \tag{B.30}$$

$$T(t) = y_p + y_h = T_{in}^{w} + cte\ e^{-\frac{he\ S_{tu_{C_{Po}}}}{M_3 c_p}t} \tag{B.31}$$

The temperature boundary conditions are the following:

$$t = 0 \rightarrow T(0) = T_{C_{Po}} = T_{in}^{w} + cte \rightarrow cte = T_{C_{Po}} - T_{in}^{w} \tag{B.32}$$

$$t = \frac{t_{cy}}{2} \rightarrow T\left(\frac{t_{cy}}{2} - t_{C_{Po}}\right) = T_D = T_{in}^{w} + (T_{C_{Po}} - T_{in}^{w})\ e^{-\frac{he\ S_{tu_{C_{Po}}}}{M_3 c_p}(\frac{t_{cy}}{2} - t_{C_{Po}})} \tag{B.33}$$

$$T\left(\frac{t_{cy}}{2} - t_{C_{Po}}\right) = T_{\mathrm{D}} = T_{in}^{w} + (T_{C_{Po}} - T_{in}^{w})\ e^{-\frac{he\ S_{tu_{C_{Po}}}}{M_{C_{Po}} c_p}(\frac{t_{cy}}{2} - t_{C_{Po}})} \tag{B.34}$$

With:

$$\frac{he\ S_{C_{Po}}}{M_{C_{Po}} c_p} = \frac{NTU}{t_{cy}} \tag{B.35}$$

and

$$NTU = \frac{4\ he\ V_{C_{Po}}}{D\ c_p\ \dot{m}_{DA}} \tag{B.36}$$

$$T_{\mathrm{D}} = T_{in}^{w} + (T_{C_{Po}} - T_{in}^{w})\ e^{-NTU\left(\frac{1}{2} - \frac{t_{C_{Po}}}{t_{cy}}\right)} \tag{B.37}$$

B.2.3. Air discharge phase (Liquid piston expander)

Equation (3.41) is a differential equation with second member that describes the phase air discharge phase after expending the compressed air (phase: C' → D').This equation is solved based on two analysis approaching the air mass $M(t)$ and tube surface $S_{tu}(t)$.

- Mass calculation $\boldsymbol{M(t)}$

$$\frac{dM}{dt} = \dot{m} \tag{B.38}$$

$$M = \dot{m}t + b \tag{B.39}$$

The mass boundary conditions are as follow:

$$t = 0 \rightarrow M = b = M_{C'_{Po}} \tag{B.40}$$

$$t = \frac{t_{cy}}{2} - t_{C'_{Po}} \rightarrow M = 0$$

Using the two above boundary conditions, the mass equation is described below:

$$M = M_{C'_{Po}} \left(1 - \frac{2t}{t_{cy}}\right) \tag{B.41}$$

Substituting Eq. (3.41):

$$M_{C'_{Po}} \left(1 - \frac{2t}{t_{cy}}\right) c_p \frac{dT}{dt} = he\, S_{tu}(t)(T_{in}^w - T) \tag{B.42}$$

- Tube surface calculation $\boldsymbol{S_{tu}(t)}$

$$S_{tu}(t) = \alpha t + \beta \tag{B.43}$$

The surface boundary conditions are the following:

$$t = 0 \rightarrow S_{tu}(0) = S_{tu_{C'_{Po}}} = \beta \tag{B.44}$$

$$t = \frac{t_{cy}}{2} \rightarrow S_{tu}\left(\frac{t_{cy}}{2}\right) = 0$$

Using the two above boundary conditions, the tube surface equation is described below:

$$S_{tu}(t) = S_{tu_{C'_{Po}}}(1 - \frac{2t}{t_{cy}}) \tag{B.45}$$

Substituting Eq. (3.41):

$$M_{C'_{Po}} c_p \frac{dT}{dt} = he\, S_{tu_{C'_{Po}}}(T_{in}^w - T) \tag{B.46}$$

$$\frac{dT}{dt} + \frac{he\, S_{tu_{C'_{Po}}}}{M_{C'_{Po}} c_p} T = \frac{he\, S_{tu_{C'_{Po}}}}{M_{C'_{Po}} c_p}\, T_{in}^w \tag{B.47}$$

The solution is therefore :

$$y(t) = \frac{c}{b} + cte\, e^{\frac{-b}{a}t} \tag{B.48}$$

$$T(t) = y_p + y_h = T_{in}^w + cte\, e^{-\frac{he\, S_{tu_{C'_{Po}}}}{M_{C'_{Po}} c_p} t} \tag{B.49}$$

The temperature boundary conditions are the following:

$$t = 0 \rightarrow T(0) = T_{C'_{Po}} = T_{in}^{w} + cte \rightarrow cte = T_{C'_{Po}} - T_{in}^{w} \quad \text{(B.50)}$$

$$t = \frac{t_{cy}}{2} \rightarrow T\left(\frac{t_{cy}}{2}\right) = T_D = T_{in}^{w} + cte\ e^{-\frac{he\ S_{tu_{C'_{Po}}}\ t_{cy}}{M_{C'_{Po}}\ c_p}} \quad \text{(B.51)}$$

$$T\left(\frac{t_{cy}}{2}\right) = T_{\mathrm{D}} = T_{in}^{w} + \left(T_{C'_{Po}} - T_{in}^{w}\right) e^{-\frac{he\ S_{tu_{C'_{Po}}}\ t_{cy}}{M_{C'_{Po}}\ c_p}} \quad \text{(B.52)}$$

With:

$$\frac{he\ S_{tu_{C'_{Po}}}}{M_{C'_{Po}}\ c_p} = \frac{NTU}{t_{cy}} \quad \text{(B.53)}$$

and

$$NTU = \frac{4\ he\ V_{C'_{Po}}}{D\ c_p\ \dot{m}_{DA}} \quad \text{(B.54)}$$

$$T_{\mathrm{D}} = T_{in}^{w} + (T_{C'_{Po}} - T_{in}^{w})\ e^{\frac{-NTU}{2}} \quad \text{(B.55)}$$

Appendix C *AIR4POWER project*

In this section a detailed description of the AIR4POWER project developed by AIA LIFE DESIGNERS is presented.

C.1. Project general description

The solution proposed in the AIR4POWER project is based on an adiabatic compressed air system (A-CAES - Adiabatic Compressed Air Energy Storage) allowing energy to be stored in order to restore it in four different energy types (electricity, heat, cold and compressed air) with a relatively important global energy efficiency. An interconnection of buildings with thermal and electrical networks (smartgrid type) is also proposed in this project in order to increase and optimize the renewable energy integration into the final energy consumption. Five applications are currently being considered:

- Urban energy storage module (smart-grid).
- Energy storage integrated into spaces and fallow volumes or undergoing conversion.
- Energy consumption peaks removal and electricity resale from industrial sites.
- Buildings with integrated energy storage (use of opportunistic voids in structures).
- Energy storage for non-interconnected areas (ZNI) (islands, mountains, nature reserves).

C.2. Project key dates

The research project, officially launched in 2013 by the AIA LIFE DESIGNERS team, had to deal with major ups and downs. In the first place, a significant part of the research work was based on the technical and numerical data provided by the LightSail Energy, an American

startup developing I-CAES (Isothermal compressed air energy storage), partner of AIA LFE DESIGNERS.

LightSail Energy has been considered for many years as one of the most promising international startups in terms of small scale CAES systems (100 kW to 1 MW). Created since 2008 by Danielle Fong and Steve Crane with a team over 30 people and they succeed to raise more than $60 million based on investors like Khosla Venture, Bill Gates, Peter Thiel, Total Energy Venture, etc.

AIA LIFE DESIGNERS signed an exclusive partnership agreement in Europe for the establishment of an incubator (laboratory) and a prototype (pilot in a real environment) in 2018, based on the equipment supplied by LightSail Energy and adapted to the European context. Research on AIR4POWER resulted in the filing of a patent in 2014 (INPI) and the international extension (PCT), filed in February 2015.

However, this agreement could not be respected by LightSail Energy due to significant delays in engine development. These delays have, moreover and since the end of 2016, led to legal proceedings by certain investors of LightSail Energy and put the reversible compressed air engine development project on hold for an indefinite period at this stage.

The AIA LIFE DESIGNERS research project team having been impacted by these difficulties from the start of the AIR4POWER research project in May 2016, they tried to adapt, as much as possible, the research to move forward.

Without having the right skills to carry out a theoretical and fundamental research, AIA LIFE DESIGNERS with the CETHIL of INSA Lyon (Center Energétique et Thermique de Lyon) has launched a PhD CIFRE project for 3 years (initiated since February 2017).

AIA LIFE DESIGNERS has completed a diagnostic and feasibility study for the installation of an AIR4POWER storage unit in a fish cannery (vacant building) on the island of Yeu in France. The study consisted of developing an analysis of the existing building (structural diagnosis, plant context, analysis of the renewable energy mix of the territory) and producing an installation diagram for the energy storage system in the old building factory (February 2018).

Another research project was carried out between AIA LIFE DESIGNERS, CSTB (Scientific and Technical Center for Building) and CETHIL for the purpose of answering the essential question of energy storage and management questioned by the ADEME. This project demonstrated the relevance of compressed air storage technology (quasi-isothermal and adiabatic) at the scale of a building from a technical, economic and social point of view. In addition, an LCA (Levilized cost analysis) method was proposed in order to compare the

AIR4POWER solution to other storage technologies in the market. In September 2018, a final report (170 pages) was delivered to ADEME.

AIA LIFE DESIGNERS was interested by ENAIRYS, a Swiss start-up which has been developing a CAES system based on liquid piston for 10 years. A lack of funding causes a delay in the development of prototype B (25 kW).

In this context, AIA LIFE DESIGNERS aims to set up a hybrid compressed air energy storage system (CAES), mainly composed of elements currently available in the market.

C.3. AIR4POWER system description

C.3.1. Building model definition

The innovative character of the AIR4POWER solution is based on the advantageous use of the architectural and structural specificities (structural voids and soil freed from the foundations) of certain buildings allowing energy to be stored in these empty spaces.

Figure 0.4: Incubator building proposed by AIR4POWER project

There are 2 types of architectural elements that can used to store energy:

- Structural voids that can store electrical energy (in the form of compressed air), and thermal energy: these are voids in SVS (Stockage dans les Vides de Structure) or CVS (Caissons dans les Vides de Structure). Such floors can be used:
    - When long-span floors are necessary (for example to free the lower floor from cross walls and ensure its modularity),
    - to ensure load transfer between 2 levels with different structural frames (for example an office floor and a housing floor (Figure 0.5).
- Soil Freed from Foundations (SLF) allows the heat produced by the gas compression process to be stored in sealed tanks located in a set of piles located in the SLF.

The figures below below illustrates two building designs likely to host the AIR4POWER solution.

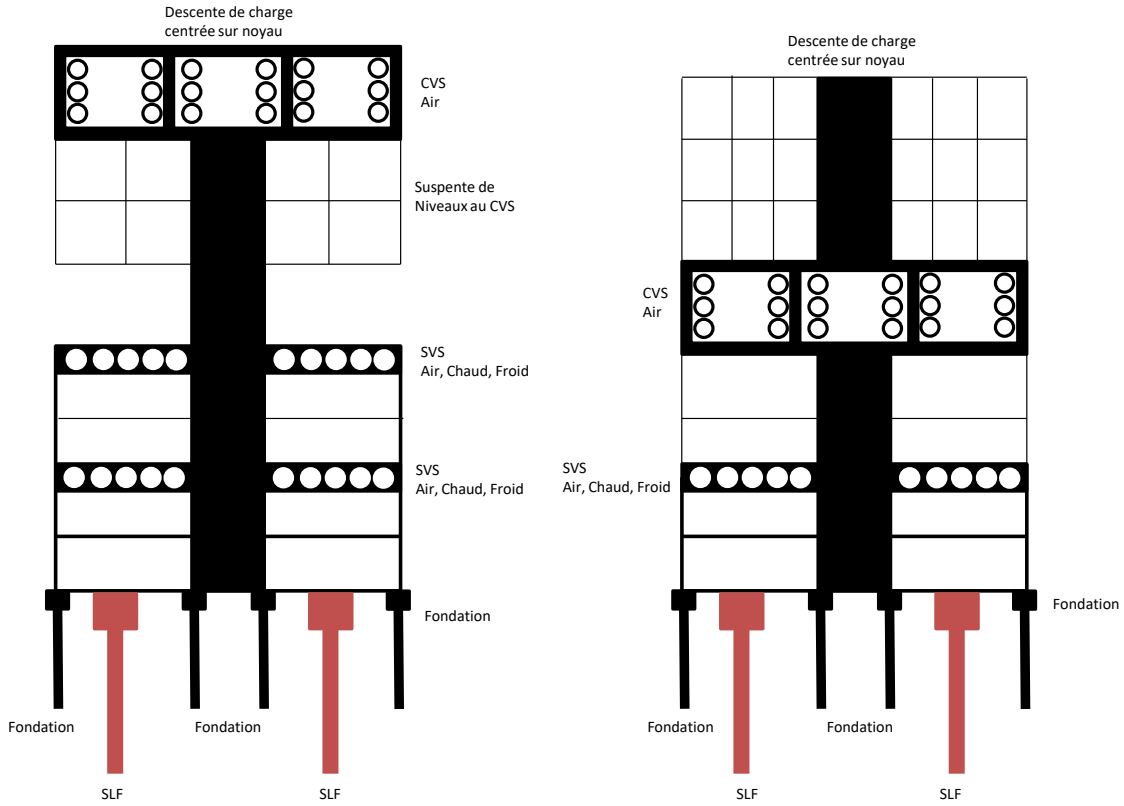

Figure 0.5: Sectional view of a building integrating the AIR4POWER solution

Figure 0.6: Structural design of the energy storage solution (a)

Figure 0.7: Structural design of the energy storage solution (b)

References

[1] I. E. Agency, “World Energy Outlook 2018,” 2018.

[2] Gouvernement Francais, “Energy transition.” [Online]. Available: https://www.gouvernement.fr/en/energy-transition.

[3] I. E. Agency, “Renewables 2018-Analysis and forcasts to 2023,” 2018.

[4] Ministère de l’environnement de l’énergie et de la mer, “PANORAMA ÉNERGIES-CLIMAT,” 2016.

[5] Ministère de la Transition écologique, “Énergie dans les bâtiments,” 2017. [Online]. Available: https://www.ecologique-solidaire.gouv.fr/energie-dans-batiments. [Accessed: 04-Aug-2020].

[6] Y. Coltier *et al.*, “Chiffres clés des énergies renouvelables - Édition 2019,” pp. 1–92, 2019.

[7] ADEME, “Les français et l’environnement,” 2019.

[8] CEA, “Le stockage stationnaire de l’énergie,” p. 41, 2012.

[9] X. Luo, J. Wang, M. Dooner, and J. Clarke, “Overview of current development in electrical energy storage technologies and the application potential in power system operation,” *Appl. Energy*, vol. 137, pp. 511–536, 2015.

[10] M. Budt, D. Wolf, R. Span, and J. Yan, “A review on compressed air energy storage: Basic principles, past milestones and recent developments,” *Appl. Energy*, vol. 170, pp. 250–268, 2016.

[11] I.-énergie Nouvelle, “Le stockage massif de l’énergie,” 2013.

[12] J. Wang, “Overview of compressed air energy storage and technology development,” *Energies*, vol. 10, no. 7, p. 22, 2017.

[13] L. Chen, T. Zheng, S. Mei, and X. Xue, “Review and prospect of compressed air energy storage system,” *J. Mod. Power Syst. Clean Energy*, vol. 4, pp. 529–541, 2016.

[14] G. Venkataramani and J. Wang, “A review on compressed air energy storage – A path way for smartgrid and polygeneration,” *Renew. Sustain. Energy Rev.*, vol. 62, pp. 895–

907, 2016.

[15] ARUP, “Five minute guide: Electricity storage technologies.” [Online]. Available: www.arup.com.

[16] aerocom, “Historique de l’évolution du système pneumatique.” [Online]. Available: https://www.aerocom-france.com/le-pneumatique-historique/.

[17] Ouest-France, “En 1879, déjà, le tram à air comprimé,” *Ouest-France*, 07-Jan-2015.

[18] “Poste pneumatique de Paris.” .

[19] M. Nakhamkin and M. Chiruvolu, “Available compressed air energy storage CAES plant concepts,” *Energy*, pp. 541–548, 2010.

[20] A. Ter-Gazarian, *Energy storage power systems*. 1994.

[21] F. Crotogino, “Le stockage d’air comprimé de HUNTOR: plus de 20 ans de succès dans l’exploitation,” p. 4, 2001.

[22] J. Walter Keeney, “Iinvestigation of compressed air energy storage effiency,” Faculty of California Polytechnic State University, 2013.

[23] E. Barbour, D. Mignard, and Y. Ding, “Adiabatic compressed air energy storage with packed bed thermalenergy storage,” *Appl. Energy*, vol. 155, pp. 801–815, 2015.

[24] INERIS (Institut national de l’environnement industriel et des Risques), “Stockage souterrain de l’air comprimé dans le contexte de la transition énergétique,” 2016.

[25] Y. Kim, “Novel concepts of compressed air energy storage and thermo-electric energy storage,” EPFL, 2012.

[26] H. Xue and A. White, “A comparative study of liquid, solid and hybrid adiabatic compressed air energy storage systems,” *J. Energy Storage*, vol. 18, pp. 349–359, 2018.

[27] J.-L. Liu and J.-H. Wang, “A comparative research of two adiabatic compressed air energy storage systems,” *Energy Convers. Manag.*, vol. 108, pp. 566–578, 2015.

[28] L.-X. Chen, P. Hu, C.-C. Sheng, and M.-N. Xie, “A novel compressed air energy storage CAES system combined with pre-cooler and using low grade waste heat as heat source,” *Energy*, vol. 131, pp. 259–266, 2017.

[29] N. Hartmann, O. Vöhringer, C. Kruck, and L. Eltrop, “Simulation and analysis of different adiabatic compressed air energy storage plant configurations,” *Appl. Energy*, vol. 93, pp. 541–548, 2011.

[30] Y. Zhang, K. Yang, X. Li, and J. Xu, “The thermodynamic effect of air storage chamber model on advanced adiabatic compressed air energy storage system,” *Renew. Energy*, vol. 57, pp. 469–478, 2013.

[31] C. Guo *et al.*, “Performance analysis of compressed air energy storage systems considering dynamic characteristics of compressed air storage,” *Energy*, vol. 135, pp. 876–888, 2017.

[32] Y. Li, X. Wang, D. Li, and Y. Ding, “A trigeneration system based on compressed air and thermal energy storage,” *Appl. Energy*, vol. 99, pp. 316–323, 2012.

[33] E. Jannelli, M. Minutillo, A. Lubrano Lavadera, and G. Falcucci, “A small-scale CAES (compressed air energy storage) system for stand-alone renewable energy power plant for a radio base station: A sizing-design methodology,” *Energy*, vol. 78, pp. 313–322, 2014.

[34] S. Simpore, F. Garde, M. David, O. Marc, and J. Castaing-Lasvignottes, “Design and dynamic simulation of a compressed air energy storage system (CAES) coupled with a building, an electric grid and a photovoltaic power plant,” *CLIMA 2016 - Proc. 12th REHVA World Congr.*, 2016.

[35] S. Lv, W. He, A. Zhang, G. Li, B. Luo, and X. Liu, “Modelling and analysis of a novel compressed air energy storage system for trigeneration based on electrical energy peak load shifting,” *Energy Convers. Manag.*, vol. 135, pp. 394–401, 2017.

[36] S. Wang, X. Zhang, L. Yang, Y. Zhou, and J. Wang, “Experimental study of compressed air energy storage system with thermal energy storage,” *Energy*, vol. 103, pp. 182–191, 2016.

[37] M. Cheayb, M. Marin Gallego, M. Tazerout, and S. Poncet, “Modelling and experimental validation of a small-scale trigenerative compressed air energy storage system,” *Appl. Energy*, vol. 239, pp. 1371–1384, 2019.

[38] S. Crane, D. Fong, and E. Berlin, “Energy storage system utilizing compressed gas,” no. US 8,247,915 B2. p. 31, 2012.

[39] S. Lemofouet, “Investigation and optimisation of hybrid electricity storage systems based on compressed air and supercapacitors,”, Ph.D dissertation, École polytechnique fédérale de Lausanne, Lausanne, 2006.

[40] SustainX, “Energy storage and generation systems and methods using coupled cylinder assemblies,” 2013.

[41] Emmanuel Barraud, “L’Etat de Vaud soutient le stockage d’énergie par air comprimé,” 2014. [Online]. Available: https://actu.epfl.ch/news/l-etat-de-vaud-soutient-le-stockage-d-energie-par-/. [Accessed: 03-Mar-2020].

[42] S. Lemofouet and A. Rufer, “Projet pilote de stockage hydropneumatique d’énergie pour le lissage de la production photovoltaïque de Mont-Soleil,” 2011.

[43] S. Lemofouet and A. Rufer, “Multistage hydraulic gas compression/expansion system and methods,” US 8,567,183,B2, 2013.

[44] S. Lemofouet, “Réalisation et Caractérisation Etendue d’un Prototype de Système de Stockage Hydro-pneumatique d’Energie,”, Office fédéral de l'énergie OFEN, Switzerland, December 2012.

[45] K. N. Nwaigwe, P. Mutabilwa, and E. Dintwa, “An overview of solar power (PV systems) integration into electricity grids,” *Mater. Sci. Energy Technol.*, vol. 2, no. 3, pp. 629–633, Dec. 2019.

[46] S. Simpore, “Modélisation, simulation et optimisation d’un système de stcokage à air comprimé couplé à un batiment et à une production photovoltaique,”, Ph.D dissertation, Université de la réunion, 2019.

[47] J. de Ven and P. Li, “Liquid Piston Gas Compression,” *Appl. Energy*, vol. 86, pp. 2183–2191, 2009.

[48] C. Qin and E. Loth, “Liquid piston compression efficiency with droplet heat transfer,” *Appl. Energy*, vol. 114, pp. 539–550, 2014.

[49] J. Guanwei, X. Weiqing, C. Maolin, and S. Yan, “Micron-sized water spray-cooled quasi-isothermal compression for compressed air energy storage,” *Exp. Therm. Fluid Sci.*, vol. 96, pp. 470–481, 2018.

[50] A. Odukomaiya, A. Abu-Heiba, S. Graham, and A. M. Momen, “Experimental and analytical evaluation of a hydro-pneumatic compressed-air Ground-Level Integrated Diverse Energy Storage (GLIDES) system,” *Appl. Energy*, vol. 221, pp. 75–85, 2018.

[51] X. Zhang *et al.*, “A near-isothermal expander for isothermal compressed air energy storage system,” *Appl. Energy*, vol. 225, pp. 955–964, 2018.

[52] B. Cretinon, “Paramètres hygrométriques,” vol. 33, no. R3047 V1, p. 12, 2004.

[53] R. Revellin, *Thermodynamique appliquée aux machines thermiques*. 2016.

[54] L. Tocci, T. Pal, I. Pesmazoglou, and B. Franchetti, “Small Scale Organic Rankine Cycle

(ORC): A Techno-Economic Review," vol. 10, pp. 1–26, 2017.

[55] A. P. Weiß, "Volumetric expander versus turbine - Which is the better choice for small ORC plants?," *3rd Int. Semin. ORC Power Syst.*, pp. 1–10, 2015.

[56] V. Lemort and A. Legros, *Positive displacement expanders for Organic Rankine Cycle systems*. Elsevier Ltd, 2017.

[57] R. Daccord *et al.*, "Integration of a piston expander for exhaust heat recovery in a long haul truck," *Exoès – Fr.*, 2016.

[58] K. Qiu, M. Thomas, and M. Douglas, "Investigation of a scroll expander driven by compressed air and its potential applications to ORC," *Appl. Therm. Eng.*, vol. 135, pp. 109–115, 2018.

[59] D. Ziviani, N. A. James, F. A. Accorsi, J. E. Braun, and E. A. Groll, "Experimental and numerical analyses of a 5 kWe oil-free open-drive scroll expander for small-scale organic Rankine cycle (ORC) applications," *Appl. Energy*, vol. 230, pp. 1140–1156, 2018.

[60] ENOGIA, "FICHE TECHNIQUE ORC ENO-10LT," 2009. [Online]. Available: http://enogia.com/wp/7-2-2/.

FOLIO ADMINISTRATIF

THESE DE L'UNIVERSITE DE LYON OPEREE AU SEIN DE L'INSA LYON

NOM : DIB DATE de SOUTENANCE : 27/10/20

Prénoms : Ghady

TITRE : Thermodynamic simulation of compressed air energy storage systems

NATURE : Doctorat Numéro d'ordre : 2020LYSEI092

Ecole doctorale : MEGA (Mécanique, Énergétique, Génie Civil, Acoustique)

Spécialité : Thermique et Énergétique

RESUME :

Un modèle numérique d'un système de stockage par air comprimé à petite échelle, couplé à un modèle de bâtiment et à des modules d'énergie renouvelable a été développé dans le but de modéliser différents compresseurs/organes de détente et structures d'installation développés par plusieurs startups (LightSail Energy et Enairys Powertech). Plusieurs scénarios énergétiques (autonomes et connectés aux réseaux), localisations géographiques et typologies de bâtiments ont été proposés et analysés. Le développement du modèle numérique CAES est basé sur la résolution de l'équation de conservation de l'énergie et des équations de transferts pour chaque composant du système (compresseur/organe de détente, échangeur, réservoir d'air haute pression, réservoir de stockage d'eau chaude/froide). Deux types de compresseurs et organes de détente (adiabatique et isotherme) ont été testés et analysés. Le système CAES adiabatique semble être réalisable à partir des composants disponibles sur le marché : compresseurs, turbines, réservoirs et autres équipements nécessaires pour le système de stockage. En ce qui concerne le système CAES isotherme, une augmentation de rendement électrique a été observée. En particulier, la technologie de compresseurs/organes de détente basée sur le piston classique a présenté une meilleure récupération thermique par rapport à la technologie de compresseurs/organes de détente basée sur le piston liquide. Ce dernier a néanmoins montré un meilleur rendement électrique à l'échelle du système.

MOTS-CLÉS : Energy storage, advanced adiabatic, quasi-isothermal, compression/expansion, numerical model, building application

Laboratoire (s) de recherche : CETHIL

Directeur de thèse: REVELLIN Rémi

Président de jury : LANZETTA François

Composition du jury : LEMORT Vincent, GROSU Lavinia, LANZETTA François, REVELLIN Rémi, RULLIÈRE Romuald.